



**Fakultät für Chemie**

**Lehrstuhl für Pharmazeutische Radiochemie**

# **Development of cyclic pentapeptide ligands for chemokine receptor targeting**

**Theresa Martina Osl**

Vollständiger Abdruck der von der Fakultät für Chemie der Technischen Universität München zur Erlangung des akademischen Grades eines

**Doktor der Naturwissenschaften (Dr. rer. nat.)**

genehmigten Dissertation.

**Vorsitzender:** Prof. Dr. Dr. h.c. Horst Kessler

**Prüfer der Dissertation:**

1. Prof. Dr. Hans-Jürgen Wester
2. apl. Prof. Dr. Klemens Scheidhauer

Die Dissertation wurde am 20.12.2016 bei der Fakultät für Chemie der Technischen Universität München eingereicht und durch die Fakultät für Chemie am 08.03.2016 angenommen.

Meiner Familie

-Have no fear of perfection, you'll never reach it.-

*Salvador Dali*

## Table of contents

<b>I. INTRODUCTION.....</b>	<b>1</b>
<b>1. Background.....</b>	<b>1</b>
1.1. Chemokines and chemokine receptors.....	1
1.2. Stromal cell-derived factor-1 (SDF-1/CXCL12) and its receptor CXCR4.....	2
1.3. The role of CXCR4/CXCL12 signaling in cancer.....	3
<b>2. Structure based development of peptide and peptidomimetic ligands for CXCR4.....</b>	<b>8</b>
2.1 Structure of CXCR4 .....	8
2.2. CXCR4 ligand development: A downsizing process.....	9
2.3. Binding mode of cyclic pentapeptides.....	13
<b>3. PET imaging of CXCR4 expression .....</b>	<b>16</b>
<b>4. CXCR4 targeted therapeutic approaches.....</b>	<b>21</b>
<b>5. Objectives .....</b>	<b>25</b>
<b>II. MATERIALS AND METHODS .....</b>	<b>27</b>
<b>1. General information.....</b>	<b>27</b>
<b>2. General synthesis protocols.....</b>	<b>28</b>
2.1. Fmoc-based solid-phase peptide synthesis.....	28
2.2. Condensation with chelating moieties and cold complexation .....	31
<b>3. Synthesis of cyclo[D-Tyr-(hexylguanidino)-D-Ala-Arg-Nal-Gly] (R1) derived ligands....</b>	<b>32</b>
<b>4. Synthesis of cyclo[D-Tyr-N(Me)-D-Orn-Arg-2-Nal-Gly] derived peptides.....</b>	<b>39</b>
4.1. Shifting the charge.....	41
4.2. Optimization of the linking unit .....	45
4.3. Precursor for radiofluorination (BF <sub>3</sub> -derivatives) .....	61
<b>5. Synthesis of CXCR7 targeting ligands .....</b>	<b>66</b>
<b>6. Radiochemistry .....</b>	<b>73</b>
6.1. Radioiodination([ <sup>125</sup> I]NaI) .....	73
6.2. <sup>68</sup> Ga <sup>III</sup> -labeling .....	75
6.3. <sup>177</sup> Lu-labeling.....	75
6.4. <sup>18</sup> F-labeling .....	76

<b>7. Cell experiments .....</b>	<b>76</b>
7.1. Cultivation of utilized cell lines .....	76
7.2. Determination of receptor binding affinity and specificity .....	77
7.3. Fluorescent microscopy .....	79
7.4. Functional assays for <i>in vitro</i> characterization.....	80
<b>8. Determination of lipophilicity, stability and blood cell binding.....</b>	<b>83</b>
<b>9. Animal experiments .....</b>	<b>85</b>
9.1. Metabolite analysis .....	85
9.2. Biodistribution.....	86
9.3. Small-animal PET imaging .....	86
<b>III. RESULTS AND DISCUSSION.....</b>	<b>87</b>
<b>1. Synthesis.....</b>	<b>87</b>
1.1. Synthesis of cyclo[D-Tyr-N(hexylguanidino)-D-Ala-Arg-Nal-D-Cys] ( <b>2</b> )-based compounds.....	89
1.2. Synthesis of cyclo[D-Tyr-N(Me)-D-Orn-Arg-Nal-Gly] ( <b>11</b> )-based compounds.....	91
1.3. Ligands based on cyclo[D-Tyr-Pro-Nal-N(Me)-Arg-Arg] ( <b>R3</b> ) for addressing the CXC chemokine receptor type 7 .....	97
1.4. Metal complexation.....	100
<b>2. Radiolabeling .....</b>	<b>100</b>
2.1. Radioiodination.....	100
2.2. <sup>68</sup> Ga-labeling .....	100
2.3. <sup>177</sup> Lu-labeling.....	101
2.4. <sup>18</sup> F-labeling .....	101
<b>3. <i>In vitro</i> evaluation .....</b>	<b>101</b>
3.1. Cyclo[D-Tyr-N(hexylguanidino)-D-Ala-Arg-Nal-D-Cys] ( <b>2</b> ) based compounds .....	102
3.2. Cyclo[D-Tyr-N(Me)-D-Orn-Arg-Nal-Gly] ( <b>11</b> )-based compounds .....	106
3.3. Ligands based on cyclo[D-Tyr-Pro-2-Nal-N(Me)-Arg-Arg] ( <b>R3</b> ) for addressing the CXC chemokine receptor type 7 .....	126
<b>4. Determination of lipophilicity and specific cell binding.....</b>	<b>129</b>
<b>5. <i>In vivo</i> evaluation .....</b>	<b>133</b>
5.1. Metabolite analysis .....	133
5.2. Biodistribution.....	134



5.3. Small-animal PET .....	144
<b>IV SUMMARY AND CONCLUSION .....</b>	<b>152</b>
<b>V SUPPLEMENTARY MATERIAL.....</b>	<b>157</b>
1. Figure and Table index.....	157
2. Abbreviations.....	164
3. References.....	167
4. Publications .....	182
5. Acknowledgements.....	184

## ABSTRACT

### ***Abstract***

Due to its pivotal role in tumor growth and metastasis in several types of human cancer, the chemokine receptor 4 (CXCR4) represents an innovative target for both diagnostic imaging and endoradiotherapeutic approaches. Several CXCR4 ligands based on the small-molecule inhibitor AMD3100, but also 14-mer cyclic peptides and cyclic pentapeptides have been evaluated pre-clinically. Increasing clinical application of [ $^{68}\text{Ga}$ ]Pentixafor PET demonstrates the capabilities of cyclic pentapeptides as lead structures for CXCR4 targeting. In addition, the therapeutic analogue, [ $^{177}\text{Lu}$ ]Pentixather, has already indicated the therapeutic potency of CXCR4-targeted endoradiotherapy (ERT). The goal of this work was the development of further optimized, CXCR4 targeting peptides for PET imaging ( $^{68}\text{Ga}$ ,  $^{18}\text{F}$ ), fluorescence microscopy (fluorescent dye), and endoradiotherapy ( $^{177}\text{Lu}$ ) of CXCR4 associated malignancies.

A combination of solid-phase peptide synthesis and solution phase chemistry was applied for the composition of the CXCR4 ligands. They generally consist of a radiometal chelator or a signaling moiety (e.g. AmBF<sub>3</sub>, QD), connected with a CXCR4 binding scaffold *via* a peptidic spacer unit. Determination of the affinity to *h*CXCR4 ( $IC_{50}$ ) was performed in a competitive binding assay using CXCR4<sup>+</sup> Jurkat cells (*h*CXCR4) and [ $^{125}\text{I}$ ]FC131 (cyclo[[ $^{125}\text{I}$ ]D-Tyr-Arg-Arg-2-Nal-Gly]) as the radioligand. Binding affinity towards the murine receptor was determined on Eμ-Myc1080 cells and [ $^{125}\text{I}$ ]CPCR4.3 (cyclo[[ $^{125}\text{I}$ ]D-Tyr-N(hexylguanidino)-D-Ala-Arg-Nal-Gly]) as the radioligand. Internalization and externalization rates of the respective radiolabeled peptides were determined on *h*CXCR4-expressing Chem\_1 cells. Further, the octanol distribution coefficient (lipophilicity) and metabolic stability of the radiopharmaceuticals was investigated, together with the *in vivo* targeting efficiency using  $\mu\text{PET}$ , as well as biodistribution in Daudi-tumor-bearing SCID mice.

Since CPCR4.3 (highly affine towards *m/h*CXCR4) lacks functionalities for the attachment of chelators or other signaling units, a D-cysteine for glycine substitution was performed in a first approach for the identification of novel peptides with feasible linkers without comprising CXCR4 affinity and species independence. Cyclo[D-Tyr-N(hexylguanidino)-D-Ala-Arg-Nal-D-Cys(1,4-phe-

## ABSTRACT

nylen-bismethanamine)ac-etamine)] proofed to be a functional CXCR4 affine ligand in conjugation with DOTA as well as on the surface of QDs. *In vitro* and *in vivo* evaluation of the respective DOTA-conjugated derivative showed high affinity towards murine as well as human CXCR4, high stability *in vivo* and favorable pharmacokinetics in healthy mice. QDs decorated with the novel CXCR4 targeting ligand showed specific accumulation on CXCR4 positive cells. PET studies investigating CXCR4-associated pathologies in a mouse model are currently limited to xenograft animal models, due to the absence of murine specific ligands. Consequently, the novel ligand could function as a valuable lead structure for the development of powerful murine CXCR4 targeting ligands with further optimized pharmacokinetic profiles especially with focus on the enhanced liver accumulation of the present ligands.

In the second part of the project, an elaborated SAR study was conducted to optimize the length and the structure of a linking unit between the pentixafor/-ther scaffold (cyclo[(3-*iodo*)D-Tyr-N(Me)-D-Orn-Arg-2-Nal-Gly]) and the signaling unit (chelator). Ligands comprising the novel linking unit “D-Arg-D-Ala-4-aminobenzoic acid” retained high binding affinity towards *h*CXCR4 (and surprisingly, *m*CXCR4 for ligands with iodinated binding scaffold), independently of the incorporated (radio)metal. In contrast to Ga-Pentixafor based ligands, which loose binding affinity towards CXCR4 in consequence of small structural changes (e.g. changing the radiometal), the novel linking unit introduce a greater flexibility towards structural modifications in regards to the development of  $^{18}\text{F}$ -,  $^{99\text{m}}\text{Tc}$ -, or fluorescent-labeled CXCR4 ligands.

DOTA-D-Arg-D-Ala-4-aminobenzoic acid-CPCR4 revealed an  $IC_{50}$  of  $0.4 \pm 0.1$  nM, fast and efficient internalization in CXCR4<sup>+</sup> cells, elevated retention in CXCR4<sup>+</sup> tumor cells, high CXCR4 specific binding and favorable pharmacokinetics *in vivo*. These traits qualify the novel ligand to be a promising CXCR4-targeting radiopharmaceutical and possible candidate for theranostic applications. An elaborated evaluation of  $^{68}\text{Ga}$ - and  $^{177}\text{Lu}$ -labeled DOTA-D-Arg-D-Ala-4-aminobenzoic acid-CPCR4 was performed in direct comparison with the established radiopharmaceuticals [ $^{68}\text{Ga}$ ]Pentixafor (for PET), as well as [ $^{177}\text{Lu}$ ]Pentixather (for ERT). The D-

## ABSTRACT

Tyr<sup>3</sup>-iodinated analogue revealed high human serum albumin (HSA) binding, extraordinary high internalization efficiency and increased specific binding to human blood cells. In order to be able to assess the full potential of novel peptides with higher binding affinity towards CXCR4, improved hydrophilicity and increased internalization in regards to endoradiotherapeutic probes, initial dosimetry studies have to be performed.

Recently, the ACKR3 (CXCR7) was identified as the second endogenous receptor of CXCL12 and its involvement in several malignancies could be proven. In a first approach, a potential anchor point for the introduction of additional functional groups (i.e. chelators, prosthetic groups) into the reference ligand FC313 (cyclo[D-Tyr-Pro-2-Nal-N(Me)-Arg-Arg]) was identified, and a reliable competitive binding assay employing CXCR7<sup>+</sup> U343 cells was established. The preliminary results of the small project can be used for more elaborated SAR studies, which could yield the first CXCR7 targeting PET probe.

In conclusion, a structural optimization of the linking unit between the binding scaffold and the chelator led to the development of novel, high affine CXCR4 ligands with favorable pharmacokinetic profiles for both diagnostic and therapeutic applications. Due to the introduction of the novel linking unit, a greater flexibility was achieved in regards to structural modifications of the targeting molecules, paving the way for the design of innovative CXCR4 targeting peptides.

## ZUSAMMENFASSUNG

### *Zusammenfassung*

Der Chemokin Rezeptor Typ 4 (CXCR4) ist unter Anderem am Wachstum und an der Metastasierung von Tumoren, sowie an Entzündungsprozessen im Körper beteiligt und eignet sich daher hervorragend als Zielstruktur sowohl für die diagnostische Bildgebung, als auch für therapeutische Ansätze. Zahlreiche Liganden basierend auf niedermolekularen Inhibitoren wie AMD3100, aber auch größere zyklische Peptide (14 Aminosäuren) und zyklische Pentapeptide wurden bereits in präklinischen Studien evaluiert. Die ansteigende Zahl an PET Untersuchungen mit [ $^{68}\text{Ga}$ ]Pentixafor zeigt die Tauglichkeit der in dieser Arbeit verwendeten, zyklischen Pentapeptide als Zielvektoren für CXCR4. Das therapeutische Analogon [ $^{177}\text{Lu}$ ]Pentixather wurde in initialen endoradiotherapeutischen Behandlungen eingesetzt und konnte bereits das Potential einer CXCR4-gerichteten Endoradiotherapie andeuten. Ziel dieser Arbeit war die Entwicklung neuer CXCR4 gerichteter Peptide für die PET-Diagnostik ( $^{68}\text{Ga}$ ,  $^{18}\text{F}$ ), Fluoreszenzmikroskopie (Fluoreszenzfarbstoffe, Quantum dots) und Endoradiotherapie ( $^{177}\text{Lu}$ ) von CXCR4 assoziierten Krankheiten. Dabei fokussierte sich das Ligandendesign auf die Einführung neuer Linkereinheiten zwischen dem Bindemotiv und der Bildgebungseinheit (Chelator oder prosthetische Gruppe), um eine hohe Bindungsaffinität an *m/hCXCR4* zu gewährleisten.

Die neuen CXCR4 Liganden wurden mittels Festphasen Peptidsynthese und Reaktionen in Lösung aufgebaut. Generell bestehen die Liganden aus einem zyklischen Bindungsmotiv und einer Bildgebungseinheit (Radiometallchelator, radiomarkierte prosthetische Gruppe oder Quantum Dots), die über einen Spacer oder Linker (zumeist ein kurzes Peptid) miteinander verbunden sind. Die Bindungsaffinität zum humanen Rezeptor ( $IC_{50}$ ) wurde mittels kompetitiver Bindungsstudien an Jurkat Zellen (*hCXCR4*<sup>+</sup>) unter Verwendung von [ $^{125}\text{I}$ ]FC131 (cyclo[[ $^{125}\text{I}$ ]D-Tyr-Arg-Arg-2-Nal-Gly]) als Radioligand bestimmt. Des Weiteren wurde die Affinität an murinen Ep-Myc1080 (*mCXCR4*<sup>+</sup>) Zellen mit [ $^{125}\text{I}$ ]CPCR4.3 (cyclo[[ $^{125}\text{I}$ ]D-Tyr-N(hexylguanidino)-D-Ala-Arg-Nal-Gly]) als Radioligand bestimmt. Für die Erhebung der funktionellen *in vitro* Daten, wie Internalisierungs- und Externalisierungsrate wurden Chem\_1 Zellen (*hCXCR4*<sup>+</sup>) verwendet. Nach Vorselektion anhand erhobener Bindungsaffinitäten wurden die

## ZUSAMMENFASSUNG

vielversprechendsten Liganden auf ihre Lipophilie und die metabolische Stabilität *in vivo* untersucht. Die abschließende Bewertung der neuen Liganden erfolgte mittels Kleintier-PET und Biodistributionsstudien in Daudi Tumor-tragenden SCID Mäusen.

Im ersten Teil der Arbeit diente cyclo[D-Tyr-N(hexylguanidino)-D-Ala-Arg-Nal-Gly] als Bindungsmotiv für die Entwicklung neuer CXCR4 affiner Liganden, welches sich durch seine außerordentlich hohe Bindungsaffinität sowohl zum murinen, als auch zum humanen Rezeptor auszeichnet. Durch die Substitution von Glycin mit D-Cystein konnte die zyklische Grundstruktur für die Einführung von verschiedenen Linkern zugänglich gemacht werden. Cyclo[D-Tyr-N(hexylguanidino)-D-Ala-Arg-Nal-D-Cys(1,4-phenylen-bismethanamine)acetamine]] erwies sich als ein hoch affines Peptid (gemessen an *h*CXCR4 und *m*CXCR4) sowohl als Konjugat mit DOTA, als auch auf der Oberfläche von QDs. Trotz hoher *in vivo* Stabilität des  $^{68}\text{Ga}$ -markierten Peptids und einer schnellen, renalen Ausscheidung, limitiert die erhöhte Anreicherung der neuen Verbindung in der Leber von gesunden Mäusen die derzeitige Verwendbarkeit des DOTA-Derivats. Dennoch könnte der neue Ligand als Ausgangspunkt für die Weiterentwicklung von potenten, spezie-unabhängigen CXCR4 Liganden dienen, um CXCR4 assoziierte Krankheitsprozesse im Mausmodel exakter untersuchen zu können.

Im zweiten Teil der Arbeit wurde eine Struktur-Wirkungsbeziehung anhand der gemessenen Bindungsaffinitäten zu *h*CXCR4 durchgeführt, um die Länge und Beschaffenheit des Linkers zwischen dem Bindungsmotiv (CPCR4 (cyclo[D-Tyr-N(Me)-D-Orn-Arg-2-Nal-Gly])) und dem Chelator zu optimieren. Liganden, die den neuen Linker "D-Arg-D-Ala-4-aminobenzoessäure" beinhalten, wiesen hohe Bindungsaffinitäten zu *h*CXCR4 (und überraschender Weise auch zu *m*CXCR4, wenn das an D-Tyr<sup>3</sup> iodierter Grundgerüst verwendet wurde) auf, unabhängig vom komplexiertem Radiometall. Im Gegensatz zu [ $^{nat}\text{Ga}$ ]Pentixafor-basierten Liganden, die eine hohe Abhängigkeit der Bindungsaffinität zum Rezeptor von strukturellen Veränderungen aufweisen, ermöglicht die neue Linkerstruktur eine höhere Flexibilität gegenüber strukturellen Modifikationen im Hinblick auf die Entwicklung von  $^{18}\text{F}$ -,  $^{99\text{m}}\text{Tc}$ -, oder Fluoreszenz-markierte CXCR4 Liganden.

## ZUSAMMENFASSUNG

Das optimierte Pentixafor-Derivat DOTA-D-Arg-D-Ala-4-ABA-CPCR4 ist ein hoch affiner ( $IC_{50}$  von  $0.4 \pm 0.1$  nM), gut internalisierender CXCR4 Ligand, der sich durch eine erhöhte Retention in Tumorzellen und eine schnellen Pharmakokinetik *in vivo* auszeichnet. Eine genaue Bewertung von  $^{68}\text{Ga}$ - und  $^{177}\text{Lu}$ -markiertem DOTA-D-Arg-D-Ala-4-ABA-CPCR4 erfolgte durch einen direkten Vergleich mit den bereits etablierten Radiopharmaka [ $^{68}\text{Ga}$ ]Pentixafor und [ $^{177}\text{Lu}$ ]Pentixather. Das iodierter Analogon DOTA-D-Arg-D-Ala-4-ABA-*iodo*CPCR4 zeigte eine außergewöhnlich gute Internalisierung, eine sehr hohe Bindung an Serumalbumin und eine nicht vernachlässigbare Bindung an humane Blutzellen. Außerdem wurde eine gesteigerte Affinität zu *m*CXCR4 bestimmt.

In einem abschließenden Projekt wurden neue ACKR3 (CXCR7) gerichtete Liganden entwickelt. Als zweiter endogener Rezeptor von CXCL12 interagiert CXCR7 nicht nur mit der bekannten CXCR4/CXCL12-Achse, sondern wurde auch mit diversen Krankheiten in Zusammenhang gebracht. Die Referenzverbindung cyclo[D-Tyr-Pro-2-Nal-N(Me)-Arg-Arg]) wurde durch Modifikationen in der Aminosäuren Sequenz auf eine geeignete Substitutionsstelle untersucht, um zusätzliche funktionelle Gruppen einzuführen (z.B. Chelatoren oder prosthetische Gruppen). Dafür musste ein verlässlicher Bindungsassay mit CXCR7<sup>+</sup> U343 Zellen etabliert werden. Die ersten Ergebnisse der Studie stellen eine Grundlage zur Entwicklung neuer CXCR7-gerichteter Liganden dar, welche durch detaillierte Struktur-Wirkungsbeziehungsstudien erarbeitet werden müssen.

Zusammenfassend konnte durch die Optimierung des Linkers zwischen Bindemotiv und Chelator ein CXCR4 affines, theranostisches Derivat entwickelt werden, welches eine hohe Toleranz bezüglich verschiedenster Radiometalle aufweist und daher breite Anwendung finden könnte. Mit Hilfe des optimierten Linkers war es zusätzlich möglich, neue Derivate zur  $^{18}\text{F}$ -Markierung und Endoradiotherapie mit erhöhten Affinitäten und verbesserten pharmakokinetischen Eigenschaften zu entwickeln.

# I. INTRODUCTION

## 1. Background

### 1.1. Chemokines and chemokine receptors

Comparable to surface adhesion molecules, chemokines are small secreted proteins that guide the migration of distinct cells to sites of their specific niches <sup>1</sup>. To date, 44 chemokines and 21 chemokine receptors have been described, with numerous receptors having more than only one endogenous chemokine <sup>2-4</sup>. The chemokine superfamily is separated into four branches, based on the number and spacing of their conserved cysteines: 2 Cys residues may be adjacent (the CC family); separated by an intervening residue (the CXC family); have only one of the first two Cys residues (C chemokines); or contain both cysteines, separated by three intervening residues (CX3C chemokines) <sup>2, 4, 5</sup>. Chemokines mediate their functions by binding to chemokine receptors often in a highly promiscuous way <sup>2, 6</sup>.

The corresponding receptors belong to the family of G-protein-coupled receptors (GPCRs or seven-transmembrane domain receptors) and are designated CXCR1 through CXCR7, CCR1 through CCR11, XCR1, and CX3CR1, based on their specific preference for certain chemokines <sup>2, 5</sup>. The interactions between such receptors and their respective chemokines coordinate the trafficking and recruitment of cells to various tissues. The dissemination of lymphocytes between blood and secondary lymphoid tissues, for example, is supposed to be a highly regulated process, which is governed by tissue-specific expression of chemokines <sup>5</sup>. Hence, in a process called “rolling”, circulating blood lymphocytes interact temporary and reversibly with vascular endothelium through adhesion molecules (selectins, integrins). An elevated concentration of chemokines on the luminal endothelial surface can activate chemokine receptors on the rolling cells, which triggers integrin activation <sup>7</sup>. Integrin activation in turn results in the trans-endothelial migration into tissues where again, chemokine concentration gradients direct the localization and retention of the respective cells <sup>5</sup>. This “homing” mechanism is an essential processes for the development of the hematopoietic, cardiovascular and nervous systems during embryogenesis, but also for organization and function of the immune system, and tissue



## INTRODUCTION

replacement <sup>1, 7-10</sup>. There is growing evidence that these physiologic mechanisms of tissue-specific recruitment are functional in neoplastic cells <sup>5, 6, 11-14</sup> and in the process of metastatic spread <sup>8, 15</sup>.

### 1.2. Stromal cell-derived factor-1 (SDF-1/CXCL12) and its receptor CXCR4

Stromal cell-derived factor-1 (SDF-1) was initially described as a pre-B-cell growth stimulating factor (PBSF) secreted by a stromal cell line <sup>16</sup>. At the same time, the function of CXCR4 as a co-receptor for the entry of T-tropic (X4) human immunodeficiency virus into CD4<sup>+</sup> T cells was discovered and ignited a broad research effort to elucidate the function of this receptor-ligand pair <sup>17-19</sup>. The activation of CXCR4 through binding of SDF-1, which is now referred to as CXCL12 <sup>20</sup>, activates the downstream protein kinase B (AKT)/mitogen-activated protein kinases (MAPK) signaling pathway, which leads to the alteration of gene expression, actin polymerization, cell skeleton rearrangement and cell migration. The physiological functions of the CXCL12/CXCR4 axis play a pivotal role in embryogenesis by regulation of embryonic stem cell migration and positioning, immune response by leucocyte trafficking to sites of inflammation, hematopoiesis through the homing of hematopoietic stem/progenitor cells to the bone marrow, brain development and neo-angiogenesis <sup>8, 17, 21-23</sup>. Not surprisingly, genetic defects displayed in *Cxcl12* and *Cxcr4* gene-deleted mice exhibit identical, lethal phenotypes with severely impaired hematopoiesis and CNS development <sup>24</sup>, indicating a monogamous relation between this chemokine and its receptor <sup>5</sup>.

Not until 2005, the concept of a monogamous relation between CXCL12 and CXCR4 was challenged after another receptor, also known as orphan receptor RDC-1 (CXCR7 or ACKR3), was shown to bind and internalize CXCL12 on T lymphocytes <sup>10</sup>. Additionally, it was noticed that murine fetal liver cells from CXCR4 knockout mice still bind radio-labeled CXCL12 <sup>25</sup>. Elevated expression of CXCR7 has been found in T lymphocytes and during B cell development and differentiation <sup>10, 19</sup>. Furthermore, CXCR7 is involved in the differentiation of B cells into plasma cells, which are competent to become antibody secreting cells <sup>26-28</sup>.

## INTRODUCTION

### 1.3. The role of CXCR4/CXCL12 signaling in cancer

The pivotal role of CXCR4 and its chemokine CXCL12 was first demonstrated with the discovery of its involvement in B-cell trafficking and tissue localization in chronic leukemia patients <sup>29</sup> as well as in the regulation of organ specific metastasis in different breast cancer models <sup>15</sup>. Based on the similarities of tumor cell migration and metastasis with leukocyte trafficking (“rolling” and “homing”, as described before) <sup>6, 22</sup>, the crucial involvement of CXCR4 and CXCL12 could be proven. A significant overexpression of CXCR4 – relative to normal breast tissue – by human breast cancer cell lines and primary and metastatic breast tumors was demonstrated <sup>15</sup>. Today, elevated CXCR4 expression is known in more than 20 human tumor types, including hematopoietic malignancies, brain neoplasm, gastrointestinal cancer and other cancer types (see Table 1). In general, CXCR4 overexpressing cancer cells are thought to exploit the CXCR4/CXCL12 axis for tumor cell survival and the development of distant organ metastasis <sup>15</sup>. The regulation of primary tumor growth and the mechanism of metastatic spread are depicted in Figure 1. Tumor associated stromal cells constitutively express CXCL12 which stimulates the proliferation and survival of CXCR4-positive tumor cells (paracrine signaling) <sup>30, 31</sup>. CXCR4-expressing bone marrow derived progenitor cells are thus recruited by the tumor, where they contribute to the process of vascularization by supporting newly formed blood vessels and by the release of other proangiogenic factors <sup>32</sup>. Moreover, malignant primary cancer cells invade their underlying extracellular matrix and subsequently circulate in the blood and lymphatic system, where they migrate along the CXCL12 gradient to distant organs showing peak levels of CXCL12 expression (see Figure 1, **B**).

## INTRODUCTION

**Table 1.** Overexpression of CXCR4 in different types of malignancies based on literature from <sup>5, 8, 15, 33</sup>

Hematopoietic malignancies	
B-cell chronic lymphocytic leukemia (CLL) <sup>29</sup>	
multiple myeloma <sup>34</sup>	
lymphoma (B-cell, T-cell and non-Hodgkin NHL) <sup>29, 35</sup>	
acute lymphoblastic leukemia (ALL) <sup>36</sup>	
acute myelogenous leukemia (AML) <sup>37</sup>	
Brain neoplasms	Gastrointestinal cancer
glioma <sup>38, 39</sup>	colorectal cancer <sup>43</sup>
neuroblastoma <sup>40</sup>	pancreatic cancer <sup>44</sup>
glioblastoma <sup>41</sup>	hepatocellular carci-noma (HCC) <sup>45</sup>
medulloblastoma <sup>42</sup>	gastric and stomach cancer <sup>46</sup>
	esophageal carcinoma <sup>47</sup>
Adrenal cancer	
	small-cell lung cancer <sup>53</sup>
breast cancer <sup>15</sup>	non-small-cell
ovarian cancer <sup>48</sup>	lung cancer <sup>53</sup>
prostate cancer <sup>49</sup>	nasopharyngeal carcinoma (NPC) <sup>54</sup>
renal cell carcinoma <sup>50</sup>	soft tissue sarcoma <sup>33</sup>
thyroid carcinoma <sup>51</sup>	melanoma <sup>55</sup>
chondrosarcoma <sup>52</sup>	

Consequently, organs and tissues, such as brain, bone marrow, lungs and liver that exhibit high expression levels of CXCL12 are common sites of metastasis <sup>15, 33, 56, 57</sup>. Supporting this hypothesis, the inhibition of the CXCR4/CXCL12 signaling axis by CXCR4 antagonists was

## INTRODUCTION

shown to result in reduced metastatic spread in many mouse models of CXCR4<sup>+</sup> cancer types <sup>15</sup>,

58.

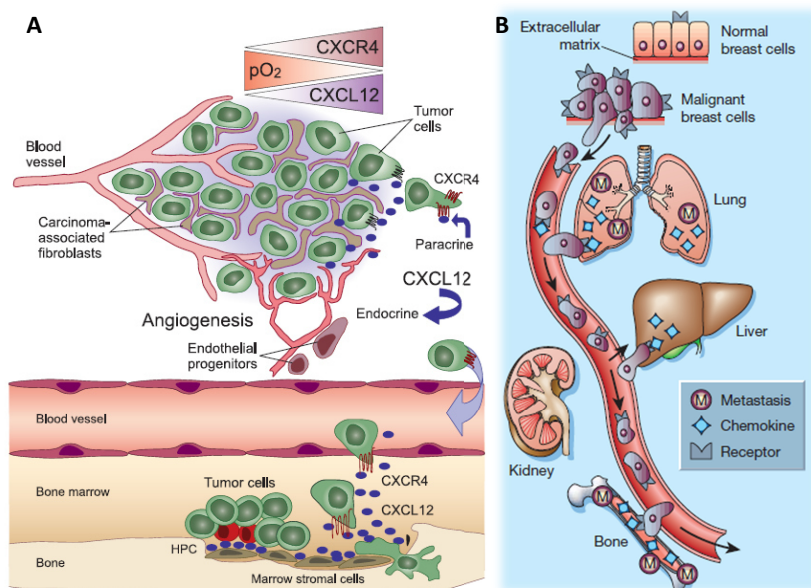


**Figure 1.** Involvement of the CXCR4 and CXCL12, in the tumor microenvironment and in the development of organ targeted metastasis. A) Within hypoxic areas of tumors, both CXCL12 and CXCR4 expression on tumor cells increases. Expression of CXCL12 promotes tumor cell growth and recruits circulating endothelial progenitors, which allow for tumor angiogenesis<sup>5</sup>. B) CXCL12 is released only by certain organs (bone marrow, liver and lung) or under certain physiological conditions (tissue damage, hypoxia etc.). CXCR4 expressing cells, such as stem cells or cancer cells are recruited by these sites and leave the circulation for differentiation or for the formation of metastasis (misuse of the physiological CXCR4/CXCL12 based stem cell axis) <sup>59</sup>.

In addition to the site specific development of metastasis, the mechanism of CXCR4 activation also involves circulating tumor cells that “hijack” the CXCR4-CXCL12 axis for homing to microenvironments that normally are restricted to hematopoietic progenitor cells (HPCs). More precisely, tumor cells utilize CXCR4 to access the CXCL12-rich bone marrow microenvironment that favors their growth and survival<sup>60</sup>.

The CXCR4/CXCL12 axis also contributes to the notion, that tumors are no insular masses of proliferating cancer cells, but complex tissues composed of multiple distinct cell types that

## INTRODUCTION

participate in heterotypic interactions with one another and establish a “tumor micro-environment” which contributes to tumorigenesis, see Figure 1, **A**<sup>61</sup>. Therefore, several factors account for the upregulation of CXCR4 in malignant cells. Most importantly, the hypoxia-inducible factor 1 (HIF-1)<sup>9, 62</sup> leads to upregulation of both CXCR4 and CXCL12 expression, but also growth factors such as vascular endothelial growth factor (VEGF)<sup>63</sup>, epidermal growth factor (EGF)<sup>64</sup> and many more.

It was shown, that CXCL12 gene expression is regulated by HIF-1 in endothelial cells, resulting in an upregulated CXCL12 expression in ischemic tissue and consequently increased adhesion, migration and homing of circulating CXCR4-positive progenitor cells to ischemic tissue<sup>9</sup>. Since neoplastic states are often characterized by profound hypoxia, studies indicate, that stem and progenitor cells together with cancer cells share the CXCR4/CXCL12 axis for selective tissue homing and therefore, contribute to tumor-tissue regeneration and tumor growth<sup>15, 65</sup>. On the other hand, CXCR4-positive cancer cells can be recruited to CXCL12-rich mesenchymal stroma niches. This recruitment mimics the “homing” of normal stem cells to the bone marrow<sup>8, 66, 67</sup>, in which they reside in a microenvironment that protects them in a CXCR4-dependent manner (e.g. from chemotherapy)<sup>58, 67</sup>. This indicates that CXCR4/CXCL12 signaling events present in the bone marrow niche can, directly or indirectly, contribute to resistance to chemotherapy in leukemia<sup>68</sup> and solid tumors<sup>8, 69</sup>.

In summary, the CXCR4/CXCL12 axis is involved in proliferation, migration and invasion of cancer cells in addition to angiogenesis of tumor tissue<sup>19</sup>. Even in regards to therapeutic resistance, the CXCR4/CXCL12 axis directly promotes cancer cell survival or homing in a pro-survival microenvironment<sup>8</sup>. Therefore, CXCR4/CXCL12 axis signaling plays a key role in tumor development and metastatic spread towards CXCL12-rich tissues (liver, lung, bone marrow, lymph nodes) and became an important target for conventional therapy as well as nuclear medicine applications<sup>70</sup>. The expression of CXCR4 has been identified as an independent biomarker of poor prognosis in several types of cancer<sup>71</sup>. Quantifying CXCR4 expression non-invasively might aid in prognostication (potential of metastatic spread) and patient stratification

## INTRODUCTION

as a mean for personalized therapy and post treatment monitoring. This could improve therapeutic outcome and reduce unnecessary toxicities <sup>72</sup>.

In some tumor cell types however, co-expression of CXCR4 and CXCR7 was identified. For example, CXCR7, but not CXCR4, is expressed by human glioblastoma cell lines, small cell lung cancer cell lines transcribe CXCR4, but not CXCR7, and mixed expression of both receptors occurs in some carcinoma cell lines as well <sup>19, 73</sup>. Therefore, the CXCR4/CXCR7 co-expression further complicates the CXCL12 mediated signaling pathway. For a long time, CXCR7 was thought to function as a scavenger receptor for CXCL12 in terms of down-tuning classical CXCL12/CXCR4 signaling, since it exhibits an almost 10 fold higher affinity for CXCL12 compared to CXCR4 <sup>10, 74</sup>. This assignment does not display the entire role of CXCR7 in cancer, since activation of CXCR7 was shown to prevent glioblastoma cells from apoptosis induced by cytotoxic drugs <sup>73</sup>. In human glioblastomas, for example, the majority of more differentiated glioblastoma cells exclusively express CXCR7. The co-expression of both receptors by distinct cell subpopulations cannot be excluded <sup>73</sup> and the cooperative function of CXCR4-CXCR7 expression are known to regulate a number of biological processes including migration and therapeutic homing of progenitor cells <sup>75, 76</sup>. Despite these various effects of CXCR7 expression, targeting of this receptor in different subpopulations of glioblastoma cells seems to be a promising approach for nuclear medicine. Given its extensive and complex involvement in cancer progression, the CXCR4/CXCR7–CXCL12 axis is an interesting target for future investigations.

## INTRODUCTION

### 2. Structure based development of peptide and peptidomimetic ligands for CXCR4

During the last decade, the clinical importance and the therapeutic implication of the CXCL12–CXCR4 interaction have become apparent <sup>77</sup>, resulting in an increasing interest in CXCR4-targeted, potential anti-tumor and anti-metastatic agents <sup>5, 78</sup>. The very first CXCR4 inhibitor was the small-molecule CXCR4 antagonist, AMD3100 (Plerixafor, *Mozobik®*), which was approved for clinical use in the United States and in Europe in 2008 and 2009, respectively <sup>79</sup>. Although AMD3100 was originally developed as an anti-HIV drug, it has been approved for mobilization of hematopoietic stem cells (HSCs) into the peripheral blood. Besides AMD3100, a great variety of CXCR4 antagonists have been developed, ranging from small-molecule inhibitors (AMD3100 derivatives and others) to peptide ligands (5-14 amino acids) as well as CXCL12-analogs (68 amino acids) and anti-CXCR4-antibodies <sup>80-82</sup>. Some are currently under clinical investigation for their therapeutic potential <sup>8, 74</sup>. The development of the peptide lead structures, used in this study, is described in more detail in the following section.

#### 2.1 Structure of CXCR4

The structure of CXCR4 is encoded on chromosome 2 (q21) and consists of 352 amino acid residues comprising an *N*-terminal domain, seven-trans membrane (TM) domains (I - VII), three extra-cellular loops (ECL), three intra-cellular loops and a *C*-terminal domain (Figure 2) <sup>83</sup>. Compared to other G protein-coupled receptors (GPCR), the binding cavity of CXCR4 is larger, more accessible and located closer to the extracellular surface <sup>83</sup>. The extracellular surface exhibits mostly negative residues, which may be important for the initial interaction of potential ligands with the receptor surface (see coloring of electrostatic potential, Figure 2).

## INTRODUCTION

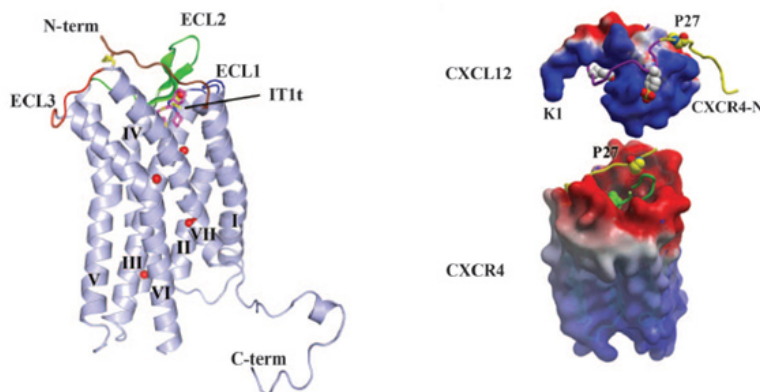


**Figure 2.** Structure of CXCR4 and electrostatic surface area representation of CXCR4 and CXCL12. **Left)** Crystal structure of CXCR4 co-crystallized with small molecule inhibitor IT1t (magenta, PDB: 3ODU). **Right)** Surface representation of CXCR4 and CXCL12, colored according to the electrostatic potential from red (negative) to blue (positive). The CVX15 peptide (green ribbon) illustrates the binding site for peptide ligands <sup>83</sup>.

The complimentary charged surface of CXCL12 strengthens this hypothesis. Crump *et al* proposed a two-site theory for the binding of the endogenous ligand CXCL12 with CXCR4 <sup>84</sup>. First, the RFFESH loop (site 1, purple circle, see Figure 3) of CXCL12 interacts with the *N*-terminal domain of CXCR4; then the *N*-terminal region (site 2, KPVSLSYR, blue circle, see Figure 3) binds to the receptor groove comprising the TM helices and the extra-cellular loops. The binding of CXCL12 triggers rapid internalization and various downstream signaling pathways that result in a plethora of responses, such as increase in intracellular calcium level, gene transcription, chemotaxis, cell survival, and proliferation <sup>33</sup>.

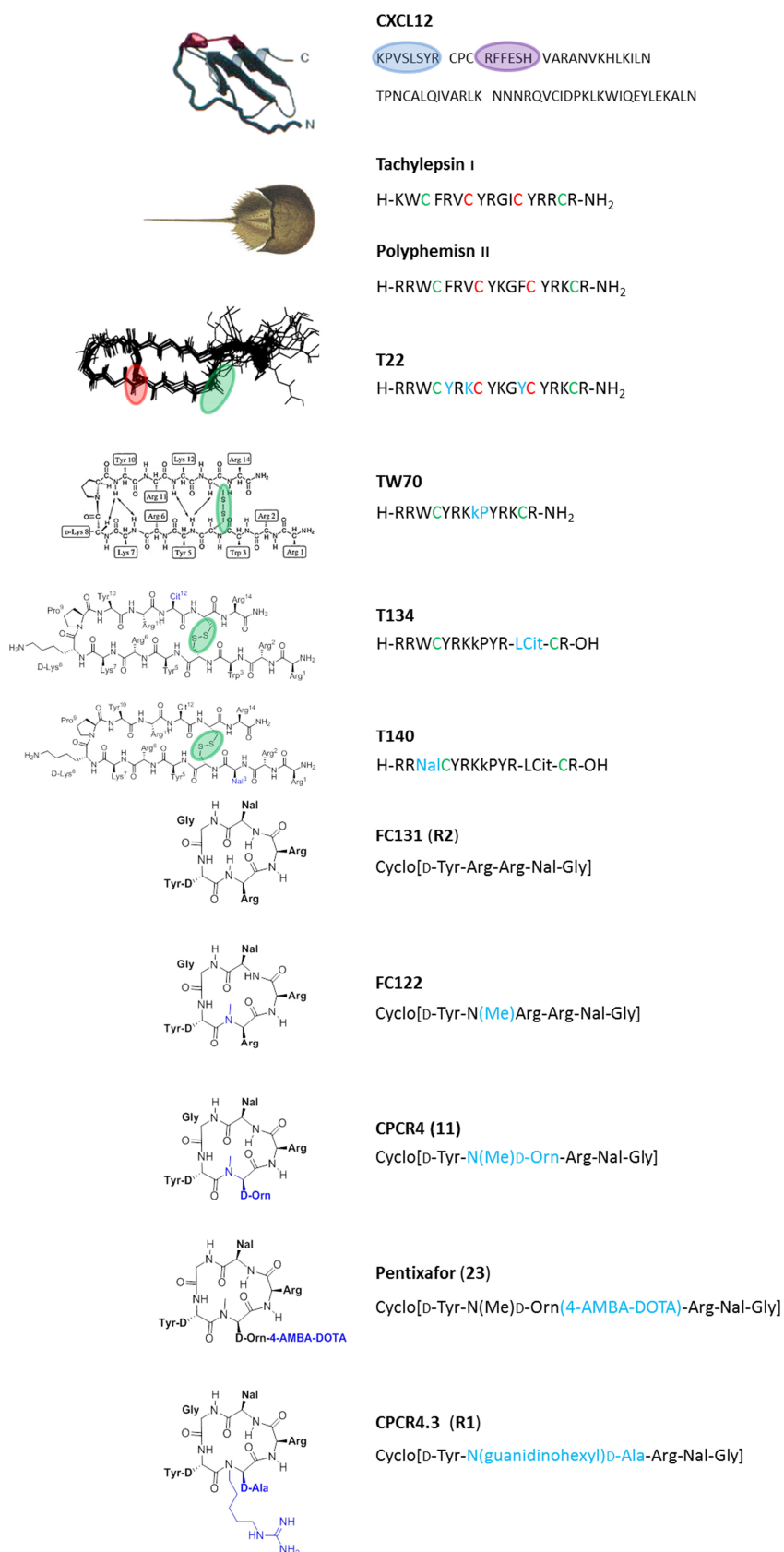
### 2.2. CXCR4 ligand development: A downsizing process

Figure 3 illustrates the ligand development of CXCR4 binding peptide antagonists starting from the identification of antimicrobial peptides down to the development of small cyclic pentapeptides, which are employed as lead structures in this study. Tachyplesin I and II and polyphemusin I and II were isolated from the hemocytes of horseshoe crabs (*Tachypleus tridentatus* and *Limulus polyphemus*) due to their potent anti-HIV properties.



## INTRODUCTION

### *A downsizing process*



**Figure 3.** Peptide and peptido-mimetic ligands for CXCR4. The amino acid sequence of CXCL12 (68 AS) is included with the two binding sites for CXCR4 labeled with purple (site 1) and blue (site 2) circles. Cysteines involved in disulfide bridges are labeled green and red, respectively. Structural modifications in the course of ligand development are indicated with blue color <sup>84-92</sup>.

## INTRODUCTION

These peptides contain two disulfide bridges (colored red and green, Figure 3), which stabilize the antiparallel  $\beta$ -sheet structure connected by a  $\beta$ -turn. Structure-activity relation (SAR) studies on the basis of these highly potent peptides resulted in the identification of T22 (substitution of two phenylalanine with tyrosine, and valine with lysine, starting from *polyphemism II*, respectively)<sup>86</sup>, which retained the anti-parallel  $\beta$ -sheet structure similar to that of *tachyplesin I*. Importantly, the two disulfide bridges and two repeated Tyr-Arg-Lys (Y-R-K) motifs were shown to be indispensable to the anti-HIV activity of T22. With focus on molecular size reduction (T22 contains 18 AS), the outer disulfide bond (indicated in green, Figure 3) of T22, together with the two crucial Tyr-Arg-Lys (Y-R-K) sequences were retained in the novel peptide structures. In addition, turn-stabilizing motifs (D-Lys-Pro or Pro-D-Lys, indicated in blue, TW70) were introduced to the peptide sequence, resulting in the first, potent 14-residue CXCR4 antagonist TW70. TW70 maintains an antiparallel  $\beta$ -sheet structure even though it has only one stabilizing disulfide bridge<sup>87</sup>.

Further derivatization of TW70 was performed with the focus on decreasing cytotoxicity, which was believed to result from the high number of basic amino acid residues. Subsequent substitution of Arg- and Lys- residues with glutamic acid and citrulline (Cit) was conducted. Consequently, T134 (substitution of lysine with L-Cit) and T140 (additional substitution of Trp with L-3-(2-naphthyl)alanine (Nal)) exhibited the highest CXCR4 binding affinities measured so far. Several different SAR studies, including an alanine scanning experiment of T140, revealed the pivotal role of Arg<sup>2</sup>, Nal<sup>3</sup>, Tyr<sup>5</sup> and Arg<sup>14</sup> for the inhibitory activity against binding of CXCL12 to CXCR4. Subsequent approaches to decrease cytotoxicity and to increase biological stability were achieved by amidation of the C-terminus and substitution of Arg with L-Cit, which resulted in TN14003 ([Cit<sup>6</sup>]-T140 with a C-terminal amide). Due to the superior stability of TN14003 in human serum, a functional group was introduced to further exploit the optimized peptide. Hence, a 4-fluorobenzoyl group constituted a novel pharmacophore for T140-based CXCR4 antagonists, providing the most potent antagonist, TF14016 (4-fluorobenzoyl-TN14003, see Figure 7), with subnanomolar binding affinity<sup>93</sup>. This peptide CXCR4 antagonist was

## INTRODUCTION

further employed for  $^{18}\text{F}$ -or  $^{68}\text{Ga}$ -based positron emission tomography (PET) imaging of CXCR4 expression *in vivo*, as discussed later <sup>94-96</sup>.

The crystal structure of a T140 peptide analogue, CVX15 clearly supported the key role of residues Arg<sup>2</sup>, Nal<sup>3</sup>, Tyr<sup>5</sup> and Arg<sup>14</sup> as determined by SAR studies so far. These key residues were employed in the following molecular-size reduction approach, wherein the four amino acids were connected with a glycine linker, resulting in a cyclic pentapeptide (FC131 (**R2**), see Figure 3) which is equipotent to T140. The indispensable functional groups of the side chains of FC131 (**R2**) were illustrated in further SAR studies including alanine scanning, *N*-methyl amino acid scanning, optimization of amino acids and design of retro-inverso sequence peptides, which all failed to improve the binding affinity of FC131 <sup>97-99</sup>. A further increase of binding affinity was only accomplished by *N*-methylation of Arg<sup>2</sup> in FC131 (**R2**) (FC122, see Figure 3), which resulted in an alternative binding mode with a flipped D-Tyr<sup>1</sup>-N(Me)Arg<sup>2</sup> peptide bond in FC122 <sup>100, 101</sup>. Within the scope of the development of molecular imaging probes for CXCR4, the *N*-methylation approach was also employed to enhance binding affinity, while all side chains of FC131 were tested for their feasibility of exchange. The substitution of Arg<sup>2</sup> with D-Ornithine and subsequent *N*-methylation of D-Orn<sup>2</sup>, yielded in CPCR4 (cyclo[D-Tyr<sup>1</sup>-N(Me)D-Orn<sup>2</sup>-Arg<sup>3</sup>-Nal<sup>4</sup>-Gly<sup>5</sup>], (**11**), see Figure 3), which exhibits high binding affinity towards CXCR4 and in addition comprises an anchor point for further modification <sup>102</sup>. Attempts to modify other side chains of FC131 resulted in a total loss of activity, however N(Me)D-Orn has been found to be a valuable attachment site for a variety of linking substituents. As expected from the massive affinity losses of residue modification in the binding scaffold of FC131, the introduction of acyl or alkyl substituents on Orn<sup>2</sup> of CPCR4 (**11**) reduced the binding affinity again, but unexpectedly, the attachment of a benzoic acids on Orn<sup>2</sup> retained most of the CXCR4 binding affinity. In a subsequent optimization step including more than 25 compounds, 1,4,7,10-tetraazacyclododecane-1,4,7,10-tetraacetic acid (DOTA) was introduced into the molecule with an optimized linking unit to yield Pentixafor (**23**, see Figure 3) as the first high affinity PET tracer for CXCR4 <sup>90, 91, 103</sup>.

## INTRODUCTION

Starting from CPCR4 (**11**) an alternative approach was initiated to further optimize the interaction of the cyclic pentapeptide ligands with the residues of CXCR4 in the binding cavity. NMR studies revealed, that FC122 ([N(Me)-Arg<sup>2</sup>]-FC131) despite its high affinity, exhibits two conformations in slow equilibrium, wherein only one was assumed to be the bioactive conformation<sup>100</sup>. In order to enhance stiffness of the cyclic peptides, the side chain of Orn<sup>2</sup> in CPCR4 (**11**) was shifted from the  $\alpha$ -carbon to the adjacent nitrogen atom assuming that the peptide bond (cis-trans) would be frozen in its *trans* conformation. The resulting peptoid compound CPCR4.3 (**R1**) exhibited a 10-fold higher affinity compared to FC131<sup>89</sup>. The binding scaffolds of **R1** and CPCR4 (**11**) were utilized in the present work for the development of high affinity molecular imaging and endoradiotherapeutic probes targeting CXCR4. Therefore, information about the binding mode of the lead compounds can be utilized to find possible attachment sites for radiolabeling moieties.

### 2.3. Binding mode of cyclic pentapeptides

An exact binding mode of FC131 (**R2**), CPCR4.3 (**R1**) or CPCR4 (**11**) is not known due to the lack of crystal structures.

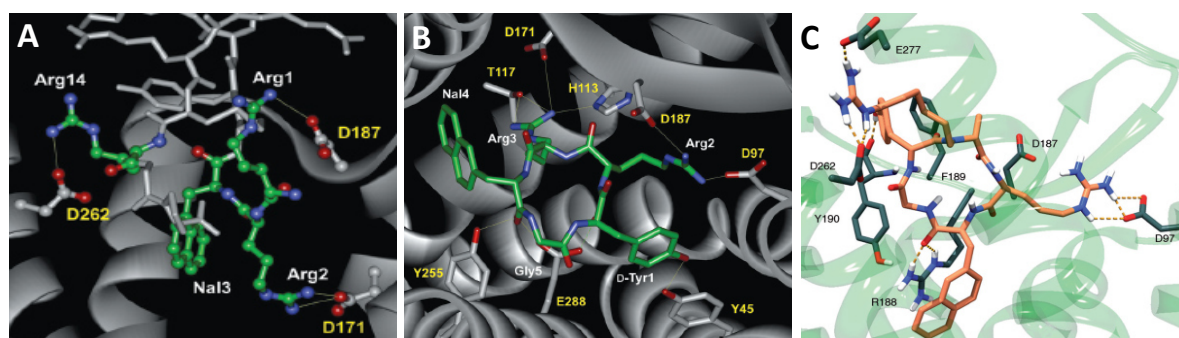


**Figure 4.** Charge interactions in the crystal structure of CXCR4 in complex with the peptide CVX15 (**A**) (PDB code: 3OE0). Calculated binding mode of FC131 (**R2**), depicted in (**B**) and of the peptidomimetic ligand CPCR4.3 (**R1**) (depicted in (**C**)) in CXCR4 using PDB code: 3OE0 and the software glide. Residues of the CXCR4 binding cavity, which are involved in ligand binding are highlighted in gray and green, respectively<sup>85, 89</sup>.

## INTRODUCTION

However, binding models were derived from the crystal structure of CXCR4 complexed with the T140 analog CVX15 (protein data bank (PDB) code: 3OE0)<sup>83</sup> in combination with molecular modeling and SAR studies. Both the crystal structure of the CVX15-CXCR4 complex and the binding models for T140 to CXCR4 revealed binding of the *N*- and *C*-terminus of the ligands into the cavity of the seven transmembrane helices of CXCR4. In the case of CVX15, Arg<sup>1</sup>, Arg<sup>2</sup>, Lys<sup>7</sup> and Arg<sup>14</sup> are the key residues to form salt bridges with the receptor residues, see Figure 4. These core-specific interactions are formed by Arg<sup>1</sup> and Asp187, and Arg<sup>2</sup> which interacts with Thr117 and Asp171. Arg<sup>14</sup> establishes a salt bridge with Asp262 in addition to an intramolecular hydrogen bond with the Tyr<sup>5</sup> side chain, which in turn makes hydrophobic contacts with helix V side chains. Finally, the bulky naphthalene ring of Nal<sup>3</sup> is anchored in a hydrophobic region bordered by helix V<sup>83</sup>. A detailed modeling study of FC131 suggested that FC131 (**R2**) binds in the major binding pocket of CXCR4 (see Figure 4 and 5) in consistence with CVX15 and T140. Arg<sup>1</sup> of FC131 forms charge-charge interactions with Asp187 in ECL-2, while Arg<sup>2</sup> interacts with His113 and Asp171 in TM-3. The aromatic 2-Nal<sup>3</sup> side chain is positioned in a tight hydrophobic pocket facing TM-5, and sandwiched between Arg188 (cation- $\pi$  interactions) and His203 ( $\pi$ - $\pi$  interactions). D-Tyr<sup>5</sup> points to the extracellular side of CXCR4 (see Figure 4). Furthermore, the backbone of FC131 interacts with the chemokine receptor-conserved Glu288 *via* two water molecules. The side chain of Arg<sup>1</sup> is exposed to the extracellular environment to some extent (see Figure 5 **B**), and thus, does not have important interactions with CXCR4. This finding was corroborated by an alanine scan, where Arg<sup>1</sup> substitution decreased the CXCR4 affinity with only a factor of 16. Ala-substitution of Nal<sup>3</sup>, D-Tyr<sup>5</sup> and Arg<sup>2</sup> however, completely diminished the affinity and alanine substitution of Gly<sup>4</sup> decreased the affinity with a factor of 43. Consequently, Gly<sup>4</sup> and Arg<sup>1</sup> appear to be the preferred attachment points for structural modifications<sup>83, 102, 104</sup>.

## INTRODUCTION

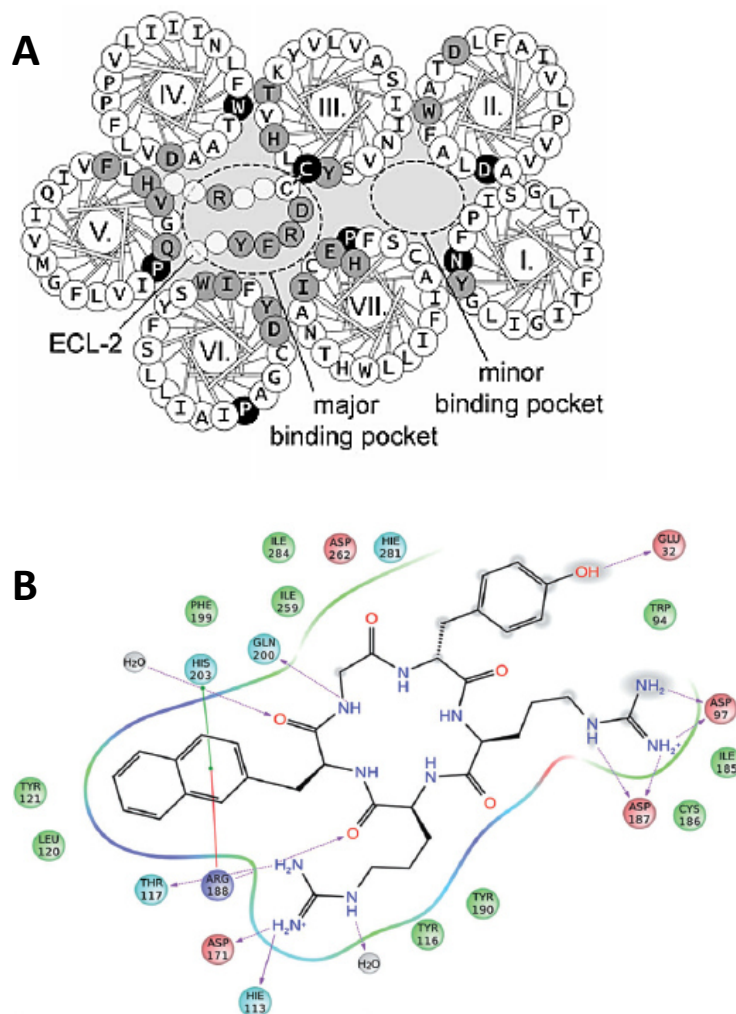


**Figure 5.** A) Helical wheel diagram of CXCR4 as seen from the extracellular side showing the upper halves of the TMs and parts of ECL-2. Residues on gray background were mutated during a site-directed mutagenesis study to determine crucial residues for FC131 interaction with CXCR4. B) Two-dimensional representation of FC131-binding to CXCR4. Residue colors: red, negative; purple, positive; cyan, polar; green, hydrophobic. Interactions: pink full and stippled arrows, H-bond with main and side chain respectively; green line,  $\pi$ - $\pi$  stacking; red line, cation- $\pi$  interaction; gray cloud, solvent-exposed atom <sup>104</sup>.

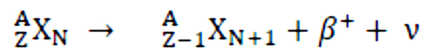
Molecular docking studies based on the crystal structure of CVX15 (PDB: 3OE0) supported a very similar binding mode of CPCR4.3 (**R1**) in the major binding pocket of CXCR4. Importantly, the *N*-alkylshift of the functional group of Orn<sup>1</sup> in CPCR4 (see Figure 3) towards the adjacent *N*-alkylated Ala<sup>1</sup> resulted in an additional strong ionic interaction of the terminal guanidine group and Asp262 and Glu277 (Figure 4). This enhanced interaction induced an

## INTRODUCTION

almost 10-fold higher affinity of **R1** in comparison to FC131 (**R2**). Furthermore, the hydrogen bonding and electrostatic interactions are also established by Arg<sup>2</sup> (not Arg<sup>1</sup> compared with FC131), which makes polar contacts with Asp97 and Asp187. NaI<sup>3</sup> is embedded in the inner portion of the receptor, establishing a well-oriented cation- $\pi$  interaction with Arg188, just like it was proposed for FC131 (Figure 4 B,C) <sup>89</sup>. Again, Gly<sup>4</sup> appeared to be the preferred attachment point for structural modifications based on the modeling data.

### 3. PET imaging of CXCR4 expression

*Positron emission tomography* (PET) utilizes the decay of positron-emitting radionuclides in which a proton in the nucleus is transformed into a neutron, a positon ( $\beta^+$ ) and a neutrino ( $\nu$ ).



After ejection from the nucleus, the positron loses its kinetic energy through interaction (collision, ionization or electronic interaction) with atoms of the surrounding matter and comes to rest, usually within a few millimeters of the site of its origin in body tissues (depending on the energy of the ejected positron and the type of surrounding matter). The positron and an ordinary electron temporary form a “pseudo-atom” called *positronium*, which has a mean lifetime of 125 picoseconds and is converted according to the mass-energy equivalence ( $E = (m_+ + m_e) \cdot c^2$ ) into two 511 keV annihilation photons ( $\gamma$ -photons) that are emitted in mutually opposite directions, see Figure 6 <sup>105</sup>. A selection of positron emitting radioisotopes used in nuclear medicine, their half-lives and maximal positron-energies is depicted in Table 2.

Near-simultaneous detection of the two annihilation photons allows PET to localize the origin of positron-emitters along a line between the detectors (Fig. 6). This mechanism is called

## INTRODUCTION

*annihilation coincidence detection* (ACD) and is usually measured within a timing window of 6 - 12 nanoseconds and an energy window of 300 – 650 keV. By incorporation of multiple opposing detectors in a complete ring around the patient, data for multiple projection angles can be acquired simultaneously. However, the quality of an image produced by PET is degraded by several physical factors like detector sensitivity differences, random coincidences or scattering.

**Table 2.** Physical properties of selected PET isotopes (positron emitters) <sup>106</sup>.

radioisotope	half-life ( $t_{1/2}$ )	maximum $\beta^+$ - energy (abundance)
<sup>11</sup> C	20.4 min	1.0 MeV (99.8%)
<sup>13</sup> N	10.0 min	1.2 MeV (100%)
<sup>15</sup> O	2.0 min	1.7 MeV (99.8%)
<sup>18</sup> F	109.7 min	0.6 MeV (96.9%)
<sup>64</sup> Cu	12.7 h	0.7 MeV (19.3%)
<sup>68</sup> Ga	67.6 min	1.9 MeV (90%)
<sup>89</sup> Zr	78.4 h	0.9 MeV (22.7%)
<sup>124</sup> I	4.2 d	2.1 MeV (25%)

Therefore flat, ring-shaped lead or tungsten septa are used, not only to reduce the number of scattered events collected, but to minimize other effects of radiation originating outside the field of view <sup>107</sup>.

To further optimize the PET signal, corrections for attenuation, dead-time and pile-up events need to be applied to the projections prior to reconstruction. Finally, algorithms for reconstructing PET images such as filtered back projection (FBP) and ordered subsets expectation maximization (OSEM) are used to process the raw data (sinograms) <sup>108</sup>. The images that result from PET provide quantitative information about the voxel intensity and the amount of radioactivity in a voxel. Calibration factors must be determined to translate the corrected counts to radioactivity values (kBq/cm<sup>3</sup>) <sup>105</sup>. The signal in a region of interest (ROI) can then be



## INTRODUCTION

described as % injected dose per mL (% ID/mL), activity per volume (Bq/cm<sup>3</sup>), or as standardized uptake value (SUV), which is defined as the *activity concentration in the volume of interest [kBq/mL] times the body weight [kg] divided by the injected activity [kBq]* <sup>109</sup>.

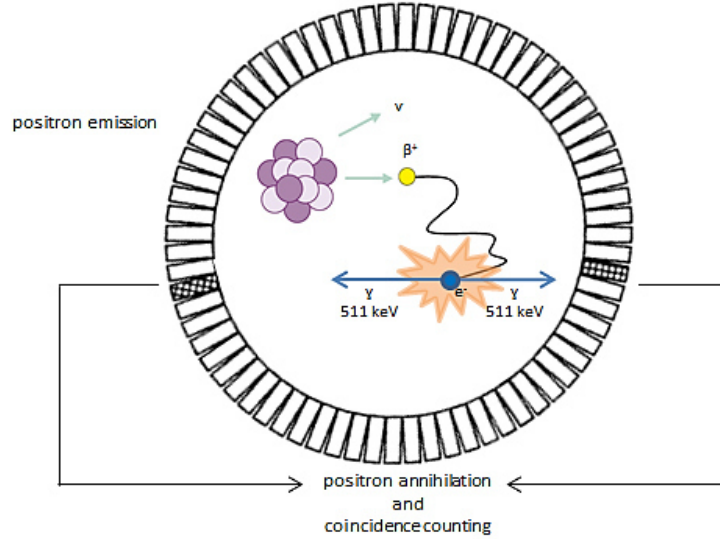


**Figure 6.** Schematic representation of a PET scanner. The radioisotope decays by  $\beta^+$ -emission. Subsequent annihilation of the formed positronium results in two 511 keV  $\gamma$ -photons, which are counted by two opposite detector units electronically connected *via* a coincidence circuit.

If signals originate from very small structures, they will have their radioactivity concentrations either overestimated or underestimated, since the activity signal (same total counts) seems to be distributed over a larger volume due to image blurring and the way of image sampling during the PET signal analysis (partial-volume effect) <sup>105, 110</sup>. In addition, the finite positron range (energy of ejected positron) and photon noncollinearity (annihilation photon are not exactly 180° apart) also contribute to the spatial resolution of the resulting PET images. The resolution of a preclinical scanner can reach up to 2.5 mm and 4 – 6 mm on whole-body PET systems, respectively <sup>105</sup>.

The *in vivo* behavior of a tracer is varying with time and depends on a number of components. Tracer delivery, extraction from the vasculature, diffusion or transport into cells, metabolism and excretion from the body (also referred to as the ADME principle in pharmacokinetics with

## INTRODUCTION

absorption, distribution, metabolism and excretion). Dynamic PET imaging allows direct measurement of the radioactivity concentration over different time frames and can therefore be employed to describe the kinetic of a radiopharmaceutical in the body <sup>105, 111</sup>. By applying ROIs on different compartments (heart for blood pool and tumor for specific binding site for example), the dynamic change of tracer concentration in these compartments can be observed and support the understanding of tracer distribution *in vivo*.

**CXCR4 ligands for PET:** As a small-molecule CXCR4 antagonist used for PET imaging of CXCR4, [<sup>64</sup>Cu]AMD3100 appeared to be fast and efficiently radiolabeled and showed rapid clearance from the blood and accumulation in CXCR4 specific tissue. However, due to high accumulation in the liver (>40% ID/g), the clinical applicability of this tracer is challenging <sup>112, 113</sup>. An optimized AMD3100 derivative, AMD3465 revealed promising target properties with very high accumulation in CXCR4<sup>+</sup> tumors (> 100% ID/g), but also significant accumulation in the liver (40% ID/g), whereas the <sup>11</sup>C-labeled analogue unfortunately exhibited low tumor-to-background ratios <sup>114, 115</sup>. Other small-molecule CXCR4 antagonist [<sup>18</sup>F]MSX-122F and [<sup>18</sup>F]M508F (see Figure 7) displayed specific binding to CXCR4 *in vitro*, but were not further evaluated <sup>116, 117</sup>.

Radiolabeled analogues of CXCL12 (<sup>125</sup>I and <sup>99m</sup>Tc) were only used for *in vivo* biodistribution, but the specificity of the signal is doubted, due to rapid enzymatic degradation <sup>118, 119</sup>. In addition <sup>125</sup>I-labeled antibodies for CXCR4 were used for *in vitro* and *in vivo* biodistribution studies, but were not able to clearly distinguish CXCR4<sup>+</sup> from CXCR4<sup>-</sup> tissue <sup>120</sup>. Very recently an <sup>89</sup>Zr-labeled human CXCR4-mAb (<sup>89</sup>Zr-CXCR4-mAb) was evaluated for detection of CXCR4 expression. *In vitro* and *in vivo* evaluation of <sup>89</sup>Zr-CXCR4-mAb showed enhanced uptake in CXCR4<sup>+</sup> xenografts.

## INTRODUCTION

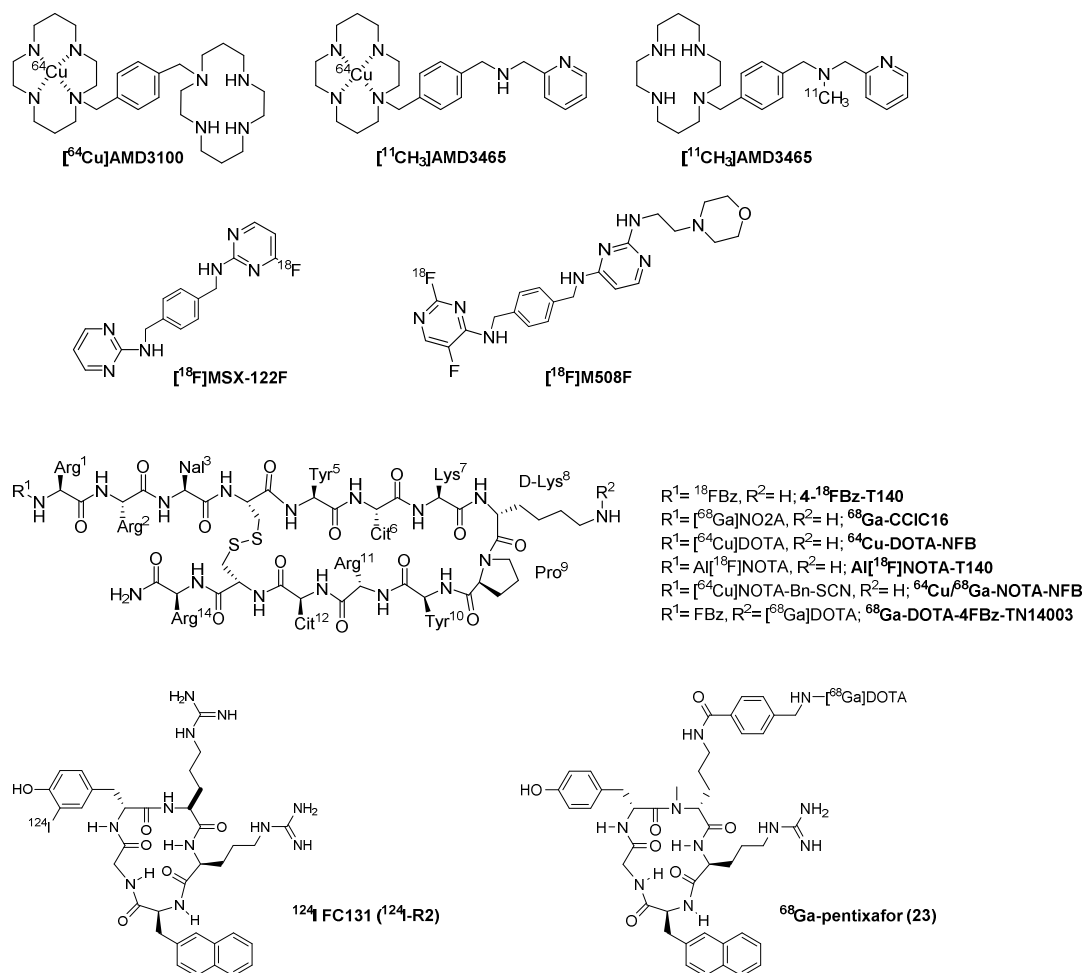


**Figure 7.** Structures of selected PET imaging agents for CXCR4 targeting.

It also demonstrated the ability to detect lymph node metastases in an experimental model of metastatic triple negative breast cancer. However, due to slow antibody clearance kinetics, late imaging time points (optimum 7 days p.i.), and thus somewhat complicated imaging protocols, the clinical applicability of  $^{89}\text{Zr}$ -CXCR4-mAb is also challenging <sup>121</sup>.

Radiolabeled derivatives of T140 (see Figure 7) were also employed for PET imaging.  $4\text{-}^{18}\text{F}$ -T140 showed low tumor-to-background ratios mostly due to enhanced binding to red blood cells and accessory elevated uptake in liver tissue <sup>96</sup>. Even though the exchange of the fluorobenzyl group with DOTA or NOTA reduced the unspecific binding to red blood cells in  $^{64}\text{Cu}$ -DOTA-NFB <sup>122</sup>,

## INTRODUCTION

$^{64}\text{Cu}$ -NOTA-NFB<sup>122</sup> and  $\text{Al}[^{18}\text{F}]\text{NOTA-T140}$ <sup>95</sup>, a significant accumulation in liver tissue remained, which resulted in low tumor-to-background ratios. First clinical application was reported for  $^{68}\text{Ga}$ -NOTA-NFB in healthy volunteers and glioma patients. Good tumor-to-background ratios and a low background uptake were reported. However,  $^{68}\text{Ga}$ -NOTA-NFB primarily accumulates in the spleen and the liver, which resulted in a slightly higher effective radiation dose compared to  $^{68}\text{Ga}$ ]Pentixafor<sup>123</sup>. The  $^{68}\text{Ga}$ -labeled T140 derivative  $^{68}\text{Ga}$ -CCIC16 demonstrated favorable pharmacokinetic properties along with CXCR4 specific accumulation (tumor-to-muscle ratio: 9.5)<sup>94</sup>.

Radioiodinated FC131 (**R2**) was the first cyclic pentapeptide based imaging agent. Unfortunately,  $^{124}\text{I}$ -FC131 is very lipophilic, which is thought to be responsible for high uptake in the liver and intestines, as lipophilic compounds are often excreted *via* the hepatobiliary route (partition coefficient  $\log P = -0.35 \pm 0.02$ , as determined in octanol/PBS)<sup>124</sup>. Intensive research and a library of peptide ligands resulted in  $^{68}\text{Ga}$ ]Pentixafor ( $^{68}\text{Ga}$ ]**23**,  $\log P = -2.90 \pm 0.08$ ), that exploits a 4-aminomethyl-benzoic acid linked hydrophilic DOTA chelator for labeling. Due to its highly specific binding to human CXCR4 and favorable pharmacokinetics,  $^{68}\text{Ga}$ ]Pentixafor is currently the only radiopharmaceutical suitable for CXCR4 imaging in patients and is assessed in a broad range of clinical proof-of-concept studies for a variety of diseases (cancer, cardiovascular diseases, stroke or inflammation)<sup>90, 91, 125-133</sup>.

## 4. CXCR4 targeted therapeutic approaches

CXCR4 antagonists are therapeutically used for stem cell mobilization alone or in combination with the granulocyte colony-stimulation factor. In addition, incorporating CXCR4-targeted therapy into cancer treatment protocols was suggested to not only increase chemosensitivity, but also prevent relapse of the disease by disruption of the interaction of residual CXCR4<sup>+</sup> cancer

## INTRODUCTION

cells with the bone marrow niche. Consequently, numerous preclinical and clinical studies currently investigate the potency of anti CXCR4 therapy <sup>8, 80, 134-137</sup>.

Endoradiotherapy is a versatile application in nuclear medicine by the specific delivery of therapeutic radionuclides to target-expressing cells. In contrast to standard therapeutic approaches, the amount of substance actually injected is significantly lower and therefore pharmacological effects are supposed to be unlikely <sup>138</sup>. The emitted particles directly affect cells in the vicinity of the targeted cell, but - depending on the energy of the emitter- can also irradiate cells within a greater radius. Hence, endoradiotherapy can also be used for treatment of tumors with heterogeneous receptor expression or with insufficient vascularization <sup>139</sup>.

**Table 3.** Physical properties of selected therapeutic radioisotopes (<sup>106, 140-142</sup>).

radio-nuclide	half-life (t <sub>1/2</sub> )	decay	average energy (keV)	Mean beta- particle range in water	γ-energy [keV]
<sup>67</sup> Cu	61.9 h	β <sup>-</sup>	141	2.9 mm	-
<sup>90</sup> Y	2.67 d	β <sup>-</sup>	935	4.0 mm	-
<sup>131</sup> I	8.0 d	β <sup>-</sup>	182	0.4 mm	364, 637, 284
<sup>161</sup> Tb	6.9 d	β <sup>-</sup>	154	0.2 mm	75
<sup>177</sup> Lu	6.7 d	β <sup>-</sup>	133	0.2 mm	113, 208
<sup>186</sup> Re	3.8 d	β <sup>-</sup>	764	3.1 mm	137
<sup>211</sup> At	7.2 h	α	6790	60 μm	687
<sup>213</sup> Bi	46 min	α	8320	84 μm	440
<sup>223</sup> Ra	11.4 d	α	6700	60 μm	269, 154, 324
<sup>111</sup> In	2.8 d	EC/Auger	0.02	> 100 nm	171, 245
<sup>125</sup> I	60.1 d	EC/Auger	0.015	> 100 nm	186

In addition to this “crossfire effect”, subsequent intracellular communication and the presence of free radicals from irradiated cells can cause cytotoxicity (radiation-induced bystander effect) in

## INTRODUCTION

the tumor lesion even outside the range of irradiation <sup>143</sup>. The effective irradiation (destruction of covalent bonds, single- and double-strand breaks within the DNA, cross-link-reactions and nucleobase modification resulting in cell death) depends on the amount of delivered energy and the characteristics of the absorbed radiation <sup>144</sup>. Only a high radiation dose (in the range of 20 – 70 Gy) induces the loss of cell vitality and long-term inability of mitosis due to chromosome aberrations <sup>145</sup>. Consequently, a detailed knowledge of the tumor volume and homogeneity is crucial for the endoradiotherapeutic efficiency. Concerning the geometrical features, radionuclides with long-range beta emission, such as <sup>90</sup>Y and <sup>188</sup>Re, are the most efficient agents for irradiation of larger tumors <sup>146</sup>. Consequently, <sup>90</sup>Y is expected to exhibit reduced efficiency and increase toxicity when targeting small metastases. A Monte Carlo simulation suggested, that <sup>177</sup>Lu irradiate smaller spheres more effectively than <sup>90</sup>Y, but with the addition, that <sup>161</sup>Tb outperform <sup>177</sup>Lu in very small metastases (< 100  $\mu$ m) mostly due to its large number of Auger electrons, which are in the low-energy domain (< 50 keV) and deposit their entire dose over short distances <sup>140</sup>. Many  $\beta$ -emitters also exhibit  $\gamma$ -emission, which generally increases the undesired whole-body radiation dose. However, <sup>177</sup>Lu possesses  $\gamma$ -emission, which has appropriate energy for whole-body distribution monitoring of the radiopharmaceutical by means of single-photon emission computed tomography (SPECT), rendering <sup>177</sup>Lu the clinical routine nuclide for ERT <sup>138</sup>. The determination of the amount and the spatial distribution of radiation dose to tissues of interest in a patient helps to calculate the patient-specific dosimetry <sup>147</sup>.

The highest linear energy transfer (LET) and accordingly a high cell damaging efficiency is feasible in alpha emitting nuclides, due to the large volume of alpha particles. Their tissue penetration is in the range of one to only a few cell diameters. Therefore, the application of alpha emitters is limited to the treatment of residual tumor margins or hematological diseases, such as leukemia <sup>138, 148</sup>. However, high target selectivity, rapid clearance from non-target organs and detailed knowledge about the fate of the daughter radionuclides is very important for the application of  $\alpha$ -emitters.

## INTRODUCTION

Auger electrons are emitted due to the rearrangement of the electron shells after electron capture or internal conversion <sup>105</sup>. Auger-electron-emitting radionuclides are known to be extremely radiotoxic and can produce extensive DNA damage. However, internalization of the radiopharmaceutical and translocation into the cell nucleus is required for the highly localized energy deposition by Auger electrons with generally very low energy (typically < 30 keV, range in the order of nanometers). Auger-electron emitters with clinical application are <sup>111</sup>In, <sup>123</sup>I, <sup>125</sup>I or <sup>99m</sup>Tc <sup>149</sup>. The radionuclide with the highest therapeutic potential of these low-energy emitters is <sup>125</sup>I with 20 electron emissions per decay in average <sup>142</sup>.

**CXCR4 targeting endoradiotherapeutic approaches:** Nuclear medicine has substantially influenced the management of patients in terms of patient stratification, peptide-receptor radionuclide therapy and therapy staging in the field of endocrine tumors <sup>150</sup>. For CXCR4 associated malignancies, targeted radionuclide therapy using anti-CD20 antibodies labeled with either <sup>131</sup>I or <sup>90</sup>Y, were successfully used to treat patients with relapsed or refractory non-Hodgkin lymphomas <sup>151, 152</sup>. Excellent preclinical results were obtained with radioimmunotherapy targeting CD38 <sup>70</sup>. Not until 2015 (within the scope of this thesis), a first-in-man endoradiotherapeutic application directly targeting CXCR4 in three heavily pretreated patients with multiple myeloma (MM) was conducted. After application of 15 and 23 GBq of [<sup>177</sup>Lu/<sup>90</sup>Y]Pentixather ([<sup>177</sup>Lu/<sup>90</sup>Y]**24**), significant reduction of metabolic activity within the lesions could be observed already within two weeks after application, therefore indicating the potential of CXCR4 targeted endoradiotherapy <sup>153, 154</sup>. Given the small number of patients and the fact, that all patients received a combination of high-dose chemotherapy, consecutive stem cell support and [<sup>177</sup>Lu/<sup>90</sup>Y]Pentixather endoradiotherapy, a clear assignment of the therapeutic effects of each individual treatment is not possible. Nevertheless, it demonstrates the general feasibility and high potential of a CXCR4-targeted endoradiotherapy approach.

## INTRODUCTION

### 5. Objectives

CXCR4 resembles a highly relevant molecular target for imaging and endoradiotherapy<sup>81, 155</sup>, due to the favorable expression profile and its high accessibility as a transmembrane receptor. Thus, several CXCR4 antagonists have already been designed and utilized in a preclinical manner. Out of this field of lead structures, cyclic peptides are known to offer excellent structural traits for the development of highly stable vectors. Based on the previous work in our group, the goal of this work was the development of novel cyclic pentapeptide CXCR4 ligands for PET imaging (labeling with <sup>68</sup>Ga, <sup>18</sup>F), fluorescence microscopy, as well as <sup>177</sup>Lu-based endoradiotherapeutic treatment of patients with CXCR4<sup>+</sup> malignancies.

In general, within the design of novel radiopharmaceuticals, properties, such as affinity, specificity, selectivity, lipophilicity, stability, and specific activity should be considered. Based on the fundamental work within our group, several cyclic pentapeptides emerged and were utilized as lead structures in this work. The first peptide scaffold (CPCR4.3 (**R1**), see Figure 3)<sup>89</sup> showed unexpectedly high affinity towards murine and human CXCR4, but lacks an attachment site for (radio)labels other than iodine isotopes. To nevertheless be able to exploit the unsurpassed CXCR4 affinity of CPCR4.3 (**R1**), an alternative concept for backbone modification of FC131-derived cyclic pentapeptides was integrated into the design of novel CPCR4.3-based analogs for molecular imaging. By combining a D-Cys<sup>2</sup> for Gly<sup>2</sup> substitution concept and the *N*-alkylation strategy employed in CPCR4.3 (**R1**), the development of novel pentapeptide-based CXCR4 radioligands with suitable characteristics for *in vivo* applications was aimed.

Driven by the success of [<sup>68</sup>Ga]Pentixafor-PET as the first radiopharmaceutical for clinical investigation of the CXCR4 receptor status in patients, the fundamental lead structure CPCR4 (**11**, Figure 3) was utilized in the development of novel CXCR4 ligands. Since Pentixafor loses its high binding affinity towards CXCR4 when labeled with <sup>177</sup>Lu or other (radio)metals<sup>91, 156</sup>, one major objective was the development of novel structural devices, which enable the complexation



## INTRODUCTION

of diagnostic and therapeutic nuclides or the introduction of other imaging moieties (such as fluorescent dyes or  $^{18}\text{F}$ -labeling prosthetic groups).

Another objective was the utilization of cyclotron produced no-carrier-added  $^{18}\text{F}$ -fluoride, which reveals the most favorable nuclide properties for PET imaging. An attempt was made to avoid conventional methods for radiofluorination, which are often based on multi-step procedures and involve prosthetic groups. Thus, a novel, fast and efficient radiolabeling procedure was integrated in high affinity peptides comprising the boron-based fluoride acceptor-motif ammonio-methyltrifluoroborate ( $\text{AmBF}_3$ )<sup>157</sup>.

Increasing evidence about the involvement of CXCR7 in the complex CXCL12/CXCR4 axis ignited the interest in the development of CXCR7 ligands, which can be utilized for PET imaging. A reported selectivity switch from CXCR4- towards CXCR7-specific ligands<sup>158</sup> served as the basis for the design of novel CXCR7 specific ligands and should pave the way for further investigations based on the results of the preliminary SAR study.

A central point within the process of ligand development was the improvement of the binding affinity towards CXCR4. Affinity determination ( $IC_{50}$ ), as well as cellular uptake and internalization kinetics assessment were performed with different cell lines to provide a solid and reproducible *in vitro* evaluation. All novel CXCR4 ligands were evaluated with respect to Pentixafor (**23**, Fig. 3) or Pentixather (**24**) for literature comparability. One very promising novel ligand was investigated in terms of agonist or antagonistic binding towards CXCR4. This was addressed during a three month stay at the Emory University Hospital of Atlanta. Further, the lipophilicity and metabolic stability was determined together with imaging and biodistribution data for the most promising candidates in tumor bearing mice.

## II. MATERIALS AND METHODS

### 1. General information

All solvents and organic chemicals were purchased from *Sigma Aldrich* (Munich, Germany) or *VWR* (Radnor, USA). Fmoc-(9-fluorenylmethoxycarbonyl-) and other protected amino acid analogues were purchased from *Iris Biotech* (Marktredwitz, Germany) or *Bachem* (Bubendorf, Switzerland). For solid-phase-peptide-synthesis (SPPS) H-D-Cys(Trt)-2CT, Cl-2CT or H-Gly-2CT resin (0.7 – 1.6 mmol/g) were used (*Iris Biotech*, Germany and *Bachem*, Switzerland). The chelators DOTA and DOTAGA were purchased from *Chematech* (Dijon, France). Solid phase peptide synthesis was carried out manually using an Intelli-Mixer syringe shaker (*Neolab*, Heidelberg, Germany). Analytical reversed-phase high performance liquid chromatography (RP-HPLC) was performed using a system from *Sykam GmbH* (Gilching, Germany) with a gradient pump S 1021, mixing chamber S 8111, controller S 2000, UV/VIS detector 200 Photometer (*LineartM Instruments Corp.*, Reno, USA) and a Nucleosil 100 C18 column (5  $\mu$ m, 125  $\times$  4 mm, *CS Chromatographie GmbH*, Langerwehe, Germany) with 1 mL/min flow rate. Pyramid software (*Waters*, Milford, USA) was used for visualization. For semi-preparative HPLC, a system from *Shimadzu Corp.* (Kyoto, Japan) with two LC-20AP gradient pumps, a CBM-20A communication module, an CTO-20A column oven, an SPD-20A UV/VIS detector and a Multospher 100 RP 18 column (5  $\mu$ m, 250  $\times$  10 mm, *CS Chromatographie GmbH*, Langerwehe, Germany) with 5 mL/min flow rate was utilized. Lab Solutions software by *Shimadzu Corp.* was used for visualization and analysis. The peptides were eluted applying different gradients of 0.1% (v/v) trifluoroacetic acid (TFA) in H<sub>2</sub>O (solvent A) and 0.1% TFA (v/v) in acetonitrile (solvent B) at a constant flow (specific gradients are cited in the text). Both retention times  $t_R$  as well as the capacity factors  $K'$  are cited in the text. Radio-HPLC of the radiolabeled ligands was carried out using a Nucleosil 100 C18 (5  $\mu$ m, 125  $\times$  4.0 mm) column. For radioactivity detection, the outlet of the UV-photometer was connected to a NaI(Tl) well-type scintillation counter from *EG&G Ortec* (Munich, Germany). Electron-spray ionization mass spectrometry (ESI-MS) was conducted on a 500-MS IT mass spectrometer by *Varian* (Agilent Technologies, Santa Clara,

## MATERIALS AND METHODS

USA) and expression LCMS mass spectrometer with electron-spray-ionization and quadrupol-analyzer (*Advion Inc.*, Ithaca, USA).

## 2. General synthesis protocols

### 2.1. Fmoc-based solid-phase peptide synthesis

**TCP-resin loading:** Following standard Fmoc strategy <sup>159</sup>, TCP-resin (1.95 mmol/g) is loaded with Fmoc-Xaa-OH (1.5 eq.) in anhydrous DCM with DIPEA (4.5 eq.) at room temperature (rt) for 2 h. The remaining tritylchloride is capped by addition of 2 mL/g methanol for 15 min. After that, the resin is filtered and thoroughly washed with DCM (2 x), with DMF (2 x) and methanol, respectively and stored under vacuum overnight. The loading is determined using the weight differences:

$$\frac{(m_{total} - m_{net\ weight}) \times 1000}{(M_{As} - M_{HCl}) \times m_{weight\ of\ resin}} = mmol/g$$

$m_{total}$ :  $\Delta$  mass of loaded resin (Fmoc-Xaa-OH and HCl);  $M_{As}$ : molar mass of amino acid

$m_{net\ weight}$ : mass of used resin;  $M_{HCl}$ : molar mass of hydrochloric acid

**TBTU/HOBt coupling:** A solution of Fmoc-Xaa-OH (2.0 eq.), TBTU (2.0 eq.), HOBt (2.0 eq.), DIPEA (5.2 eq.) in NMP (8 mL/g resin) was added to the resin-bound free amine peptide and shaken for 2 h at rt and washed with NMP (6 x 2 min).

The coupling with secondary or aromatic amines was performed employing a different protocol. 3.0 eq. of Fmoc-Xaa-OH was dissolved in DMF (8 mL/g resin) together with HATU (3.0 eq.), HOAt (3.0 eq.) and DIPEA (6.0 eq.) and stirred for 15 min. The pre-activated solution was added to the resin bound secondary peptide and shaken for 2 h at rt. After completion of the reaction, the resin was washed 6 times with NMP.

## MATERIALS AND METHODS

**On-resin Fmoc-deprotection:** The resin-bound Fmoc peptide was treated with 20% piperidine in DMF (v/v) for 5 min and a second time for 15 min. The resin was washed thoroughly with NMP (8 x 2 min).

**Dde-deprotection:** The Dde-protected peptide (1.0 eq.) was dissolved in a solution of 2% hydrazine monohydrate in DMF (v/v). After 15 min, the deprotected peptide was washed with DMF (6 x), if bound to resin, or precipitated in diethyl ether to give the crude product.

***p*-Ns protection:** A solution of 4-nitrobenzenesulfonylchloride (*p*-Ns-Cl) (4.0 eq.) and 2,3,4-collidine (10 eq.) in NMP (1 ml/g resin) was added to the resin-bound free amine peptide and shaken for 20 min at rt. The resin was washed with NMP (3 x 2 min) and with dry THF (3 x 2 min). The reaction was repeated if unprotected free amide could be detected with ESI-MS.

***N*-alkylation under Mitsunobu conditions:** The *N*-alkylation reactions were performed according to recently published protocols<sup>103</sup>. A solution of triphenylphosphine (5.0 eq.), DIAD (5.0 eq.) and MeOH or Alkyl-OH (10 eq.), respectively in dry THF (1 ml/g resin) was carefully added to the resin-bound *p*-Ns protected peptides and shaken for 10 to 15 min at rt. The resin was filtered off, washed with dry THF (3 x) and with NMP (3 x 2 min) subsequently.

**On-resin *p*-Ns deprotection.** For *p*-Ns deprotection, the resin-bound *p*-Ns-peptides were stirred in a solution of mercaptoethanol (10 eq.) and DBU (5.0 eq.) in NMP (1 ml/g resin) for 20 min. The deprotection procedure was repeated once and the resin was washed with NMP (5 x) afterwards.

### Peptide cleavage from the resin:

**A) With preservation of side chain protecting groups:** The fully protected, resin-bound peptide was dissolved in a mixture of DCM/TFE/AcOH (v/v/v; 6/3/1) and shaken for 30 min. The solution was filtered off and the resin was dissolved in another cleavage solution for another

## MATERIALS AND METHODS

30 min. The fractions were combined and the solvent was concentrated under reduced pressure. The filtrate was redissolved in toluene and concentrated under reduced pressure to remove the acetic acid. Precipitation in water resulted in the crude, side chain protected peptide.

**B) Cleavage with concurrent deprotection of all acid labile protecting groups:** The fully protected, resin bound peptide was dissolved in a mixture of TFA/TIPS/water (v/v/v; 95/2.5/2.5) and shaken for 30 min. The solution was filtered off and the resin was treated in the same way for another 30 min. Afterwards, the fractions were combined and the solvent was concentrated under a constant flow of nitrogen. The crude peptide was precipitated in diethyl ether and left to dry overnight.

**Cyclization of fully protected linear peptides:** To a 5 mM solution of crude product in dry DMF,  $\text{NaHCO}_3$  (5.0 eq.) and diphenylphosphoryl azide (DPPA; 3.0 eq.) were added at rt and the suspension was stirred for 5 h or until no linear peptide could be observed *via* ESI-MS. The solution was concentrated under reduced pressure and the peptide was precipitated in water and washed thoroughly to remove  $\text{NaHCO}_3$ .

**Iodination of tyrosine side chain:** The introduction of a iodine into the side chain of potent cyclic peptides was performed using a recently developed protocol <sup>160</sup>. Briefly, to a 9.0 mM solution of HPLC-purified peptide in MeCN/water (v/v; 1/1), 0.4 – 0.7 eq. of a 0.1 M solution of *N*-iodosuccinimide (NIS) in MeCN was added and the solution was injected into the semi-preparative HPLC immediately. The amount of *N*-iodosuccinimide added equivalents was optimized to yield a maximal ratio of mono-iodinated to di-iodinated product. The required amount varies in the range of 0.3 to 0.7 eq. according to the purity and chemical structure of the precursor and the solvents.

## MATERIALS AND METHODS

### 2.2. Condensation with chelating moieties and cold complexation

**Condensation of the peptides with the chelating moieties:** The condensation of the peptides and the respective chelators are described in several publications and summarized as follows <sup>161-163</sup>.

**DOTAGA-anhydride:** 1.0 eq. of the N-terminal deprotected peptide was dissolved together with 1.5 eq. DOTAGA-anhydride and 10.0 eq. DIPEA in dry DMF. The reaction was allowed to stir overnight and precipitated in diethyl ether or directly used for HPLC purification afterwards.

**DOTA:** DOTA condensation was performed according to a method published previously. Briefly, DOTA • 6 H<sub>2</sub>O was activated prior to the condensation reaction. Therefore, DOTA • 6 H<sub>2</sub>O (1.0 eq.) was dissolved together with NHS (1.25 eq.) and EDCI (1.25 eq.) in water and after addition of DIPEA (2.0 eq), it was allowed to activate for 15 to 30 min. The activated DOTA solution was then slowly added to the peptide (0.25 eq., dissolved in DMF and water as a function of solubility) and stirred at rt for 1 h. After completion, the crude product was purified using semi-preparative HPLC.

**Chelation of the DOTA- or DOTAGA-conjugated ligands with Lutetium, Gallium, Yttrium and Bismuth for use in *in vitro* studies:** <sup>nat</sup>Lu<sup>III</sup>-complexation. A solution of DOTA- or DOTAGA-peptide (2.0 mM in tracepure water (*Sigma Aldrich*)) was treated 1:1 (v/v) with a 20 mM solution of LuCl<sub>3</sub> (0.1 M CH<sub>3</sub>COONH<sub>4</sub>, pH = 6) and stirred for 30 min at 95 °C. After cooling to rt, the formation of the <sup>nat</sup>Lu<sup>III</sup>-chelate was confirmed using analytical HPLC and ESI-MS.

<sup>nat</sup>Ga<sup>III</sup>-complexation. For labeling with native gallium, a 2.0 mM solution of DOTA-peptide was treated 1:1 (v/v) with a 2.0 mM solution of Ga(NO<sub>3</sub>)<sub>3</sub> in 1 M NaOAc buffer. The mixture was stirred for 30 min at 95 °C and the completion of the <sup>nat</sup>Ga<sup>III</sup>-chelate formation was determined using analytical HPLC and ESI-MS.

<sup>nat</sup>Y<sup>III</sup>-complexation. A solution of DOTA- or DOTAGA-peptide (2 mM in tracepure water (*Sigma Aldrich*)) was treated 1:1 (v/v) with a 20 mM solution of YCl<sub>3</sub> (0.1 M CH<sub>3</sub>COONH<sub>4</sub>, pH = 6) and

## MATERIALS AND METHODS

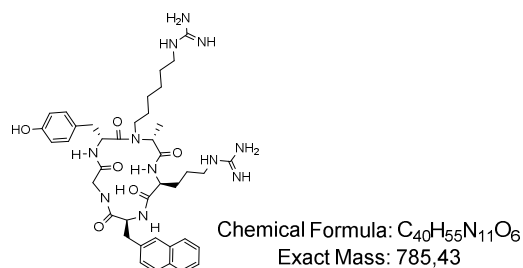
stirred for 30 min at 95 °C. After cooling to rt, the formation of the  $^{nat}\text{Y}^{\text{III}}$ -chelate was confirmed using analytical HPLC and ESI-MS.

*$^{nat}\text{Cu}^{\text{II}}$ -complexation.* For labeling with native copper, a 2.0 mM solution of DOTA-peptide was treated 1:1 (v/v) with a 2.0 mM solution of  $\text{Cu}(\text{OAc})_2$  in 1 M NaOAc buffer. The mixture was stirred for 20 min at rt and the completion of the  $^{nat}\text{Cu}^{\text{II}}$ -chelate formation was determined using analytical HPLC and ESI-MS.

*$^{nat}\text{Bi}^{\text{III}}$ -complexation.* Bismuth complexation was performed using a 2.0 mM solution of DOTA-peptide, which was treated 1:1 (v/v) with a 20 mM solution of  $\text{Bi}(\text{OAc})_3$  in 1 M NaOAc buffer (pH= 4.5). The mixture was stirred for 15 min at rt. Formation of the  $^{nat}\text{Bi}^{\text{III}}$ -chelate was confirmed using HPLC and ESI-MS.

### 3. Synthesis of cyclo[D-Tyr-(hexylguanidino)-D-Ala-Arg-Nal-Gly] (R1) derived ligands

**cyclo[D-Tyr-N(hexylguanidino)-D-Ala-Arg-Nal-Gly] (CPCR4.3, R1):** The synthesis of

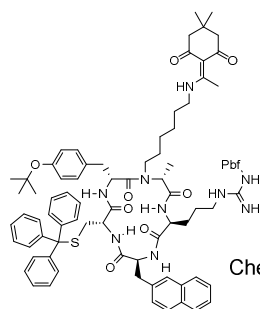


the radioligand was performed according to a published protocol <sup>89</sup> and in accordance to the synthesis of compounds **2**. The peptide synthesis, cleavage from the resin and subsequent modifications were performed according to the standard protocols

described in II.2.1. HPLC (10 to 90% B in 15 min):  $t_R = 5.4$  min;  $K' = 2.6$ . Calculated monoisotopic mass ( $\text{C}_{40}\text{H}_{55}\text{N}_{11}\text{O}_6$ ): 785.43, found:  $m/z = 786.6$   $[\text{M}+\text{H}]^+$ , 394.1  $[\text{M}+2\text{H}]^{2+}$ .

## MATERIALS AND METHODS

**cyclo[D-Tyr(t-Bu)-N(Dde-aminohexyl)-D-Ala-Arg(Pbf)-2-Nal-D-Cys(Trt)] (1):** The



Chemical Formula:  $C_{86}H_{105}N_9O_{11}S_2$   
Exact Mass: 1503,74

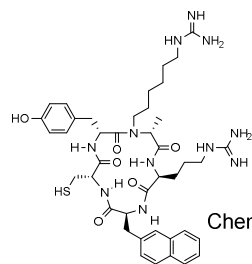
synthesis of the cyclic pentapeptide scaffold was performed according to a published protocol<sup>89</sup> with small modification. Therefore, 0.5 g of preloaded H-D-Cys-TCP resin (loading = 1.60 mmol/g; 0.80 mmol) were allowed to pre-swell for 30 min and the amino acids Fmoc-L-2-Nal-OH,

Fmoc-L-Arg(Pbf)-OH and Fmoc-D-Ala-OH were coupled using the standard procedure with 184 mg (1.20 mmol, 1.5 eq.) HOBt, 385 mg (1.20 mmol, 1.5 eq.) TBTU and 611  $\mu$ L (3.60 mmol, 4.5 eq.) of DIPEA. After Fmoc-deprotection, the resin was dissolved in NMP together with 710 mg (3.2 mmol, 4.0 eq.) of *p*-NCl and 1.0 mL (8.00 mmol, 10 eq.) of 2,3,4-collidine. After 20 min, the resin was washed with NMP (6 x2 min) and the solvent was changed to THF. 2.2 g (8.00 mmol, 10 eq.) of Dde-aminohexanol were dissolved with 1.05 g (4.00 mmol, 5.0 eq.) triphenylphosphine and stirred for 5 min. 785  $\mu$ L (4.00 mmol, 5.0 eq.) diisopropyl azodicarboxylate (DIAD) were slowly added to the resin within 5 min and the mixture was allowed to stir for 15 min afterwards. The resin was washed thoroughly and the *p*-Ns deprotection was performed according to the procedure described in (II.2.1). Fmoc-D-Tyr(t-Bu)-OH was added with the protocol for secondary amines (II.2.1). The fully protected linear peptide was cleaved from the resin (according to II.2.1) and precipitated in water to yield 746 mg (0.49 mmol, 60%) yellowish powder. For cyclization, the crude product was dissolved in 98 mL of dry DMF (5.0 mM) together with 288 mg (2.45 mmol, 5.0 eq.)  $NaHCO_3$  and 317  $\mu$ L (1.47 mmol, 3.0 eq.) of DPPA and stirred for 5 h or until no linear peptide could be observed *via* ESI-MS. The solution was concentrated under reduced pressure and the peptide was precipitated in water and washed two times. The crude product was dried and used for further reaction steps without further purification. HPLC (70 to 100% B in 15 min):  $t_R$  = 17.7 min;  $K'$  = 10.8. Calculated monoisotopic mass ( $C_{86}H_{105}N_9O_{11}S_2$ ): 1503.74, found:  $m/z$  = 1505.8  $[M+H]^+$ , 1527.8  $[M+Na]^+$ .



## MATERIALS AND METHODS

**cyclo[D-Tyr-N(hexylguanidino)-D-Ala-Arg-2-Nal-D-Cys] (2):** For Dde-deprotection according to protocol II.2.1., 118 mg (0.08 mmol, 1.0 eq.)

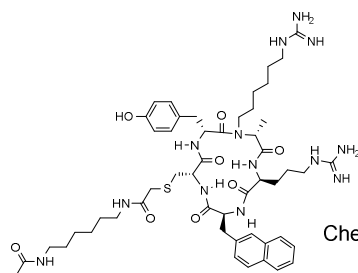


Chemical Formula:  $C_{41}H_{57}N_{11}O_6S$   
Exact Mass: 831.42

of **1** were dissolved in DMF. 129 mg (0.88 mmol, 10 eq.) of 1-H-pyrazol-1-carboxamidine were added and the reaction started after addition of 299  $\mu$ L (1.76 mmol, 20 eq.) of DIPEA. The solution was

stirred for 6 h at rt and subsequently treated with trifluoroacetic acid, Triisopropylsilane (TIPS) and water (95, 2.5, 2.5; v/v/v) for 40 min and precipitated in diethyl ether to yield **2** as yellowish powder. HPLC (10 - 90% B in 15 min):  $t_R$  = 11.9 min;  $K'$  = 4.9; Calculated monoisotopic mass ( $C_{41}H_{57}N_{11}O_6S$ ): 831.42, found by ESI-MS:  $m/z$  = 832.8  $[M+H]^+$ .

**cyclo[D-Tyr-N(hexylguanidino)-D-Ala-Arg-2-Nal-D-Cys(N,N'-(hexane-1,6-diyl)di-**



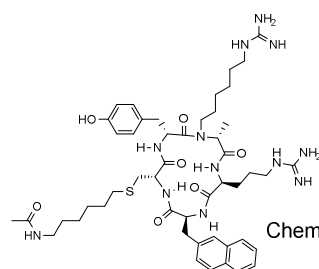
Chemical Formula:  $C_{51}H_{75}N_{13}O_8S$   
Exact Mass: 1029.56

**acetamide)] (3):** 30 mg (0.04 mmol, 1.0 eq.) of **2** was dissolved in 50  $\mu$ L DMF. 48.0 mg (0.12 mmol, 3.0 eq.) of Fmoc-(6-aminohexyl)-carbamic chloride were dissolved in 800  $\mu$ L of a MeCN/water solution

(9/1; v/v). The solutions were combined and after addition of 40  $\mu$ L (0.24 mmol, 6.0 eq.) DIPEA to adjust the pH to 9, the white suspension was stirred overnight. After precipitation in water, the white powder was freeze-dried and used without further purification. App. 38.0 mg (0.03 mmol) were used for Fmoc-deprotection and after precipitation in diethyl ether, the crude peptide was dissolved in a solution of acetic anhydride, DIPEA and DMF (10:5:85; v/v/v) and stirred for 1 h at rt. At once, the mixture was purified using semi-preparative HPLC (30 - 60% B in 20 min) to receive 7.5 mg (7.3  $\mu$ mol, 18%) of white powder. HPLC (15 - 45% B in 15 min):  $t_R$  = 9 min;  $K'$  = 5.4; calculated monoisotopic mass ( $C_{51}H_{75}N_{13}O_8S$ ): 1029.56, found by ESI-MS:  $m/z$  = 1030.7  $[M+H]^+$ , 1052.6  $[M+Na]^+$ .

## MATERIALS AND METHODS

### cyclo[D-Tyr-N(hexylguanidino)-D-Ala-Arg-2-Nal-D-Cys(N-hexylacetamide)] (4):

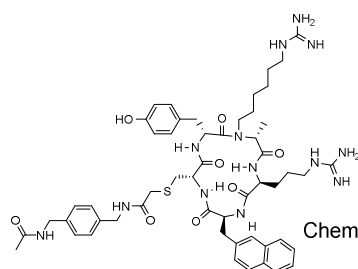


Chemical Formula:  $C_{49}H_{72}N_{12}O_7S$   
Exact Mass: 972.54

30 mg (0.04 mmol, 1.0 eq.) of **2** was dissolved in 50  $\mu$ L DMF. 48.3 mg (0.12 mmol, 3.0 eq.) of Fmoc-(6-bromohexyl)carbamate were dissolved in 800  $\mu$ L of a MeCN/water solution (9/1; v/v). The solutions were combined and after addition

of 40  $\mu$ L (0.24 mmol, 6.0 eq.) DIPEA, the white suspension was stirred overnight at rt (pH = 9-10). After precipitation in water, the white powder was freeze-dried and used without further purification. App. 20 mg (0.02 mmol, 43%) were used for Fmoc-deprotection and after precipitation in diethyl ether, the crude peptide was dissolved in a solution of acetic anhydride, DIPEA and DMF (10:5:85; v/v/v) and stirred for 1 h at rt. The mixture was purified immediately using semi-preparative HPLC (30 - 60% B in 20 min) to receive 2.0 mg (2.0  $\mu$ mol, 5%). HPLC (15 - 45% B in 15 min):  $t_R$  = 10 min;  $K'$  = 5.6; calculated monoisotopic mass ( $C_{49}H_{72}N_{12}O_7S$ ): 972.54; found by ESI-MS:  $m/z$  = 973.6  $[M+H]^+$ , 995.5  $[M+Na]^+$ .

### cyclo[D-Tyr-N(hexylguanidino)-D-Ala-Arg-2-Nal-D-Cys((1,3-phenylen-bismethan-



Chemical Formula:  $C_{53}H_{71}N_{13}O_8S$   
Exact Mass: 1049.53

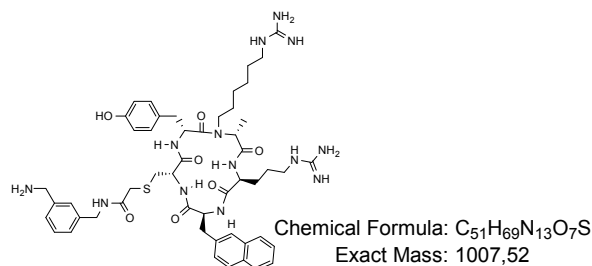
amine)diacetamine)] (**5**): 30 mg (0.04 mmol, 1.0 eq.) of **2** was dissolved in 50  $\mu$ L DMF. 50 mg (0.12 mmol, 3.0 eq.) of Fmoc-(4-(((chlorocarbonyl)amino)methyl)benzyl) carbamate were dissolved in 800  $\mu$ L of a

MeCN/water solution (9/1; v/v). The solutions were combined and the pH was adjusted to 9 using 40  $\mu$ L (0.24 mmol, 6.0 eq.) of DIPEA. After 18 h, the product was precipitated in water and freeze-dried. Without further purification, app. 35 mg (0.03 mmol, 71%) were used for Fmoc-deprotection and after precipitation in diethyl ether, the crude peptide was dissolved in a solution of acetic anhydride, DIPEA and DMF (10:5:85; v/v/v) and stirred for one hour at rt. The mixture was purified immediately with semi-preparative HPLC (30 - 60% B in 20 min) to receive 5.4 mg (5.1  $\mu$ mol, 13%). HPLC (15 - 45% B in 15 min):  $t_R$  = 8.7 min;  $K'$  = 5.2;

## MATERIALS AND METHODS

calculated monoisotopic mass ( $C_{53}H_{71}N_{13}O_8S$ ): 1049.53, found by ESI-MS:  $m/z = 1050.6$   $[M+H]^+$ , 1072.6  $[M+Na]^+$ , 525.8  $[M+2H]^{2+}$ .

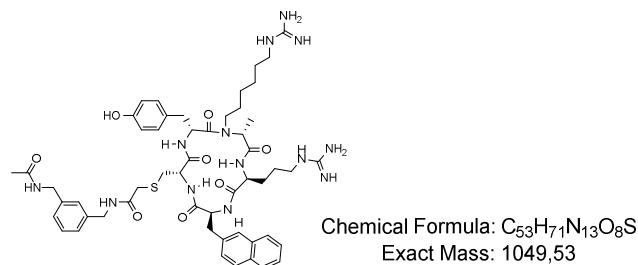
### cyclo[D-Tyr-N(hexylguanidino)-D-Ala-Arg-2-Nal-D-Cys(1,4-phenylen-bismethan-



**amine)acetamine)] (6):** 30 mg (0.04 mmol, 1.0 eq.) of **2** was dissolved in 50  $\mu$ L DMF. 50 mg (0.12 mmol, 3.0 eq.) of Fmoc-3-(((chlorocarbonyl)amino)methyl)benzyl)carbamate were dissolved in 800  $\mu$ L of a MeCN/water

solution (9/1; v/v). The solutions were combined and after addition of 40.0  $\mu$ L (0.24 mmol, 6.0 eq.) DIPEA the white suspension was stirred overnight at a pH of 9-10. After precipitation in water, the compound was freeze-dried and used without further purification. App. 32 mg (0.03 mmol, 65%) were used for Fmoc-deprotection and after precipitation in diethyl ether, the crude peptide was purified using semi-preparative HPLC (30 - 60% B in 20 min) to receive 4.0 mg (3.9  $\mu$ mol, 10%). HPLC (35 - 45% B in 15 min):  $t_R = 6.2$  min;  $K' = 2.9$ ; calculated monoisotopic mass ( $C_{51}H_{69}N_{13}O_7S$ ): 1007.52, found by ESI-MS:  $m/z = 1008.7$   $[M+H]^+$ , 1030.6  $[M+Na]^+$ .

### cyclo[D-Tyr-N(hexylguanidino)-D-Ala-Arg-2-Nal-D-Cys(1,4-phenylen-bismethan-



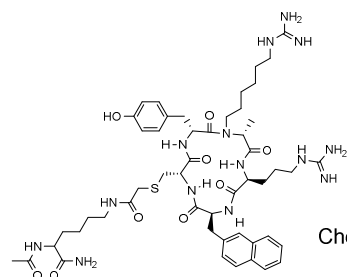
**amine)diacetamine)] (7):** 30 mg (0.04 mmol, 1.0 eq.) of **2** was dissolved in 50  $\mu$ L DMF. 50.0 mg (0.12 mmol, 3.0 eq.) of Fmoc(3(((chloro-carbonyl)amino)methyl)-benzyl)carbamate were dis-solved in 800  $\mu$ L

of a MeCN/water solution (9/1; v/v). The solutions were combined and after addition of 40.0  $\mu$ L (0.24 mmol, 6.0 eq.) DIPEA the white suspension was stirred overnight at rt. After precipitation in water, the compound was freeze-dried. After Fmoc-deprotection of 32 mg (0.03 mmol, 65%),

## MATERIALS AND METHODS

the crude peptide was dissolved in a solution of acetic anhydride, DIPEA and DMF (10:5:85; v/v/v) and stirred for one hour at rt. The mixture was purified immediately with semi-preparative HPLC (30 - 60% B in 20 min) to receive 4.6 mg (4.4  $\mu$ mol, 11%). HPLC (15 - 45% B in 15 min):  $t_R$  = 8.8 min;  $K'$  = 5.7; calculated monoisotopic mass ( $C_{53}H_{71}N_{13}O_8S$ ): 1049.53; found by ESI-MS:  $m/z$  = 1050.8  $[M+H]^+$ , 1072.7  $[M+Na]^+$ , 525.9  $[M+2H]^{2+}$ .

**cyclo[D-Tyr-N(hexylguanidino)-D-Ala-Arg-2-Nal-D-Cys(N,N'-(6-amino-6-oxohexane-1,5-diyl)diacet-amide)] (8):** 30 mg



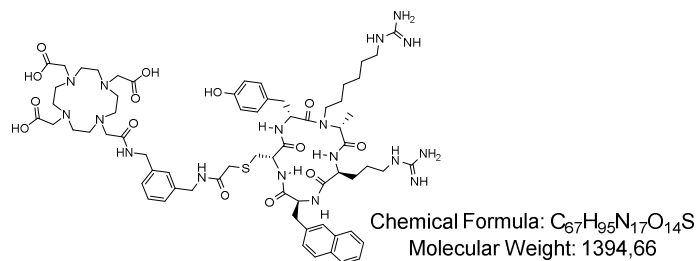
Chemical Formula:  $C_{51}H_{74}N_{14}O_9S$   
Exact Mass: 1058,55

(0.04 mmol, 1.0 eq.) of **2** was dissolved in 50  $\mu$ L DMF. 65.0 mg (0.12 mmol, 3.0 eq.) of Fmoc-*tert*-butyl(6-(2-chloro-acetamido)-1-oxohexane-1,2-diyl)dicarbamate were dissolved in 800  $\mu$ L of a MeCN/water solution (9/1; v/v). The solutions were combined and after addition of 40.0  $\mu$ L (0.24 mmol, 6.0 eq.) DIPEA the white suspension was stirred overnight at a pH of 9-10. After precipitation in water, the compound was freeze dried and used without further purification. App. 28 mg (0.02 mmol, 52%) were used for Fmoc-deprotection. After precipitation in diethyl ether and drying, Boc-deprotection was performed using a mixture of TFA/TIPS/water (95/2.5/2.5) for 30 min. The cleavage mixture was concentrated under reduced pressure and dissolved in a solution of acetic anhydride, DIPEA and DMF (10:5:85; v/v/v) without further purification. After 1 h, the mixture was purified immediately with semi-preparative HPLC (30 - 60% B in 20 min) to receive 1.3 mg (1.2  $\mu$ mol, 3%). HPLC (15 - 45% B in 15 min):  $t_R$  = 6.8 min;  $K'$  = 4.2; calculated monoisotopic mass ( $C_{51}H_{74}N_{14}O_9S$ ): 1058.55; found by ESI-MS:  $m/z$  = 1059.8  $[M+H]^+$ , 1081.8  $[M+Na]^+$ , 1097.6  $[M+K]^+$ .

solved in 800  $\mu$ L of a MeCN/water solution (9/1; v/v). The solutions were combined and after addition of 40.0  $\mu$ L (0.24 mmol, 6.0 eq.) DIPEA the white suspension was stirred overnight at a pH of 9-10. After precipitation in water, the compound was freeze dried and used without further purification. App. 28 mg (0.02 mmol, 52%) were used for Fmoc-deprotection. After precipitation in diethyl ether and drying, Boc-deprotection was performed using a mixture of TFA/TIPS/water (95/2.5/2.5) for 30 min. The cleavage mixture was concentrated under reduced pressure and dissolved in a solution of acetic anhydride, DIPEA and DMF (10:5:85; v/v/v) without further purification. After 1 h, the mixture was purified immediately with semi-preparative HPLC (30 - 60% B in 20 min) to receive 1.3 mg (1.2  $\mu$ mol, 3%). HPLC (15 - 45% B in 15 min):  $t_R$  = 6.8 min;  $K'$  = 4.2; calculated monoisotopic mass ( $C_{51}H_{74}N_{14}O_9S$ ): 1058.55; found by ESI-MS:  $m/z$  = 1059.8  $[M+H]^+$ , 1081.8  $[M+Na]^+$ , 1097.6  $[M+K]^+$ .

## MATERIALS AND METHODS

**cyclo[D-Tyr-N(hexylguanidino)-D-Ala-Arg-2-Nal-D-Cys(DOTA-1,4-phenylen-di-**



**methanamine)] (9):** DOTA conden-

sation was performed according to the method described under (II.2.2.). After

completion, the mixture was purified using semi-preparative HPLC (25 – 55%

B in 20 min). HPLC (15 - 35% B in 15

min):  $t_R = 11.9$  min;  $K' = 6.4$ ; calculated monoisotopic mass ( $C_{67}H_{95}N_{17}O_{14}S$ ): 1394.66, found by ESI-MS:  $m/z = 1396.1$   $[M+H]^+$ , 698.4  $[M+2H]^{2+}$ .

Complexation of DOTA-conjugate **9** was performed according to the protocol described in II.2.2.

**cyclo[D-Tyr-N(hexylguanidino)-D-Ala-Arg-2-Nal-D-Cys(<sup>nat</sup>Ga-DOTA-1,4-phenylen-di-**

**methanamine)] ([<sup>nat</sup>Ga]**9**):** HPLC (15 - 35% B in 15 min):  $t_R = 12.5$  min;  $K' = 6.8$ ; calculated

monoisotopic mass ( $C_{67}H_{93}GaN_{17}O_{14}S$ ): 1460.61; found by ESI-MS:  $m/z = 1463.0$   $[M+H]^+$ , 732.1  $[M+2H]^{2+}$ .

**cyclo[D-Tyr-N(hexylguanidino)-D-Ala-Arg-Nal-D-Cys(<sup>nat</sup>Lu-DOTA-1,4-phenylen-**

**dimethanamine)] ([<sup>nat</sup>Lu]**9**):** HPLC (15 - 35% B in 15 min):  $t_R = 11.7$  min;  $K' = 6.3$ ;

calculated monoisotopic mass ( $C_{67}H_{92}LuN_{17}O_{14}S$ ): 1565.61; found by ESI-MS:  $m/z = 1567.0$   $[M+H]^+$ , 784.5  $[M+2H]^{2+}$ .

**cyclo[D-Tyr-N(hexylguanidino)-D-Ala-Arg-Nal-D-Cys(<sup>nat</sup>Cu-DOTA-1,4-phenylen-**

**dimethanamine)] ([<sup>nat</sup>Cu]**9**):** HPLC (15 - 35% B in 15 min):  $t_R = 12.9$  min;  $K' = 7.0$ ;

calculated monoisotopic mass ( $C_{67}CuH_{92}N_{17}O_{14}S$ ): 1455.62; found by ESI-MS:  $m/z = 1456.1$   $[M+H]^+$ , 729.1  $[M+2H]^{2+}$ .

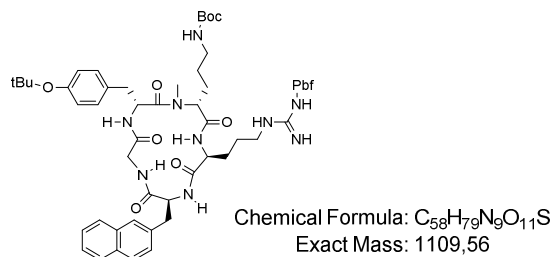
**Decoration of carboxyl-modified quantum dots with 6:** Carboxyl quantum dots (*Life technologies*, Qdot® 655 ITK™ Carboxyl Quantum Dots) (0.8 nmol in 100  $\mu$ l 50 mM borate buffer (pH=8.3)) were diluted with 10 mM borate buffer (pH=7.4) to a total volume of 920  $\mu$ l.

## MATERIALS AND METHODS

Then, 1-ethyl-3-(3-dimethylamino-propyl)carbodiimide (800 eq., 640 nmol) in 12.2  $\mu$ L 10 mM borate buffer and deprotected **6** (40 eq., 32 nmol) dissolved in 64  $\mu$ L 10 mM borate buffer were added. Consumption of unreacted peptide from the reaction mixture was monitored *via* RP-HPLC. Upon completion of the coupling reaction (30-60 min at rt), excess coupling reagent was removed from the **QD-6** suspension by repeated buffer exchanges using 50 mM borate buffer (pH = 8.3) and Amicon Ultra-4 ultrafiltration units with 100 kDa cutoff (4 mL, *Millipore*). Final reconstitution with 50 mM borate buffer yielded the peptide coated quantum dots **QD-6** as a 4.0  $\mu$ M suspension. According to the chosen stoichiometry, coating efficiency of the quantum dots was calculated to be app. 40% of reactive carboxylates.

## 4. Synthesis of cyclo[D-Tyr-N(Me)-D-Orn-Arg-2-Nal-Gly] derived peptides

**cyclo[D-Tyr(tBu)-N(Me)-D-Orn-Arg(Pbf)-2-Nal-Gly] (10):** The synthesis of cyclic



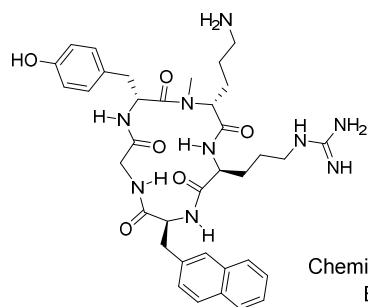
pentapeptide scaffold was performed according to a previously published protocol with small modification<sup>102</sup>. 2.5 g of preloaded H-Gly-TCP resin (loading = 0.4 mmol/g; 1.0 mmol) was allowed to pre-swell for 30 min and the amino acids

Fmoc-L-2-Nal-OH, Fmoc-L-Arg(Pbf)-OH and Fmoc-D-Orn(Boc)-OH were coupled using the standard procedure with 202.7 mg (1.5 mmol, 1.5 eq.) HOBt, 481.7 mg (1.5 mmol, 1.5 eq.) TBTU and 765.3  $\mu$ L (4.5 mmol, 4.5 eq.) of DIPEA. After Fmoc-deprotection, *p*-Ns protection was performed according to II.2.1. After 20 min, the resin was washed (6 x 2 min NMP) and the solvent was changed to THF. 405  $\mu$ L (10.0 mmol, 10 eq.) of MeOH were dissolved with 1.31 g (5.0 mmol, 5.0 eq.) triphenylphosphine in dry THF and stirred for 5 min. 981  $\mu$ L (5.0 mmol, 5.0 eq.) DIAD were carefully added to the resin within 5 min and the mixture was allowed to stir for another 15 min. The resin was washed thoroughly and the *p*-NS deprotection was performed

## MATERIALS AND METHODS

according to the procedure described in (II.2.1). Fmoc-D-Tyr(t-Bu)-OH was added with the protocol for secondary amines (II.2.1). The fully protected linear peptide was cleaved from the resin and precipitated in water to yield 970 mg (0.86 mmol, 86%) yellowish powder. For peptide cyclization, the crude product was dissolved in 275 mL of dry DMF together with 812.0 mg (5.0 mmol, 5.0 eq.) NaHCO<sub>3</sub>. 893  $\mu$ L (3.0 mmol, 3.0 eq.) of DPPA were added at rt and the suspension was stirred for 5 h or until no linear peptide could be observed *via* ESI-MS. The solution was concentrated under reduced pressure and the peptide was precipitated in water and washed two times. HPLC (30 to 100% B in 15 min):  $t_R$  = 10.68 min;  $K'$  = 6.1; calculated monoisotopic mass (C<sub>58</sub>H<sub>79</sub>N<sub>9</sub>O<sub>11</sub>S<sub>2</sub>): 1109.56 found:  $m/z$  = 1110.3 [M+H]<sup>+</sup>.

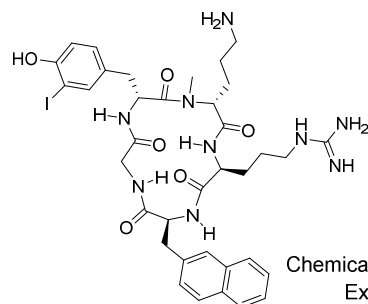
**cyclo[D-Tyr-N(Me)-D-Orn-Arg-2-Nal-Gly], CPCR4 (11):** **10** was dissolved in TFA, TIPS



and water (v/v/v; 95/2.5/2.5) and stirred for 30 min. The solvent was concentrated under a constant nitrogen flow and after dissolving in MeCN and water, the crude product was purified using semi-preparative HPLC (20 to 45% B in 20 min). 450 mg (0.64 mmol, 64%) of

the purified peptide **11** was stored under 8 °C until further applications. HPLC (10 to 50% B in 15 min):  $t_R$  = 9.7 min;  $K'$  = 3.7; calculated monoisotopic mass (C<sub>36</sub>H<sub>47</sub>N<sub>9</sub>O<sub>6</sub>): 701.36 found:  $m/z$  = 702.37 [M+H]<sup>+</sup>.

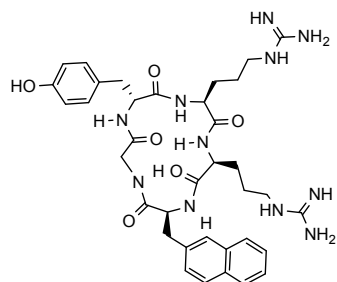
**cyclo[(3-iodo)-D-Tyr-N(Me)-D-Orn-Arg-2-Nal-Gly] (12):** **11** was converted to **12**



employing 0.45 eq. of NIS as described in II.2.1. HPLC (25 to 55% B in 15 min):  $t_R$  = 8.2 min;  $K'$  = 4.8; calculated monoisotopic mass (C<sub>36</sub>H<sub>46</sub>IN<sub>9</sub>O<sub>6</sub>): 827.26; found:  $m/z$  = 829.4 [M+H]<sup>+</sup>.

## MATERIALS AND METHODS

**cyclo[D-Tyr-Arg-Arg-2-Nal-Gly], FC131 (R2):** The synthesis of FC131 (R2) was



Chemical Formula:  $C_{36}H_{47}N_{11}O_6$   
Exact Mass: 729,37

performed according to the protocol described for peptide **11**. Therefore, standard solid phase peptide synthesis was performed employing the amino acids Fmoc-L-2-Nal-OH, Fmoc-L-Arg(Pbf)-OH and Fmoc-L-

Arg(Pbf)-OH and Fmoc-D-Tyr(tBu)-OH. Cleavage from the resin, cyclization and subsequent cleavage of all side chain protecting groups was performed according to II.2.1. The crude purified using semi-preparative HPLC (15 to 45% B in 20 min) to collect 8.2 mg (0.011 mmol) of white powder. HPLC (15 to 45% B in 15 min):  $t_R = .8$  min;  $K' = 5.5$ ; calculated monoisotopic mass ( $C_{36}H_{47}N_{11}O_6$ ): 729.37 found:  $m/z = 730.7$   $[M+H]^+$ .

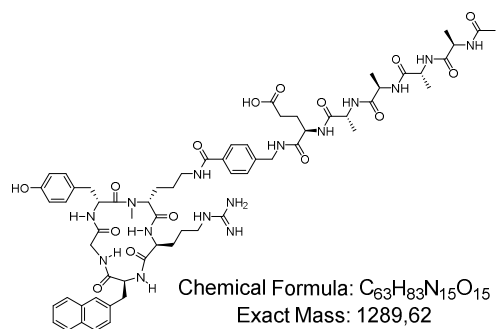
### 4.1. Shifting the charge

The respective amino acid linkers were constructed using Fmoc-based solid-phase peptide synthesis according to II.2.1. The TCP-resin bound 4-(Fmoc-aminomethyl)benzoic acid (in the following referred to 4-Fmoc-AMBA) was coupled with the respective Fmoc-protected amino acids. After cleavage from the resin under preservation of the protecting groups, the peptides were condensed with peptide **11** employing 1.5 eq. HOBt, 1.5 eq. TBTU and 4.5 eq. DIPEA. After final Fmoc-deprotection, the terminal amine was acetylated using a mixture of acetic anhydride, diisopropylamine and DMF (v/v/v; 10/5/85) for 1 h. The solvent was concentrated under reduced pressure and the residue was precipitated in diethyl ether. After dissolving the precipitate in TFA/TIPS/water (v/v/v; 95/2.5/2.5) for 30 min, the mixture was employed for semi-preparative HPLC (27 to 35% in 20 min).



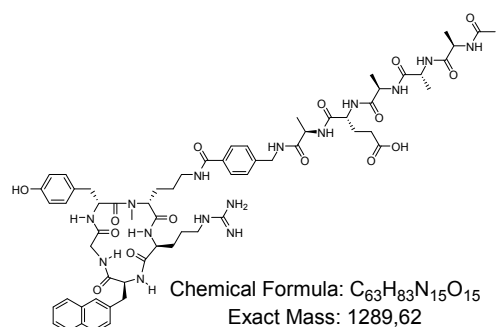
## MATERIALS AND METHODS

### cyclo[D-Tyr-N(Me)-D-Orn(Ac-D-Ala-D-Ala-D-Ala-D-Ala-D-Glu-AMBA)-Arg-2-Nal-



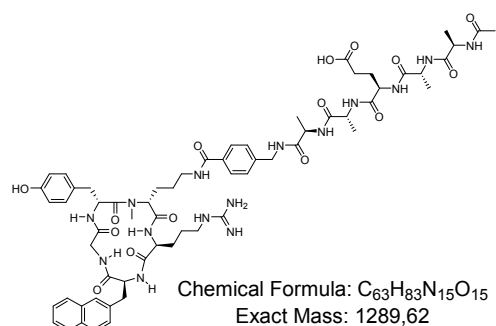
**Gly] (13):** HPLC (20 to 70% B in 15 min):  $t_R = 8.2$  min;  $K' = 3.8$ . Calculated monoisotopic mass ( $C_{63}H_{83}N_{15}O_{15}$ ): 1289.62; found:  $m/z = 1290.0$   $[M+H]^+$ , 1312.1  $[M+Na]^+$ .

### cyclo[D-Tyr-N(Me)-D-Orn(Ac-D-Ala-D-Ala-D-Ala-D-Glu-D-Ala-AMBA)-Arg-2-Nal-



**Gly] (14):** HPLC (20 to 70% B in 15 min):  $t_R = 10.8$  min;  $K' = 4.1$ . Calculated monoisotopic mass ( $C_{63}H_{83}N_{15}O_{15}$ ): 1289.62; found:  $m/z = 1290.9$   $[M+H]^+$ , 1312.9  $[M+Na]^+$ .

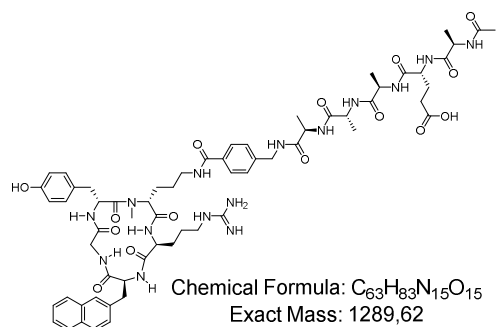
### cyclo[D-Tyr-N(Me)-D-Orn(Ac-D-Ala-D-Ala-D-Glu-D-Ala-D-Ala-AMBA)-Arg-2-Nal-



**Gly] (15):** HPLC (30 to 80% B in 15 min):  $t_R = 9.1$  min;  $K' = 3.8$ . Calculated monoisotopic mass ( $C_{63}H_{83}N_{15}O_{15}$ ): 1289.62; found:  $m/z = 1290.6$   $[M+H]^+$ , 1312.6  $[M+Na]^+$ .

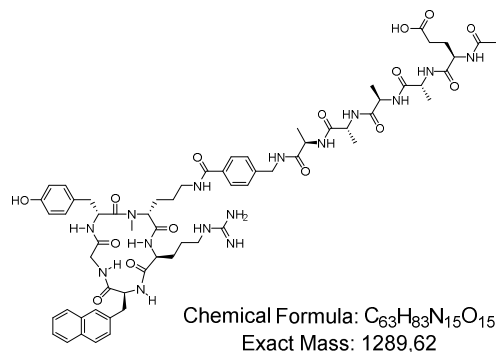
## MATERIALS AND METHODS

### cyclo[D-Tyr-N(Me)-D-Orn(Ac-D-Ala-D-Glu-D-Ala-D-Ala-D-Ala-AMBA)-Arg-2-Nal-



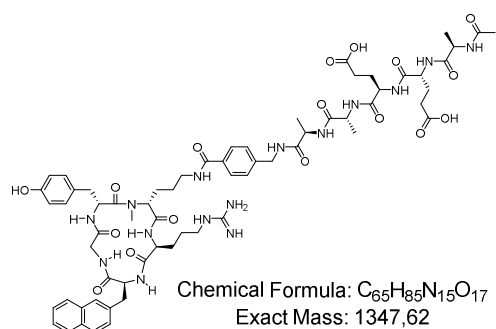
**Gly] (16):** HPLC (10 to 90% B in 15 min):  $t_R = 12.3$  min;  $K' = 5.4$ . Calculated monoisotopic mass ( $C_{63}H_{83}N_{15}O_{15}$ ): 1289.62; found:  $m/z = 1290.9$   $[M+H]^+$ , 1328.9  $[M+K]^+$ .

### cyclo[D-Tyr-N(Me)-D-Orn(Ac-D-Glu-D-Ala-D-Ala-D-Ala-D-Ala-AMBA)-Arg-2-Nal-



**Gly] (17):** HPLC (35 to 50% B in 15 min):  $t_R = 7.6$  min;  $K' = 3.8$ . Calculated monoisotopic mass ( $C_{63}H_{83}N_{15}O_{15}$ ): 1289.62; found:  $m/z = 1290.8$   $[M+H]^+$ , 1329.9  $[M+K]^+$ .

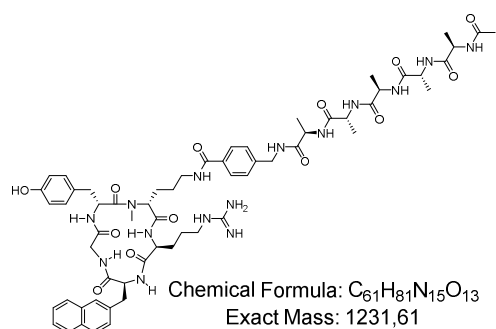
### cyclo[D-Tyr-N(Me)-D-Orn(Ac-D-Ala-D-Glu-D-Glu-D-Ala-D-Ala-AMBA)-Arg-2-Nal-



**Gly] (18):** HPLC (35 to 50% B in 15 min):  $t_R = 8.2$  min;  $K' = 3.6$ . Calculated monoisotopic mass ( $C_{65}H_{85}N_{15}O_{17}$ ): 1347.62; found:  $m/z = 1348.8$   $[M+H]^+$ , 1370.7  $[M+K]^+$ .

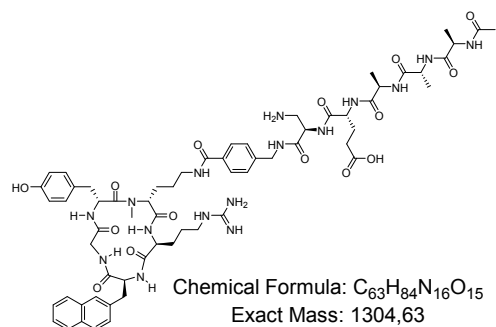
## MATERIALS AND METHODS

### cyclo[D-Tyr-N(Me)-D-Orn(Ac-D-Ala-D-Ala-D-Ala-D-Ala-D-Ala-AMBA)-Arg-2-Nal-



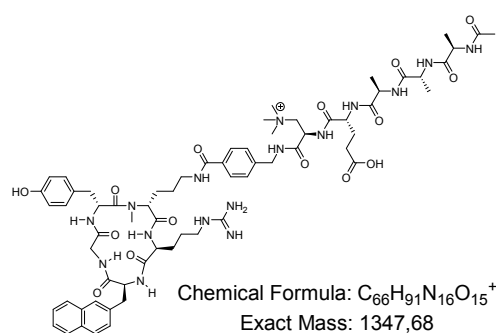
**Gly] (19):** HPLC (20 to 70% B in 15 min):  $t_R = 10.1$  min;  $K' = 4.1$ . Calculated monoisotopic mass ( $C_{61}H_{81}N_{15}O_{13}$ ): 1231.61; found:  $m/z = 1232.8$   $[M+H]^+$ .

### cyclo[D-Tyr-N(Me)-D-Orn(Ac-D-Ala-D-Ala-D-Ala-D-Glu-D-Dap-AMBA)-Arg-2-Nal-



**Gly] (20):** HPLC (25 to 55% B in 15 min):  $t_R = 12.2$  min;  $K' = 5.4$ . Calculated monoisotopic mass ( $C_{63}H_{84}N_{16}O_{15}$ ): 1304.63; found:  $m/z = 1306.2$   $[M+H]^+$ , 1327.9  $[M+Na]^+$ , 1344.0  $[M+K]^+$ .

### cyclo[D-Tyr-N(Me)-D-Orn(Ac-D-Ala-D-Ala-D-Ala-D-Glu-D-Dap(NMe)<sub>3</sub>-AMBA)-Arg-

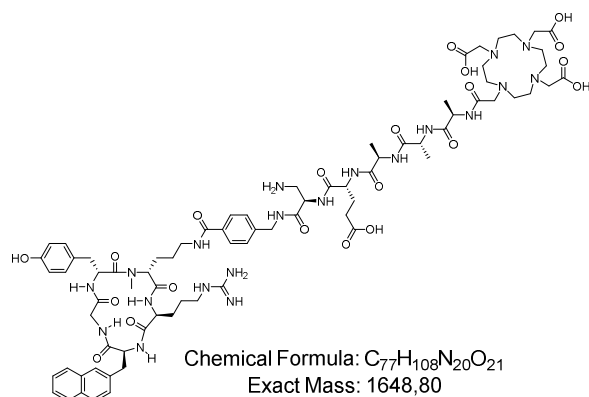


**2-Nal-Gly] (21):** The synthesis of the respective amino acid chain was performed as described for **20** on solid support. Methylation of the side chain of D-Dap on solid support was achieved employing 8.0 eq. of iodomethane and 4.0 eq. of silver oxide in dry DMF. After 5 h, the resin was washed with DMF and the

linear peptide was cleaved from the resin using DCM, TFE and AcOH. After purification of the linear peptide, the linker was combined with **11** as described in the standard procedure for this chapter. HPLC (35 to 55% B in 15 min):  $t_R = 7.2$  min;  $K' = 3.2$ . Calculated monoisotopic mass ( $C_{66}H_{91}N_{16}O_{15}^+$ ): 1347.68; found:  $m/z = 1348.0$   $[M+H]^+$ , 675.0  $[M+2H]^{2+}$ .

## MATERIALS AND METHODS

### cyclo[D-Tyr-N(Me)-D-Orn(DOTA-D-Ala-D-Ala-D-Ala-D-Glu-D-Dap-AMBA)-Arg-2-



**Nal-Gly] (22):** Condensation of the *N*-terminal free peptide was performed according to the protocol described in II.2.1. HPLC (25 to 55% B in 15 min):  $t_R = 12.2$  min;  $K' = 5.4$ . Calculated monoisotopic mass ( $C_{77}H_{108}N_{20}O_{21}$ ): 1648.80; found:  $m/z = 1650.2$   $[M+H]^+$ , 825.4  $[M+H+H]^{2+}$ .

$^{nat}Ga$  and  $^{nat}Lu$ -complexation of DOTA-conjugate **21** was performed according to the protocol described in II.2.2.

### cyclo[D-Tyr-N(Me)-D-Orn( $^{nat}Ga$ -DOTA-D-Ala-D-Ala-D-Ala-D-Glu-D-Dap-AMBA)-

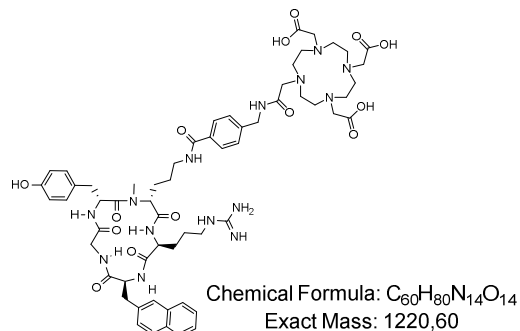
**Arg-2-Nal-Gly] ( $[^{nat}Ga]$ 22):** HPLC (15 to 55% B in 15 min):  $t_R = 7.7$  min;  $K' = 3.5$ . Calculated monoisotopic mass ( $C_{77}H_{106}GaN_{20}O_{21}$ ): 1715.71; found:  $m/z = 1717.3$   $[M+H]^+$ , 859.8  $[M+H+H]^{2+}$ .

### cyclo[D-Tyr-N(Me)-D-Orn( $^{nat}Lu$ -DOTA-D-Ala-D-Ala-D-Ala-D-Glu-D-Dap-AMBA)-

**Arg-2-Nal-Gly]RNaIG ( $[^{nat}Lu]$ 22):** HPLC (25 to 55% B in 15 min):  $t_R = 12.2$  min;  $K' = 5.4$ . Calculated monoisotopic mass ( $C_{77}H_{105}LuN_{20}O_{21}$ ): 1820.72; found:  $m/z = 1823.3$   $[M+H]^+$ , 912.2  $[M+H+H]^{2+}$ .

## 4.2. Optimization of the linking unit

### cyclo[D-Tyr-N(Me)-D-Orn(DOTA-AMBA)-Arg-2-Nal-Gly], Pentixafor (23):

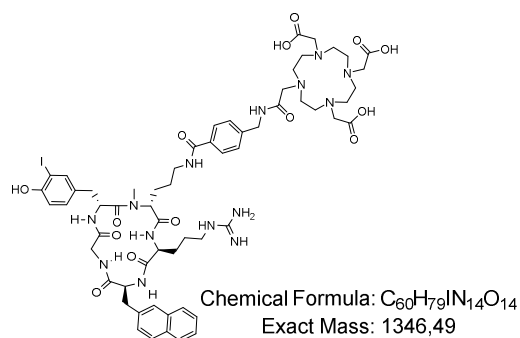


The synthesis of Pentixafor was performed according to earlier published procedures<sup>90, 91, 103</sup>. Briefly, 40 mg (0.05 mmol, 1.0 eq.) of **11** dissolved in 100  $\mu$ L of DMF was added to a mixture of 27.9 mg (0.075 mmol, 1.5 eq.) of 4-(Fmoc-aminomethyl)-benzoic acid (4-

## MATERIALS AND METHODS

Fmoc-AMBA), 10.1 mg (0.075 mmol, 1.5 eq.) HOAt, 11.6  $\mu$ L (0.075 mmol, 1.5 eq.) DIC and 38.2  $\mu$ L (0.225 mmol, 4.5 eq.) of DIPEA in 500  $\mu$ L of DMF. After 3 h, 120  $\mu$ L of piperidine was added to the solution for 30 min at rt. The solvent was concentrated under reduced pressure and the crude product was precipitated in diethyl ether. After removal of the solvent, condensation with DOTA was performed according to the protocol in II.2.2. The resulting peptide was purified using semi-preparative HPLC (20-30% B in 20 min) to give 2.3 mg (1.8  $\mu$ mol, 4%) white solid. HPLC (15 to 45% B in 15 min):  $t_R$  = 9.0 min;  $K'$  = 5.4. Calculated monoisotopic mass ( $C_{60}H_{80}N_{14}O_{14}$ ): 1220.60; found:  $m/z$  = 1221.9  $[M+H]^+$ , 611.2  $[M+H+H]^{2+}$ .

### cyclo[(3-iodo)D-Tyr-N(Me)-D-Orn(DOTA-AMBA)-Arg-2-Nal-Gly], Pentixather (24):

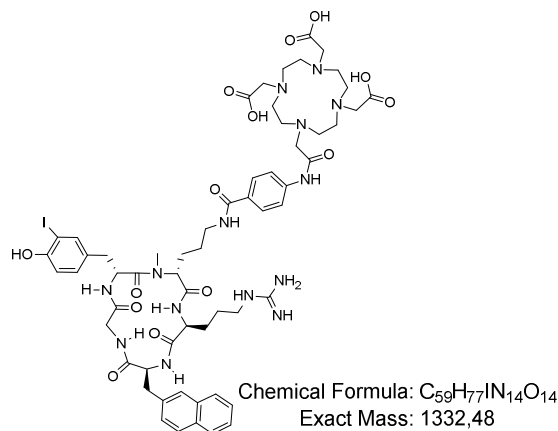


6.0 mg (4.9  $\mu$ mol, 1.0 eq.) of **23** were used in the direct iodination protocol described in II.2.1 employing 0.45 eq. NIS. 2.8 mg (2.0  $\mu$ mol, 41%) of a white powder were collected. HPLC (15 to 45% B in 15 min):  $t_R$  = 10.6 min;  $K'$  = 5.2. Calculated monoisotopic mass ( $C_{60}H_{79}IN_{14}O_{14}$ ): 1346.49; found:

$m/z$  = 1347.7  $[M+H]^+$ , 737.5  $[M+H+H]^{2+}$ , 1369.7  $[M+Na]^+$ .

### cyclo[(3-iodo)D-Tyr-N(Me)-D-Orn(DOTA-ABA)-Arg-2-Nal-Gly] (25):

20.3 mg



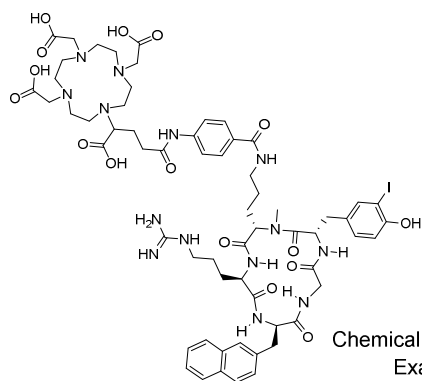
(0.086 mmol, 1.5 eq.) of 4-(Boc-amino)benzoic acid (from now on referred to as Boc-ABA) were dissolved together with 11.6 mg (0.086 mmol, 1.5 eq.) HOAt, 13.4  $\mu$ L (0.086 mmol, 1.5 eq.) DIC and 43.5  $\mu$ L (0.256 mmol, 4.5 eq.) of DIPEA in DMF and stirred for 15 min. The mixture was added to 40.0 mg (0.057 mmol, 1.0 eq.) of **11** in DMF and the solution was stirred for 3h at rt. The

solvent was concentrated under reduced pressure and the crude product was precipitated in

## MATERIALS AND METHODS

diethyl ether. 31.6 mg (0.034 mmol, 60%) of the crude product were dissolved in TFA, TIPS and water (v/v/v; 95/2.5/2.5) and stirred for 30 min. After removal of the solvent, condensation with DOTA was performed according to the protocol in II.2.2. The resulting peptide was purified using semi-preparative HPLC (26-32% B in 20 min) to give 8.3 mg (6.8  $\mu$ mol, 12%) of the iodination precursor. To receive peptide **25**, the direct iodination of the tyrosine side chain was performed with 0.55 eq. NIS as described in II.2.1. 3.8 mg (2.8  $\mu$ mol, 5%) of a white powder were collected. HPLC (35 to 60% B in 15 min):  $t_R$  = 6.8 min;  $K'$  = 2.7. Calculated monoisotopic mass ( $C_{59}H_{77}IN_{14}O_{14}$ ): 1332.48; found:  $m/z$  = 1333.9  $[M+H]^+$ , 667.8  $[M+H+H]^{2+}$ , 1355.8  $[M+Na]^+$ .

**cyclo[(3-iodo)D-Tyr-N(Me)-D-Orn(DOTAGA-ABA)-Arg-2-Nal-Gly]** (**26**): 20.0 mg

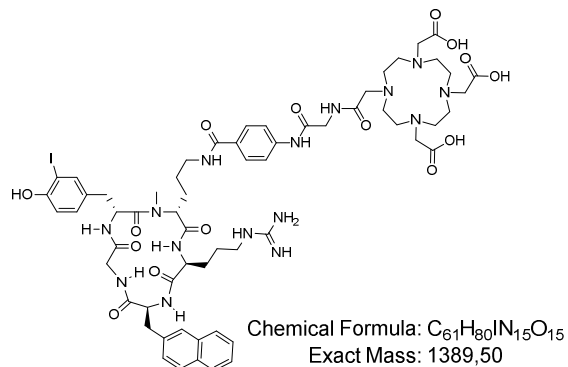


(0.084 mmol, 1.5 eq.) of Boc-ABA were dissolved together with 11.3 mg (0.084 mmol, 1.5 eq.) HOAt, 13.1  $\mu$ L (0.084 mmol, 1.5 eq.) DIC and 42.8  $\mu$ L (0.252 mmol, 4.5 eq.) of DIPEA in DMF and stirred for 15 min. The mixture was added to 39.0 mg (0.056 mmol, 1.0 eq.) of

**11** in DMF and the solution was stirred for 3 h at rt. The solvent was concentrated under reduced pressure and the crude product was precipitated in diethyl ether. 25.0 mg (0.027 mmol, 49%) of the crude product were dissolved in TFA, TIPS and water (v/v/v; 95/2.5/2.5) and stirred for 30 min. After removal of the solvent, condensation with DOTAGA anhydride was performed according to the protocol in II.2.2. The resulting peptide was purified using semi-preparative HPLC (22-40% B in 20 min) to give 7.2 mg (5.6  $\mu$ mol, 10%) of the iodination precursor. The purified peptide was directly iodinated using 0.6 eq. NIS. 4.9 mg (3.4  $\mu$ mol, 6%) of a white powder were collected. HPLC (35 to 60% B in 15 min):  $t_R$  = 9.2 min;  $K'$  = 4.1. Calculated monoisotopic mass ( $C_{62}H_{81}IN_{14}O_{16}$ ): 1404.50; found:  $m/z$  = 1405.9  $[M+H]^+$ , 703.7  $[M+H+H]^{2+}$ .

## MATERIALS AND METHODS

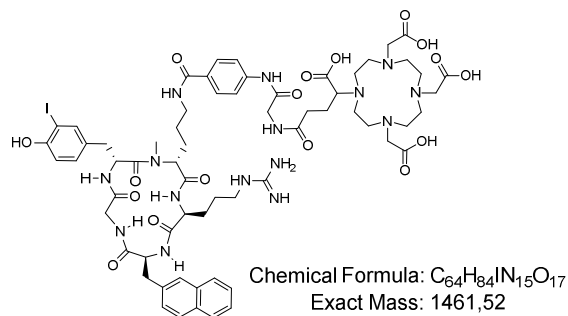
**cyclo[(3-*iodo*)D-Tyr-N(Me)-D-Orn(DOTA-Gly-ABA)-Arg-2-Nal-Gly] (27):** 20.3 mg



(0.086 mmol, 1.5 eq.) of Boc-ABA were dissolved together with 11.6 mg (0.086 mmol, 1.5 eq.) HOAt, 13.4  $\mu$ L (0.086 mmol, 1.5 eq.) DIC and 43.5  $\mu$ L (0.256 mmol, 4.5 eq.) of DIPEA in DMF and stirred for 15 min. The mixture was added to 40.0 mg (0.057 mmol, 1.0 eq.) of **11** in DMF and the solution was stirred for 3 h at rt. The peptide

was precipitated in diethyl ether and freeze-dried overnight. After Fmoc-deprotection, 34.0 mg (0.047 mmol, 1.0 eq.) were dissolved in DMF together with 18.2 mg (0.06 mmol, 1.5 eq.) Fmoc-Gly-OH, 8.2 mg (0.06 mmol, 1.5 eq.) HOAt, 9.5  $\mu$ L (0.06 mmol, 1.5 eq.) DIC and 31.0  $\mu$ L (0.18 mmol, 4.5 eq.) of DIPEA and stirred for 3 h at rt. The peptide was precipitated in diethyl ether and Fmoc-deprotected. Afterwards, the deprotected peptide was precipitated in cold diethyl ether and freeze-dried overnight. Conjugation with DOTA was performed according to the protocol in II.2.2. and the resulting product was purified using HPLC (15-45% B in 20 min). 11.1 mg (8.78  $\mu$ mol, 15%) of the iodination precursor were treated with 0.5 eq. NIS as described in II.2.1. 3.78 mg (2.7  $\mu$ mol, 5%) of a yellowish powder were collected. HPLC (35 to 60% B in 15 min):  $t_R$  = 8.8 min;  $K'$  = 3.8. Calculated monoisotopic mass ( $C_{61}H_{80}IN_{15}O_{15}$ ): 1389.50; found:  $m/z$  = 1390.9  $[M+H]^+$ , 696.3  $[M+H+H]^{2+}$ .

**cyclo[(3-*iodo*)D-Tyr-N(Me)-D-Orn(DOTAGA-Gly-ABA)-Arg-2-Nal-Gly] (28):**



20.3 mg (0.086 mmol, 1.5 eq.) of Boc-ABA were dissolved together with 11.6 mg (0.086 mmol, 1.5 eq.) HOAt, 13.4  $\mu$ L (0.086 mmol, 1.5 eq.) DIC and 43.5  $\mu$ L (0.256 mmol, 4.5 eq.) of DIPEA in DMF and stirred for 15 min. The mixture was added to 40.0 mg (0.06 mmol, 1.0 eq.) of **11** in

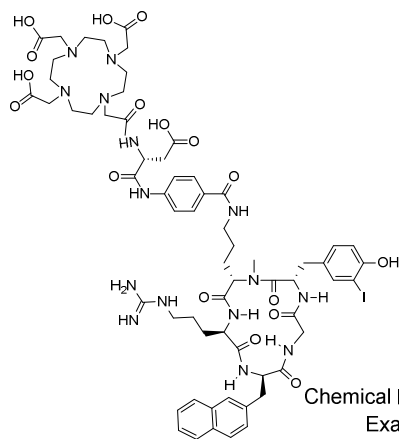
DMF and the solution was stirred for 3 h at rt. The peptide was precipitated in diethyl ether

## MATERIALS AND METHODS

and freeze-dried overnight. After Fmoc-deprotection, 34.0 mg (0.047 mmol, 1.0 eq.) were dissolved in DMF together with 18.2 mg (0.06 mmol, 1.5 eq.) Fmoc-Gly-OH, 8.2 mg (0.06 mmol, 1.5 eq.) HOAt, 9.5  $\mu$ L (0.06 mmol, 1.5 eq.) DIC and 31.0  $\mu$ L (0.18 mmol, 4.5 eq.) of DIPEA and stirred for 3 h at rt. The peptide was precipitated in diethyl ether and Fmoc-deprotected directly. Afterwards, the deprotected peptide was precipitated in cold diethyl ether and freeze-dried overnight. Conjugation with DOTAGA anhydride was performed according to the protocol in II.2.2. and the resulting product was purified using HPLC (22-42% B in 20 min). 13.7 mg (0.01 mmol, 18%) of the iodination precursor were treated with 0.45 eq. NIS. 1.5 mg (1.0  $\mu$ mol, 2%) of a white powder were collected. HPLC (30 to 55% B in 15 min):  $t_R$  = 12.2 min;  $K'$  = 5.7. Calculated monoisotopic mass ( $C_{64}H_{84}IN_{15}O_{17}$ ): 1461.52; found:  $m/z$  = 1462.8  $[M+H]^+$ , 732.2  $[M+H+H]^{2+}$ .

Ligands containing more than one amino acid between the benzyl spacer and the chelator DOTA or DOTAGA were synthesized utilizing two separate synthesis pathways. The linking unit was constructed starting with 1.018 g resin bound 4-(Fmoc-amino)benzoic acid (Fmoc-ABA) (1.12 mmol, 1.1 mmol/g resin) as described in II.2.1. Following standard Fmoc-protocol, the respective amino acids were introduced as described in II.2.1 using HOBt, TBTU and DIPEA as a base. After completion of the linking peptide chain, the linear peptide was cleaved from the resin and used directly for the combination with the respective binding scaffold.

**cyclo[(3-*iodo*)D-Tyr-N(Me)-D-Orn(DOTA-D-Asp-ABA)-Arg-2-Nal-Gly] (29):** 0.2 g of



Chemical Formula:  $C_{63}H_{82}N_{15}O_{17}$   
Exact Mass: 1447,51

resin bound Fmoc-ABA (0.224 mmol, 1.0 eq.) were allowed to pre-swell for 30 min in DMF. 276.5 mg (0.672 mmol, 3.0 eq.) Fmoc-D-Asp(tBu)-OH was dissolved together with 255.4 mg (0.672 mmol, 3.0 eq.) HATU, 91.5 mg (0.672 mmol, 3.0 eq.) HOAt and 228.1  $\mu$ L (1.34 mmol, 6.0 eq.) DIPEA 20.3 mg

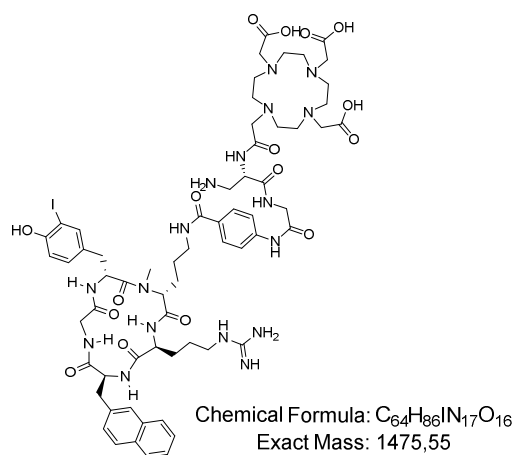


## MATERIALS AND METHODS

(0.086 mmol, 1.5 eq.) in DMF and stirred for 15 min. The mixture was added to the resin and the reaction was shaken for 3 h at rt. The linear peptide was cleaved from the resin under standard conditions, precipitated in diethyl ether and freeze-dried overnight.

45.0 mg (0.086 mmol, 1.5 eq.) of Fmoc-D-Asp(tBu)-ABA-OH were dissolved together with 11.6 mg (0.086 mmol, 1.5 eq.) HOAt, 13.4  $\mu$ L (0.086 mmol, 1.5 eq.) DIC and 43.5  $\mu$ L (0.256 mmol, 4.5 eq.) of DIPEA in DMF and stirred for 15 min. The mixture was added to 40.0 mg (0.057 mmol, 1.0 eq.) of **11** in DMF and stirred for 3 h at rt. After precipitation of the peptide in diethyl ether and freeze-drying overnight, the crude peptide was used without further purification. After Fmoc-deprotection, conjugation with DOTA was performed and the resulting product was purified using HPLC (27 to 37% B in 20 min). 3.38 mg (2.56  $\mu$ mol, 5%) of the iodination precursor were treated with 0.55 eq. NIS. 1.6 mg (1.1  $\mu$ mol, 2%) of a white solid were collected. HPLC (25 to 55% B in 15 min):  $t_R$  = 8.3 min;  $K'$  = 4.9. Calculated monoisotopic mass ( $C_{63}H_{82}IN_{15}O_{17}$ ): 1447.51; found:  $m/z$  = 1448.8  $[M+H]^+$ , 725.3  $[M+H+H]^{2+}$ .

### cyclo[(3-*iodo*)D-Tyr-N(Me)-D-Orn(DOTA-D-Dap-Gly-(ABA)-Arg-2-Nal-Gly)] (30):



0.2 g of resin bound Fmoc-ABA (0.224 mmol, 1.0 eq.) were allowed to pre swell for 30 min in DMF. 199.6 mg (0.672 mmol, 3.0 eq.) Fmoc-Gly-OH was dissolved together with 255.4 mg (0.672 mmol, 3.0 eq.) HATU, 91.5 mg (0.672 mmol, 3.0 eq.) HOAt and 228.1  $\mu$ L (1.34 mmol, 6.0 eq.) DIPEA 20.3 mg (0.086 mmol, 1.5 eq.) in DMF and stirred for 15 min. The mixture was added to the resin and the reaction

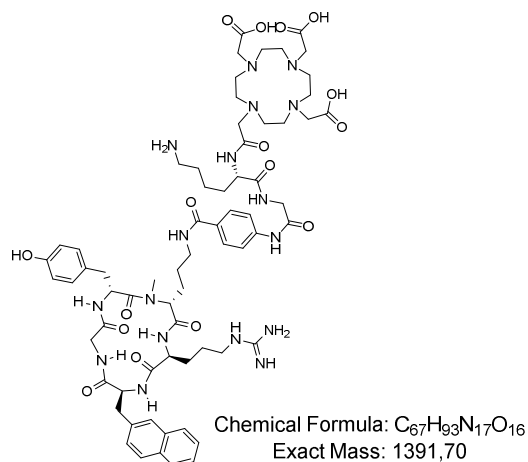
was shaken for 3 h at rt. After washing and Fmoc-deprotection, a solution of 109.6 mg (0.34 mmol, 1.5 eq.) of Fmoc-D-Dap(Boc)-OH, 45.4 mg (0.34 mmol, 1.5 eq.) HOBt, 107.9 mg (1.5 mmol, 1.5 eq.) TBTU and 259.7  $\mu$ L (1.53 mmol, 4.5 eq.) of DIPEA was added and the mixture was stirred for 3 h. The linear peptide was cleaved from the resin under standard conditions (see II.2.1), precipitated in diethyl ether and freeze-dried overnight to give the linking

## MATERIALS AND METHODS

unit. HPLC (10 to 90% B in 15 min):  $t_R = 12.0$  min;  $K' = 5.3$ . Calculated monoisotopic mass ( $C_{32}H_{34}N_4O_8$ ): 602.24; found:  $m/z = 502.5$  [(M-Boc)+H] $^+$ .

51.8 mg (0.086 mmol, 1.5 eq.) of Fmoc-D-Dap(Boc)-Gly-ABS-OH were dissolved together with 11.6 mg (0.086 mmol, 1.5 eq.) HOAt, 13.4  $\mu$ L (0.086 mmol, 1.5 eq.) DIC and 43.5  $\mu$ L (0.256 mmol, 4.5 eq.) of DIPEA in DMF and stirred for 15 min. The mixture was added to 40.0 mg (0.057 mmol, 1.0 eq.) of **11** in DMF and the solution was stirred for 3 h at rt. After precipitation of the peptide in diethyl ether and freeze drying overnight, the crude peptide was used without further purification. After Fmoc-deprotection, conjugation with DOTA was performed according to the protocol in II.2.2. and the resulting product was purified using HPLC (28 to 50% B in 20 min). 4.0 mg (2.8  $\mu$ mol, 5%) of the iodination precursor were treated with 0.50 eq. NIS as described in II.2.1. 1.4 mg (0.95  $\mu$ mol, 2%) of a white solid were collected. HPLC (25 to 65% B in 15 min):  $t_R = 11.89$  min;  $K' = 5.2$ . Calculated monoisotopic mass ( $C_{64}H_{86}IN_{17}O_{16}$ ): 1475.55; found:  $m/z = 1476.8$  [M+H] $^+$ , 739.3 [M+H+H] $^{2+}$ .

**cyclo[D-Tyr-N(Me)-D-Orn(DOTA-D-Lys-Gly-ABA)-Arg-2-Nal-Gly] (31):** The linking



unit was synthesized according to the previous protocol using 159.2 mg (0.34 mmol, 1.5 eq.) of Fmoc-D-Lys(Boc)-OH, 45.4 mg (0.34 mmol, 1.5 eq.) The linear peptide was cleaved from the resin under standard conditions (see II.2.1), precipitated in diethyl ether and freeze-dried overnight. HPLC (10 to 90% B in 15 min):  $t_R = 13.0$  min;  $K' = 5.8$ . Calculated monoisotopic mass ( $C_{32}H_{34}N_4O_8$ ): 644.28;

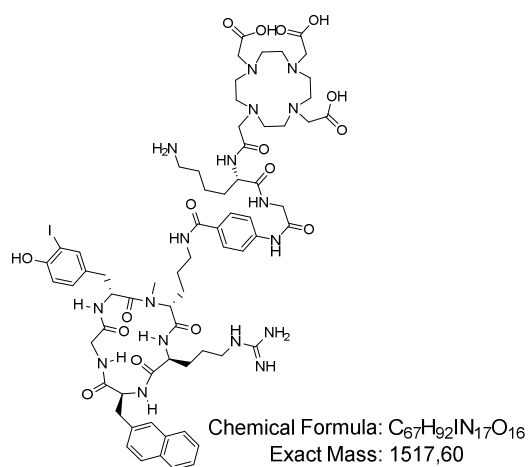
found:  $m/z = 545.4$  [(M-Boc)+H] $^+$ .

55.4 mg (0.086 mmol, 1.5 eq.) of Fmoc-D-Lys(Boc)-Gly-ABS-OH were dissolved together with 11.6 mg (0.086 mmol, 1.5 eq.) HOAt, 13.4  $\mu$ L (0.086 mmol, 1.5 eq.) DIC and 43.5  $\mu$ L (0.256 mmol, 4.5 eq.) of DIPEA in DMF and stirred for 15 min. The mixture was added to 40.0 mg (0.057 mmol, 1.0 eq.) of **11** in DMF and the solution was stirred for 3 h at rt. After

## MATERIALS AND METHODS

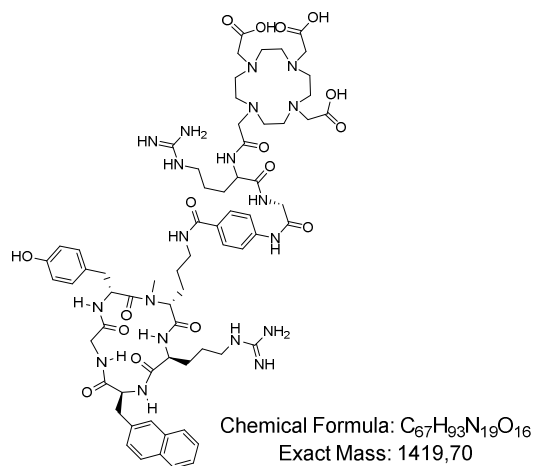
precipitation of the peptide in diethyl ether and drying, the crude peptide was Fmoc-deprotected. After Fmoc-deprotection, DOTA•6 H<sub>2</sub>O was conjugated according to the protocol in II.2.2 and the resulting product was purified using HPLC (22 to 38% B in 20 min). 13.9 mg (9.9 μmol, 18%). HPLC (15 to 55% B in 15 min):  $t_R$  = 7.9 min;  $K'$  = 7.0. Calculated monoisotopic mass (C<sub>67</sub>H<sub>93</sub>N<sub>17</sub>O<sub>16</sub>): 1391.70; found:  $m/z$  = 1393.2 [M+H]<sup>+</sup>.

### cyclo[(3-*iodo*)D-Tyr-N(Me)-D-Orn(DOTA-D-Lys-Gly-ABA)-Arg-2-Nal-Gly] (**32**):



6.0 mg (4.3 μmol, 1.0 eq.) of **31** were treated with 0.40 eq. NIS as described in II.2.1. 2.2 mg (1.45 μmol, 2.5%) of a yellowish solid were collected. HPLC (25 to 55% B in 15 min):  $t_R$  = 12.8 min;  $K'$  = 7.0. Calculated monoisotopic mass (C<sub>67</sub>H<sub>92</sub>IN<sub>17</sub>O<sub>16</sub>): 1517.60; found:  $m/z$  = 1519.1 [M+H]<sup>+</sup>, 760.4 [M+H+H]<sup>2+</sup>.

### cyclo[D-Tyr-N(Me)-D-Orn(DOTA-D-Arg-Gly-ABA)-Arg-2-Nal-Gly] (**33**):



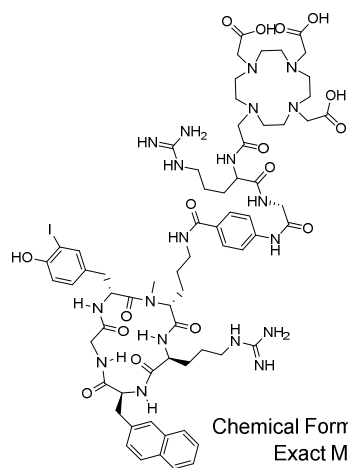
The linking unit was synthesized according to the previous protocol using 220.4 mg (0.34 mmol, 1.5 eq.) of Fmoc-D-Arg(Pbf)-OH. HPLC (10 to 90% B in 15 min):  $t_R$  = 12.6 min;  $K'$  = 5.3. Calculated monoisotopic mass (C<sub>30</sub>H<sub>32</sub>N<sub>6</sub>O<sub>6</sub>): 572.24; found:  $m/z$  = 573.5 [M+H]<sup>+</sup>.

49.2 mg (0.086 mmol, 1.5 eq.) of Fmoc-D-Arg-Gly-ABA were dissolved together with 11.6 mg (0.086 mmol, 1.5 eq.) HOAt, 13.4 μL (0.086 mmol, 1.5 eq.) DIC and 43.5 μL (0.256 mmol, 4.5 eq.) of DIPEA in DMF and stirred for 15 min. The mixture was added to 40.0 mg (0.057 mmol, 1.0 eq.) of **11** in DMF and the solution was stirred for 3 h at rt. After precipitation

## MATERIALS AND METHODS

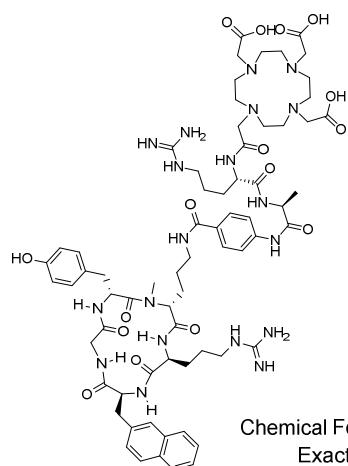
of the peptide in diethyl ether and freeze-drying overnight, the crude peptide was used without further purification. Conjugation with DOTA•6 H<sub>2</sub>O was performed according to the protocol described in II.2.2 and the resulting product was purified using HPLC (32 to 40% B in 20 min). 5.6 mg (3.9 μmol, 7%) of a yellowish solid were collected. HPLC (15 to 55% B in 15 min):  $t_R$  = 8.2 min;  $K'$  = 4.8. Calculated monoisotopic mass (C<sub>67</sub>H<sub>93</sub>N<sub>19</sub>O<sub>16</sub>): 1419.70; found:  $m/z$  = 1421.5 [M+H]<sup>+</sup>.

### cyclo[(3-iodo)D-Tyr-N(Me)-D-Orn(DOTA-D-Arg-Gly-ABA)-Arg-2-Nal-Gly] (34):



4.0 mg (2.5 μmol, 1.0 eq.) of **33** were treated with 0.70 eq. NIS as described in II.2.1. 1.1 mg (0.71 μmol, 1.2%) of a yellowish solid was collected. HPLC (25 to 55% B in 15 min):  $t_R$  = 13.3 min;  $K'$  = 5.6. Calculated monoisotopic mass (C<sub>67</sub>H<sub>92</sub>IN<sub>19</sub>O<sub>16</sub>): 1545.60; found:  $m/z$  = 1547.2 [M+H]<sup>+</sup>, 774.5 [M+H+H]<sup>2+</sup>.

### cyclo[D-Tyr-N(Me)-D-Orn(DOTA-D-Arg-D-Ala-ABA)-Arg-2-Nal-Gly] (35):



0.2 g of resin bound Fmoc-ABA (0.224 mmol, 1.0 eq.) were allowed to pre swell for 30 min in DMF. 209.0 mg (0.672 mmol, 3.0 eq.) Fmoc-D-Ala-OH was dissolved together with 255.4 mg (0.672 mmol, 3.0 eq.) HATU, 91.5 mg (0.672 mmol, 3.0 eq.) HOAt and 228.1 μL (1.34 mmol, 6.0 eq.) DIPEA 20.3 mg (0.086 mmol, 1.5 eq.) in DMF and stirred for 15 min. The mixture was added to the resin

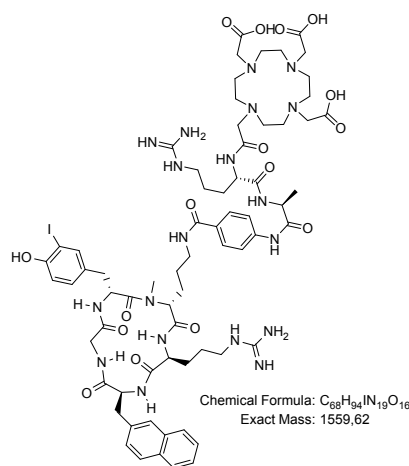
and the reaction was shaken for 3 h at rt. After washing and Fmoc-deprotection, a solution of 220.4 mg (0.34 mmol, 1.5 eq.) of Fmoc-D-Arg(Pbf)-OH, 45.4 mg (0.34 mmol, 1.5 eq.) HOBt,

## MATERIALS AND METHODS

107.9 mg (1.5 mmol, 1.5 eq.) TBTU and 259.7  $\mu\text{L}$  (1.53 mmol, 4.5 eq.) of DIPEA was added and the mixture was stirred for 3 h. The linear peptide was cleaved from the resin under standard conditions (see II.2.1), precipitated in diethyl ether and freeze-dried overnight to yield the linking unit. HPLC (10 to 90% B in 15 min):  $t_R = 11.6$  min;  $K' = 5.4$ . Calculated monoisotopic mass ( $\text{C}_{31}\text{H}_{34}\text{N}_6\text{O}_6$ ): 586.25; found:  $m/z = 587.5$   $[\text{M}+\text{H}]^+$ .

50.4 mg (0.086 mmol, 1.5 eq.) of Fmoc-D-Arg-D-Ala-ABA were dissolved together with 11.6 mg (0.086 mmol, 1.5 eq.) HOAt, 13.4  $\mu\text{L}$  (0.086 mmol, 1.5 eq.) DIC and 43.5  $\mu\text{L}$  (0.256 mmol, 4.5 eq.) of DIPEA in DMF and stirred for 15 min. The mixture was added to 40.0 mg (0.057 mmol, 1.0 eq.) of **11** in DMF and the solution was stirred for 3 h at rt. After Fmoc-deprotection, conjugation with DOTA was performed according to the protocol in II.2.2 and the resulting product was purified using HPLC (30 to 42% B in 20 min). 7.3 mg (5.1  $\mu\text{mol}$ , 8.9%) of a yellowish solid were collected. HPLC (15 to 55% B in 15 min):  $t_R = 8.0$  min;  $K' = 3.0$ . Calculated monoisotopic mass ( $\text{C}_{68}\text{H}_{95}\text{N}_{19}\text{O}_{16}$ ): 1433.72; found:  $m/z = 1435.1$   $[\text{M}+\text{H}]^+$ , 717.3  $[\text{M}+\text{H}+\text{H}]^{2+}$ .

### cyclo[(3-*iodo*)D-Tyr-N(Me)-D-Orn(DOTA-D-Arg-D-Ala-ABA)-Arg-2-Nal-Gly] (**36**):



4.0 mg (2.8  $\mu\text{mol}$ , 1.0 eq.) of **35** were treated with 0.60 eq. NIS as described in II.2.1. 1.5 mg (0.96  $\mu\text{mol}$ , 1.6%) of a yellowish solid were collected. HPLC (25 to 55% B in 15 min):  $t_R = 12.1$  min;  $K' = 7.0$ . Calculated monoisotopic mass ( $\text{C}_{68}\text{H}_{94}\text{IN}_{19}\text{O}_{16}$ ): 1559.62; found:  $m/z = 1560.2$   $[\text{M}+\text{H}]^+$ , 781.5  $[\text{M}+\text{H}+\text{H}]^{2+}$ .

## MATERIALS AND METHODS

Metal complexation for *in vitro*  $IC_{50}$  studies.

**$^{nat}\text{Ga}$ -compounds:**  $^{nat}\text{Ga}^{\text{III}}$ -chelate formation was achieved using the protocol described in II.2.2. The resulting 1 mM aqueous solutions of the respective  $^{nat}\text{Ga}$ -complexes were diluted (serial dilution  $10^{-4}$  to  $10^{-11}$  M in *Hanks salt solution* (HBSS) with 1% BSA) and used in the *in vitro*  $IC_{50}$  studies without further processing. Pentixafor and Pentixather were used as intern standards for comparison of affinity and pharmacological behavior of the novel compounds.

**cyclo[D-Tyr-N(Me)-D-Orn( $^{nat}\text{Ga}$ -DOTA-AMBA)-Arg-2-Nal-Gly] ( $^{nat}\text{Ga}$ 23):** HPLC (30 to 55% B in 15 min):  $t_R = 9.0$  min;  $K' = 5.0$ ; Calculated monoisotopic mass ( $\text{C}_{60}\text{H}_{78}\text{GaN}_{14}\text{O}_{14}$ ): 1,287.50; found by ESI-MS:  $m/z = 1,287.7$   $[\text{M}+\text{H}]^+$ , 1,311.7  $[\text{M}+\text{Na}]^+$ .

**cyclo[(3-*iodo*)D-Tyr-N(Me)-D-Orn( $^{nat}\text{Ga}$ -DOTA-AMBA)-Arg-2-Nal-Gly] ( $^{nat}\text{Ga}$ 24):** HPLC (30 to 55% B in 15 min):  $t_R = 10.8$  min;  $K' = 5.8$ ; Calculated monoisotopic mass ( $\text{C}_{60}\text{H}_{77}\text{GaIN}_{14}\text{O}_{14}$ ): 1,413.40; found by ESI-MS:  $m/z = 1,414.9$   $[\text{M}+\text{H}]^+$ , 1,437.2  $[\text{M}+\text{Na}]^+$ , 707.6  $[\text{M}+2\text{H}]^{2+}$ .

**cyclo[(3-*iodo*)D-Tyr-N(Me)-D-Orn( $^{nat}\text{Ga}$ -DOTA-ABA)-Arg-2-Nal-Gly] ( $^{nat}\text{Ga}$ 25):** HPLC (35 to 60% B in 15 min):  $t_R = 8.1$  min;  $K' = 4.4$ ; Calculated monoisotopic mass ( $\text{C}_{59}\text{H}_{74}\text{ILuN}_{14}\text{O}_{14}$ ): 1,504.40; found by ESI-MS:  $m/z = 1,505.9$   $[\text{M}+\text{H}]^+$ , 1,527.7  $[\text{M}+\text{Na}]^+$ , 1,543.7  $[\text{M}+\text{K}]^+$ , 753.6  $[\text{M}+2\text{H}]^{2+}$ .

**cyclo[(3-*iodo*)D-Tyr-N(Me)-D-Orn( $^{nat}\text{Ga}$ -DOTAGA-ABA)-Arg-2-Nal-Gly] ( $^{nat}\text{Ga}$ 26):** HPLC (35 to 60% B in 15 min):  $t_R = 7.0$  min;  $K' = 4.0$ ; Calculated monoisotopic mass ( $\text{C}_{62}\text{H}_{79}\text{IGaN}_{14}\text{O}_{16}$ ): 1471.42, found by ESI-MS:  $m/z = 1472.6$   $[\text{M}+\text{H}]^+$ , 736.8  $[\text{M}+2\text{H}]^{2+}$ .

**cyclo[(3-*iodo*)D-Tyr-N(Me)-D-Orn( $^{nat}\text{Ga}$ -DOTA-Gly-ABA)-Arg-2-Nal-Gly] ( $^{nat}\text{Ga}$ 27):** HPLC (35 to 60% B in 15 min):  $t_R = 9.1$  min;  $K' = 5.5$ ; Calculated monoisotopic mass ( $\text{C}_{61}\text{H}_{78}\text{GaIN}_{15}\text{O}_{15}$ ): 1456.41, found by ESI-MS:  $m/z = 1456.8$   $[\text{M}+\text{H}]^+$ , 1,478.5  $[\text{M}+\text{Na}]^+$ .

**cyclo[(3-*iodo*)D-Tyr-N(Me)-D-Orn( $^{nat}\text{Ga}$ -DOTAGA-Gly-ABA)-Arg-2-Nal-Gly] ( $^{nat}\text{Ga}$ 28):** HPLC (30 to 55% B in 15 min):  $t_R = 12.8$  min;  $K' = 6.1$ ; Calculated monoisotopic mass ( $\text{C}_{64}\text{H}_{82}\text{GaIN}_{15}\text{O}_{17}$ ): 1528.43, found by ESI-MS:  $m/z = 1528.4$   $[\text{M}+\text{H}]^+$ , 1552.7  $[\text{M}+\text{Na}]^+$ , 765.9  $[\text{M}+2\text{H}]^{2+}$ , 776.7  $[\text{M}+\text{H}+\text{Na}]^{2+}$ .

## MATERIALS AND METHODS

**cyclo[(3-*iodo*)D-Tyr-N(Me)-D-Orn(<sup>nat</sup>Ga-DOTA-D-Dap-Gly-ABA)-Arg-2-Nal-Gly]**

(<sup>[natGa]</sup>**30**): HPLC (25 to 65% B in 15 min):  $t_R = 11.4$  min;  $K' = 5.3$ ; Calculated monoisotopic mass (C<sub>64</sub>H<sub>84</sub>GaN<sub>17</sub>O<sub>16</sub>): 1542.46, found by ESI-MS:  $m/z = 1544.8$  [M+H]<sup>+</sup>, 772.4 [M+2H]<sup>2+</sup>.

**cyclo[D-Tyr-N(Me)-D-Orn(<sup>nat</sup>Ga-DOTA-D-Lys-Gly-ABA)-Arg-2-Nal-Gly] (<sup>[natGa]</sup>**31**):**

HPLC (15 to 55% B in 15 min):  $t_R = 7.6$  min;  $K' = 3.0$ ; Calculated monoisotopic mass (C<sub>67</sub>H<sub>91</sub>GaN<sub>17</sub>O<sub>16</sub>): 1458.61, found by ESI-MS:  $m/z = 1459.8$  [M+H]<sup>+</sup>, 730.2 [M+2H]<sup>2+</sup>.

**cyclo[(3-*iodo*)D-Tyr-N(Me)-D-Orn(<sup>nat</sup>Ga-DOTA-D-Lys-Gly-ABA)-Arg-2-Nal-Gly]**

(<sup>[natGa]</sup>**32**): HPLC (25 to 55% B in 15 min):  $t_R = 12.9$  min;  $K' = 6.1$ ; Calculated monoisotopic mass (C<sub>67</sub>H<sub>90</sub>GaN<sub>17</sub>O<sub>16</sub>): 1584.51, found by ESI-MS:  $m/z = 1585.0$  [M+H]<sup>+</sup>, 1608.9 [M+Na]<sup>+</sup>, 793.7 [M+2H]<sup>2+</sup>.

**cyclo[D-Tyr-N(Me)-D-Orn(<sup>nat</sup>Ga-DOTA-D-Arg-Gly-ABA)-Arg-2-Nal-Gly] (<sup>[natGa]</sup>**33**):**

HPLC (15 to 55% B in 15 min):  $t_R = 7.7$  min;  $K' = 3.2$ ; Calculated monoisotopic mass (C<sub>67</sub>H<sub>91</sub>GaN<sub>19</sub>O<sub>16</sub>): 1468.61, found by ESI-MS:  $m/z = 745.3$  [M+2H]<sup>2+</sup>.

**cyclo[(3-*iodo*)D-Tyr-N(Me)-D-Orn(<sup>nat</sup>Ga-DOTA-D-Arg-Gly-ABA)-Arg-2-Nal-Gly]**

(<sup>[natGa]</sup>**34**): HPLC (25 to 55% B in 15 min):  $t_R = 12.6$  min;  $K' = 6.8$ ; Calculated monoisotopic mass (C<sub>67</sub>H<sub>90</sub>GaN<sub>19</sub>O<sub>16</sub>): 1612.51, found by ESI-MS:  $m/z = 1614.9$  [M+H]<sup>+</sup>, 808.0 [M+2H]<sup>2+</sup>.

**cyclo[D-Tyr-N(Me)-D-Orn(<sup>nat</sup>Ga-DOTA-D-Arg-D-Ala-ABA)-Arg-2-Nal-Gly]**

(<sup>[natGa]</sup>**35**): HPLC (15 to 55% B in 15 min):  $t_R = 6.8$  min;  $K' = 3.5$ ; Calculated monoisotopic mass (C<sub>68</sub>H<sub>93</sub>GaN<sub>19</sub>O<sub>16</sub>): 1500.63, found by ESI-MS:  $m/z = 751.5$  [M+2H]<sup>2+</sup>, 787.2 [M+2K]<sup>2+</sup>.

**cyclo[(3-*iodo*)D-Tyr-N(Me)-D-Orn(<sup>nat</sup>Ga-DOTA-D-Arg-D-Ala-ABA)-Arg-2-Nal-Gly]**

(<sup>[natGa]</sup>**36**): HPLC (25% to 55% B in 15 min):  $t_R = 7.9$  min;  $K' = 3.9$ ; Calculated monoisotopic mass (C<sub>68</sub>H<sub>92</sub>GaN<sub>19</sub>O<sub>16</sub>): 1626.53, found by ESI-MS:  $m/z = 1626.8$  [M+H]<sup>+</sup>, 815.0 [M+2H]<sup>2+</sup>.

**<sup>nat</sup>Lu-compounds:** <sup>nat</sup>Lu<sup>III</sup>-chelate formation was achieved using the protocol described under II.2.2. The resulting 1 mM aqueous solutions of the respective <sup>nat</sup>Lu-complexes were diluted (serial dilution 10<sup>-4</sup> to 10<sup>-11</sup> M in HBSS with 1% BSA) and used in the *in vitro* IC<sub>50</sub> studies without further processing.

## MATERIALS AND METHODS

**cyclo[(3-*iodo*)D-Tyr-N(Me)-D-Orn(<sup>nat</sup>Lu-DOTA-AMBA)-Arg-2-Nal-Gly] ([<sup>nat</sup>Lu]24):**

HPLC (15 to 55% B in 15 min):  $t_R = 6.3$  min;  $K' = 4.3$ ; Calculated monoisotopic mass ( $C_{60}H_{76}ILuN_{14}O_{14}$ ): 1,518.41; found by ESI-MS:  $m/z = 1,520.1$   $[M+H]^+$ , 760.8  $[M+2H]^{2+}$ .

**cyclo[(3-*iodo*)D-Tyr-N(Me)-D-Orn(<sup>nat</sup>Lu-DOTA-ABA)-Arg-2-Nal-Gly] ([<sup>nat</sup>Lu]25):**

HPLC (35 to 60% B in 15 min):  $t_R = 8.1$  min;  $K' = 4.4$ ; Calculated monoisotopic mass ( $C_{59}H_{74}ILuN_{14}O_{14}$ ): 1,504.40; found by ESI-MS:  $m/z = 1,505.9$   $[M+H]^+$ , 1,527.7  $[M+Na]^+$ , 1,543.7  $[M+K]^+$ , 753.6  $[M+2H]^{2+}$ .

**cyclo[(3-*iodo*)D-Tyr-N(Me)-D-Orn(<sup>nat</sup>Lu-DOTAGA-ABA)-Arg-2-Nal-Gly] ([<sup>nat</sup>Lu]26):**

HPLC (35 to 60% B in 15 min):  $t_R = 9.2$  min;  $K' = 4.1$ ; Calculated monoisotopic mass ( $C_{62}H_{78}ILuN_{14}O_{16}$ ): 1576.42, found by ESI-MS:  $m/z = 1577.6$   $[M+H]^+$ , 1,600.5  $[M+Na]^+$ , 789.5  $[M+2H]^{2+}$ , 800.5  $[M+H+Na]^{2+}$ .

**cyclo[(3-*iodo*)D-Tyr-N(Me)-D-Orn(<sup>nat</sup>Lu-DOTA-Gly-ABA)-Arg-2-Nal-Gly]**

**([<sup>nat</sup>Lu]27):** HPLC (35 to 60% B in 15 min):  $t_R = 9.1$  min;  $K' = 5.5$ ; Calculated monoisotopic mass ( $C_{61}H_{77}ILuN_{15}O_{15}$ ): 1561.42, found by ESI-MS:  $m/z = 1562.6$   $[M+H]^+$ , 1,584.5  $[M+Na]^+$ , 782.0  $[M+2H]^{2+}$ , 792.9  $[M+H+Na]^{2+}$ .

**cyclo[(3-*iodo*)D-Tyr-N(Me)-D-Orn(<sup>nat</sup>Ga-DOTAGA-Gly-ABA)-Arg-2-Nal-Gly]**

**([<sup>nat</sup>Lu]28):** HPLC (35 to 60% B in 15 min):  $t_R = 9.3$  min;  $K' = 4.2$ ; Calculated monoisotopic mass ( $C_{64}H_{81}ILuN_{15}O_{17}$ ): 1633.44, found by ESI-MS:  $m/z = 1634.7$   $[M+H]^+$ , 1,656.6  $[M+Na]^+$ , 818.1  $[M+2H]^{2+}$ , 829.0  $[M+H+Na]^{2+}$ .

**cyclo[(3-*iodo*)D-Tyr-N(Me)-D-Orn(<sup>nat</sup>Lu-DOTA-D-Asp-ABA)-Arg-2-Nal-Gly]**

**([<sup>nat</sup>Lu]29):** HPLC (35 to 65% B in 15 min):  $t_R = 8.0$  min;  $K' = 3.4$ ; Calculated monoisotopic mass ( $C_{63}H_{79}ILuN_{15}O_{17}$ ): 1619.42, found by ESI-MS:  $m/z = 1620.9$   $[M+H]^+$ , 1,642.8  $[M+Na]^+$ , 811.2  $[M+2H]^{2+}$ , 822.0  $[M+H+Na]^{2+}$ .

**cyclo[(3-*iodo*)D-Tyr-N(Me)-D-Orn(<sup>nat</sup>Lu-DOTA-D-Dap-Gly-ABA)-Arg-2-Nal-Gly]**

**([<sup>nat</sup>Lu]30):** HPLC (25 to 65% B in 15 min):  $t_R = 10.8$  min;  $K' = 9.8$ ; Calculated monoisotopic mass ( $C_{64}H_{83}ILuN_{17}O_{16}$ ): 1647.47, found by ESI-MS:  $m/z = 1648.9$   $[M+H]^+$ , 825.2  $[M+2H]^{2+}$ , 860.5  $[M+2K]^{2+}$ .



## MATERIALS AND METHODS

**cyclo[D-Tyr-N(Me)-D-Orn(<sup>nat</sup>Lu-DOTA-D-Lys-Gly-ABA)-Arg-2-Nal-Gly] ([<sup>nat</sup>Lu]31):**

HPLC (15 to 55% B in 15 min):  $t_R = 7.5$  min;  $K' = 4.0$ ; Calculated monoisotopic mass ( $C_{67}H_{90}LuN_{17}O_{16}$ ): 1563.62, found by ESI-MS:  $m/z = 1565.4$   $[M+H]^+$ .

**cyclo[(3-*iodo*)D-Tyr-N(Me)-D-Orn(<sup>nat</sup>Lu-DOTA-D-Lys-Gly-ABA)-Arg-2-Nal-Gly]**

([<sup>nat</sup>Lu]32): HPLC (25 to 55% B in 15 min):  $t_R = 13.1$  min;  $K' = 7.7$ ; Calculated monoisotopic mass ( $C_{67}H_{89}ILuN_{17}O_{16}$ ): 1689.51, found by ESI-MS:  $m/z = 1691.8$   $[M+H]^+$ , 1712.7  $[M+Na]^+$ , 846.4  $[M+2H]^{2+}$ , 857.1  $[M+H+Na]^{2+}$ .

**cyclo[D-Tyr-N(Me)-D-Orn(<sup>nat</sup>Lu-DOTA-D-Arg-Gly-ABA)-Arg-2-Nal-Gly] ([<sup>nat</sup>Lu]33):**

HPLC (15 to 55% B in 15 min):  $t_R = 7.2$  min;  $K' = 4.1$ ; Calculated monoisotopic mass ( $C_{67}H_{90}LuN_{19}O_{16}$ ): 1591.62, found by ESI-MS:  $m/z = 1592.5$   $[M+H]^+$ , 1631.0  $[M+K]^+$ .

**cyclo[(3-*iodo*)D-Tyr-N(Me)-D-Orn(<sup>nat</sup>Lu-DOTA-D-Arg-Gly-ABA)-Arg-2-Nal-Gly]**

([<sup>nat</sup>Lu]34): HPLC (25 to 55% B in 15 min):  $t_R = 13.4$  min;  $K' = 7.9$ ; Calculated monoisotopic mass ( $C_{67}H_{89}IN_{19}O_{16}$ ): 1717.52, found by ESI-MS:  $m/z = 1719.9$   $[M+H]^+$ , 860.5  $[M+2H]^{2+}$ , 871.1  $[M+H+Na]^{2+}$ , 895.7  $[M+2K]^{2+}$ .

**cyclo[D-Tyr-N(Me)-D-Orn(<sup>nat</sup>Lu-DOTA-D-Arg-D-Ala-ABA)-Arg-2-Nal-Gly]**

([<sup>nat</sup>Lu]35): HPLC (15 to 55% B in 15 min):  $t_R = 7.5$  min;  $K' = 4.0$ ; Calculated monoisotopic mass ( $C_{68}H_{92}LuN_{19}O_{16}$ ): 1605.64, found by ESI-MS:  $m/z = 1607.2$   $[M+H]^+$ , 804.6  $[M+2H]^{2+}$ .

**cyclo[(3-*iodo*)D-Tyr-N(Me)-D-Orn(<sup>nat</sup>Lu-DOTA-D-Arg-D-Ala-ABA)-Arg-2-Nal-Gly]**

([<sup>nat</sup>Lu]36): HPLC (25 to 55% B in 15 min):  $t_R = 6.5$  min;  $K' = 2.3$ ; Calculated monoisotopic mass ( $C_{68}H_{91}ILuN_{19}O_{16}$ ): 1731.53, found by ESI-MS:  $m/z = 1732.8$   $[M+H]^+$ , 867.3  $[M+2H]^{2+}$ , 902.6  $[M+2K]^{2+}$ .

The <sup>nat</sup>Y-complexes were prepared as described under II.2.2. After cooling, the <sup>nat</sup>Y<sup>III</sup>-chelate formation was confirmed using HPLC and MS. The resulting 1 mM aqueous solutions of the respective <sup>nat</sup>Y-complexes were diluted (serial dilution  $10^{-4}$  to  $10^{-11}$  M in HBSS with 1% BSA) and used in the *in vitro*  $IC_{50}$  studies without further processing.

## MATERIALS AND METHODS

**cyclo[(3-*iodo*)D-Tyr-N(Me)-D-Orn(<sup>nat</sup>Y-DOTA-AMBA)-Arg-2-Nal-Gly] ([<sup>nat</sup>Y]24):**

HPLC (15 to 55% B in 15 min):  $t_R = 6.5$  min;  $K' = 3.6$ ; Calculated monoisotopic mass ( $C_{60}H_{76}IN_{14}O_{14}Y$ ): 1432.38; found by ESI-MS:  $m/z = 1,433.6$   $[M+H]^+$ , 1,455.8  $[M+Na]^+$ , 717.4  $[M+2H]^{2+}$ .

**cyclo[(3-*iodo*)D-Tyr-N(Me)-D-Orn(<sup>nat</sup>Y-DOTA-ABA)-Arg-2-Nal-Gly] ([<sup>nat</sup>Y]25):**

HPLC (35 to 60% B in 15 min):  $t_R = 4.9$  min;  $K' = 2.3$ ; Calculated monoisotopic mass ( $C_{59}H_{74}IN_{14}O_{14}Y$ ): 1418.36; found by ESI-MS:  $m/z = 1,419.8$   $[M+H]^+$ , 1,442.7  $[M+Na]^+$ , 710.4  $[M+2H]^{2+}$ .

**cyclo[(3-*iodo*)D-Tyr-N(Me)-D-Orn(<sup>nat</sup>Y-DOTAGA-ABA)-Arg-2-Nal-Gly] ([<sup>nat</sup>Y]26):**

HPLC (35 to 60% B in 15 min):  $t_R = 9.2$  min;  $K' = 4.4$ ; Calculated monoisotopic mass ( $C_{62}H_{78}IN_{14}O_{16}Y$ ): 1490.38, found by ESI-MS:  $m/z = 1491.6$   $[M+H]^+$ , 1513.5  $[M+Na]^+$ , 746.5  $[M+2H]^{2+}$ , 757.4  $[M+H+Na]^{2+}$ .

**cyclo[(3-*iodo*)D-Tyr-N(Me)-D-Orn(<sup>nat</sup>Y-DOTA-Gly-ABA)-Arg-2-Nal-Gly] ([<sup>nat</sup>Y]27):**

HPLC (35 to 60% B in 15 min):  $t_R = 8.2$  min;  $K' = 7.2$ ; Calculated monoisotopic mass ( $C_{61}H_{77}IN_{15}O_{15}Y$ ): 1475.38, found by ESI-MS:  $m/z = 1476.7$   $[M+H]^+$ , 1498.5  $[M+Na]^+$ , 739.0  $[M+2H]^{2+}$ , 750.0  $[M+H+Na]^{2+}$ .

**cyclo[(3-*iodo*)D-Tyr-N(Me)-D-Orn(<sup>nat</sup>Y-DOTAGA-Gly-ABA)-Arg-2-Nal-Gly]**

**([<sup>nat</sup>Y]28):** HPLC (35 to 65% B in 15 min):  $t_R = 9.2$  min;  $K' = 4.1$ ; Calculated monoisotopic mass ( $C_{64}H_{81}IN_{15}O_{17}Y$ ): 1547.40, found by ESI-MS:  $m/z = 1548.6$   $[M+H]^+$ , 1570.4  $[M+Na]^+$ , 775.0  $[M+2H]^{2+}$ , 785.9  $[M+H+Na]^{2+}$ .

**cyclo[(3-*iodo*)D-Tyr-N(Me)-D-Orn(<sup>nat</sup>Y-DOTA-D-Dap-Gly-ABA)-Arg-2-Nal-Gly]**

**[<sup>nat</sup>Y]30):** HPLC (25 to 65% B in 15 min):  $t_R = 11.5$  min;  $K' = 6.1$ ; Calculated monoisotopic mass ( $C_{64}H_{83}IN_{17}O_{16}Y$ ): 1561.43, found by ESI-MS:  $m/z = 1562.7$   $[M+H]^+$ , 782.3  $[M+2H]^{2+}$ , 793.0  $[M+H+Na]^{2+}$ .

**cyclo[D-Tyr-N(Me)-D-Orn(<sup>nat</sup>Y-DOTA-D-Lys-Gly-ABA)-Arg-2-Nal-Gly] ([<sup>nat</sup>Y]31):**

HPLC (15 to 55% B in 15 min):  $t_R = 7.8$  min;  $K' = 2.7$ ; Calculated monoisotopic mass ( $C_{67}H_{90}N_{17}O_{16}Y$ ): 1477.58, found by ESI-MS:  $m/z = 1478.9$   $[M+H]^+$ , 740.4  $[M+2H]^{2+}$ .

## MATERIALS AND METHODS

**cyclo[(3-iodo)D-Tyr-N(Me)-D-Orn(<sup>nat</sup>Y-DOTA-D-Lys-Gly-ABA)-Arg-2-Nal-Gly]**

(<sup>[natY]</sup>**32**): HPLC (25 to 55% B in 15 min):  $t_R = 12.9$  min;  $K' = 7.6$ ; Calculated monoisotopic mass ( $C_{67}H_{89}IN_{17}O_{16}Y$ ): 1603.48, found by ESI-MS:  $m/z = 1605.7$   $[M+H]^+$ , 1626.6  $[M+Na]^+$ , 803.4  $[M+2H]^{2+}$ , 814.1  $[M+H+Na]^{2+}$ .

**cyclo[D-Tyr-N(Me)-D-Orn(<sup>nat</sup>Y-DOTA-D-Arg-Gly-ABA)-Arg-2-Nal-Gly]** (<sup>[natY]</sup>**33**):

HPLC (15 to 55% B in 15 min):  $t_R = 8.0$  min;  $K' = 2.8$ ; Calculated monoisotopic mass ( $C_{67}H_{90}N_{19}O_{16}Y$ ): 1505.59, found by ESI-MS:  $m/z = 1506.2$   $[M+H]^+$ , 754.3  $[M+2H]^{2+}$ .

**cyclo[(3-iodo)D-Tyr-N(Me)-D-Orn(<sup>nat</sup>Y-DOTA-D-Arg-Gly-ABA)-Arg-2-Nal-Gly]**

(<sup>[natY]</sup>**34**): HPLC (25 to 55% B in 15 min):  $t_R = 13.3$  min;  $K' = 7.9$ ; Calculated monoisotopic mass ( $C_{67}H_{89}IN_{19}O_{16}Y$ ): 1631.48, found by ESI-MS:  $m/z = 1632.9$   $[M+H]^+$ , 817.4  $[M+2H]^{2+}$ , 828.1  $[M+H+Na]^{2+}$ , 852.7  $[M+2K]^{2+}$ .

**cyclo[D-Tyr-N(Me)-D-Orn(<sup>nat</sup>Y-DOTA-D-Arg-D-Ala-ABA)-Arg-2-Nal-Gly]** (<sup>[natY]</sup>**35**):

HPLC (15 to 55% B in 15 min):  $t_R = 7.0$  min;  $K' = 3.6$ ; Calculated monoisotopic mass ( $C_{68}H_{92}N_{19}O_{16}Y$ ): 1519.60, found by ESI-MS:  $m/z = 761.0$   $[M+2H]^{2+}$ .

**cyclo[(3-iodo)D-Tyr-N(Me)-D-Orn(<sup>nat</sup>Y-DOTA-D-Arg-D-Ala-ABA)-Arg-2-Nal-Gly]**

(<sup>[natY]</sup>**36**): HPLC (25 to 55% B in 15 min):  $t_R = 9.6$  min;  $K' = 2.8$ ; Calculated monoisotopic mass ( $C_{68}H_{91}IN_{19}O_{16}Y$ ): 1645.50, found by ESI-MS:  $m/z = 1646.9$   $[M+H]^+$ , 824.1  $[M+2H]^{2+}$ , 859.5  $[M+2K]^{2+}$ .

Bismuth complexation was performed using the protocol described in II.2.2. Formation of the <sup>nat</sup>Bi<sup>III</sup>-chelate was confirmed using HPLC and ESI-MS. The resulting 1 mM aqueous solutions of the respective <sup>nat</sup>Bi-complexes were diluted (serial dilution  $10^{-4}$  to  $10^{-10}$  M in HBSS with 1% BSA) and used in the *in vitro*  $IC_{50}$  studies without further processing.

**cyclo[(3-iodo)D-Tyr-N(Me)-D-Orn(<sup>nat</sup>Bi-DOTA-AMBA)-Arg-2-Nal-Gly]** (<sup>[natBi]</sup>**24**):

HPLC (15 to 55% B in 15 min):  $t_R = 9.6$  min;  $K' = 4.3$ ; Calculated monoisotopic mass ( $C_{60}H_{76}BiIN_{14}O_{14}$ ): 1552.45; found by ESI-MS:  $m/z = 1,554.2$   $[M+H]^+$ , 778.2  $[M+2H]^{2+}$ .

## MATERIALS AND METHODS

**cyclo[(3-*iodo*)D-Tyr-N(Me)-D-Orn(<sup>nat</sup>Bi-DOTA-ABA)-Arg-2-Nal-Gly] ([<sup>nat</sup>Bi]25):**

HPLC (15 to 55% B in 15 min):  $t_R = 9.6$  min;  $K' = 5.0$ ; Calculated monoisotopic mass ( $C_{59}H_{74}BiN_{14}O_{14}$ ): 1538.44; found by ESI-MS:  $m/z = 1,540.6$   $[M+H]^+$ , 770.1  $[M+2H]^{2+}$ .

**cyclo[(3-*iodo*)D-Tyr-N(Me)-D-Orn(<sup>nat</sup>Bi-DOTA-Gly-ABA)-Arg-2-Nal-Gly] ([<sup>nat</sup>Bi]27):**

HPLC (15 to 55% B in 15 min):  $t_R = 9.5$  min;  $K' = 4.3$ ; Calculated monoisotopic mass ( $C_{61}H_{77}BiN_{15}O_{15}Y$ ): 1595.46, found by ESI-MS:  $m/z = 1597.4$   $[M+H]^+$ , 799.5  $[M+2H]^{2+}$ .

**cyclo[(3-*iodo*)D-Tyr-N(Me)-D-Orn(<sup>nat</sup>Bi-DOTA-D-Dap-Gly-ABA)-Arg-2-Nal-Gly]**

**([<sup>nat</sup>Bi]30):** HPLC (15 to 55% B in 15 min):  $t_R = 8.9$  min;  $K' = 3.9$ ; Calculated monoisotopic mass ( $C_{64}H_{83}BiN_{17}O_{16}$ ): 1681.51, found by ESI-MS:  $m/z = 1682.2$   $[M+H]^+$ , 839.8  $[M+2H]^{2+}$ .

**cyclo[(3-*iodo*)D-Tyr-N(Me)-D-Orn(<sup>nat</sup>Bi-DOTA-D-Lys-Gly-ABA)-Arg-2-Nal-Gly]**

**([<sup>nat</sup>Bi]32):** HPLC (15 to 55% B in 15 min):  $t_R = 8.9$  min;  $K' = 3.3$ ; Calculated monoisotopic mass ( $C_{67}H_{89}BiN_{17}O_{16}$ ): 1724.56, found by ESI-MS:  $m/z = 1726.2$   $[M+H]^+$ , 863.2  $[M+2H]^{2+}$ .

**cyclo[(3-*iodo*)D-Tyr-N(Me)-D-Orn(<sup>nat</sup>Bi-DOTA-D-Arg-Gly-ABA)-Arg-2-Nal-Gly]**

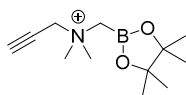
**([<sup>nat</sup>Bi]34):** HPLC (15 to 55% B in 15 min):  $t_R = 9.0$  min;  $K' = 3.7$ ; Calculated monoisotopic mass ( $C_{67}H_{89}BiN_{19}O_{16}$ ): 1751.56, found by ESI-MS:  $m/z = 1752.3$   $[M+H]^+$ .

**cyclo[(3-*iodo*)D-Tyr-N(Me)-D-Orn(<sup>nat</sup>Bi-DOTA-D-Arg-D-Ala-ABA)-Arg-2-Nal-Gly]**

**([<sup>nat</sup>Bi]36):** HPLC (15 to 55% B in 15 min):  $t_R = 9.1$  min;  $K' = 4.0$ ; Calculated monoisotopic mass ( $C_{68}H_{91}BiN_{19}O_{16}$ ): 1765.57, found by ESI-MS:  $m/z = 1767.5$   $[M+H]^+$ , 885.1  $[M+2H]^{2+}$ .

### 4.3. Precursor for radiofluorination (BF<sub>3</sub>-derivatives)

***N*-propargyl-*N,N*-dimethyl-ammoniomethylboronylpinacolate (37):** A dry round



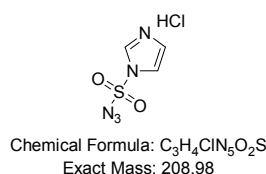
Chemical Formula:  $C_{12}H_{23}BNO_2^+$   
Exact Mass: 224,18

bottom flask was loaded with 53.8  $\mu$ L (0.5 mmol, 1.0 eq.) of *N,N*-dimethylpropargylamine and 3 mL of dry DCM under a nitrogen atmosphere. 80.1  $\mu$ L (0.5 mmol, 1.0 eq.) of iodomethyl-boronylpinacolate was added dropwise at rt. On stirring, the solution became cloudy and the white precipitated was filtered of after 2h of vigorously stirring at 0 °C. The precipitate was washed with ice cold

## MATERIALS AND METHODS

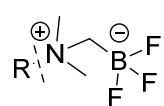
diethyl ether two times and used without further purification. 104 mg (0.45 mmol, 93%) of **37** were collected as a white solid. Calculated monoisotopic mass ( $C_{12}H_{23}BNO_2^+$ ): 224.18, found by ESI-MS:  $m/z = 224.2$   $[M]^+$ . **<sup>1</sup>H-NMR** (400 MHz [Bruker],  $CD_3CN$ ):  $\delta$  [ppm] = 1.31 (s, 12H), 3.17 (s, 6H), 3.21 (t, 2H), 3.23 (s, 1H), 4.22 (d, 2H).

**imidazole-1-sulfonyl azide hydrochloride (38):** The synthesis of **38** was performed



according to a published protocol<sup>164</sup>. Briefly, sulfonylchloride (1.62 mL, 20.0 mmol, 1.0 eq.) was added drop-wise to an ice-cooled suspension of  $NaN_3$  (1.3 g, 20.0 mmol, 1.0 eq.) in MeCN (20 mL) and the mixture was stirred overnight at rt. While stirring vigorously, imidazole (2.5 g, 38.0 mmol, 2.0 eq.) was added carefully to the ice-cooled solution and stirred for 3 h at rt. The solution was diluted with EtOAc (40 mL) and washed with water (2 x 40 mL) and saturated aqueous  $NaHCO_3$  (2 x 20 mL), dried over  $MgSO_4$  and filtered. A fresh solution of HCl in EtOH (obtained through drop-wise addition of AcCl (10.0 mL) to ice-cooled dry ethanol (25 mL)) was added slowly to the filtrate while stirring at 0 °C. The crystallized product was filtered off on ice and the white crystals were washed with ice cold EtOAc to give **38** as colorless needles (2.0 g, 9.5 mmol, 48%). The compound was used without further purification and stored at -20 °C.

**Ammoniomethyltrifluoroborate (AmBF<sub>3</sub>):** In the following synthesis procedures,

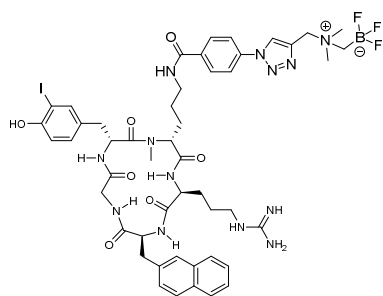


ammoniomethyltrifluoroborate (AmBF<sub>3</sub>) is produced *in situ* prior to the 1,3-cycloaddition as described in literature<sup>157, 165, 166</sup> and is always referred to as AmBF<sub>3</sub>.

**cyclo[(3-iodo)D-Tyr-N(Me)-D-Orn(AmBF<sub>3</sub>(methyl(1H-1,2,3-triazol-4-yl)4-amino)-**

**benzoyl)-Arg-Nal-Gly] (39):** Fmoc-ABA loaded TCP-resin (0.53 mmol, 1.0 eq.) was treated with 20% piperidine in DMF (v/v) to remove the Fmoc-protection group. After washing the resin with DMF two times, 204  $\mu$ L of DIPEA (1.2 mmol, 2.25 eq.) together with 2 mL of DMF were added to the resin and shaken for 10 min while cooling down to 0 °C. **38** (166 mg, 0.79 mmol, 1.5 eq.) dissolved in ice cold DMF was added to the resin bound peptide. 0.5 mg of

## MATERIALS AND METHODS

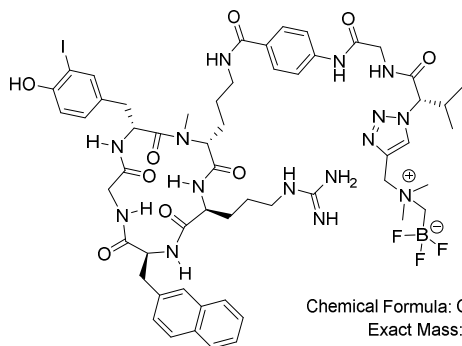


Chemical Formula: C<sub>49</sub>H<sub>60</sub>BF<sub>3</sub>IN<sub>13</sub>O<sub>7</sub>  
Exact Mass: 1137.38

CuSO<sub>4</sub> (catalytic amount) and 337  $\mu$ L (1.98 mmol, 3.75 eq.) DIPEA was dissolved in 1 ml of water and added to the peptide. Cooling was continued for 2 h and the resin bound peptide was shaken overnight while warming to rt. The peptide was cleaved from the resin and freeze-dried overnight. **37** (176.9 mg, 0.79 mmol, 1.5 eq.) dissolved in 700  $\mu$ L H<sub>2</sub>O and 2.1 mL DMF was combined with a solution of 1.05 mL KHF<sub>2</sub> (3 M solution in

water, 1.4 mmol, 2.6 eq.) and 1.1 mL HCl (4 M solution in water, 1.9 mmol, 3.6 eq.) and heated to 45 °C for 2 h. After addition of 1.2 mL of NH<sub>4</sub>OH (1 M in water) to adjust the pH to 3 to 4, the solution was added to the dry peptide, which was dissolved in <sup>t</sup>BuOH and water (v/v; 1/1). To start the cycloaddition 400  $\mu$ L of a 1 M CuSO<sub>4</sub> solution was added together with 350 mg (1.7 mmol, 3.3 eq.) sodium ascorbate. The slurry mixture was heated to 55 °C for 15 h and purified using HPLC (15 to 25% in 20 min). The purified fragment was coupled to **12** employing HOBt, TBTU and DIPEA under standard conditions. After final HPLC purification (25 to 45% in 20 min) the product was collected as yellowish powder (1.5 mg, 2%). HPLC (25 to 65% B in 15 min):  $t_R$  = 10.3 min;  $K'$  = 4.4; calculated monoisotopic mass (C<sub>49</sub>H<sub>60</sub>BF<sub>3</sub>IN<sub>13</sub>O<sub>7</sub>): 1137.38, found by ESI-MS:  $m/z$  = 1138.6 [M+H]<sup>+</sup>.

cyclo[(**3-iodo**)D-Tyr-N(Me)-D-Orn(AmBF<sub>3</sub>(methyl(1H-1,2,3-triazol-4-yl)-(R)-((1-(1-((2-((4-carboxyphenyl)-amino)-2-oxoethyl)amino)-3-methyl-1-oxobutan-2-yl))Arg-



Chemical Formula: C<sub>56</sub>H<sub>72</sub>BF<sub>3</sub>IN<sub>15</sub>O<sub>9</sub>  
Exact Mass: 1293.47

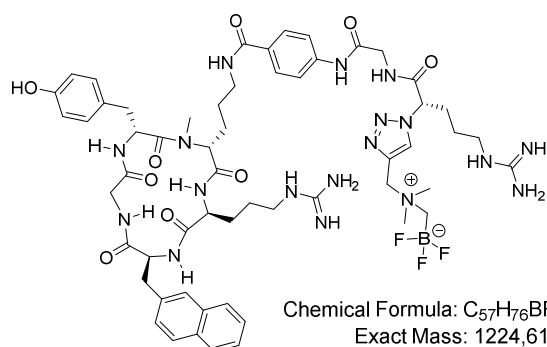
Nal-Gly] (**40**): Starting with Fmoc-ABA loaded resin, the introduction of Fmoc-Gly-OH and Fmoc-D-Val-OH was performed as described earlier (II.2.1.). After Fmoc-deprotection, the amine was converted to the respective azide as described for **39** employing **38**, DIPEA and CuSO<sub>4</sub>. The azide-peptide

fragment was cleaved from the resin and combined with **37** as described before (employing **39**).

## MATERIALS AND METHODS

After purification of the linear AmBF<sub>3</sub>-linking unit, it was converted to its respective pentafluorophenylester. Therefore, 23.5 mg of AmBF<sub>3</sub>(methyl(1H-1,2,3-triazol-4-yl)-D-Val-Gly-ABA (0.05 mmol, 1.0 eq.) were dissolved in dry DMF together with 25  $\mu$ L 0.1 M DMAP (10% solution in DMF; 5.0  $\mu$ mol, 0.1 eq.), 22.8 mg 2,3,4,5,6-pentafluorophenol (0.125 mmol, 2.5 eq.) and 31.4  $\mu$ L DIC (0.2 mmol, 4.0 eq.) and stirred at rt for 1.5 h. After purification using HPLC, 19.5 mg (0.03 mmol, 63%) of yellow slur were collected. The combination of the active ester and compound **12** in presence of 10.0 eq. of DIPEA resulted in 3.8 mg of a white solid after purification using semi-preparative HPLC (30 to 55% B in 20 min). HPLC (25 to 65% B in 15 min):  $t_R$  = 11.1 min;  $K'$  = 4.8; calculated monoisotopic mass (C<sub>56</sub>H<sub>72</sub>BF<sub>3</sub>N<sub>15</sub>O<sub>9</sub>): 1293.47, found by ESI-MS:  $m/z$  = 1294.8 [M+H]<sup>+</sup>.

**cyclo[D-Tyr-N(Me)-D-Orn(AmBF<sub>3</sub>(methyl(1H-1,2,3-triazol-4-yl)-(R)-(1-(1-((2-(4-carboxyphenyl)-amino)-2-oxoethyl)amino)-5-guanidino-1-oxopentan-2-yl)-Arg-2-Nal-**

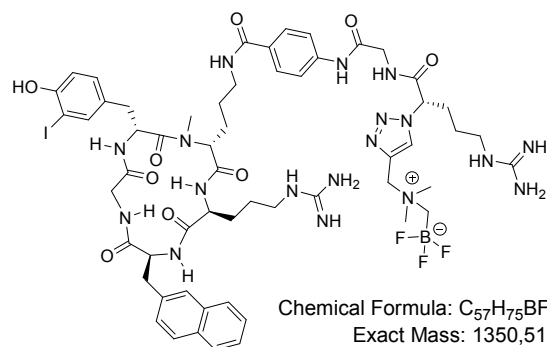


**Gly] (41):** Starting with Fmoc-ABA loaded resin, the introduction of Fmoc-Gly-OH and Fmoc-D-Arg(Pbf)-OH was performed as described earlier (II.2.1.). After Fmoc-deprotection, the amine was converted to the respective azide as described for **39** employing

DIPEA, **38** and CuSO<sub>4</sub>. After cleavage from the resin and concurrent removal of protecting groups (HPLC (15 to 65% B in 15 min):  $t_R$  = 6.2 min;  $K'$  = 2.6; calculated monoisotopic mass (C<sub>15</sub>H<sub>20</sub>N<sub>8</sub>O<sub>4</sub>): 376.16, found by ESI-MS:  $m/z$  = 377.3 [M+H]<sup>+</sup>), the combination with **37** was performed as described for **39** and resulted in AmBF<sub>3</sub>(methyl(1H-1,2,3-triazol-4-yl)-D-Arg-Gly-ABA. The peptide was converted to its respective pentafluorophenylester as described before. The combination of the active ester and compound **11** in presence of 10 eq. of DIPEA resulted in 1.2 mg (0.98  $\mu$ mol) of a white solid after purification using HPLC (28 to 50% B in 15 min). HPLC (15 to 55% B in 15 min):  $t_R$  = 8.7 min;  $K'$  = 5.2; calculated monoisotopic mass (C<sub>57</sub>H<sub>76</sub>BF<sub>3</sub>N<sub>18</sub>O<sub>9</sub>): 1224.61, found by ESI-MS:  $m/z$  = 1226.2 [M+H]<sup>+</sup>.

## MATERIALS AND METHODS

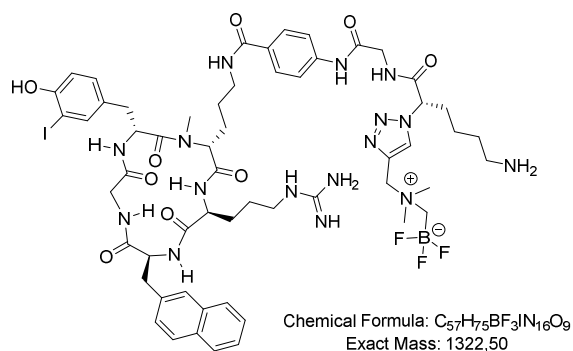
cyclo[(3-iodo)D-Tyr-N(Me)-D-Orn(AmBF<sub>3</sub>(methyl(1H-1,2,3-triazol-4-yl)-(R)-(1-(1-((2-(4-carboxyphenyl)-amino)-2-oxoethyl)amino)-5-guanidino-1-oxopentan-2-yl)-Arg-



2-Nal-Gly] (**42**): Starting with Fmoc-ABA loaded resin, the introduction of Fmoc-Gly-OH and Fmoc-D-Arg(Pbf)-OH was performed as described earlier (II.2.1.). After Fmoc-deprotection, the amine was converted to the respective azide as described for **39** employing **38**, DIPEA and CuSO<sub>4</sub>. After

cleavage from the resin and concurrent removal of protecting groups (HPLC (15 to 65% B in 15 min):  $t_R$  = 6.2 min;  $K'$  = 2.6; calculated monoisotopic mass (C<sub>15</sub>H<sub>20</sub>N<sub>8</sub>O<sub>4</sub>): 376.16, found by ESI-MS:  $m/z$  = 377.3 [M+H]<sup>+</sup>), the combination with **37** was performed as described before. The peptide was converted to its respective pentafluorophenylester and combined with compound **12** (iodoCPCR4) in presence of 10 eq. of DIPEA. 2.5 mg (1.8 μmol) of white solid was collected after purification using HPLC (28 to 45% B in 20 min). The solid was stored at -20 °C. HPLC (15 to 65% B in 15 min):  $t_R$  = 11.3 min;  $K'$  = 4.9; calculated monoisotopic mass (C<sub>57</sub>H<sub>75</sub>BF<sub>3</sub>IN<sub>18</sub>O<sub>9</sub>): 1350.51, found by ESI-MS:  $m/z$  = 1352.0 [M+H]<sup>+</sup>, 1374.0 [M+Na]<sup>+</sup>, 676.8 [M+2H]<sup>2+</sup>.

cyclo[(3-iodo)D-Tyr-N(Me)-D-Orn(AmBF<sub>3</sub>(methyl(1H-1,2,3-triazol-4-yl)-(R)-(1-(1-(2-(4-carboxyphenyl)-amino)-2-oxoethyl)amino)-1-oxohexan-2-yl))-Arg-2-Nal-Gly]



(**43**): Starting with Fmoc-ABA loaded resin, the introduction of Fmoc-Gly-OH and Fmoc-D-Lys(Boc)-OH was performed as described earlier (II.2.1.). After Fmoc-deprotection, the amine was converted to the respective azide as described for **39** employing **38**, DIPEA and CuSO<sub>4</sub>. The peptide was cleaved from the resin with the



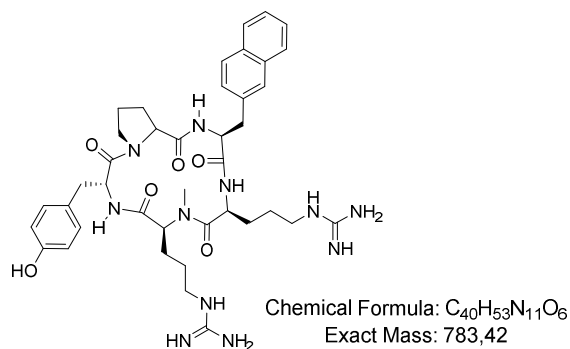
## MATERIALS AND METHODS

protecting group still bound to the peptide (HPLC (10 to 90% B in 15 min):  $t_R = 9.5$  min;  $K' = 5.3$ ; calculated monoisotopic mass ( $C_{20}H_{28}N_6O_6$ ): 448.21, found by ESI-MS:  $m/z = 348.15$   $[M+H(-Boc)]^+$ ). The  $AmBF_3$  group was introduced *via* combination with **37** as described before and resulted in  $AmBF_3$ (methyl(1H-1,2,3-triazol-4-yl)-D-Lys(Boc)-Gly-ABA. The peptide was converted to its respective pentafluorophenylester employing DMAP, 2,3,4,5,6-pentafluorophenol and DIC as described earlier. The pentafluorophenylester was combined with **12** in presence of 10 eq. of DIPEA. The solvent was removed under reduced pressure and the crude peptide was dissolved in TFA, TIPS and water (v/v/v; 95/2.5/2.5) for 30 min at rt. The solution was diluted in water and MeCN and directly injected into an analytical HPLC for purification (15 to 45% in 15 min). 2.5 mg (1.89  $\mu$ mol) white solid was collected and stored at -20 °C. HPLC (15 to 55% B in 15 min):  $t_R = 12.1$  min;  $K' = 5.3$ ; calculated monoisotopic mass ( $C_{57}H_{75}BF_3IN_{16}O_9$ ): 1322.50, found by ESI-MS:  $m/z = 1323.8$   $[M+H]^+$ .

## 5. Synthesis of CXCR7 targeting ligands

The synthesis of cyclic pentapeptides was performed according to a recently published protocol<sup>158</sup>. The published CXCR7 specific ligand cyclo[D-Tyr-Pro-Nal-N(Me)-Arg-Arg], also called FC313 was synthesized and included in the study as the CXCR7 specific standard and utilized as the radioligand for  $IC_{50}$  determination.

**cyclo[D-Tyr-Pro-2-Nal-N(Me)-Arg-Arg] (FC313; R3):** 0.8 g TCP-resin (1.66 mmol/g,



1.29 mmol) was loaded with 1.23 g (3.63 mmol, 2.8 eq.) Fmoc-L-Pro-OH according to the procedure described in II.2.1 resulting in a resin loading of 1.06 mmol/g resin. 1.2 g (1.27 mmol, 1.0 eq.) of loaded resin was allowed to pre-swell

## MATERIALS AND METHODS

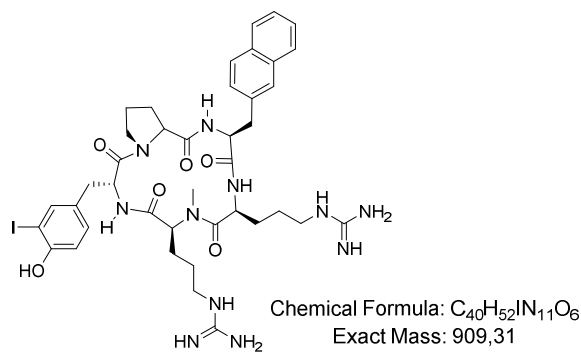
for 30 min in NMP. 1.67 g (3.82 mmol, 3.0 eq.) Fmoc-L-2-Nal-OH, 1.45 g (3.82 mmol, 3.0 eq.) HATU, 520 mg (3.82 mmol, 3.0 eq.) HOAt and 1.29 mL (7.64 mmol, 6.0 eq.) DIPEA were dissolved in NMP and stirred for 15 min. The solution was combined with the resin bound peptide and shaken for 3 h at rt. After washing (NMP, 6 x 2 min), a major amount of resin bound peptide was stored under vacuum until further utilization.

A smaller amount of resin, app. 0.42 mmol (1.0 eq.) was treated with 0.41 g (0.64 mmol, 1.5 eq.) Fmoc-L-Arg(Pbf)-OH, 85.9 mg (0.64 mmol, 1.5 eq.) HOBt, 204.5 mg (0.64 mmol, 1.5 eq.) TBTU and 324.4  $\mu$ L (1.91 mmol, 4.5 eq.) of DIPEA dissolved in NMP for 2 h at rt. After Fmoc-deprotection, the resin bound *N*-terminal free peptide was *p*-Ns protected as described in II.2.1. After 20 min, the resin was washed with NMP (6 x 2 min) and with THF (3 x 2 min) subsequently. 170  $\mu$ L (4.2 mmol, 10 eq.) of MeOH were dissolved with 550.8 mg (2.1 mmol, 5.0 eq.) triphenylphosphine in dry THF and stirred for 5 min. 414  $\mu$ L (2.1 mmol, 5.0 eq.) DIAD were carefully added to the resin within 5 min and the mixture was allowed to stir for another 15 min. The resin was washed thoroughly and the *p*-Ns deprotection was performed according to the procedure described in II.2.1. 0.81 g (1.26 mmol, 3.0 eq.) Fmoc-L-Arg(Pbf)-OH was dissolved together with 478 mg (1.26 mmol, 3.0 eq.) HATU, 171.5 mg (1.26 mmol, 3.0 eq.) HOAt and 425  $\mu$ L (2.52 mmol, 6.0 eq.) DIPEA in NMP and stirred for 15 min before adding to the resin bound peptide. The reaction was shaken for 3 h and washed three times with NMP. After Fmoc-deprotection, 459.5 mg (0.64 mmol, 1.5 eq.) Fmoc-D-Tyr(t-Bu), 85.9 mg (0.64 mmol, 1.5 eq.) HOBt, 204.5 mg (0.64 mmol, 1.5 eq.) TBTU and 324.4  $\mu$ L (1.91 mmol, 4.5 eq.) of DIPEA dissolved in NMP were added to the resin and shaken for 2 h. The fully protected linear peptide was cleaved from the resin (II.2.1) and precipitated in water to yield 385 mg (0.29 mmol, 86%, 1.0 eq.) yellowish powder. The crude product was dissolved in 110 mL of dry DMF (3 mM) together with 236 mg (1.45 mmol, 5.0 eq.) NaHCO<sub>3</sub> and 259  $\mu$ L (0.87 mmol, 3 eq.) of DPPA for peptide cyclization. After <sup>t</sup>Bu and Pbf-deprotection employing a mixture (v/v/v) of 95% TFA, 2.5% TIBS and 2.5% water, the product was purified using semi-preparative HPLC (20 to 55% B in 20 min). 3.5 mg (4.4  $\mu$ mol) of the white solid were collected. HPLC (15 to 55% B in 15

## MATERIALS AND METHODS

min):  $t_R = 12.8$  min;  $K' = 5.7$ . Calculated monoisotopic mass ( $C_{40}H_{53}N_{11}O_6$ ): 738.42 found:  $m/z = 785.0$   $[M+H]^+$ , 392.9  $[M+2H]^{2+}$ .

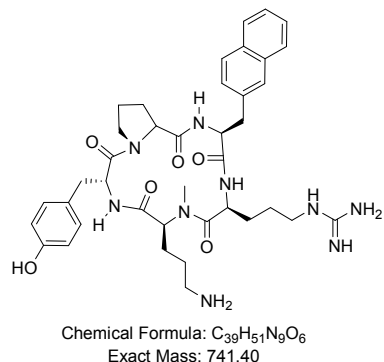
**cyclo[(3-iodo)D-Tyr-Pro-2-Nal-N(Me)-Arg-Arg] (44):** 4.0 (5.1  $\mu$ mol, 1.0 eq.) of **R3** were



treated with 0.5 eq. NIS as described in II.2.1.

1.4 mg (1.53  $\mu$ mol, 30%) of a white solid was collected. HPLC (15 to 65% B in 15 min):  $t_R = 9.8$  min;  $K' = 4.1$ . Calculated monoisotopic mass ( $C_{40}H_{52}IN_{11}O_6$ ): 909.31; found:  $m/z = 910.8$   $[M+H]^+$ , 456.0  $[M+2H]^{2+}$ .

**cyclo[D-Tyr-Pro-2-Nal-N(Me)-Arg-Orn] (45):** App. 0.42 mmol (1.0 eq.) of resin loaded



with L-proline and L-2-Naphtylalanine was treated with 0.41 g (0.64 mmol, 1.5 eq.) Fmoc-L-Arg(Pbf)-OH, 85.9 mg (0.64 mmol, 1.5 eq.) HOBt, 204.5 mg (0.64 mmol, 1.5 eq.) TBTU and 324.4  $\mu$ L (1.91 mmol, 4.5 eq.) of DIPEA dissolved in NMP for 2 h at rt as described for **43**. After Fmoc-deprotection, *Ns*-protection, *N*-methylation and subsequent *Ns*-deprotection as described for **43**, 516 mg (1.26 mmol, 3.0 eq.) Fmoc-L-Orn(<sup>t</sup>Bu)-

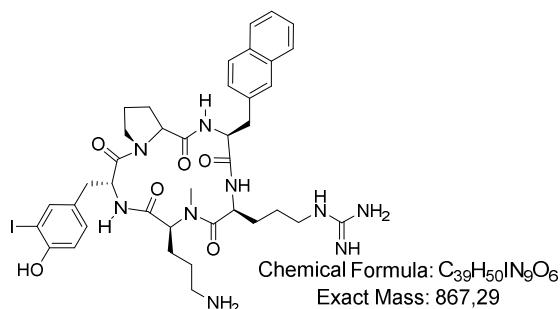
OH were dissolved together with 478 mg (1.26 mmol, 3.0 eq.) HATU, 171.5 mg (1.26 mmol, 3.0 eq.) HOAt and 425  $\mu$ L (2.52 mmol, 6.0 eq.) DIPEA in NMP and stirred for 15 min before adding to the resin bound peptide. The reaction was shaken for 3 h and washed three times with NMP. After Fmoc-deprotection, 459.53 mg (0.64 mmol, 1.5 eq) Fmoc-D-Tyr(<sup>t</sup>Bu), 85.9 mg (0.64 mmol, 1.5 eq.) HOBt, 204.5 mg (0.64 mmol, 1.5 eq.) TBTU and 324.4  $\mu$ L (1.91 mmol, 4.5 eq.) of DIPEA dissolved in NMP were added to the resin and shaken for 2 h. The fully protected linear peptide was cleaved from the resin (according to II.2.1) and precipitated in water to yield 340 mg (0.3 mmol, 72%) yellowish powder. After cyclization, the crude peptide was deprotected and precipitated in diethyl ether. The peptide was purified using HPLC (25 to

## MATERIALS AND METHODS

38% B in 20 min) to yield 4.6 mg (6.2  $\mu$ mol, 2%) of yellowish solid. HPLC (15 to 65% B in 15 min):  $t_R$  = 8.2 min;  $K'$  = 3.3. Calculated monoisotopic mass ( $C_{39}H_{51}IN_9O_6$ ): 741.40; found:  $m/z$  = 742.7  $[M+H]^+$ , 371.8  $[M+2H]^{2+}$ .

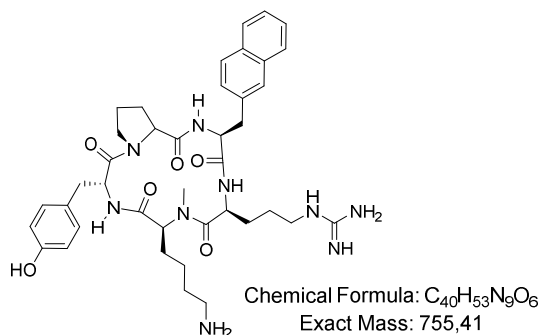
**cyclo[D-Tyr-Pro-2-Nal-N(Me)-Arg-D-Orn] (46):** 5.2 mg (7.0  $\mu$ mol, 2%); HPLC (15 to 65% B in 15 min):  $t_R$  = 7.9 min;  $K'$  = 3.4. Calculated monoisotopic mass ( $C_{39}H_{51}IN_9O_6$ ): 741.40; found:  $m/z$  = 742.9  $[M+H]^+$ , 371.9  $[M+2H]^{2+}$ .

**cyclo[(3-*iodo*)D-Tyr-Pro-2-Nal-N(Me)-Arg-Orn] (47):** 3.0 mg (4.0  $\mu$ mol) of **45** were



treated with 0.55 eq. NIS as described in II.2.1. 1.2 mg (1.38  $\mu$ mol, 34%) of a white solid was collected. HPLC (15 to 65% B in 15 min):  $t_R$  = 10.2 min;  $K'$  = 4.3. Calculated monoisotopic mass ( $C_{39}H_{50}IN_9O_6$ ): 867.29; found:  $m/z$  = 742.9  $[M+H]^+$ , 371.9  $[M+2H]^{2+}$ .

**cyclo[D-Tyr-Pro-2-Nal-N(Me)-Arg-Lys] (48):** The linear peptide was constructed on solid

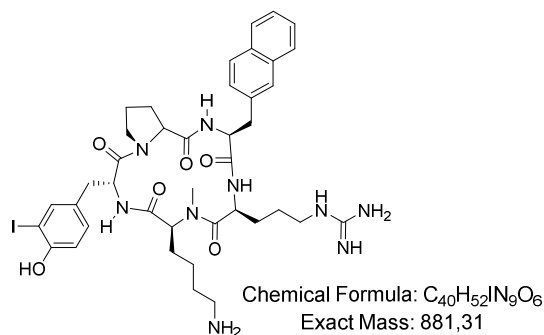


support as described before. After cleavage from the resin and cyclization, the crude peptide was deprotected according to the protocol in II.2.1 and precipitated in diethyl ether and purified using semi-preparative HPLC (25 to 43% B in 20 min) to yield 5.5 mg (7.3  $\mu$ mol) of yellowish solid. HPLC (15

to 55% B in 15 min):  $t_R$  = 9.1 min;  $K'$  = 3.7. Calculated monoisotopic mass ( $C_{40}H_{53}N_9O_6$ ): 755.41; found:  $m/z$  = 756.8  $[M+H]^+$ , 378.6  $[M+2H]^{2+}$ .

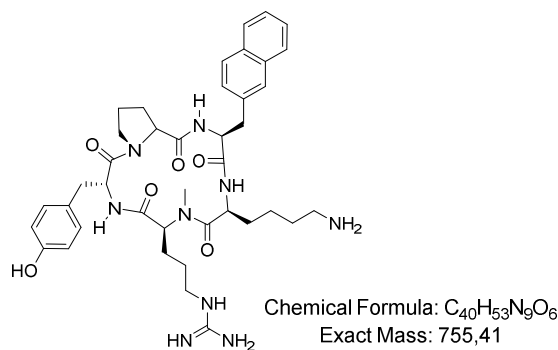
## MATERIALS AND METHODS

**cyclo[(3-iodo)D-Tyr-Pro-2-Nal-N(Me)-Arg-Lys] (49):** 3.0 mg (4.0  $\mu$ mol) of **48** were



treated with 0.6 eq. NIS as described in II.2.1. 0.8 mg (0.9  $\mu$ mol, 28%) of a white solid was collected. HPLC (15 to 65% B in 15 min):  $t_R$  = 10.3 min;  $K'$  = 4.7. Calculated monoisotopic mass (C<sub>40</sub>H<sub>52</sub>IN<sub>9</sub>O<sub>6</sub>): 881.31; found:  $m/z$  = 883.1 [M+H]<sup>+</sup>, 442.1 [M+2H]<sup>2+</sup>.

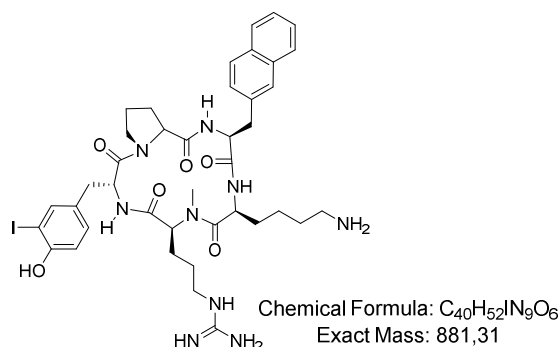
**cyclo[D-Tyr-Pro-2-Nal-N(Me)-Lys-Arg] (50):** The linear peptide was constructed on solid



support as described before. The fully protected linear peptide was cleaved from the resin and precipitated in water to yield 442.0 mg (0.37 mmol, 88%) yellowish powder. After cyclization, the crude peptide was deprotected according to the protocol in II.2.1 and precipitated

in diethyl ether. The peptide was purified using HPLC (25 to 45% B in 20 min) to yield 3.5 mg (4.6  $\mu$ mol) of the white solid. HPLC (15 to 65% B in 15 min):  $t_R$  = 9.0 min;  $K'$  = 3.7. Calculated monoisotopic mass (C<sub>40</sub>H<sub>53</sub>N<sub>9</sub>O<sub>6</sub>): 755.41; found:  $m/z$  = 756.7.1 [M+H]<sup>+</sup>, 378.8 [M+2H]<sup>2+</sup>.

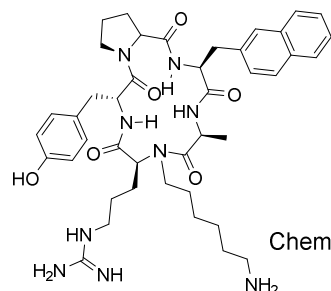
**cyclo[(3-iodo)D-Tyr-Pro-2-Nal-N(Me)-Lys-Arg] (51):** 3.0 mg (4.0  $\mu$ mol) of **50** were



treated with 0.6 eq. NIS as described in II.2.1. 1.4 mg (1.6  $\mu$ mol, 39%) of a white solid were collected. HPLC (15 to 65% B in 15 min):  $t_R$  = 10.4 min;  $K'$  = 4.2. Calculated monoisotopic mass (C<sub>40</sub>H<sub>52</sub>IN<sub>9</sub>O<sub>6</sub>): 881.31; found:  $m/z$  = 882.4 [M+H]<sup>+</sup>, 441.9 [M+2H]<sup>2+</sup>.

## MATERIALS AND METHODS

**cyclo[D-Tyr-Pro-2-Nal-N(aminohexyl)-Ala-Arg] (52):** App. 0.42 mmol (1.0 eq.) of resin



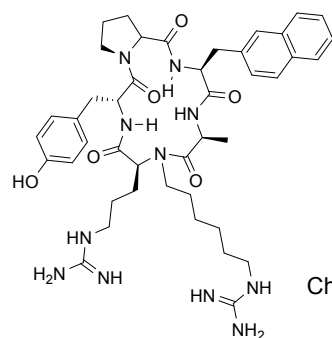
Chemical Formula:  $C_{42}H_{57}N_9O_6$   
Exact Mass: 783.44

loaded with L-proline and L-2-Naphtylalanine was treated with 0.20 g (0.64 mmol, 1.5 eq.) Fmoc-Ala-OH, 85.9 mg (0.64 mmol, 1.5 eq.) HOBt, 204.5 mg (0.64 mmol, 1.5 eq.) TBTU and 324.4  $\mu$ L (1.91 mmol, 4.5 eq.) of DIPEA dissolved in NMP for 2 h at rt as described for

**43.** After Fmoc-deprotection, *Ns*-protection was performed on resin as described for **43** and in II.2.1. For *N*-alkylation, 1.1 g triphenylphosphine (4.2 mmol, 10 eq.) together with 944 mg Dde-aminohexanol (3.36 mmol, 8.0 eq.) were dissolved in dry THF and added to the resin-bound peptide for 15 min. 826.9  $\mu$ L (4.2 mmol, 10 eq.) DIAD dissolved in THF were added to the solution of the resin bound peptide very carefully within 5 min and the reaction was allowed to continue for another 15 min. After washing the resin with NMP, *Ns*-deprotection was performed as described for **43**. 816.5 mg (1.26 mmol, 3.0 eq.) Fmoc-L-Arg(Pbf)-OH were dissolved together with 478 mg (1.26 mmol, 3.0 eq.) HATU, 171.5 mg (1.26 mmol, 3.0 eq.) HOAt and 425  $\mu$ L (2.52 mmol, 6.0 eq.) DIPEA in NMP and stirred for 15 min before adding to the resin bound peptide. The reaction was shaken for 3 h and washed three times with NMP. After Fmoc-deprotection, 459.5 mg (0.64 mmol, 1.5 eq.) Fmoc-D-Tyr(*t*-Bu), 85.9 mg (0.64 mmol, 1.5 eq.) HOBt, 204.5 mg (0.64 mmol, 1.5 eq.) TBTU and 324.4  $\mu$ L (1.91 mmol, 4.5 eq.) of DIPEA dissolved in NMP were added to the resin and shaken for 2 h. The fully protected linear peptide was cleaved from the resin (according to II.2.1) and precipitated in water to yield 500 mg (0.39 mmol, 93%) yellowish powder. After cyclization, the crude peptide was deprotected according to II.2.1. and precipitated in diethyl ether. A small amount was purified using HPLC (20 to 40% B in 20 min) to yield 8.2 mg (0.01 mmol, 33%) of the white solid. HPLC (15 to 65% B in 15 min):  $t_R$  = 9.7 min;  $K'$  = 4.4. Calculated monoisotopic mass ( $C_{42}H_{67}N_9O_6$ ): 783.44; found:  $m/z$  = 784.7  $[M+H]^+$ , 807.8  $[M+Na]^+$ , 392.9  $[M+2H]^{2+}$ .

## MATERIALS AND METHODS

**cyclo[D-Tyr-Pro-2-Nal-N(guanidinohexyl)-Ala-Arg] (53):** For guanidinylation, **52**

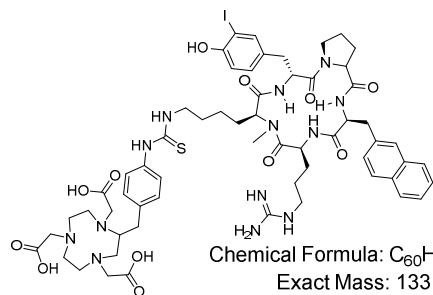


Chemical Formula:  $C_{43}H_{59}N_{11}O_6$   
Exact Mass: 825.46

(0.126 mmol, 1.0 eq.) was dissolved together with 184.7 mg (1.26 mmol, 10 eq.) 1-H-pyrazol-1-carboxamidine • HCl in 2.5 mL DMF. After addition of 428  $\mu$ L (20 eq.) DIPEA, the solution was allowed to stir for 6 h at rt. The peptide was purified using

HPLC (20 to 40% B in 20 min) to yield 4.1 mg (5.0  $\mu$ mol) of the white solid. HPLC (15 to 65% B in 15 min):  $t_R$  = 10.3 min;  $K'$  = 4.4. Calculated monoisotopic mass ( $C_{43}H_{59}N_{11}O_6$ ): 825.46; found:  $m/z$  = 826.6  $[M+H]^+$ , 848.7  $[M+Na]^+$ , 413.8  $[M+2H]^{2+}$ .

**cyclo[(3-iodo)D-Tyr-Pro-2-Nal-N(Me)-Arg-Lys(NOTA-Bn-SCN)] (54):** 0.8 mg



Chemical Formula:  $C_{60}H_{78}IN_{13}O_{12}S$   
Exact Mass: 1331.47

(0.7  $\mu$ mol, 1.0 eq.) of **49** were dissolved in DMF together with 1.4  $\mu$ L (8.4  $\mu$ mol, 12.0 eq.) of DIPEA. 0.5 mg (0.8  $\mu$ mol, 1.1 eq.) of 2,2',2''-(2-(4-methanethioamidobenzyl)-1,4,7-triazonane-1,4,7-triyl)triacetic acid (NOTA-Bn-SCN; Macro-cyclics, USA) were added to the solution and stirred for 16

h at rt. The crude mixture was purified using analytical HPLC (20 to 40% B in 15 min) to give 0.5 mg (0.38  $\mu$ mol, 53%) of white powder. HPLC (15 to 65% B in 15 min):  $t_R$  = 12.4 min;  $K'$  = 5.5. Calculated monoisotopic mass ( $C_{60}H_{78}IN_{13}O_{12}S$ ): 1331.47; found:  $m/z$  = 1333.1  $[M+H]^+$ , 666.9  $[M+2H]^{2+}$ .

**cyclo[(3-iodo)D-Tyr-Pro-2-Nal-N(Me)-Arg-Lys( $^{nat}Cu$ -NOTA-Bn-SCN)] ( $[^{nat}Cu]$ 54):**

Complexation was performed as described in II.2.2. Formation of the  $^{nat}Cu^{II}$ -chelate was confirmed using HPLC and ESI-MS. The resulting 0.5 mM aqueous solutions of the respective  $^{nat}Cu$ -complexes were diluted (serial dilution  $10^{-4}$  to  $10^{-11}$  M in HBSS with 1% BSA) and used in the *in vitro*  $IC_{50}$  studies without further processing. HPLC (15 to 65% B in 15 min):  $t_R$  =

## MATERIALS AND METHODS

11.5 min;  $K' = 4.7$ . Calculated monoisotopic mass ( $C_{60}H_{75}CuIN_{13}O_{12}S$ ): 1391.37; found:  $m/z = 696.1$   $[M+2H]^{2+}$ .

### cyclo[(3-iodo)D-Tyr-Pro-2-Nal-N(Me)-Arg-Lys(<sup>nat</sup>Ga-NOTA-Bn-SCN)] ([<sup>nat</sup>Ga]54):

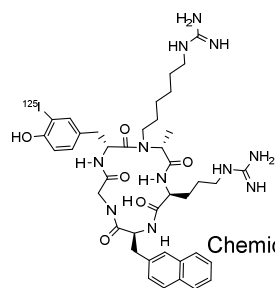
Complexation was performed as described in II.2.2. Formation of the <sup>nat</sup>Ga<sup>III</sup>-chelate was confirmed using HPLC and ESI-MS. The resulting 0.5 mM aqueous solutions of the respective <sup>nat</sup>Ga-complexes were diluted (serial dilution  $10^{-4}$  to  $10^{-11}$  M in HBSS with 1% BSA) and used in the *in vitro*  $IC_{50}$  studies without further processing. HPLC (15 to 65% B in 15 min):  $t_R = 11.5$  min;  $K' = 4.6$ . Calculated monoisotopic mass ( $C_{60}H_{75}GaIN_{13}O_{12}S$ ): 1397.37; found:  $m/z = 1400.1$   $[M+H]^+$ , 699.8  $[M+2H]^{2+}$ .

## 6. Radiochemistry

### 6.1. Radioiodination(<sup>125</sup>I]NaI)

The radioligands (**R1-3**) were iodinated applying the Iodogen-method as described previously<sup>167-169</sup>. 1.5 mg Iodogen (1,3,4,6-tetrachloro-3R,6R-diphenylglycoluril, *Pierce*, Rockford, IL) were dissolved in 1.0 mL dry DCM and apportioned in 10 Eppendorf Caps (100  $\mu$ L iodogen solution each cap). DCM was evaporated under nitrogen flow and the Iodogen-coated Eppendorf caps were stored under nitrogen at -20 °C until further application.

### cyclo[[<sup>125</sup>I]D-Tyr-N(hexylguanidino)-D-Ala-Arg-2-Nal-Gly]; [<sup>125</sup>I]CPCR4.3 ([<sup>125</sup>I]R1):



Chemical Formula:  $C_{40}H_{54}^{125}IN_{11}O_6$   
Exact Mass: 909,33

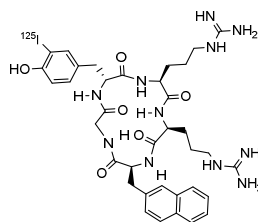
Approximately 0.5 mg (0.5  $\mu$ mol) of **R1** were dissolved in 20  $\mu$ L DMSO and 200  $\mu$ L of Tris buffer (25 mM in water). 5  $\mu$ L (20.1 MBq) [<sup>125</sup>I]NaI (74 TBq/mmol, 3.1 GBq/mL 40 mM NaOH, *Hartmann Analytic*, Braunschweig, Germany) were added to the solution and incubated for 15 min at



## MATERIALS AND METHODS

rt. The crude product was loaded onto a semi-preparative HPLC to afford the desired product (10.2 MBq, 50%). (25 - 55% B in 20 min; 220 nm);  $t_R = 19.1$  min,  $K' = 9.6$ .

**cyclo[[<sup>125</sup>I]D-Tyr-Arg-Arg-2-Nal-Gly]; [<sup>125</sup>I]FC131 ([<sup>125</sup>I]R2):** Approximately 0.5 mg (0.5 μmol) of **R2** were dissolved in 20 μL

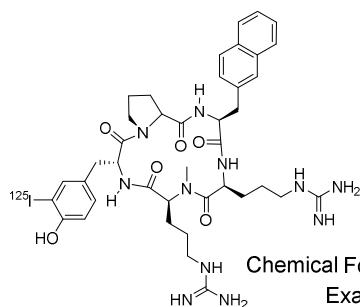


Chemical Formula:  $C_{36}H_{46}^{125}IN_{11}O_6$   
Exact Mass: 853,27

DMSO and 200 μL of Tris buffer (25 mM in water). 5 μL (23.1 MBq) [<sup>125</sup>I]NaI (74 TBq/mmol, 3.1 GBq/mL 40 mM NaOH) were added to the solution and incubated for

15 min at rt. The crude product was isolated from unlabeled FC131 *via* RP-HPLC to afford the desired product (9.62 MBq, 42%) (20 - 40% B in 20 min; 220 nm);  $t_R = 18.0$  min,  $K' = 9.0$ .

**cyclo[[<sup>125</sup>I]D-Tyr-Pro-2-Nal-N(Me)-Arg-Arg] [<sup>125</sup>I]FC313 ([<sup>125</sup>I]R3):** Approximately 0.5 mg (0.5 μmol) of **R3** were dissolved in



Chemical Formula:  $C_{40}H_{52}^{125}IN_{11}O_6$   
Exact Mass: 907,31

20 μL DMSO and 200 μL of Tris buffer (25 mM in water). 5 μL (15.88 MBq) [<sup>125</sup>I]NaI (74 TBq/mmol, 3.1 GBq/mL 40 mM NaOH) were added to the solution and incubated for 15 min at rt. The crude product was isolated from

unlabeled **R3** *via* RP-HPLC to afford the desired product (10.2 MBq, 64%) (25 to 60% B in 20 min; 220 nm);  $t_R = 14.6$  min,  $K' = 8.7$ . The radioligands were stored in the HPLC solvent at 8 °C until further utilization. Prior to the *in vitro* experiments, the radioligand was dissolved in HBSS to achieve a final concentration in the assay of 0.1 nM. The radioligands were used for 8 to 10 weeks without purification and were replaced with freshly prepared radioligands afterwards.

## MATERIALS AND METHODS

### 6.2. $^{68}\text{Ga}^{\text{III}}$ -labeling

The  $^{68}\text{Ga}$ -labeling was performed with a  $^{68}\text{Ge}/^{68}\text{Ga}$  generator (*iTHEMBA Labs*, South Africa) as published previously <sup>161, 170</sup> in our group.  $^{68}\text{Ga}$  labeling was performed within 15 min using a GallElut<sup>+</sup> system (*SCINTOMICS GmbH*, Germany). The  $^{68}\text{Ge}/^{68}\text{Ga}$ -generator with  $\text{SnO}_2$  matrix was eluted with 1.0 M aqueous HCl. A fraction of 1.25 mL, containing approx. 80% of the entire activity (ca. 1 GBq), was transferred into a glass vial (ALLTECH, 5 mL) containing 5 nmol of the precursor and an aq. solution of HEPES (270 mg HEPES in 220  $\mu\text{L}$  water, resulting pH of reaction mixture was 2). Reaction was performed for 5 min at 95 °C, followed by fixation of the labeled peptides on pre-conditioned SPE cartridge (*Waters SepPak® C18 light*). After purging of the cartridge with 10 mL of water, the labeled product was eluted with a mixture of ethanol and water (v/v; 1:1), PBS buffer (1mL) and 1 additional mL of water <sup>171</sup>. For animal studies, the ethanol for eluting the labeled tracer from the cartridge was evaporated *in vacuo*. After cooling, labeling efficiency and radiochemical purity were determined using radio-TLC (0.1 M sodium citrate buffer or 0.06 M ammonium acetate/methanol (1/1), respectively). Radiochemical purity of all  $^{68}\text{Ga}$ -labeled conjugates was  $\geq 95\%$ .

### 6.3. $^{177}\text{Lu}$ -labeling

For *in vitro* studies, 7.5  $\mu\text{L}$  (0.75 nmol) of the chelator coupled peptide (0.1 mM in Tracepure water (*Merck*, Darmstadt, Germany)) was added to 20 MBq of a [ $^{177}\text{Lu}$ ]LuCl<sub>3</sub> solution (3000 GBq/mg, 740 MBq/mL, 0.04 M HCl, *ITG Garching*, Germany). 10  $\mu\text{L}$  of 1 M NH<sub>4</sub>OAc (pH= 5) was added to the solution, followed by water to reach a final reaction volume of 100  $\mu\text{L}$ . After 40 min at 90 °C, the labeling efficiency was examined by radio-TLC and radio-HPLC. Radiochemical purity of all  $^{177}\text{Lu}$ -labeled conjugates was  $\geq 97\%$ . Hence, the tracers were diluted and used for *in vitro* experiments without further purification. For *in vivo* experiments, the  $^{177}\text{Lu}$ -labeled compounds were loaded on a C<sub>18</sub>-light cartridge (*Waters GmbH*, Eschborn, Germany), which was conditioned with 5 mL of ethanol and 5 mL of water prior to use, flushed with water and eluted with ethanol (0.1 % acetic acid). The solution of the product was diluted with PBS (% of ethanol < 5 %) for *in vivo* application.

## MATERIALS AND METHODS

### 6.4. $^{18}\text{F}$ -labeling

For  $^{18}\text{F}$ -labeling, the respective  $\text{AmBF}_3$ -conjugated precursor (100 to 150 nmol) was resuspended in 20  $\mu\text{L}$  DMF and 20  $\mu\text{L}$  of aqueous pyridazine-HCl buffer (1 M, pH 2). No-carrier-added  $^{18}\text{F}$ -fluoride, 2 – 5 GBq (50 – 130 mCi) were trapped on an anion exchange resin (loading was performed in the reverse; 9 mg, quaternary ammonium, chloride form, preconditioned with 6 mL of deionized water, 6 mL of sat. NaCl solution and 6 mL of deionized water, respectively). The aqueous  $^{18}\text{F}$ -fluoride was eluted with 60  $\mu\text{L}$  of isotonic saline into the reaction vial (polypropylene Eppendorf cap, 1.5 mL) containing the labeling precursor. The vial was placed in a heating block set at 80 °C for 20 min, whereupon the reaction was quenched by the injection of 0.2 mL of 5%  $\text{NH}_4\text{OH}$  in water. The reaction mixture was loaded onto a  $\text{C}_{18}$  classic cartridge that was conditioned with 5 mL of ethanol and 5 mL of water prior to use, flushed with water (to remove e.g.,  $^{18}\text{F}$ -fluoride, pyridazine), and eluted with ethanol (0.1 % acetic acid). The solution of the product was diluted with PBS (% of ethanol < 5 %) for *in vivo* application.

## 7. Cell experiments

### 7.1. Cultivation of utilized cell lines

All cell experiments were carried out at the Department of Nuclear Medicine at Klinikum rechts der Isar (TUM). For *in vitro* experiments, the following cell lines were used: Jurkat human T-cell leukemia cells (CLS: 300223), E $\mu$ -Myc1080 mouse B-cell lymphoma cells <sup>172</sup>, Daudi B-lymphoblast cell line (ATCC® CCL-213™) (suspension cell lines) and the hCXCR4-expressing cell line Chem-1 (*Millipore Sigma*: HTS004C), MBA-MD 231 cells (ATCC® HTB-26™), human glioma U87 cells overexpressing CD4 and CXCR4 (U87CD4CXCR4) and the hCXCR7<sup>+</sup> glioblastoma cell line U343 (CLS: 300365) (adherent cell lines). Chinese hamster ovarian (CHO) cells were used for transfection with h, mCXCR4 and h, mCXCR7 for specificity studies.

Jurkat and U343 cells were cultivated in RPMI 1640 medium (*Biochrom*, United Kingdom) containing 10% fetal calf serum (FCS; *Biochrom*). Daudi and E $\mu$ -Myc1080 cells were grown in

## MATERIALS AND METHODS

RPMEI 1640 medium supplemented with 20% FCS, 1% non-essential amino acids (Biochrom, United Kingdom) and 0.1% of 2-Mercaptoethanol (*Sigma-Aldrich*, Germany). MBA-MD 231 and U87CXCR4CD4 cells were cultivated in Dulbecco's Modified Eagle Medium/Nutrition Mix F-12 with Glutamax-I (1:1) (DMEM/F-12) (*Invitrogen*, *Life Technologies*, Darmstadt, Germany) supplemented with 10% of FCS, Chem\_1 cells were cultured in DMEM/F-12 supplemented with 10% FCS, 1% of non-essential amino acids (*Biochrom*), 1% HEPES (1.0 M) and 0.1 % of gentamycin.

Cultures were maintained at 37 °C in a 5% CO<sub>2</sub> humidified air atmosphere and passaged two to three times a week, depending on denseness of the cells. Adherent cell lines were harvested using Trypsin/EDTA (0.05% and 0.02%) in phosphate-buffered-saline (PBS) (*Biochrom*) for 5 min at 37 °C. After centrifugation and resuspension with culture medium, cells were counted with a Countesse automated cell counter (*Invitrogen*), or manually employing a Burkers counting chamber. Suspension cells were centrifuged and resuspended in fresh medium prior to counting. All *in vitro* studies were performed using vital cells. Adherent cells were seeded one day prior to the experiment in 24-well plates (1.0 mL/well; *Biochrom*). Applied cell lines and cell numbers for specific assays are described in the scope of the experimental setup and were kept constant over the time of repetitions.

### 7.2. Determination of receptor binding affinity and specificity

**Competitive binding assay using Jurkats (hCXCR4):** Competition studies addressing the human CXCR4 were performed using CXCR4 positive Jurkat human T-cell leukemia cells and [<sup>125</sup>I]FC131 ([<sup>125</sup>I]**R2**) as radioligand. The cells were separated from their normal medium and resuspended in HBSS containing 1% BSA with a concentration of 2×10<sup>6</sup> cells per mL. 200 µl of the cell suspension, containing approximately 400,000 Jurkat cells, were incubated with 25 µl of the radioligand solution (containing 3.1 kBq, approx. 0.1 nM) and 25 µl of the competitor at different concentrations of 10<sup>-11</sup> to 10<sup>-5</sup>. After shaking for 2 h at rt, the incubation was terminated by centrifugation at 600 x g (1,200 rpm, Biofuge 15) for 3 min. The

## MATERIALS AND METHODS

activity in the supernatant was separated and the cell pellets were washed twice with cold HBSS. Cell bound radioactivity was determined by using a  $\gamma$ -counter (1480 Wizard<sup>3</sup> gamma-counter from *Wallac*, Turku, Finland). Experiments were repeated at least three times in triplicates.  $IC_{50}$  values of the compounds were calculated by nonlinear regression using GraphPad Prism (GraphPad Prism 4.0 *Software Inc.*, San Diego, USA). Each data point is the average of at least three determinations.

**Competitive binding assay using Ep-Myc1080 (mCXCR4):** The determination of murine CXCR4 affinity was performed according to the affinity assay described for Jurkats cells, but with 200,000 cells/sample and [<sup>125</sup>I]**R1** as the radioligand.

**Competitive binding assay using U343 (hCXCR7):** Adherent cell lines were harvested using Trypsin/EDTA (0.05% and 0.02%) in PBS for 5 min at 37 °C. After centrifugation and resuspension with culture medium, cells were counted. 150,000 cells/well were seeded one day prior to the experiment in 24-well plates (1.0 mL/well). On the day of the experiment, the culture medium was removed and the cells were washed once with 500  $\mu$ L of HBSS containing 1% BSA, before being left to equilibrate in 200  $\mu$ L of HBSS (1% BSA) on ice for 15 min. Then, 25  $\mu$ L/well of either (1% BSA; Control) or of solutions containing the respective test compound (cold metal complex) in increasing concentrations ( $10^{-10}$  -  $10^{-4}$  M in HBSS 1% BSA) were added, followed by the addition of 25  $\mu$ L of [<sup>125</sup>I]**R3** in HBSS (1% BSA) as the radioligand (app. 3.1 kBq, 0.1 nM). Experiments were carried out in triplicate for each concentration. Cells were incubated on ice for 2 h. By removal of the incubation medium, incubation was terminated and the cells were thoroughly rinsed with cold 250  $\mu$ L of HBSS twice. The washing medium was combined with the supernatant of the previous step. This fraction represents the amount of unbound radioligand. Cells were then lysed using 250  $\mu$ L of 1 N NaOH, the lysate was transferred to vials and combined with another 250  $\mu$ L of NaOH used for rinsing the wells. Quantification of the amount of unbound and bound activity was performed in a  $\gamma$ -counter.

## MATERIALS AND METHODS

**Specificity of radioligand cell binding:** Cell transfection and cell binding experiments were all performed at the Department of Nuclear Medicine at Klinikum rechts der Isar (TUM). CHO cells were transfected with h/mCXCR4/CXCR7 vectors 24 h before start of the experiment, as described by our group before <sup>127</sup>. In brief, transient transfection was accomplished using jetPRIME reagent (*PEQLAB Biotechnology*, Erlangen, Germany; #13-114) according to manufacturer's instructions. CHO-K1 cells were seeded at a density of 50000 cells/well in poly-L-lysine-coated 24-well plates, transfected with 0.5 µg/well of receptor-encoding constructs (kindly supplied by Prof. Dr. S. Schulz and Prof. Dr. R. Stumm, Institute of Pharmacology and Toxicology, Jena University Hospital, Germany) 16 h after plating, and used for assay 24 h after transfection.

On the day of the experiment, the culture medium was removed and the cells were washed once with 500 µL of DEMEM containing 5% BSA, before being left to equilibrate in 200 µL of DEMEM (5% BSA) for 15 min. Then, 25 µL per well of either DEMEM (5% BSA; Control) or 25 µL of AMD3100 (100 µM; blockade) were added, followed by 25 µL of the radiolabeled peptide (10 nM; final concentration in the assay: 1 nM). The plates were incubated at 4 °C for 30 min. The incubation was terminated by removing the supernatant and thoroughly rinsing the cells with cold PBS. The wash media were combined and the cells were lysed by addition of 250 µL of 1 N NaOH. The lysate was transferred to vials and combined with another 250 µL of NaOH used for rinsing the wells. The fractions of unbound and bound activity for the control and the blocking experiment were quantified in a γ-counter. The experiment was conducted in triplicates for every compound (control and blockade).

### 7.3. Fluorescent microscopy

**Fluorescent imaging:** Eµ-Myc1080 mouse B-cell lymphoma cells, Chemicon's Wild-Type Chem-1 cells and Daudi human B-Lymphoblast cells were utilized for fluorescent imaging of the CXCR4 surface expression. The suspension cells (Daudi and Eµ-Myc1080) were separated from their normal medium and re-suspended in DEMEM (5% BSA). 200 µL of the cell suspension, containing app. 200,000 cells, were incubated with 25 µL of **QDs-6** (final

## MATERIALS AND METHODS

concentration: 25 nM) or unlabeled quantum dots for control for 1 h at rt. The supernatant was separated and the cells were rinsed with HBSS thoroughly. The Chem\_1 cells were seeded 24 h prior to experiments (approximately 50,000 cells per vial) on cover slides (micro cover slides, VWR). On the day of the experiment, the cells were washed and treated with QDs according to the procedure described above. Fluorescence images were obtained on a fluorescence microscope BZ9000 (*Keyence*, Japan) with TxRed SB filter. Wavelengths: Ex.: 562/40; DM: 593, EM: 624/40. Fluorescence imaging was conducted in triplicates; images were obtained and used without further modification (except enhancing contrast).

**Binding affinity assay using biotin-labeled TN14003 (performed at Emory University; Atlanta):** To determine the inhibitory effectiveness of selected CXCR4 targeted peptides, a binding assay utilizing the biotin-labeled CXCR4 inhibitor TN14003 as the standard ligand was performed. Therefore, app.  $2 \times 10^4$  MBA-MD-231 cells were seeded in 8 well glass slides (Chamber Slide, Thermo Fisher Science, USA) containing 300  $\mu$ L of DEMEM (10% FCS) the day before the experiment. The incubation medium was removed and the slides were washed two times with serum free medium. The test compounds were dissolved in 180  $\mu$ L serum free medium at different concentrations (1 nM, 10 nM, 100 nM and 1000 nM) and incubated for 15 min at 37 °C. The incubation was terminated by washing two times with cold PBS. The chamber walls were removed as described by the provider and the cells were fixed for 20 min with cold 3.8% formaldehyde in PBS (v/v). The cells were washed with PBS and treated with 60  $\mu$ L of biotinylated TN14003 (0.1  $\mu$ g/mL; *Thermo Fisher*; USA) for 30 min at rt. After washing, incubation with streptavidin conjugated Rhodamine and Hoechst core staining was performed for another 30 min. Fluorescent microscopy was performed on an Axioplan 2 microscope (*Zeiss*, Germany) and a rhodamine filter.

### 7.4. Functional assays for *in vitro* characterization

**Internalization and cell binding kinetics (hCXCR4, hCXCR7):** For internalization studies addressing the hCXCR4 receptor, Chem\_1 cells were utilized. In studies

## MATERIALS AND METHODS

focusing on the hCXCR7, U343 cells were employed. Conditions (cell number, assay medium, incubation time) were identical for both experiments. Therefore, the cells were harvested using Trypsin/EDTA (0.05% and 0.02%) in PBS for 5 min at 37 °C. After centrifugation and resuspension with culture medium, cells were counted. 100,000 cells/well were seeded one day prior to the experiment in 24-well plates (1.0 mL/well). On the day of the experiment, the culture medium was removed and the cells were washed once with 500  $\mu$ L of warm DMEM-F12 (5% BSA) before being left to equilibrate in 200  $\mu$ L DMEM-F12 (5% BSA) at 37 °C for a minimum of 15 min. Then, 25  $\mu$ L (per well) of either DMEM-F12 (5% BSA) or 100  $\mu$ M AMD3100 solution (control or blocking) was added, followed by the addition of 25  $\mu$ L of radiolabeled peptide. The final radioligand concentration was 1.0 nM in all internalization studies. To determine internalization kinetics, cells were incubated at 37 °C for 5, 15, 30 and 60 min, respectively. Experiments were carried out in triplicate for each time point. Incubation was terminated by placing the plate on ice for approximately 1 min and by subsequent removal of the incubation medium. Cells were thoroughly rinsed with 200  $\mu$ L of ice cold PBS. The supernatant was combined with the fractions of the previous step. To remove membrane associated radioactivity, the cells were washed with 200  $\mu$ L of ice cold acid wash (0.02 M NaOAc in saline, buffered with AcOH to pH = 5.0). After removal of the supernatant, the cells were thoroughly rinsed with another 200  $\mu$ L of acid wash. Both fractions were combined and represent the amount of membrane bound radioligand. The internalized activity was released by incubation with 300  $\mu$ L of 1 N NaOH, transferred to vials and combined with 300  $\mu$ L of 1 N NaOH used for rinsing the wells. Quantification of the amount of free, membrane bound and internalized activity was performed in a  $\gamma$ -counter. Internalized and membrane associated radioactivity was corrected with the activity found in the blocking study (co-incubation with 100  $\mu$ M of AMD3100) to give CXCR4 specific results.

**Radioligand externalization and recycling kinetics (hCXCR4):** To determine externalization kinetics, Chem\_1 cells were prepared in the same way as described for internalization assay. After the cells were washed with DMEM-F12 (5% BSA) and left to



## MATERIALS AND METHODS

equilibrate for at least 15 min at 37 °C, the cells were incubated with 25 µL of radiolabeled peptides (1.0 nM) at 37 °C for 120 min in a total volume of 250 µL. After the initial incubation, the medium was removed and kept for the calculation of total added radioactivity. No acid wash was performed to ensure the receptor integrity during the subsequent externalization and recycling study. In the experiment allowing ligand recycling, 250 µL of fresh assay medium was added to the cells. In the experiment inhibiting ligand recycling, 225 µL fresh assay medium and 25 µL of 100 µM AMD3100 were added to the cells. The cells were then incubated for 5, 15, 30 and 60 min at 37 °C. Subsequently, the supernatant was removed and the cells were washed with 200 µL cold HBSS. The combined fraction of supernatant and HBSS represents the amount of externalized radioligand. The cells were then washed with 200 µL cold acid wash twice, which represents the fraction of membrane-bound radioligand. Cells were lysed as described for the internalization assay and the amount of free, externalized, membrane-bound and internalized radioligand was quantified in a γ-counter.

**Matrigel Invasion assay (hCXCR4):** MBA-MD 231 cells were washed with serum free RPMI-1640 medium 4 h prior to the experiment. 500 µL containing app.  $5 \times 10^4$  cells per well were seeded into insert of Matrigel invasion 24-well plates (*Fisher Scientific*) cups and inserted in the wells. The bottom chamber was employed with 700 µL of serum free medium and 20 ng/mL SDF-1 to induce chemotaxis. The test compounds were mixed with the cells and added carefully to the upper chamber. A positive control (no additional added compound, except SDF-1 in the bottom chamber) and a negative control (no added SDF-1) were included in every experiment. To determine the antagonistic nature of test compounds, concentrations of 100 nM of the test compound were added to the cells in the upper chamber. The cells were incubated at 37 °C for 16 h. The matrigel was removed and the cells were fixed, stained and counted using an Axioplan 2 microscope (*Zeiss*).

**cAMP assay (hCXCR4):** Human glioma U87 cells overexpressing CD4 and CXCR4 (U87CD4CXCR4) cells were kept in cultivation at least one week before starting the experiment.

## MATERIALS AND METHODS

The cells were washed and harvested according to the standard procedure for adherent cells. App. 1500 – 2000 cells per well were seeded in a 384-well plate in 2% FCS 1% penicillin 24 h before the test. *Perkin-Elmer's* LANCE cAMP assay kit (catalog #AD0262) based on time-resolved fluorescence resonance energy transfer (TR-FRET) was utilized to determine a compound's ability to block cAMP modulation induced by CXCR4/SDF-1 interaction (antagonistic approach). The experiment was performed according to the manufacturer's instructions using 5  $\mu$ M Forskolin to induce cAMP production that is reduced by the presence of SDF-1 ( $G_i$  production and subsequent inhibition of adenylyl cyclase). For the agonistic approach, SDF-1 was replaced with different concentrations of the test compound to test its ability to inhibit cAMP production. Results were measured in a Perkin-Elmer Envision 2102 multilabel reader with the following parameters: flash energy area = low, flash energy level = 239, counting cycle = 1 ms, and ex/em = 340 nm/665 nm.

## 8. Determination of lipophilicity, stability and blood cell binding

**Determination of  $\text{Log}P_{(\text{octanol/PBS})}$ :** To determine the distribution coefficient of  $^{68}\text{Ga}$ -or  $^{177}\text{Lu}$ -labeled compounds in n-octanol and PBS buffer, approximately 0.8 – 2.0 MBq of radiolabeled peptide was diluted in 0.5 mL of phosphate buffered saline (n=6, pH = 7.4). After addition of an equal volume of n-octanol, the solution was vigorously vortexed for 3 min. The vials were centrifuged at 6000 g for 5 min in a Biofuge 15 (*Heraeus Sepatech*, Osterode, Germany) for quantitative separation of the layers. 100  $\mu$ L samples were taken from both the aqueous and the organic layer, and radioactivity was measured in a 1480 Wizard<sup>3</sup> gamma-counter. The partition coefficient  $P_{(\text{o/PBS})}$ , which is defined as the molar concentration ratio of a compound between n-octanol and PBS at equilibrium, and  $\text{log}P_{(\text{o/PBS})}$ , which is an important parameter used to characterize lipophilicity of a compound, were calculated.

## MATERIALS AND METHODS

**Plasma protein binding:** To determine the ratio of free radiolabeled peptide and plasma protein-bound peptide, a 500  $\mu\text{L}$  sample of human blood from a Heparin- or EDTA coated vial was centrifuged at  $3,000 \times g$  (6,000 rpm, Biofuge 15) for 3 min. The resulting plasma was incubated with app. 0.5 – 1.0 MBq of the radiolabeled peptide at 37 °C for 15 min before ultracentrifugation in a modified polyethersulfone ultracentrifugation vial (low-protein binding, 30 kDa, *VWR International GmbH*) at  $7,500 \times g$  (15,000 rpm, Biofuge 15). A sample of the plasma and an equal volume of ultra-filtered plasma (plasma protein free) were measured in a  $\gamma$ -counter. The resulting value was corrected for unspecific adhesion to the ultra-filtration vials using PBS for incubation.

**Blood cell binding:** To distinguish the binding of CXCR4 targeted peptides to different blood cells, 1.0 mL samples of human blood from a Heparin- or EDTA coated vial were incubated with 225  $\mu\text{L}$  of a 1.0 nM solution of the radiolabeled compound and 25  $\mu\text{L}$  of either PBS or AMD3100 (100  $\mu\text{M}$ ) in 1.5 mL Eppendorf Caps for 15 min. Stepwise centrifugation separated the different blood compartments. First, the erythrocytes were collected after centrifugation at  $700 \times g$  (1,400 rpm, Biofuge 15) for 5 min. The pellet was washed with 500  $\mu\text{L}$  of cold PBS and centrifuged a second time. The supernatant was combined and centrifuged at  $3,100 \times g$  (6,200 rpm) to collect the leukocytes. After washing with PBS and centrifugation, the radioactivity of the pellets (erythrocytes and leukocytes) and the supernatant was measured in a  $\gamma$ -counter. CXCR4 specificity of binding was shown by co-incubation of 100  $\mu\text{M}$  AMD3100. Specific binding is shown as the difference of radioactivity measured with radioligand and with co-incubation of AMD3100.

**Metabolic stability in human blood:** To evaluate the metabolic stability in human blood app. 5 MBq of the radiolabeled peptide were incubated in 1 mL of fresh blood samples (Heparin- or EDTA coated vials) at 37 °C for 1 and 3 h, respectively. After incubation, the blood samples were centrifuged at  $3,100 \times g$  (6,200 rpm) for 5 min. The plasma proteins were precipitated in ice cold MeCN for 10 min at 0 °C and collected by centrifugation at  $3,100 \times g$  (6,200 rpm) for

## MATERIALS AND METHODS

5 min. Samples of all pellets were measured in a  $\gamma$ -counter. The supernatant was ultrafiltrated and directly analyzed with radioHPLC (Chromolith Performance 18 E 4.6 x 100 mm; flow rate = 3mL/min; applied gradient: 3 to 95% B in 6 min, 220 nm). The resulting chromatogram was compared with the quality control after synthesis to detect radiometabolites. Samples from every step of blood preparation were measured in a  $\gamma$ -counter to calculate the extraction efficiency (%/ID).

### 9. Animal experiments

All animal experiments were conducted in accordance with German Animal Welfare Act (Deutsches Tierschutzgesetz, approval #55.2-1-54-2532-71-13) and at the Department of Nuclear Medicine at the Klinikum rechts der Isar (TUM). The B-Lymphoma cell line Daudi was suspended 1/1 in serum-free medium and matrigel (*BD Biosciences*, Germany) and approximately  $10^7$  cells in 200  $\mu$ L were inoculated subcutaneously on the right shoulder of 6 - 8 weeks old mice (CB-17 SCID, *Charles River Laboratories*, Germany). Tumors were grown for and 2 - 4 weeks to reach 8 – 10 mm in diameter.

#### 9.1. Metabolite analysis

The respective radiolabeled tracers (25 – 40 MBq) were injected into the tail vein of anaesthetized SCID mice. The animals were allowed to wake up and after 30 min they were sacrificed applying CO<sub>2</sub>. Samples from urine, blood, liver and kidney were taken immediately. The collected urine was dissolved in PBS and directly measured using radioHPLC. Parts of the liver and one kidney were frozen in liquid nitrogen, homogenized with a ball mill and extracted with 0.2 – 1 mL PBS containing 50  $\mu$ g of AMD3100. The suspension was first centrifuged (15,000 g) and after ultrafiltration the extracts were analyzed by radioHPLC (Chromolith Performance 18 E 4.6 x 100 mm; flow rate = 3 mL/min; applied gradient: 3 to 95% B in 6 min,

## MATERIALS AND METHODS

220 nm). The blood samples were centrifuged to separate the plasma from the blood cells. Plasma proteins were removed by precipitation with cold acetonitrile (50% (v/v), 10 min, 4 °C) and subsequent centrifugation and ultrafiltration as described before. The blood extract was also analyzed by radioHPLC. For all extracts the extraction efficiency was determined in a  $\gamma$ -counter.

### 9.2. Biodistribution

For biodistribution studies, the respective radiolabeled CXCR4 ligands (0.1 – 0.3 nmol) were injected into the tail vein of isoflurane anesthetized mice. The uptake of the radiopharmaceuticals in selected organs, tissues and body fluids (e.g. blood, heart, lungs, liver, spleen, pancreas, stomach (without content), intestine (with content), kidney, uterus, muscle, bone, skin, brain, tumor and tail) was examined at different time points p.i.. Weighted samples were quantified in a  $\gamma$ -counter. Specificity of binding was demonstrated by coinjection of 50  $\mu$ g of AMD3100 together with the radiolabeled peptide one hour p.i. (n = 3-4). Specific activity of the tracer, injected mass, molarity and determined time points are cited in the text with the respective experiment.

### 9.3. Small-animal PET imaging

PET imaging was performed using a *Siemens Inveon* small animal PET (Department of Nuclear Medicine, Klinikum rechts der Isar, TUM), followed by data analysis using the Inveon Research Workplace software. The animals were anesthetized with isoflurane, weighted and injected via tail vein with 2 – 10 MBq (0.1 – 0.25 nmol) of tracer. Injected activity is cited with the respective study in the text. Dynamic imaging was performed after on-bed injection for 1.5 h. Static images were recorded at 1 h post injection (p.i.) with an acquisition time of 15 min. For the competition study, animals were co-injected with 5 mg/kg of AMD3100 and static images were recorded 1 h p.i. for 15 min. Images were reconstructed using 3D ordered-subsets expectation maximization (OSEM3D) algorithm without scanner and attenuation correction.

### III. RESULTS AND DISCUSSION

#### 1. Synthesis

The development of cyclic peptide CXCR4 inhibitors starting from the endogenous ligand of CXCR4 CXCL12 (SDF-1) showed a complex relation between binding affinity and structural modifications. Based on SAR studies starting from T22 ([Tyr<sup>5,12</sup>, Lys<sup>7</sup>]-polyphemusin II, see Figure 3), *Fujii et al* developed the first cyclic pentapeptide FC131 (**R2**) with high affinity towards CXCR4 and high potency for HIV entry inhibition <sup>85, 86, 88, 97, 98, 100, 173, 174</sup>.

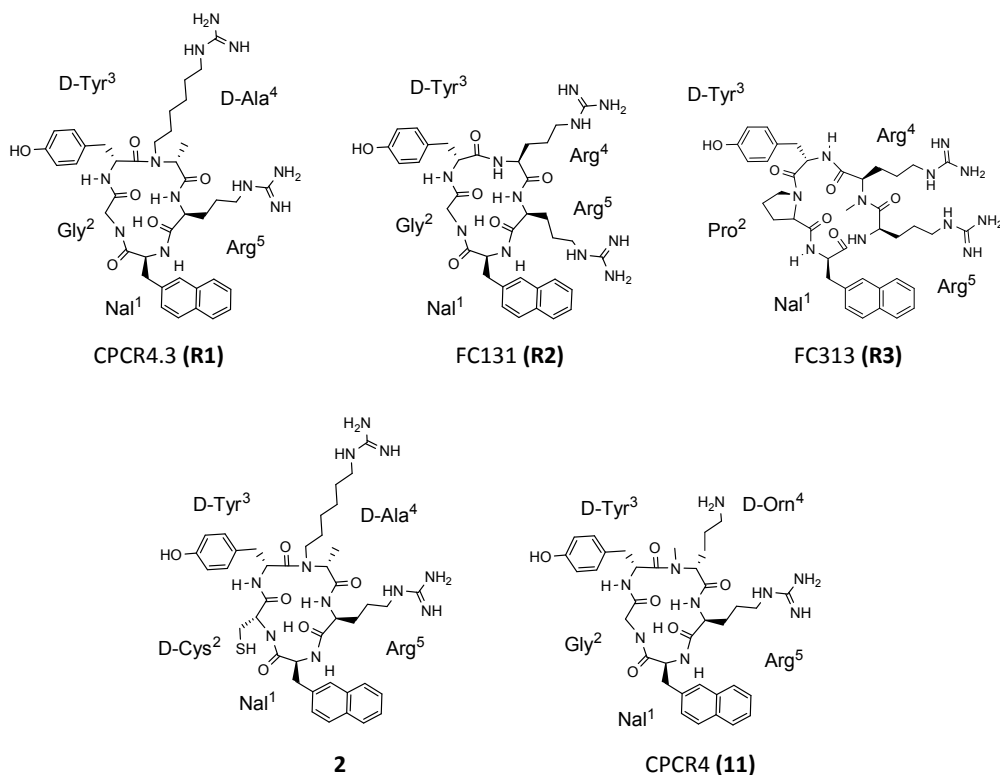


**Figure 8.** Structures of CXCR4 targeting lead scaffolds **R1** <sup>89</sup> and **R2** <sup>88</sup> with thereof derived cyclic pentapeptides **2** and **11** <sup>91</sup> and the chemical structure of CXCR7 targeting lead scaffold FC313 (**R3**) <sup>158</sup>.

In order to design novel CXCR4 affine ligands, different binding scaffolds developed in our group <sup>89, 91</sup>, were utilized for further modification and introduction of signaling units like chelators (for

## RESULTS AND DISCUSSION

radio metals), fluorescent dyes or  $^{18}\text{F}$ -labeled prosthetic groups. Recently, the group of *Fujii et al* reported the development of novel CXCR7-selective ligands through an SAR study based on the CXCR4-specific antagonist FC131 (**R2**)<sup>158</sup>. The respective pentapeptides **R1**, **R2** and **R3** (see Figure 8) were synthesized and employed as reference ligands, lead structures for further modifications and as precursor for radioiodination to be used as radioligands for *in vitro* evaluation of the novel ligands. The synthesis of all cyclic pentapeptides was performed on solid support applying standard Fmoc-protocol<sup>159, 175</sup> and recently published methods for *N*-Alkylation or *N*-Methylation, respectively<sup>103</sup>.

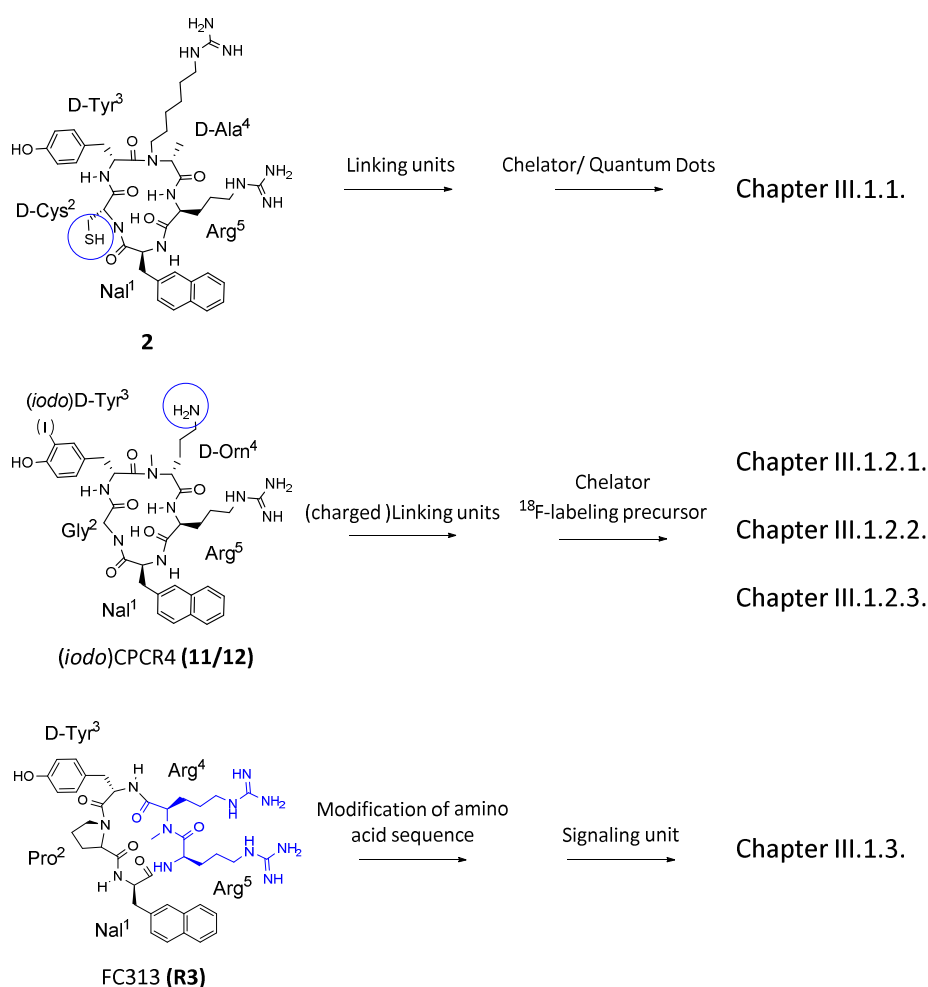


**Figure 9.** Overview of the synthetic routes and the separation into chapters according to the utilized lead structure.

## RESULTS AND DISCUSSION

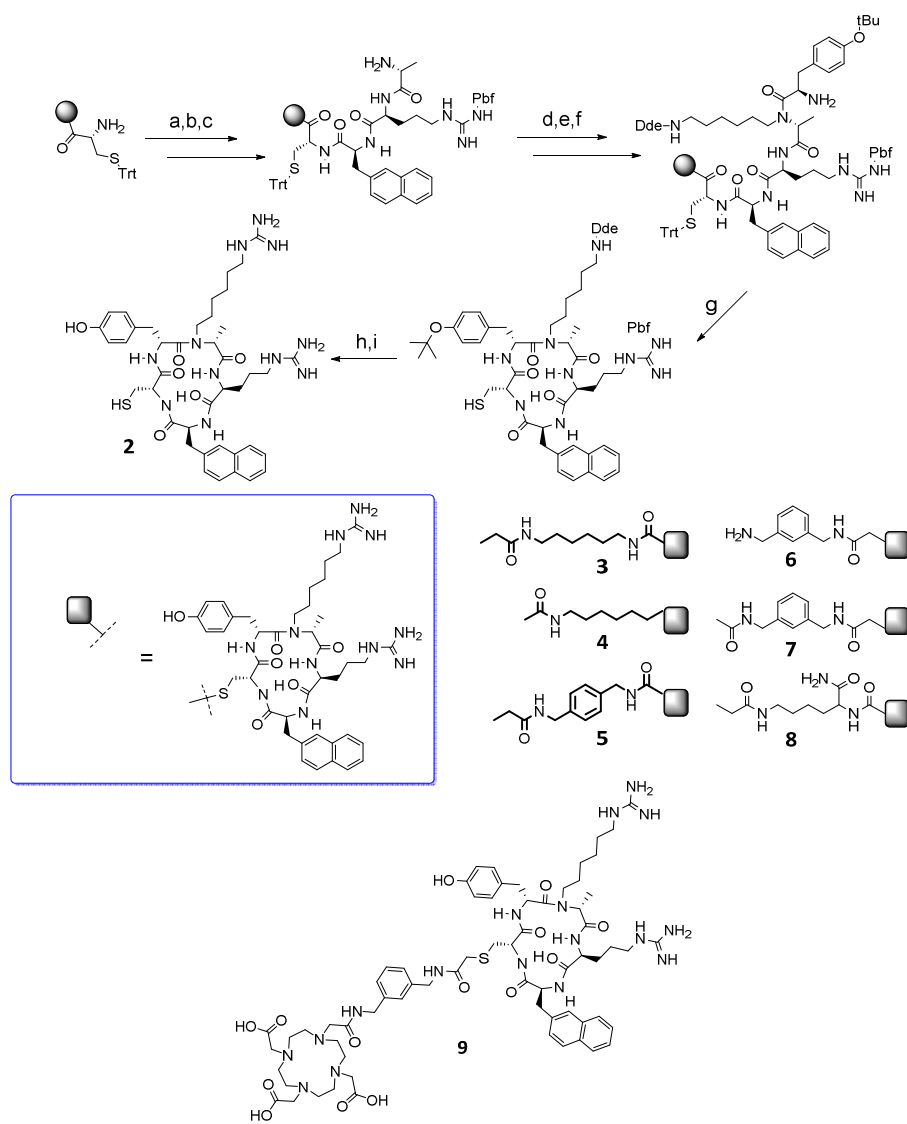
After cleavage from the resin and subsequent cyclization, the protected peptides were obtained with a reaction yield of 70% on average. On the basis of peptides **2** and **11** (Fig. 9), different linking units were introduced (III.1.1, III.1.2) to determine the influence of structural modifications on the receptor targeting traits of the novel compounds (III.1.2.1. *shifting the charge*, III.1.2.2. *optimization of the linking unit*). In addition, the novel derivatives were combined with imaging modalities (chelators, quantum dots (III.1.1), or  $^{18}\text{F}$ -radiosynthons (III.1.2.3.  *$^{18}\text{F}$ -labeling precursor*)). The following chapters are ordered by the utilized binding scaffold, starting with peptide **2**-based ligands (Fig. 9, III.1.1), then (*iodo*)CPCR4 (**11/12**)-based ligands (see III.1.2) and finally FC313 (**R3**)-based ligands for the targeting of CXCR7 (see III.1.3.).

### 1.1. Synthesis of cyclo[D-Tyr-N(hexylguanidino)-D-Ala-Arg-Nal-D-Cys] (**2**)-based compounds

To be able to utilize **R1** for a new series of molecular imaging agents, an alternative concept for backbone modification of FC131-derived cyclic pentapeptides was successfully integrated into the design of novel **R1**-based analogues. *Tanaka et al* had demonstrated that the substitution of glycine<sup>2</sup> by D-cysteine<sup>2</sup> in FC131 (**R2**) (Fig. 10) caused an only moderate loss of affinity and provided novel degrees of freedom for additional peptide modifications<sup>98, 100, 176</sup>. By combining this substitution concept and the *N*-alkylation strategy employed in **R1**, novel pentapeptide-based CXCR4 radioligands were developed (Fig. 10). Therefore, suitable linking units between the pentapeptide **2** and a “signaling unit” (fluorescent dye or chelator), were investigated. The linking units were introduced by reaction of the thiol group with acyl chloride- or alkylbromide-modified precursors in MeCN and H<sub>2</sub>O with DIPEA as base. The final products were acetylated on the *N*-terminus (acetic anhydride/DIPEA) and purified using RP-HPLC. The products were obtained in approximately 20% yield (based on **2**).



## RESULTS AND DISCUSSION



a) Fmoc-2Nal-OH, HOBt, TBTU, DIPEA [NMP], rt, 2h; 20% piperidine [DMF] 10 min; b) Fmoc-Arg(Pbf)-OH, HOBt, TBTU, DIPEA [NMP], rt, 2h; 20% piperidine [DMF] 10 min; c) Fmoc-D-Ala-OH, HOBt, TBTU, DIPEA [NMP], rt, 2h; 20% piperidine [DMF] 10 min; d) p-Ns-Cl and collidine [NMP], rt, 20 min; e) Triphenylphosphin, (Dde)aminohexanol, DIAD, 15 min, rt [THF]; then mercaptoethanol, DBU [NMP], 15 min, rt; f) Fmoc-D-Tyr(tBu)-OH, HATU, HOAt, DIPEA, rt, 3h [DMF]; 20% piperidine in DMF 10 min; g) DCM, Trifluoroethanol, acetic acid (6:3:1; v/v/v), 30 min, rt; NaHCO<sub>3</sub>, DPPA, 10 h, rt [DMF]; h) 3 % Hydrazine Monohydrate, 15 min, rt [DMF]; 1-H-Pyrazol-1-carboxamide, DIPEA, 6 h, rt [DMF]; i) trifluoroacetic acid, TIPS, H<sub>2</sub>O (95, 2.5, 2.5; v/v/v), 40 min, rt;

**Figure 10.** Synthetic route for the CXCR4 binding peptide (**2**). CXCR4 affine ligands in combination with different linkers (**3-8**).

The most affine compound **7** was utilized as its *N*-terminal free analog **6** for condensation with DOTA (**9**) and decoration of carboxyl-modified quantum dots (QD-**6**) for further investigation.

## RESULTS AND DISCUSSION

### 1.2. Synthesis of cyclo[D-Tyr-N(Me)-D-Orn-Arg-Nal-Gly] (**11**)-based compounds

#### 1.2.1. Shifting the charge

Detailed SAR studies revealed a pronounced dependency of CXCR4 affinity on the type and spatial arrangement of functional groups within the structure of FC131 (**R2**). Especially the side chains and the conformation of the backbone influence the binding affinity of cyclic pentapeptides, see Figure 3<sup>83, 97, 98, 100, 173, 174, 177</sup>. Nevertheless, a selection and iteration process including more than 200 compounds led to the development of [<sup>68</sup>Ga]Pentixafor ([<sup>68</sup>Ga]**23**), a first CXCR4 targeted PET agent with high affinity and selectivity for *h*CXCR4 and excellent *in vivo* pharmacokinetics<sup>90, 91, 125, 127</sup>. The binding affinity of **23** varies with the chelated metal and is therefore highly dependent on complex formation<sup>90, 91, 156</sup>. This phenomenon was reported for the somatostatin analogue DOTATOC<sup>178</sup>, as well as for inhibitors of the prostate specific membrane antigene (PSMA), before<sup>161, 178-180</sup>.

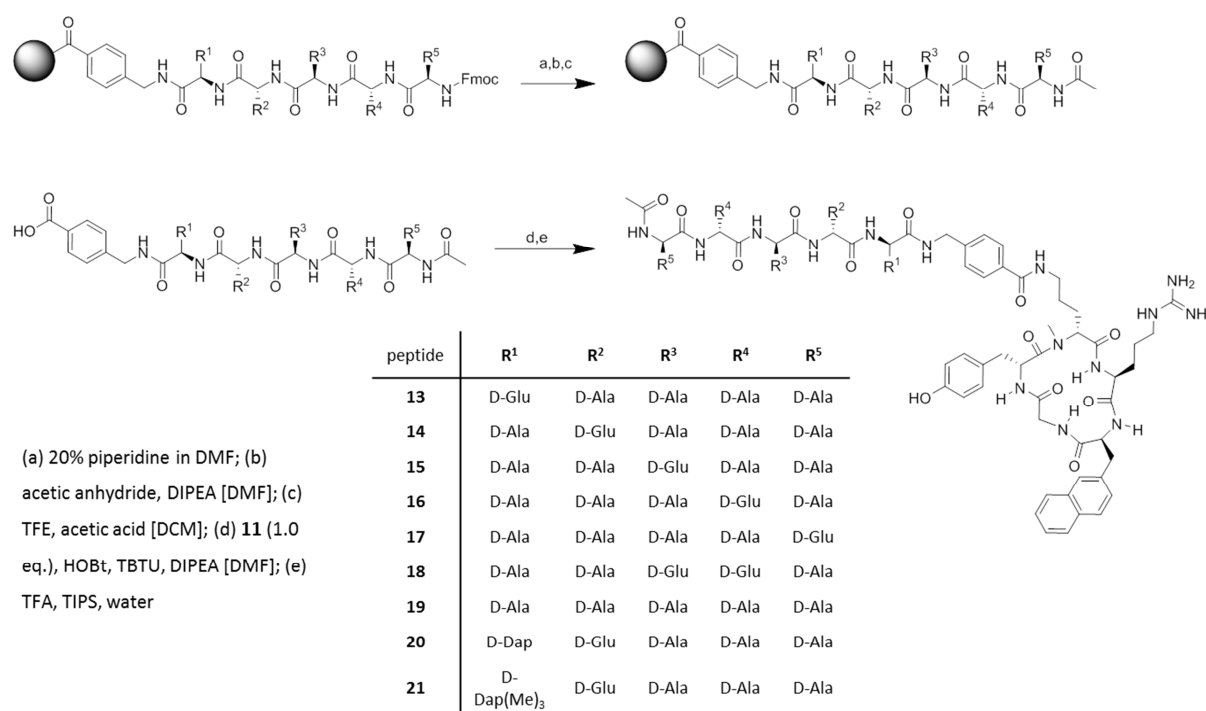


**Figure 11.** Schematic synthesis route for peptides employed in the “shifting the charge” study. For *in vitro* evaluation, the respective linear peptides were acetylated at the *N*-terminus to mimic an amide bond of further conjugation.

## RESULTS AND DISCUSSION

To address the pronounced variations in binding affinities for different  $M^{II/III}$ -chelates of **23**, a series of specifically designed linking peptides were synthesized and evaluated *in vitro* in terms of CXCR4 binding affinity. By shifting glutamic acid (negative charge) from the 4-aminomethyl benzoic acid (4-AMBA) spacer between DOTA and **11** (CPCR4) (employed in **23**), alongside a D-alanine-based peptide chain, the influence on the binding affinity was monitored. All amino acid spacer were constructed on solid support and either acetylated on the *N*-terminus or cleaved from the resin with terminal Fmoc-protection. After cleavage from the resin and HPLC purification, the linear peptides were combined with **11** (CPCR4) (see Figure 11). Conjugation to the chelator was performed in solution after HPLC purification.

**Amino acid spacer:** The different five-amino acid spacers were synthesized according to a standard Fmoc-protocol solid-phase peptide synthesis (using HOBt, TBTU and DIPEA in NMP). Therefore, TCP resin was loaded with 4-(aminomethyl)benzoic acid and the peptides with D-Glu at stepwise altering positions, together with (D-Ala)<sub>3</sub>-D-Glu-D-dap and (D-Ala)<sub>3</sub>-D-Glu[N(Me)<sub>3</sub>]D-dap were prepared similarly (Figure 11). Coupling steps were quantitative within 1.5 h, though for the first amino acid, the coupling time had to be prolonged to 3 h to obtain reasonable conjugation. To confirm quantitative coupling yields, a small amount of peptide was cleaved from the resin and analyzed by HPLC and ESI-MS. For optimal synthesis yields, all side chain functionalities (for glutamic acid and diaminopropionic acid) were orthogonally protected.

**Peptide acetylation:** For *in vitro* evaluation, the amino acid spacer had to be acetylated at the *N*-terminus. Quantitative acetylation of the unprotected *N*-terminal amine was achieved with incubation of the resin-bound peptides with acetic anhydride and DIPEA for 30 min at rt.

**Fragment condensation:** For fragment condensation between the acetylated or Fmoc-protected amino acid spacer (1.5 eq.) and **11**, HOBt, TBTU and DIPEA were used. Condensation of the fragments was quantitative within 2 h and the products were purified using HPLC.

## RESULTS AND DISCUSSION

**Chelator conjugation:** DOTA was conjugated to the D-Ala-D-Ala-D-Ala-D-Ala-D-dap spacer. Quantitative coupling of DOTA in solution <sup>162</sup> *via in situ* formation of the NHS ester was achieved by preincubation of unprotected DOTA (4.0 eq.) with NHS, EDC and DIPEA for 10 min and subsequent reaction with the peptides for another 15 min.

### 1.2.2.1. Iodination of the cyclic binding scaffold *CPCR4* (11)

A second approach for modifications of **23** (Pentixafor) was prompted by a detailed *in vitro* evaluation of [<sup>nat</sup>Ga]**23**. The results revealed, that the radioiodinated analogue of [<sup>nat</sup>Ga]**23**, [<sup>125</sup>I]-[<sup>nat</sup>Ga]**23** inherits a significant higher binding affinity for *hCXCR4* <sup>181, 182</sup>. However, the *de novo* synthesis of *iodo-23* was not successful by means of standard Fmoc-synthesis, because of the fact that Fmoc-3-*iodo*-D-Tyr-OH is not available in its sidechain protected form. A variety of side products decreased the reaction yield during solid phase synthesis.

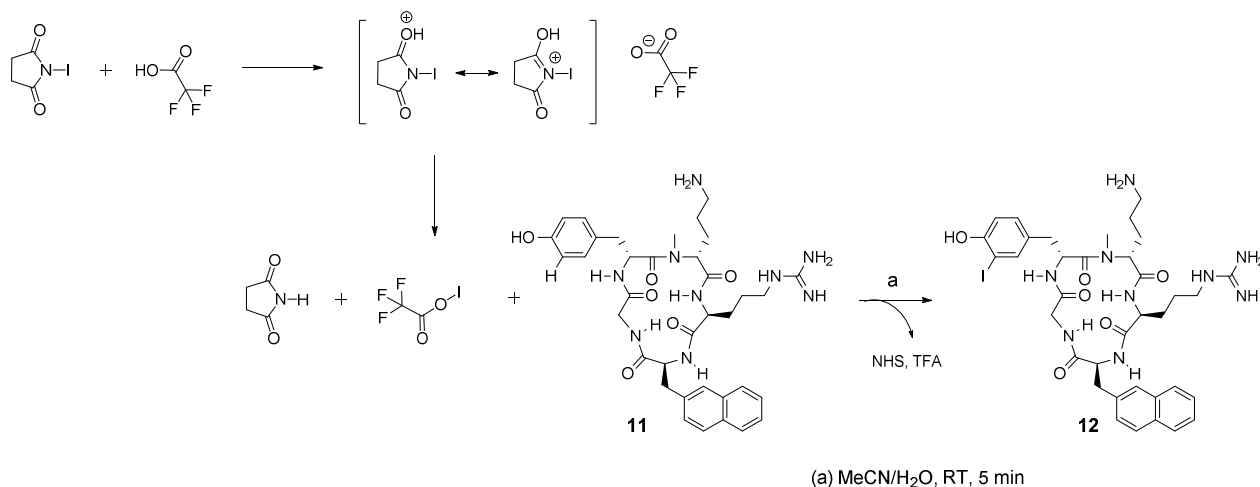


**Figure 12.** Proposed reaction scheme of TFA catalyzed, direct iodination of peptide **11**.

The *N*-methylated D-Orn<sup>4</sup> which had to be reacted with Fmoc-3-iodo-D-Tyr-OH further decreased the reaction yield and made the synthesis of **24** on solid support not practicable. Fortunately, within the scope of this work, *Schottelius et al* designed a method for direct iodination of bioactive small peptides under mild conditions <sup>160</sup>. This method employs *N*-iodo-

## RESULTS AND DISCUSSION

succinimide (NIS) on HPLC purified peptides. The presence of even catalytic amounts of TFA has been shown to greatly enhance the iodination yields of deactivated aromatic compounds using NIS due to the *in situ* formation of a highly electrophilic trifluoroacetyl hypoiodite<sup>183</sup>. This method could be smoothly applied for **23**, resulting in good yields ( $28 \pm 8\%$ ) of **24** after HPLC purification (see Figure 12). The effects of structural modification in the linking unit on binding affinity (III.3.2.), receptor internalization (III.3.2.) and lipophilicity (III.4.) were determined within this project.

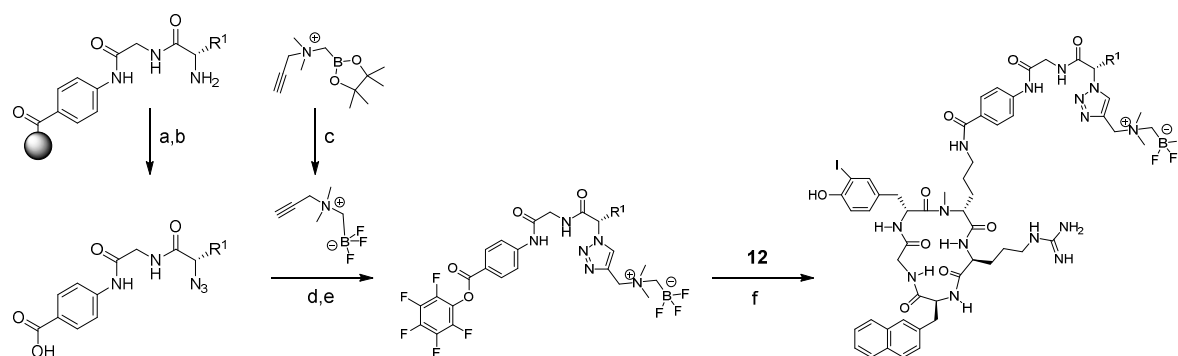
### 1.2.2.2. Optimization of the “linking unit”

Again, the ligands were synthesized using fragment condensation between the activated ester of the amino acid spacer (still Fmoc-protected) and the binding scaffold **11** (CPCR4). Subsequent Fmoc-deprotection, combination with the chelator, HPLC purification and iodination of D-tyrosine resin resulted in the novel CXCR4 ligands. Therefore, 4-((Fmoc)amino)-benzoic acid (4-Fmoc-ABA) was loaded on TCP-resin employing DIPEA as the base. Fmoc-glycine, D-alanine or D-asparagine was coupled utilizing HATU, HOAt and DIPEA due to the reduced reactivity of the aniline analogue. Additional amino acids could be reacted with the Fmoc-deprotected peptides using HOBt, TBTU and DIPEA. Quantitative coupling was achieved within 2 h. The Fmoc-protected peptides were cleaved from the resin. After precipitation in water, the peptides were reacted with **11** in the presence of HOBt, TBTU and DIPEA in DMF. The purified, *N*-terminal free peptides were then reacted with either DOTAGA-anhydride and DIPEA as the base at rt for 16 h, or with unprotected DOTA within 2 h employing NHS, EDCI\*HCl and DIPEA. Purification and subsequent iodination of D-tyrosine resulted in the desired iodinated derivatives of **24**. In most cases, relatively low yields (1 to 5%) were received, caused by high losses during multiple purification steps. Resin-bound conversion of peptides and chelator and subsequent combination with iodinated **11** (**12**) might improve the efficiency of the synthesis.

## RESULTS AND DISCUSSION

### 1.2.3. $^{18}\text{F}$ -labeling precursor

Several  $^{18}\text{F}$ -labeled CXCR4 targeting probes have been reported <sup>95, 96, 184</sup> so far. However, the tumor to background ratios are decreased due to extensive binding to red blood cells <sup>96</sup>, or unfavorable physiological distribution *in vivo* <sup>95</sup>. Conventional radiofluorination of small peptides is limited to multi-step procedures, involving prosthetic groups, which often results in prolonged reaction times <sup>185</sup> and low radiochemical yields <sup>186</sup>. In contrast, direct radiofluorination can be achieved by the utilization of  $[\text{Al}^{18}\text{F}]^{2+}$ -chelates with 1,4,7-triazacyclononane-triacetic acid (NOTA) or isotopic exchange reactions <sup>187-193</sup>. Isotopic exchange has successfully been utilized for  $^{18}\text{F}$ -labeling of both  $\text{R-BF}_3$  and SiFA-modified ligands. For these radiosyntheses, isotopic exchange conditions are milder than those of nucleophilic displacement, performed at lower temperature under moderately acidic conditions between  $\text{pH} \sim 1.5 - 2.5$  for  $\text{R-BF}_3$  and  $\text{pH} \sim 5.0 - 7.0$  for SiFA <sup>187</sup>. Consequently, to guarantee the stability of the  $\text{R-BF}_3$  group against hydrolysis during isotopic exchange and *in vivo* application, ((ethynyldimethyl-ammonio)methyl)-trifluoroborate ( $\text{AmBF}_3$ ) was published as a *radio-synthon* for  $^{18}\text{F}$ - $^{19}\text{F}$  isotopic exchange <sup>166, 194-197</sup>. Reported radiolabeling yields of up to 40% and specific activities of  $\geq 3 \text{ Ci}/\mu\text{mol}$  (98% radio purity) overcome the former limitations of isotopic exchange reactions <sup>166</sup>.



(a) **38**, DIPEA,  $\text{CuSO}_4$  [DMF]; (b) TFE, DCM, acetic acid; (c)  $\text{KHF}_2$ ,  $\text{HCl}$ ,  $\text{H}_2\text{O}$  [DMF]; (d)  $\text{CuSO}_4$ ,  $\text{C}_6\text{H}_7\text{NaO}_8$ , [ $^t\text{Bu-OH}/\text{H}_2\text{O}$ ]; (e)  $\text{C}_6\text{HF}_5\text{O}$ , DMAP, DIC [DMF] (f) DIPEA [DMF]

**Figure 13.** Reaction route for  $^{18}\text{F}$ -labeling precursor: I) construction of the peptidic linker on solid support ( $\text{R}^1$  represents different amino acids), II) diazo-transfer on solid support (a, b), III) preparation of  $\text{AmBF}_3$  synthon and *in situ* 1,3-dipolar cycloaddition (c, d), IV) preparation of the respective pentafluorophenolester (e), V) combination of iodinated scaffold **12** and the linker (f).

## RESULTS AND DISCUSSION

Therefore, **37** (pinakol ester of AmBF<sub>3</sub>) was utilized as a synthetic unit to guarantee *in vivo* stability of the novel <sup>18</sup>F-labeled ligands. The boronylpinakolester **37** was available for synthesis according to literature <sup>166, 198</sup>. Under dry conditions *N,N*-dimethylpropargylamine was reacted with iodomethylboronyl-pinacolate in high yields (93 ± 5%). The synthetic route of AmBF<sub>3</sub> modified peptides affords 1,3-dipolar cycloaddition as described in literature <sup>195, 198, 199</sup>. Therefore, an azido residue has to be introduced at a primary amine (*N*-terminus or side chain) of the respective ligands. A diazo-transfer reaction on solid support could be established according to previously published procedures <sup>164</sup>. Upon addition of catalytic amounts of CuSO<sub>4</sub>, the *N*-terminus could be converted to the respective azide within few hours (Figure 13). Due to the sensitivity of the BF<sub>3</sub>-group against reductive conditions, the synthesis of the <sup>18</sup>F-precursor was divided into several synthesis steps (mainly the preparation of the linking unit as fluorination precursor and the preparation of the cyclic binding scaffold).

First, the linking unit was prepared on solid support, converted to its respective azide and combined with the AmBF<sub>3</sub> synthon (Figure 13). The linking unit was transformed to the pentafluorophenyl ester and purified using semi-preparative HPLC. Then, the binding scaffold (CPCR4, **11**) was constructed on solid support, cyclized and iodinated subsequently, using NIS in MeCN and water (Fig. 13). After purification, the novel CXCR4 ligands were obtained after fragment condensation of the activated ester (AmBF<sub>3</sub>-(Xaa)<sub>n</sub>-4-ABA-Pfp) and the iodinated binding scaffold **12** (*iodoCPCR4*).

**Synthesis of the activated ester AmBF<sub>3</sub>-(Xaa)<sub>n</sub>-4-ABA-Pfp:** The peptide spacer were synthesized according to a standard Fmoc-protocol solid-phase peptide synthesis (using HATU, HOAt, DIPEA in DMF). 4-aminobenzoic acid was loaded on a TCP resin in quantitative yields. The peptides Fmoc-D-Lys-Gly-4-ABA (**43**), Fmoc-D-Arg-Gly-4-ABA (**42**, **41**), Fmoc-D-Val-Gly-4-ABA (**40**) and 4-Fmoc-ABA (**39**) were prepared accordingly. To confirm quantitative coupling yields, a small amount of peptide was cleaved from the resin and analyzed by HPLC and MS. After Fmoc-deprotection (20% piperidine in DMF), the primary amine was reacted with imidazole-1-sulfonyl azide hydrochloride (**38**) in the presence of catalytic amounts of CuSO<sub>4</sub> and

## RESULTS AND DISCUSSION

DIPEA in DMF. Quantitative conversion to the azide was monitored after 16 h, in general. Thus, after cleavage from the resin, the azide-peptides were purified using HPLC. For the 1,3-dipolar cycloaddition, **37** was converted to ((dimethyl(prop-2-yn-1-yl)ammonio)methyl)-trifluoroborate (AMBF<sub>3</sub>) in the presence aqueous KHF<sub>2</sub> and HCl in DMF (see Figure 13) and reacted *in situ* with the respective azide-peptides at 60 °C over night. After purification, quantitative formation of the pentafluorophenyl ester was achieved by incubation of AMBF<sub>3</sub>-(Xaa)<sub>n</sub>-4-ABA together with DMAP, 2,3,4,5,6-pentafluorophenol and DIC for 1.5 h. The resulting active esters were purified using HPLC and can be stored at −20 °C until further application.

**Combination with the binding scaffold:** For the fragment condensation, the activated peptide esters (1.1 eq.) were dissolved in dry DMF. The deprotected binding scaffold **11** or **12** was also dissolved in DMF together with DIPEA and added to the mixture. Quantitative conjugation was achieved within 1 h. After final HPLC purification the <sup>18</sup>F-labeling precursor could be received with yields of 5 to 15%. Due to the optimized strategy utilizing the pentafluorophenyl ester, a minimum amount of binding scaffold is needed and unreacted peptide can be recovered during HPLC purification.

### 1.3. Ligands based on cyclo[D-Tyr-Pro-Nal-N(Me)-Arg-Arg] (R3) for addressing the CXC chemokine receptor type 7

For a long time, CXCR4 was thought to be the only receptor for CXCL12, with CXCL12 being its only (endogenous) ligand <sup>19</sup>. However, only recently, the orphan receptor RDC-1/CXCR7 was shown to bind and internalize CXCL12 on T lymphocytes <sup>10</sup>. Routinely performed binding assays with liver cells from CXCR4-deficient mice supported this hypothesis later on. Radio-labeled CXCL12 showed persistent affinity which also led to the identification of the former orphan receptor RDC-1/CXCR7 as alternative receptor for CXCL12. In addition, CXCL11 also binds to CXCR7, but with about 10-fold lower affinity <sup>25</sup>. Interestingly, Plerixafor



## RESULTS AND DISCUSSION

or AMD3100, a known antagonist for CXCR4<sup>79, 200</sup> works as an allosteric agonist of the  $\beta$ -arrestin pathway of CXCR7<sup>201</sup>.

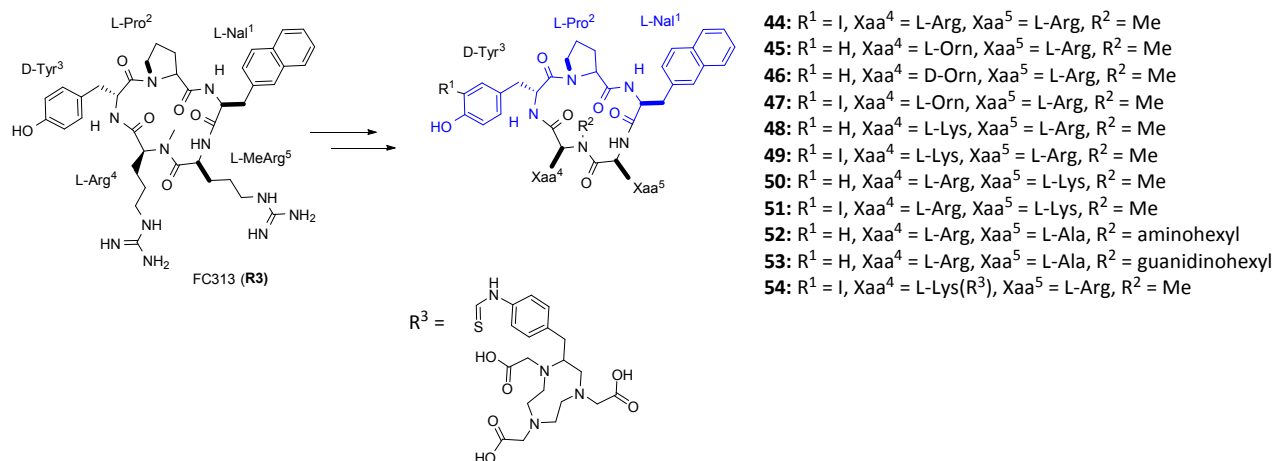


**Figure 14.** Structural modifications used in the SAR study starting from FC313 (**R3**). Blue amino acids were kept constant during the structural modification process.

Several analog observations with 17mer peptides and allosteric agonists imply that CXCR7 and CXCR4 share at least parts of the receptor surface to recognize similar scaffolds or substructures<sup>202</sup>. *Oishi et al*<sup>158</sup> recently published a SAR study based on the CXCR4 specific ligand FC131 (**R2**) in which they identify novel CXCR7 selective ligands. Based on published hexapeptides, which induced CXCR7-mediated  $\beta$ -arrestin recruitment, the substructure motif Arg-Arg-Nal was found to be responsible for the binding affinity<sup>203</sup>. This indicated the possibility that both CXCR4 and CXCR7 may recognize identical functional groups. *Oishi et al* speculated that novel CXCR7 ligands with a cyclic pentapeptide scaffold can be developed *via* selectivity switch from **R2**. This led to the development of FC313 (**R3**), a potent ( $IC_{50} = 0.80 \pm 0.3 \mu M$ , measured against [ $^{125}I$ ]SDF-1 $\alpha$  binding to CXCR7<sup>158</sup>), CXCR7-selective ligand (selectivity:  $IC'_{50}$  measured on CXCR4+ cells vs. CXCR7+ cells:  $>30 \mu M$  vs.  $0.80 \pm 0.3 \mu M$ <sup>158</sup>). Therefore, **R3** was utilized as a lead structure for the development of novel CXCR7 specific radiotracer with potential for PET-imaging. Since **R3** is the only known CXCR7-specific ligand, [ $^{125}I$ ]**R3** was utilized as the

## RESULTS AND DISCUSSION

radioligand for the *in vitro* evaluation. All modifications on the scaffold were introduced on solid support according to standard Fmoc-protocol and methods described in literature<sup>103, 158</sup>.

**Peptide synthesis:** Since three amino acids were shown to be crucial for CXCR7 binding (D-Tyr<sup>3</sup>-L-Pro<sup>2</sup>-L-Nal<sup>1</sup> are labeled blue in Figure 14)<sup>158</sup>, all potential CXCR7 ligands were constructed starting from L-proline loaded resin. The five amino acid chain was assembled according to a standard Fmoc-protocol solid-phase peptide synthesis (using HATU, HOAt and DIPEA in NMP). The peptides Pro-Nal-N(Me)-Arg-Arg-D-Tyr (FC313, **R3**), Pro-Nal-N(Me)-Arg-Orn-D-Tyr (**45**), Pro-Nal-N(Me)-Arg-D-Orn-D-Tyr (**46**), Pro-Nal-N(Me)-Arg-Lys-D-Tyr (**48**), Pro-Nal-N(Me)-Lys-Arg-D-Tyr (**50**), Pro-Nal-N(aminohexyl)-Ala-Arg-D-Tyr (**52**) and Pro-Nal-N(guanidinoethyl)-Ala-Arg-D-Tyr (**53**) were prepared similarly. Amino acid coupling steps were quantitative within 2 h, shown by reaction control with a small amount of peptide (HPLC and MS). *N*-methylation or *N*-alkylation was conducted on solid support as described in literature<sup>103, 158</sup> and generally worked in almost quantitative yields. For optimal synthesis, all side chain functionalities were orthogonally protected. After cleavage from the resin (DCM, TFE and acetic acid), the fully protected linear peptides were treated with NaHCO<sub>3</sub> (5.0 eq.) and DPPA (3.0 eq.) in DMF to yield the cyclic pentapeptides. After precipitation in water and final deprotection, employing TFA, TIPS and water, the CXCR7 ligands were collected in 60 to 80% yield.

**Iodination of the D-tyrosine side chain:** For the iodination of D-tyrosine side chains, the cyclic peptides were purified using HPLC. Due to altering iodination yield ratios (unreacted/ mono-iodinated/ di-iodinated), the optimal amount of NIS (0.2 - 0.6 eq.) had to be determined for every iodination step. Therefore, to avoid the formation of unwanted di-iodo species and since unreacted equivalents of starting peptide could be recovered during HPLC purification, low amounts of NIS were employed, resulting in reaction yields of maximum 40%.

**Introduction of the chelator:** To enable PET-imaging, the isothiocyanat-modified chelator NOTA was conjugated to peptide **53**. Coupling in solution required only a 1.1-fold molar excess

## RESULTS AND DISCUSSION

of SCN-Bn-NOTA and DIPEA (10 eq.) in DMF (16 h) and resulted in 53% yield after HPLC purification.

### 1.4. Metal complexation

All novel CXCR4 and CXCR7 targeted compounds and reference ligands, as well as their metal complexes evaluated in this study, are summarized in section III.3.. Quantitative metal complex formation was confirmed by HPLC and MS. The metal chelates were directly used for *in vitro* evaluation without further purification.

## 2. Radiolabeling

### 2.1. Radioiodination

The radioiodinated ligands [ $^{125}\text{I}$ ]**R1**, [ $^{125}\text{I}$ ]**R2** and [ $^{125}\text{I}$ ]**R3** served as radioligands in all competitive binding assays. For standard determination of  $IC_{50}$  on CXCR4<sup>+</sup> Jurkat cells, [ $^{125}\text{I}$ ]**R2** was utilized. All modifications of assay conditions are stated within the respective experiment. As an established experimental radionuclide,  $^{125}\text{I}$  was selected. Suitable radiation characteristics ( $E_{\text{max}, \gamma} = 35 \text{ keV}$ ,  $t_{1/2} = 59.4 \text{ days}$ ) and convenient practicability (radioligands are useful for up to 6 weeks) are key advantages of  $^{125}\text{I}$ . Based on procedures known from the literature, the iodogen method<sup>204</sup> was utilized for the introduction of  $^{125}\text{I}$  in the tyrosine sidechains of all reference ligands. After HPLC purification, the final products were obtained in radiochemical yields of 40 - 66% and radiochemical purities of > 95%. Radiolysis or degradation within 4 to 6 weeks was never detected using HPLC, most likely due to the low concentration of the radioligands in solution.

### 2.2. $^{68}\text{Ga}$ -labeling

Preparation of  $^{68}\text{Ga}^{\text{III}}$  for labeling of DOTA-conjugated peptides was performed by a combination of previously described methods<sup>170, 171, 205</sup>. The  $^{68}\text{Ga}$ -labeling for *in vivo* biodistribution and PET imaging studies was carried out using a fully automated GMP-

## RESULTS AND DISCUSSION

compliant procedure on a GRP synthesizer (Scintomics GmbH, Germany) <sup>206</sup>. The obtained specific activities were 60 – 110 GBq/ $\mu$ mol.

### 2.3. <sup>177</sup>Lu-labeling

The <sup>177</sup>Lu-labeling protocol was obtained after optimization of reaction buffer, pH and reaction time <sup>207-209</sup>. The obtained RCY were > 97% for complexation of DOTA-conjugated peptides, resulting in specific activities of  $A_s \geq 30$  GBq/ $\mu$ mol.

### 2.4. <sup>18</sup>F-labeling

The radiolabeling was performed manually with starting activities of 2 - 4 GBq of trapped <sup>18</sup>F-fluoride on a small QMA cartridge. Due to low reaction yields in the range of 2 - 4% RCY and precursor amounts of 100 - 150 nmol, the obtained specific activities were 0.3 GBq/ $\mu$ mol. For comparison, the RCYs and specific activities reported for AmBF<sub>3</sub>-mediated isotopic exchange reactions in the literature are 25% and 11.1 GBq/ $\mu$ mol <sup>157</sup>. This is mostly due to the elevated starting activities (up to 45 GBq) used for the isotopic exchange reaction <sup>165, 198</sup>. Consequently, in order to determine the entire potential of AmBF<sub>3</sub>-conjugated CXCR4 ligands, the <sup>18</sup>F-labeling protocol has to be further optimized in respect to a fully automated synthesis.

## 3. *In vitro* evaluation

A variety of different assays for affinity determination of novel ligands for CXCR4 and CXCR7 are reported in literature. Since some are based on the inhibition of the [<sup>125</sup>I]SDF-1 binding and others use a competitive binding assay with other reference ligands, comparison of published binding affinities with experimentally achieved results using different assays is of limited value <sup>88, 98, 210, 211</sup>. Therefore, published CXCR4 or CXCR7 ligands were synthesized and

## RESULTS AND DISCUSSION

included in the *in vitro* evaluation to enable direct and valid comparison. In addition, as shown for development of other ligands evaluated in our group (e.g. Glutamate Carboxypeptidase II inhibitors, ‘PSMA-inhibitors’) <sup>161</sup>, vital cells with endogenous CXCR4 or CXCR7 expression were employed rather than transfected cell lines <sup>95</sup> or membrane aliquots <sup>158</sup> to establish a reproducible and valid test system. To compare the binding affinities of the various ligands towards the respective receptor, the half maximal inhibitory concentration ( $IC_{50}$ ) was determined in a competitive binding assay using the radioligands ( $[^{125}I]$ **R1-R3**). A defined low concentration of the radioligands (0.1 to 0.2 nM) ensures low occupancy of the G-protein coupled receptor and allows reproducible measurement using a  $\gamma$ -counter. For data normalization, as well as assay validation (especially for CXCR7 binding assays), the  $IC_{50}$  for the literature compounds **R2** <sup>88</sup> and **R3** <sup>158</sup> were included in our assay.

### 3.1. Cyclo[D-Tyr-N(hexylguanidino)-D-Ala-Arg-Nal-D-Cys] (2) based compounds

To investigate the influence of D-cystein<sup>2</sup> for glycine<sup>2</sup> substitution and subsequent introduction of linking units (*N*-terminal acetylated), the binding affinities were measured. Starting from CPCR4.3 (**R1**), the substitution of glycine<sup>2</sup> with D-cysteine<sup>2</sup> resulted in a 12-fold decrease ( $IC_{50}$  (**2**) =  $35 \pm 2$  nM) of binding affinity compared to **R1** ( $IC_{50}$  (**R1**) =  $2.8 \pm 1.1$  nM), see Table 4 and also Figure 10.

**Introduction of a linking unit:** As shown by the  $IC_{50}$  values in Table 4, the introduction of *N,N'*-(hexane-1,6-diyl)diacetamide (**3**) or *N*-hexylacetamide (**4**) as linking units resulted mostly in massive losses of binding affinity towards *h*CXCR4. Based on the SAR studies of FC131 <sup>88</sup>, the positively charged linking unit *N,N'*-(6-amino-6-oxohexane-1,5-diyl)diacetamide of **8** was speculated to increase CXCR4 affinity, but showed only moderate *h*CXCR4 binding ( $61 \pm 8$  nM). Compared to the lead structure **R1**, the aromatic spacer of compound **5** and **7** (1,3 and 1,4-phenylen-dimethanamine, respectively), however exhibited a more promising (only 5-fold lower) binding affinity. In fact, with an  $IC_{50}$  of  $14 \pm 2$  nM, ligand **7** was more potent than any

## RESULTS AND DISCUSSION

other ligand tested in this approach and was therefore chosen for further evaluation (conjugation of the *N*-terminal free analogue **6** with the chelator (DOTA) and decoration of QDs).

**Table 4.** The half maximal inhibitory concentration ( $IC_{50}$  [nM]) of *h*CXCR4 targeting cyclic pentapeptides determined in a competitive binding assay using Jurkat cells ( $4.0 \times 10^5$  cells/well, 2 h, rt, HBSS + 1% BSA) and ( $[^{125}\text{I}]\mathbf{R2}$  ( $c = 0.1$  nM) as the radioligand. Data are expressed as mean  $\pm$  SD of at least three independent determinations.

Cyclo[D-Tyr-N(hexylguanidino)-D-Ala-Arg-Nal-D-Cys] ( <b>2</b> ) based ligands			
Peptide	$IC_{50}$ [nM]	peptide	$IC_{50}$ [nM]
CPCR4.3 ( <b>R1</b> )	$2.8 \pm 1.1$	<b>8</b>	$61 \pm 8$
FC131 ( <b>R2</b> )	$10 \pm 2.3$	<b>9</b>	$78 \pm 4$
<b>2</b> (D-Cys <sup>2</sup> -CPCR4.3)	$35 \pm 2.1$	$[\text{natGa}]\mathbf{9}$	$31 \pm 3$
<b>3</b>	$> 400$	$[\text{natLu}]\mathbf{9}$	$51 \pm 4$
<b>4</b>	$57 \pm 14$	$[\text{natCu}]\mathbf{9}$	$78 \pm 5$
<b>5</b>	$53 \pm 16$	QDs- <b>6</b>	$6.1 \pm 0.3$
<b>7</b>	$14 \pm 2.0$		

**Conjugation with DOTA:** As anticipated, the introduction of the chelator DOTA into the 1,4-phenylen-dimethanamine modified peptide **6** decreased the binding affinity towards CXCR4 almost 6-fold. This has been reported for CXCR4 antagonists before<sup>91</sup>. Nonetheless, compared to the free DOTA-conjugate, the  $\text{natGa}^{\text{III}}$ -chelate **9** exhibits a 2.5-fold increase in binding affinity. In addition,  $[\text{natGa}]\mathbf{9}$  exhibited a 1.6-fold increased affinity compared to  $[\text{natLu}]\mathbf{9}$  and even 2.5-fold increase compared to  $[\text{natCu}]\mathbf{9}$  ( $IC_{50} = 31 \pm 3$  nM,  $51 \pm 4$  nM and  $78 \pm 5$  nM, respectively). The high dependence of the binding affinity of the peptide and its chelation state was reported before for pentixafor-based ligands<sup>156</sup> and also DOTA-coupled octreotide analogues<sup>90, 178</sup>.

## RESULTS AND DISCUSSION

**Decoration of QDs:** The decorated QDs (QDs-6) featured very high binding affinity with an  $IC_{50}$  of  $6.1 \pm 0.3$  nM (Tab. 4); the elevated concentration of functional ligand on the surface of the QDs, positively enhance the apparent binding affinity. In addition to the  $IC_{50}$  values for human CXCR4, the affinity towards murine CXCR4 was evaluated as well (Tab. 5). Since **R1** shows very high binding affinity towards murine CXCR4 (previously evaluated within our group, not published yet), this radioligand was utilized for the competitive *m*CXCR4 binding assay. Both [<sup>nat</sup>Ga]**9** and QDs-6 demonstrated high binding affinities for murine CXCR4 (Tab. 5) and were hence further evaluated in terms of PET-imaging and fluorescent microscopy.

**Table 5.**  $IC_{50}$  values of selected ligands for murine CXCR4 determined with Eμ-Myc1080 mouse B-cell lymphoma cells ( $2 \times 10^5$  cells/well, 2 h, rt, HBSS + 1% BSA) using [<sup>125</sup>I]CPCR4.3 ([<sup>125</sup>I]**R1**) ( $c = 0.1$  nM) as radioligand.

<i>IC<sub>50</sub> for mCXCR4</i>	
peptide	$IC_{50}$ [nM]
FC131 ( <b>R2</b> )	$119 \pm 69$
CPCR4.3 ( <b>R1</b> )	$0.8 \pm 0.1$
[ <sup>nat</sup> Ga] <b>9</b>	$63 \pm 19$
QDs-6	$3.3 \pm 0.7$

**Fluorescence imaging with QDs-6:** Fluorescent imaging of CXCR4 expression was performed on three different cell lines, Chemicon's Wild-Type Chem-1 cells, Daudi human B-Lymphoblast cells and Eμ-Myc1080 mouse B-cell lymphoma cells, all known to intensively express CXCR4. QDs-6 showed intense binding to Daudi, Eμ-Myc1080 and Chem\_1 cells at a concentration of 25 – 100 nM (Figure 15). Under internalization inhibiting conditions (incubation at rt) binding of QDs-6 on the cell membrane is clearly visible.

## RESULTS AND DISCUSSION

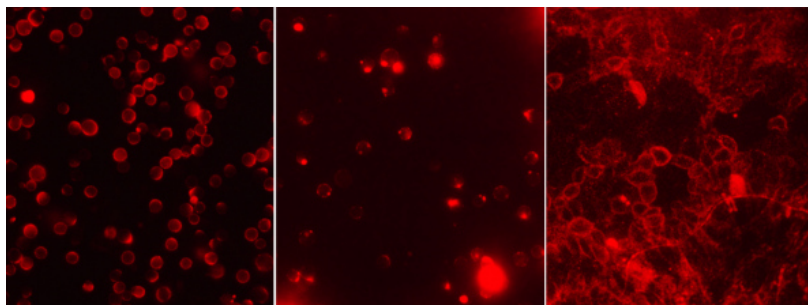


**Figure 15.** Fluorescent microscopy of different CXCR4<sup>+</sup> cells. QDs-6 binding to (left) Daudi cells (100 nM, 1 h, rt), (middle) to Eμ-Myc1080 mouse B-cell lymphoma (25 nM, 1 h, rt), (right) to Chem\_1 cells (25 nM, 1 h, rt).

To demonstrate specificity of CXCR4 binding, QDs-6 was compared with control QDs (no decoration with ligand **6**) under otherwise identical conditions. The fluorescent images depicted in Figure 16 show only negligible binding for the control QDs, thus confirming the high specificity of QDs-6.

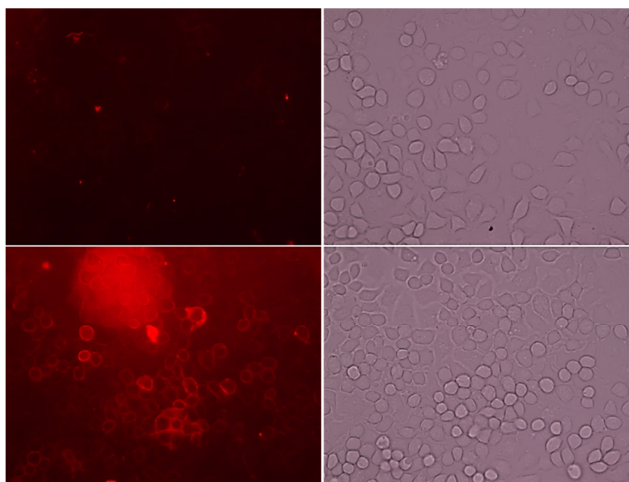


**Figure 16.** Fluorescent microscopy of CXCR4 targeting specificity. (upper row) negative control with uncoated QDs on Chem\_1 cells (25 nM, 100.000 cells) and corresponding light microscopy image, (lower row) positive control with 25 nM QDs-6 on Chem\_1 cells (25 nM, 100.000 cells) with corresponding light microscopy image.



## RESULTS AND DISCUSSION

The experimental displacement study first utilized antibodies, however probably due to the very high local concentration of the CXCR4 binding ligand on the surface of the QDs, only negligible displacement could be observed. In summary, as a proof of concept experiment, decorated QDs-**6** could detect CXCR4 expression on different cell lines of human and murine origin at concentrations as low as 25 nM in specific manner compared to control QDs.

QDs are widely used for fluorescent imaging mostly due to their size- and composition-adjustable fluorescence emission wavelengths, narrow emission bands, and very high levels of brightness and photo stability. In addition, the decoration with specific peptides (like peptide **6**) provides a toll for specific targeting of desired organs or tissues <sup>212-216</sup>. However, for a rational design of molecular targeting quantum dots, it has to be considered, that the size and charge preclude their efficient clearance from the body as intact nanoparticles. Indeed, only extremely small targeting molecules (final hydrodynamic diameter  $\leq 5.5$  nm) will be cleared from the circulation by renal excretion <sup>217</sup>. However, the increased affinity associated with multimerization of such ligands on the quantum dot surface may permit further evaluation, but due to the ongoing discussion about potential toxicity of CdSe-based QDs *in vivo* and the unlikely application of expensive carboxylate-modified quantum dots in comparison to commercial available fluorescence dyes, QDs-**6** were not further investigated <sup>218</sup>.

### 3.2. Cyclo[D-Tyr-N(Me)-D-Orn-Arg-Nal-Gly] (**11**)-based compounds

#### 3.2.1. *Shifting the charge*

To investigate the influence of negatively charged amino acids in the close proximity of the binding scaffold of **23** (Pentixafor), which only has 4-(aminomethyl)benzoic acid as spacer, the D-ala based, *N*-terminal acetylated linkers conjugated to the binding scaffold CPCR4 (**11**) were evaluated. The successive placement of an anionic amino acid (D-Glu) along a D-alanine-based amino acid chain did not show a clear correlation between the position of charge and the affinity towards *h*CXCR4 (Tab. 6). Interestingly, the neutral linker of ligand **20** (Ac-D-Ala-D-

## RESULTS AND DISCUSSION

Ala-D-Ala-D-Glu-D-Dap-4-AMBA-CPCR4) revealed the highest binding affinity ( $IC_{50} = 130 \pm 22$  nM). The respective DOTA-conjugate of the neutral ligand **20** [<sup>nat</sup>Ga]**22** still exhibited a more than four-fold decrease of binding affinity compared to the golden standard [<sup>nat</sup>Ga]**23** ( $112 \pm 34$  nM vs.  $24.8 \pm 2.5$  nM, respectively).

**Table 6.** The half maximal inhibitory concentration ( $IC_{50}$  [nM]) of *h*CXCR4 targeting cyclic pentapeptides determined in a competitive binding assay using Jurkat cells ( $4.0 \cdot 10^5$  cells/well, 2 h, rt, HBSS + 1% BSA) and ( $[^{125}\text{I}]\mathbf{R2}$  ( $c = 0.1$  nM) as radioligand. Data are expressed as mean  $\pm$  SD of three independent determinations. [<sup>nat</sup>Ga]Pentixafor ([<sup>nat</sup>Ga]**23**)<sup>91</sup> was also included in the study.

<i>Shifting the charge</i>		
CPCR4-linking unit-Ac	Cpd	$IC_{50}$ [nM]
CPCR4-4-AMBA-D-Glu-D-Ala-D-Ala-D-Ala-D-Ala-Ac	<b>13</b>	$732 \pm 378$
CPCR4-4-AMBA-D-Ala-D-Glu-D-Ala-D-Ala-D-Ala-Ac	<b>14</b>	$819 \pm 80$
CPCR4-4-AMBA-D-Ala-D-Ala-D-Glu-D-Ala-D-Ala-Ac	<b>15</b>	$> 1800$
CPCR4-4-AMBA-D-Ala-D-Ala-D-Ala-D-Glu-D-Ala-Ac	<b>16</b>	$730 \pm 11$
CPCR4-4-AMBA-D-Ala-D-Ala-D-Ala-D-Ala-D-Glu-Ac	<b>17</b>	$> 1200$
CPCR4-4-AMBA-D-Ala-D-Ala-D-Glu-D-Glu-D-Ala-Ac	<b>18</b>	$> 3000$
CPCR4-4-AMBA-D-Ala-D-Ala-D-Ala-D-Ala-D-Ala-Ac	<b>19</b>	$251 \pm 67$
CPCR4-4-AMBA-D-Dap-D-Glu-D-Ala-D-Ala-D-Ala-Ac	<b>20</b>	$130 \pm 22$
CPCR4-4-AMBA-N(Me) <sub>3</sub> -D-Dap-D-Glu-D-Ala-D-Ala-D-Ala-Ac	<b>21</b>	$446 \pm 81$
CPCR4-linking unit-DOTA		
CPCR4-4-AMBA-DOTA	[ <sup>nat</sup> Ga] <b>23</b>	$24.8 \pm 2.5$
CPCR4-4-AMBA-D-Dap-D-Glu-D-Ala-D-Ala-D-Ala-DOTA	[ <sup>nat</sup> Ga] <b>22</b>	$112 \pm 34$
CPCR4-4-AMBA-D-Dap-D-Glu-D-Ala-D-Ala-D-Ala-DOTA	[ <sup>nat</sup> Lu] <b>22</b>	$147 \pm 27$

In conclusion, the SAR study based on the insertion of a negative charge on an alanine based peptide chain did not show a preferred position of anionic residues (see Table 6). However, when compared with all glutamic acid containing linking units (**13-18**), the introduction of a cationic

## RESULTS AND DISCUSSION

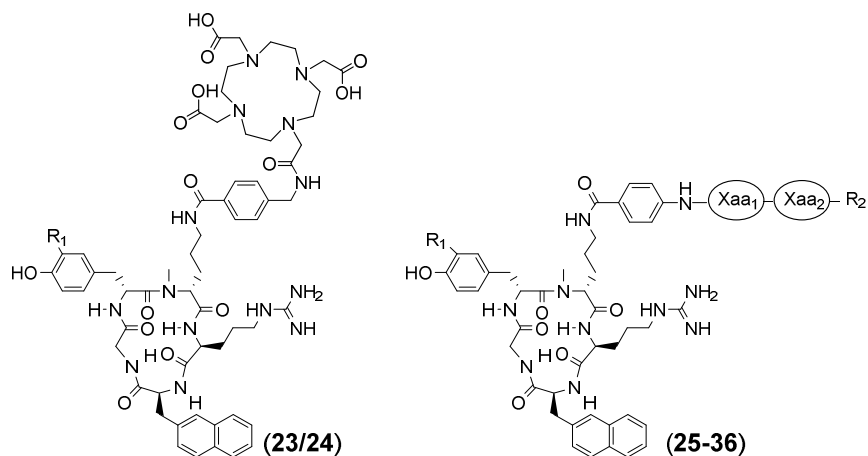
amino acid improved the binding affinity of peptide **20**. This observation was used in the following SAR-study.

### 3.2.2. Optimization of the linking unit

As part of the preclinical evaluation of [<sup>nat</sup>Ga]Pentixafor ([<sup>nat</sup>Ga]**23**), its <sup>125</sup>I-labeled analogue, [<sup>125</sup>I]-[<sup>nat</sup>Ga]**23** showed a significant increase of binding affinity, cell uptake and internalization rate compared to the parent peptide [<sup>nat</sup>Ga]**23**<sup>181, 182</sup>. Based on these promising data, the influence of modified amino acid spacer and different chelators (DOTA vs. DOTAGA) on the binding affinity of this optimized binding scaffold (iodoCPCR4, **12**) towards CXCR4 was investigated. Furthermore, internalization and externalization rates were determined. To investigate the influence of the aromatic linking unit on the binding affinity towards CXCR4, 4-(aminomethyl)benzoic acid (4-AMBA, linker of **24**, see Figure 17) was substituted with 4-aminobenzoic acid (4-ABA). In fact, [<sup>nat</sup>Lu]**25** showed a moderate increase in binding affinity compared to [<sup>nat</sup>Lu]**24** (12.5 ± 3.2 nM vs. 14.6 ± 1.0 nM), Tab.7. Since 4-AMBA was already utilized for other SAR studies on pentixafor and pentixather (**23** and **24**)<sup>156</sup> and the difference in binding affinity was not significant (or rather beneficial for 4-ABA), 4-ABA was chosen as the phenylene linker in further studies. Then, to determine the influence of metal chelator and the metal complex on the *IC*<sub>50</sub>'s of the resulting CXCR4 ligands, the <sup>nat</sup>Ga/<sup>nat</sup>Lu and <sup>nat</sup>Y analogs of DOTA vs. DOTAGA-conjugates were evaluated. Comparison of the metal-complexes of **25** to **28** (DOTA-4-ABA (**25**), DOTAGA-4-ABA (**26**), DOTA-Gly-4-ABA (**27**) and DOTAGA-Gly-4-ABA (**28**)) demonstrated a distinct influence of the chelator on the binding affinity of the ligands. All metal complexes (<sup>nat</sup>Ga, <sup>nat</sup>Lu and <sup>nat</sup>Y) of **28** exhibited a 6-fold decreased affinity compared to [<sup>nat</sup>M]**27** (47.4 ± 8.1 nM vs. 7.9 ± 1.1 nM for <sup>nat</sup>Ga, 38.8 ± 1.3 nM vs. 5.9 ± 0.3 nM for <sup>nat</sup>Lu and 43.3 ± 1.5 nM vs. 6.7 ± 1.2 nM for <sup>nat</sup>Y, respectively). The same tendencies were found for the metal complexes of DOTAGA-4-ABA (**26**). Consequently, DOTA was selected and utilized in further ligand modifications. Additionally, the presence of glycine in the spacer

## RESULTS AND DISCUSSION

positively contributed to the binding affinity of the CXCR4 ligands ( $12.5 \pm 3.2$  nM for [ $^{nat}\text{Lu}$ ]**25** (DOTA-4-ABA) vs.  $5.9 \pm 0.3$  nM for [ $^{nat}\text{Lu}$ ]**27** (DOTA-Gly-4-ABA), respectively).



D-Tyr (R <sub>1</sub> )	Spacer	Xaa <sub>1</sub>	Xaa <sub>2</sub>	R <sub>2</sub>	Cpd
H	4-AMBA	-	-	DOTA	<b>23</b>
I	4-AMBA	-	-	DOTA	<b>24</b>
I	4-ABA	-	-	DOTA	<b>25</b>
I	4-ABA	-	-	DOTAGA	<b>26</b>
I	4-ABA	Gly	-	DOTAGA	<b>28</b>
I	4-ABA	Gly	-	DOTA	<b>27</b>
I	4-ABA	Gly	D-Dap	DOTA	<b>30</b>
I	4-ABA	Gly	D-Lys	DOTA	<b>32</b>
H	4-ABA	Gly	D-Lys	DOTA	<b>31</b>
I	4-ABA	Gly	D-Arg	DOTA	<b>34</b>
H	4-ABA	Gly	D-Arg	DOTA	<b>33</b>
I	4-ABA	D-Ala	D-Arg	DOTA	<b>36</b>
H	4-ABA	D-Ala	D-Arg	DOTA	<b>35</b>
I	4-ABA	D-Asp	-	DOTA	<b>29</b>

**Figure 17.** Structural Modifications (incl. Spacer, amino acids in the linking unit and the chelator) during the SAR study *Optimization of the linking unit* and the corresponding nomenclature of the peptides.

## RESULTS AND DISCUSSION

**Table 7.** The half maximal inhibitory concentration ( $IC_{50}$  [nM]) of *h*CXCR4 targeting cyclic pentapeptides determined in a competitive binding assay with Jurkat cells ( $4.0 \times 10^5$  cells/well, 2 h, rt, HBSS + 1% BSA) using ( $[^{125}\text{I}]\mathbf{R2}$  ( $c = 0.1$  nM) as the radioligand. Data are expressed as mean  $\pm$  SD of three independent determinations.  $[\text{natM}]\text{Pentixafor}$  ( $[\text{natM}]\mathbf{23}$ )<sup>91, 156</sup> and  $[\text{natM}]\text{Pentixather}$  ( $[\text{natM}]\mathbf{24}$ )<sup>182</sup> were included in the study for comparison.

<i>Optimization of the linking unit</i>			
peptide	$IC_{50}$ [nM]	peptide	$IC_{50}$ [nM]
<b><math>\text{natGa}</math>-complexes</b>			
$[\text{natGa}]\text{Pentixafor}$ ( $[\text{natGa}]\mathbf{23}$ )	$24.8 \pm 2.5$	$[\text{natGa}]\mathbf{31}$	$8.9 \pm 3.8$
$[\text{natGa}]\text{Pentixather}$ ( $[\text{natGa}]\mathbf{24}$ )	$6.1 \pm 1.5$	$[\text{natGa}]\mathbf{32}$	$2.4 \pm 0.1$
$[\text{natGa}]\mathbf{25}$	$282 \pm 90$	$[\text{natGa}]\mathbf{33}$	$9.7 \pm 2.8$
$[\text{natGa}]\mathbf{26}$	$14.4 \pm 0.3$	$[\text{natGa}]\mathbf{34}$	$1.4 \pm 0.2$
$[\text{natGa}]\mathbf{27}$	$7.9 \pm 1.1$	$[\text{natGa}]\mathbf{35}$	$0.4 \pm 0.1$
$[\text{natGa}]\mathbf{28}$	$47.4 \pm 8.1$	$[\text{natGa}]\mathbf{36}$	$2.6 \pm 1.0$
$[\text{natGa}]\mathbf{30}$	$3.6 \pm 0.7$		
<b><math>\text{natLu}</math>-complexes</b>			
$[\text{natLu}]\text{Pentixafor}$ ( $[\text{natLu}]\mathbf{23}$ )	$41 \pm 12$	$[\text{natLu}]\mathbf{30}$	$3.5 \pm 0.3$
$[\text{natLu}]\text{Pentixather}$ ( $[\text{natLu}]\mathbf{24}$ )	$14.6 \pm 1.0$	$[\text{natLu}]\mathbf{31}$	$8.0 \pm 3.1$
$[\text{natLu}]\mathbf{25}$	$12.5 \pm 3.2$	$[\text{natLu}]\mathbf{32}$	$3.6 \pm 1.1$
$[\text{natLu}]\mathbf{26}$	$28.3 \pm 9.1$	$[\text{natLu}]\mathbf{33}$	$5.4 \pm 1.6$
$[\text{natLu}]\mathbf{27}$	$5.9 \pm 0.3$	$[\text{natLu}]\mathbf{34}$	$2.1 \pm 0.3$
$[\text{natLu}]\mathbf{28}$	$38.8 \pm 1.3$	$[\text{natLu}]\mathbf{35}$	$1.5 \pm 0.1$
$[\text{natLu}]\mathbf{29}$	$106 \pm 10$	$[\text{natLu}]\mathbf{36}$	$1.7 \pm 0.6$
<b><math>\text{natY}</math>-complexes</b>			
$[\text{natY}]\text{Pentixafor}$ ( $[\text{natY}]\mathbf{23}$ )	$40.2 \pm 27$	$[\text{natY}]\mathbf{31}$	$6.3 \pm 2.5$
$[\text{natY}]\text{Pentixather}$ ( $[\text{natY}]\mathbf{24}$ )	$20.4 \pm 0.3$	$[\text{natY}]\mathbf{32}$	$2.4 \pm 0.2$
$[\text{natY}]\mathbf{25}$	$216.3 \pm 33$	$[\text{natY}]\mathbf{33}$	$8.7 \pm 2.9$
$[\text{natY}]\mathbf{26}$	$83 \pm 30$	$[\text{natY}]\mathbf{34}$	$2.1 \pm 0.3$
$[\text{natY}]\mathbf{27}$	$6.7 \pm 1.2$	$[\text{natY}]\mathbf{35}$	$0.3 \pm 0.1$

## RESULTS AND DISCUSSION

$[\text{natY}]$ <b>28</b>	$43.3 \pm 1.5$	$[\text{natY}]$ <b>36</b>	$1.6 \pm 0.5$
$[\text{natY}]$ <b>30</b>	$4.1 \pm 1.3$		
<hr/> <b><math>\text{natBi}</math>-complexes</b> <hr/>			
$[\text{natBi}]$ Pentixather ( $[\text{natBi}]$ <b>24</b> )	$24.4 \pm 3.7$	$[\text{natBi}]$ <b>32</b>	$38 \pm 25$
$[\text{natBi}]$ <b>25</b>	$27.0 \pm 14$	$[\text{natBi}]$ <b>34</b>	$2.9 \pm 0.1$
$[\text{natBi}]$ <b>27</b>	$14.5 \pm 0.2$	$[\text{natBi}]$ <b>36</b>	$1.8 \pm 0.8$
$[\text{natBi}]$ <b>30</b>	$3.5 \pm 0.4$		

Computational models for binding of the reference ligands CPCR4.3 (**R1**) and FC131 (**R2**) suggested that the positive charged moieties (Arg<sup>4</sup> and Arg<sup>5</sup> in **R2** and Arg<sup>5</sup> and *N*(guanidino-hexyl)-D-Ala<sup>4</sup> in **R1**) in the pentapeptide strongly interact through the establishment of salt bridges with negatively charged residues in the binding pocket of CXCR4<sup>89, 101, 104, 219-222</sup>. This mode of binding was also reported for CXCR7 specific ligand (TC14012), in which Arg<sup>2</sup> and Arg<sup>14</sup> dominantly contribute to the binding towards the receptor<sup>203</sup>. Thus, we speculated, that an additional positively charged amino acid in addition to the optimized “linking unit” of DOTA-Gly-4-ABA (**27**), could further enhance binding affinity. (*R*)-2,3-diaminopropanoic acid (D-Dap) was introduced, since it already showed a beneficial effect for the binding affinity in “shifting the charge” (III.3.2.1.), resulting in DOTA-D-Dap-Gly-4-ABA (**30**), see Fig. 17. This structural modification increased the binding affinities almost 2-fold for all investigated metal complexes (e.g.  $3.6 \pm 0.7$  nM  $[\text{natGa}]$ **30** vs.  $7.9 \pm 1.1$  nM  $[\text{natGa}]$ **27**, respectively). Mutation of the cationic amino acid at this position resulted in further improvement of the  $IC_{50}$  values with DOTA-D-Arg-Gly-4-ABA (**34**) ( $1.4 \pm 0.1$  nM for  $\text{natGa}$ ,  $2.1 \pm 0.3$  nM for  $\text{natLu}$ ,  $2.1 \pm 0.3$  nM for  $\text{natY}$  and  $2.9 \pm 0.1$  nM for  $\text{natBi}$ , respectively) as the most potent ligand. The hypothesis of cationic amino acids was supported by compound  $[\text{natLu}]$ **29** (DOTA-D-Asp-4-ABA), which showed a clearly decreased binding affinity towards CXCR4 with  $106 \pm 10$  nM, most probably due to the negative charged side chain.

## RESULTS AND DISCUSSION

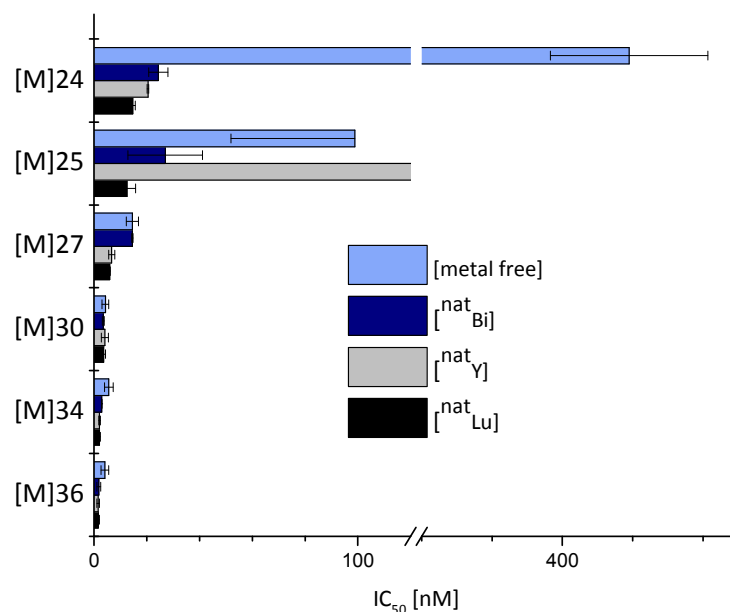


**Figure 18.** Graphical summary of the SAR study *Optimization of the linking unit*.  $IC_{50}$  values were taken from Table 7 and represent  $IC_{50}$  values of at least three independent determinations.

In a final optimization step, Glycine was substituted with D-Alanine in the peptide chain to prevent possible enzymatic degradation *in vivo*. This resulted in compound DOTA-D-Arg-D-Ala-4-ABA (**36**) having an additional almost 2-fold increase in affinity compared to DOTA-D-Dap-Gly-4-ABA (**30**) in all metal complexes, making it the most affine CXCR4 ligand measured in this study so far ( $2.6 \pm 1.0$  nM vs.  $3.6 \pm 0.7$  nM for <sup>nat</sup>Ga,  $1.7 \pm 0.6$  nM vs.  $3.5 \pm 0.3$  nM for <sup>nat</sup>Lu,  $1.6 \pm 0.5$  nM vs.  $4.1 \pm 1.3$  nM for <sup>nat</sup>Y and  $1.8 \pm 0.8$  nM vs.  $3.5 \pm 0.4$  nM for <sup>nat</sup>Bi, respectively). Figure 18 graphically summarizes the subsequent improvement of the  $IC_{50}$  values of the respective CXCR4 ligands, starting with the exchange of 4-AMBA with 4-ABA (**24** to **25**), then introduction of glycine in the “linking unit” (**25** to **27**) and finally, the introduction of cationic amino acids (**30**, **34**, **36**). To avoid unspecific uptake *in vivo* due to enzymatic deiodination by deiodinases or increased lipophilicity<sup>169, 223</sup>, the most affine CXCR4 ligands **32**, **34** and **36** were investigated as their D-Tyr<sup>3</sup> uniodinated analogues, resulting in ligands **31**, **33** and **35**, see Fig. 17. Surprisingly, all compounds exhibited good binding affinities with  $8.0 \pm 3.1$  nM for [<sup>nat</sup>Lu]**31**,  $5.4 \pm 1.6$  nM [<sup>nat</sup>Lu]**33** and especially  $1.5 \pm 0.1$  nM for [<sup>nat</sup>Lu]**35**,

## RESULTS AND DISCUSSION

respectively. [<sup>nat</sup>Ga]**35** (DOTA-D-Arg-D-Ala-4-ABA-CPCR4) is the most affine CXCR4 ligand measured up to this point with an  $IC_{50}$  value of  $0.4 \pm 0.1$  nM for the <sup>nat</sup>Ga-complex.

**Murine CXCR4 binding affinity:** As previously reported, [<sup>68</sup>Ga]Pentixafor ([<sup>68</sup>Ga]**23**), shows virtually no tracer uptake in CXCR4-expressing mouse organs such as spleen, lung, adrenal glands, or the bone marrow, as it is highly specific for *h*CXCR4<sup>90, 91, 127, 131</sup>. Its D-Tyr<sup>3</sup> iodinated analogue [<sup>177</sup>Lu]Pentixather ([<sup>177</sup>Lu]**24**), however showed enhanced binding affinity towards *m*CXCR4 and consequently slightly elevated activity accumulation in *m*CXCR4 expressing organs during *in vivo* evaluation within our group (data not published yet). Thus, to be able to compare the novel CXCR4 ligands with established probes like [<sup>nat</sup>Ga]**23** and [<sup>nat</sup>Lu]**24** in a murine model, determination of the binding affinities towards murine CXCR4 is essential. This allows a more balanced comparison of the *in vivo* properties, observed in the utilized xenograft mouse model.

**Table 8.**  $IC_{50}$  values of selected ligands for murine CXCR4 determined with Eμ-Myc1080 mouse B-cell lymphoma cells (2 h, rt, HBSS + 1% BSA) using [<sup>125</sup>I]CPCR4.3 ([<sup>125</sup>I]**R1**) ( $c = 0.1$  nM) as reference and radioligand.

<i>IC<sub>50</sub> values for murine CXCR4</i>		
Peptide	Cpd	IC <sub>50</sub> [nM]
CPCR4.3	<b>R1</b>	$0.8 \pm 0.1$
FC131	<b>R2</b>	$119 \pm 69$
[ <sup>nat</sup> Ga]Pentixafor	[ <sup>nat</sup> Ga] <b>23</b>	>1000
[ <sup>nat</sup> Lu]Pentixather	[ <sup>nat</sup> Lu] <b>24</b>	$567 \pm 62$
[ <sup>nat</sup> Lu]DOTA-D-Lys-Gly-4-ABA- <i>iodo</i> CPCR4	[ <sup>nat</sup> Lu] <b>32</b>	$61.4 \pm 17$
[ <sup>nat</sup> Lu]DOTA-D-Arg-Gly-4-ABA- <i>iodo</i> CPCR4	[ <sup>nat</sup> Lu] <b>34</b>	$37.1 \pm 2.9$
[ <sup>nat</sup> Lu] DOTA-D-Arg-D-Ala-4-ABA-CPCR4	[ <sup>nat</sup> Lu] <b>35</b>	$182 \pm 26$
[ <sup>nat</sup> Lu] DOTA-D-Arg-D-Ala-4-ABA- <i>iodo</i> CPCR4	[ <sup>nat</sup> Lu] <b>36</b>	$48.5 \pm 0.5$



## RESULTS AND DISCUSSION

All cationic compounds exhibited an increased murine affinity compared to [<sup>nat</sup>Lu]Pentixather ([<sup>nat</sup>Lu]**24**) (Tab. 8: [<sup>nat</sup>Lu]**32**:  $IC_{50} = 61.4 \pm 17$  nM, [<sup>nat</sup>Lu]**34**:  $IC_{50} = 37.1 \pm 2.9$  nM, [<sup>nat</sup>Lu]**36**:  $IC_{50} = 48.5 \pm 0.5$  nM and [<sup>nat</sup>Lu]**24**:  $567 \pm 67$  nM, respectively), whereas, as expected, [<sup>nat</sup>Ga]**23** showed no measurable affinity towards murine CXCR4. Interestingly, [<sup>nat</sup>Lu]**35** inherited a lower affinity ( $182 \pm 26$  nM) compared to its iodinated analogue **36**. In direct comparison with [<sup>nat</sup>Ga]Pentixafor, which shares the same binding scaffold (CPCR4), it still has a clearly enhanced binding affinity towards the murine receptor. In addition, based on these preliminary data, there might be a cooperative influence of a cationic linker and the iodinated binding scaffold, which influences the affinity of novel CXCR4 ligands towards murine CXCR4. Consequently, increased tracer uptake in CXCR4-expressing mouse tissue can be expected for the novel designed CXCR4 ligands during *in vivo* evaluation compared with the references Pentixafor and Pentixather (see III.5.1.-3.).

**Internalization kinetics:** High internalization efficiency may be important for therapeutic interventions, where a long retention of the radioactive isotope in the target tissue may have a beneficial influence on therapy efficiency. However, in the case of comparable  $IC_{50}$  values of the metal-free ligands and their respective radiometal chelates, the specific activity of the tracer preparation (total amount of peptide used in the assay) can have a significant effect on the cellular uptake/internalization rate. Concentrations above 1.0 nM caused a reduction of the tracer binding capacity due to increased occupancy of the binding sites by the unlabeled peptide precursor (cellular uptake of [<sup>177</sup>Lu]**24** after 60 min incubation at 37 °C (n = 3):  $7.49 \pm 0.87\%$  (1.0 nM),  $6.0 \pm 0.3\%$  (2.5 nM),  $4.8 \pm 0.5\%$  (5 nM) and  $3.6 \pm 0.1\%$  (10 nM), respectively). Consequently, to minimize these effects, radiolabeling conditions have been standardized and the concentrations of the radiolabeled peptides were kept constant throughout the study at 1.0 nM. As determined before, the <sup>nat</sup>Lu-complexes of **35** and **36** (DOTA-D-Arg-D-Ala-4-ABA-(*iodo*)CPCR4) have an almost 10-fold higher binding affinity compared to [<sup>nat</sup>Lu]**24** ([<sup>nat</sup>Lu]Pentixather) and [<sup>nat</sup>Lu]**25** ([<sup>nat</sup>Lu]DOTA-4-ABA-*iodo*CPCR4).

## RESULTS AND DISCUSSION

The optimized binding affinities due to the introduction of the novel linking unit is also reflected by the internalization kinetics in Fig. 19. Surprisingly, even minimal structural changes (e.g. exchange of 4-AMBA and 4-ABA in **24** and **25**, respectively) clearly influence the internalization kinetics. [ $^{177}\text{Lu}$ ]**36** showed the highest internalization of all tested ligands.

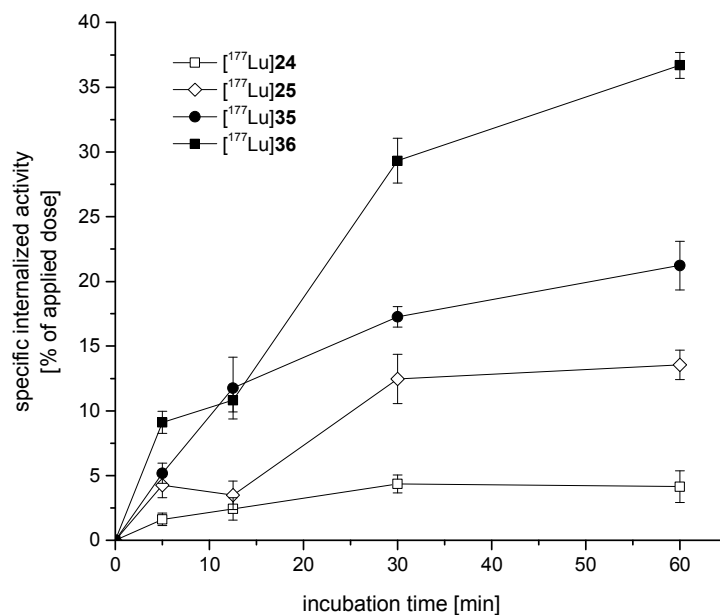


**Figure 19.** Internalization kinetics of [ $^{177}\text{Lu}$ ]**24** ([ $^{177}\text{Lu}$ ]Pentixather), [ $^{177}\text{Lu}$ ]**25** ([ $^{177}\text{Lu}$ ]DOTA-4-ABA-*iodo*CPCR4), [ $^{177}\text{Lu}$ ]**35** ([ $^{177}\text{Lu}$ ]DOTA-D-Arg-D-Ala-4-ABA-CPCR4) and [ $^{177}\text{Lu}$ ]**36** ([ $^{177}\text{Lu}$ ]DOTA-D-Arg-D-Ala-4-ABA-*iodo*CPCR4) into Chem\_1 cells. 100,000 cells/well were incubated with the respective radioligand ( $c = 1.0$  nM) at 37 °C in RPMI-medium (5% BSA). The total cellular activity was corrected for non-specific binding (10  $\mu\text{M}$  AMD3100). All data are expressed as mean  $\pm$  SD ( $n = 3$ ).

As shown in Figure 20, the increased affinity of **35** and **36** not only resulted in higher internalization rates, but also had a beneficial effect on the absolute cellular uptake of the respective radiotracer. With a total uptake of  $40.4 \pm 1.5\%$  of applied dose, [ $^{177}\text{Lu}$ ]**36** exhibits a 4-fold increase of cellular uptake compared to  $9.9 \pm 1.4\%$  of [ $^{177}\text{Lu}$ ]**24**, respectively. Importantly, the ratio of total cellular uptake and internalized activity increased from 39% for [ $^{177}\text{Lu}$ ]**24** to 91% for [ $^{177}\text{Lu}$ ]**36**, as shown in Figure 20, leading to a higher absolute dose of activity, which is transported to the  $h\text{CXCR4}^+$  cells.

## RESULTS AND DISCUSSION

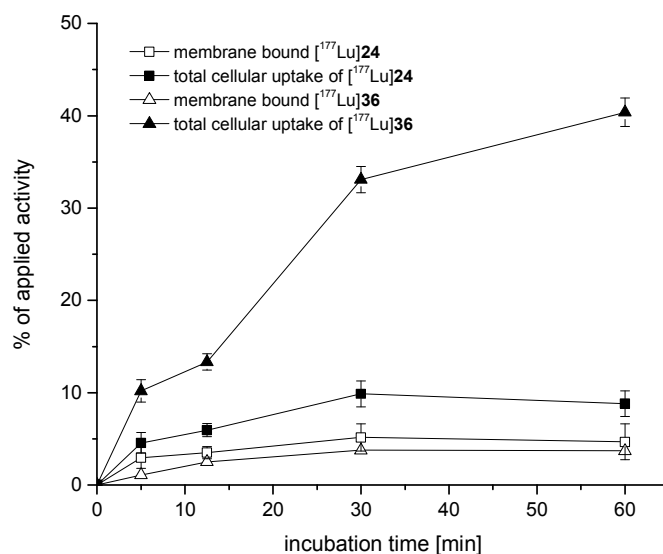


**Figure 20.** Activity uptake kinetics (membrane bound and total cellular uptake) of [<sup>177</sup>Lu]**24** ([<sup>177</sup>Lu]Pentixather) and [<sup>177</sup>Lu]**36** ([<sup>177</sup>Lu]DOTA-D-Arg-D-Ala-4-ABA-*iodo*CPCR4) in Chem\_1 cells. 100,000 cells/well were incubated with the respective radioligand ( $c = 1.0$  nM) at 37 °C in RPMI-medium (5% BSA). The total cellular activity was corrected for non-specific binding (10  $\mu$ M AMD3100). All data are expressed as mean  $\pm$  SD ( $n = 3$ ).

The internalized activity, the total cellular uptake of activity, as well as the ratio of internalized activity to total tracer uptake are summarized in Table 9. In consistence with the higher affinities, all ligands with cationic “linking units” showed increased internalization and cellular uptake, whereas the iodinated and therefore more lipophilic ligands showed an additionally higher ratio of internalization (e.g. [<sup>177</sup>Lu]**35** 65% vs. [<sup>177</sup>Lu]**36** 91%, see Table 9). This observation is also supported by the fact that [<sup>68</sup>Ga]**34** exhibits a lower cellular uptake and internalization rate than [<sup>177</sup>Lu]**34**, most probably due to the additional free carboxylate in the chelator (see lipophilicity in III.4.). In conclusion, peptide **36**, but also peptide **35** seems to be highly effective in receptor internalization and showed high cellular uptake. This was further investigated in animal models, see III.5.3.. The rationale for the development of potent probes for endoradiotherapy has been that agonists are superior to antagonists <sup>223-225</sup>. Due to the internalization of the ligand–receptor complex after high affinity agonist binding, was believed to be the basis for an efficient accumulation of the radioligand in a target cell <sup>226-228</sup>.

## RESULTS AND DISCUSSION

**Table 9.** Summary of the total cellular activity, the internalized activity and the ratio of internalized activity to total cellular uptake at 60 min as % of applied activity of radiolabeled CXCR4 ligands, determined on Chem\_1 cells (37 °C, RPMI + 5% BSA, 100,000 cells/well, c = 1.0 nM for  $^{68}\text{Ga}$ - and  $^{177}\text{Lu}$ -labeled ligands). Data are corrected for non-specific binding (10  $\mu\text{M}$  AMD3100) and expressed as mean  $\pm$  SD (n = 3).

*Internalization data of CXCR4 ligands*

CXCR4 ligand	Cpd	Internalization	Total cell binding	Ratio
[ $^{177}\text{Lu}$ ]DOTA-4-AMBA- <i>iodo</i> CPCR4	[ $^{177}\text{Lu}$ ] <b>24</b>	4.2 $\pm$ 1.2%	8.8 $\pm$ 1.4%	47%
[ $^{177}\text{Lu}$ ]DOTA-4-ABA- <i>iodo</i> CPCR4	[ $^{177}\text{Lu}$ ] <b>25</b>	13.6 $\pm$ 1.1%	17.4 $\pm$ 1.9%	78%
[ $^{177}\text{Lu}$ ]DOTA-D-Lys-Gly-4-ABA-CPCR4	[ $^{177}\text{Lu}$ ] <b>31</b>	11.5 $\pm$ 1.7%	24.6 $\pm$ 1.5%	47%
[ $^{177}\text{Lu}$ ]DOTA-D-Arg-Gly-4-ABA-CPCR4	[ $^{177}\text{Lu}$ ] <b>33</b>	13.5 $\pm$ 1.6%	26.5 $\pm$ 0.7%	51%
[ $^{177}\text{Lu}$ ]DOTA-D-Arg-Gly-4-ABA- <i>iodo</i> CPCR4	[ $^{177}\text{Lu}$ ] <b>34</b>	34.4 $\pm$ 2.3%	38.3 $\pm$ 2.0%	90%
[ $^{177}\text{Lu}$ ]DOTA-D-Arg-D-Arg-4-ABA-CPCR4	[ $^{177}\text{Lu}$ ] <b>35</b>	21.2 $\pm$ 1.9%	32.9 $\pm$ 1.0%	65%
[ $^{177}\text{Lu}$ ]DOTA-D-Arg-D-Arg-4-ABA- <i>iodo</i> CPCR4	[ $^{177}\text{Lu}$ ] <b>36</b>	36.7 $\pm$ 1.0%	40.4 $\pm$ 1.5%	91%
[ $^{68}\text{Ga}$ ]DOTA-D-Arg-Gly-4-ABA- <i>iodo</i> CPCR4	[ $^{68}\text{Ga}$ ] <b>34</b>	20.6 $\pm$ 0.4%	28.1 $\pm$ 0.8%	73%

It was believed that efficient internalization would result in elevated accumulation of radioactivity in tumor cells and thus beneficial effect therapy outcome. However, as shown with  $^{177}\text{Lu}$ -labeled somatostatin receptor (SSTR) targeting peptides, antagonists showed higher tumor uptake compared to SSTR-agonists <sup>229-232</sup>. The increased tumor uptake resulted in an elevated tumor radiation dose and therefore, to a more feasible therapeutic outcome in a preclinical study <sup>233</sup>. The beneficial effect of antagonists compared to SSTR-agonists was correlated with the elevated rate of cell binding. This observation led to the conclusion, that agonists only bind to activated receptors, whereas antagonists bind to both, activated and not activated receptors, leading to an elevated level of total cell binding <sup>229</sup>. This correlation was also observed with bombesine analogues <sup>234</sup>. In addition, the investigated antagonists showed prolonged retention at the tumor sites and consequently, increased the tumor radiation dose over time. In summary, the beneficial effects of antagonistic analogues on endoradiotherapeutic efficiency are due to elevated total cellular binding of the radiotracer compared to their antagonistic analogues.

## RESULTS AND DISCUSSION

Independently of agonistic or antagonistic characteristics, the novel ligands **35** and **36** exhibit an elevated rate of internalization, which is also accompanied by a clearly enhanced amount of total bound activity, see Table 9. This should also lead to elevated tumor radiation doses, as just described. To determine the effect of elevated internalization on the retention in the tumor cells more precisely, the externalization kinetics of the novel CXCR4 ligands were determined (Fig. 21). Further, the characteristics of the ligands **23** (Pentixafor), **24** (Pentixather) and **35** (DOTA-D-Arg-D-Ala-4-ABA-CPCR4) were investigated in terms of antagonistic, agonistic or neutral ligand behavior upon receptor binding.

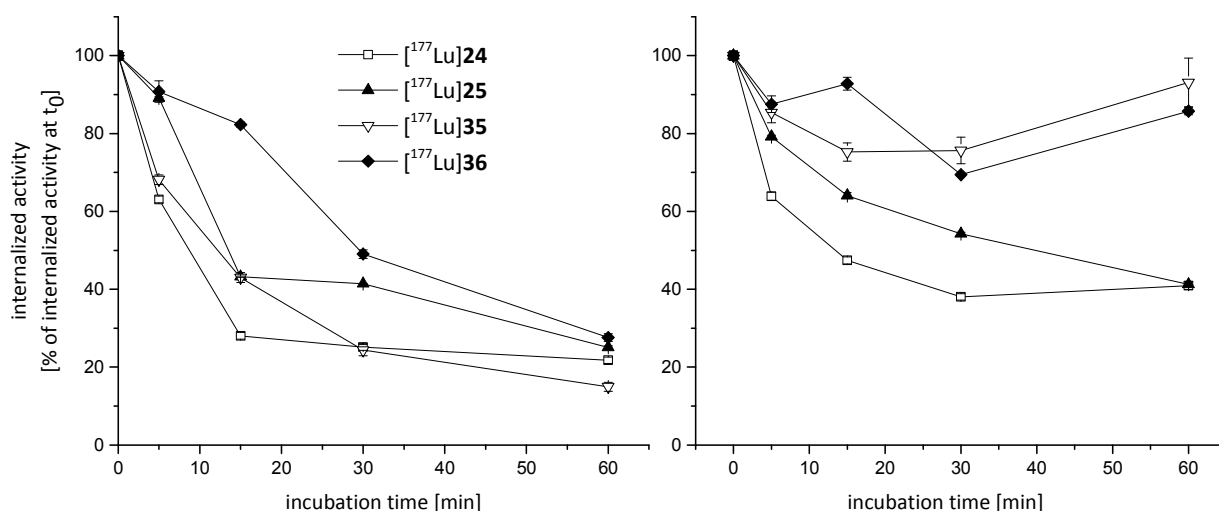


**Figure 21.** Externalization kinetics of selected CXCR4 ligands from Chem\_1 cells. 100,000 cells/well were incubated for 2 h with the respective radioligand ( $c = 1.0$  nM) at 37 °C in RPMI-medium (5% BSA). Then (**left**) RPMI-medium (5% BSA and 10  $\mu$ M AMD3100) or (**right**) only RPMI-medium (5% BSA) was added for replacement. The total cellular internalized activity at  $t = 0$  min was corrected for non-specific binding (10  $\mu$ M AMD3100) and normalized to 100%. All data are expressed as mean  $\pm$  SD ( $n = 3$ ).

Interestingly, the clearance from the tumor cells is similar for all tested <sup>177</sup>Lu-labeled tracers, if the membrane bound receptors are blocked with an excess of AMD3100 in the incubation medium (**no** ligand recycling, Fig. 21, left). Whereas for [<sup>177</sup>Lu]**35** and [<sup>177</sup>Lu]**36** the cell retention over 60 min of incubation was considerably enhanced when re-internalization of the respective

## RESULTS AND DISCUSSION

radioligands was enabled. After 60 min,  $41.0 \pm 1.0\%$  of [ $^{177}\text{Lu}$ ]**24** was located in the cells, by contrast,  $93.1 \pm 6.3\%$  of [ $^{177}\text{Lu}$ ]**35** was still cell associated after that time (Fig. 21, right). Table 10 depicts the values for remaining internalized activity after 60 min of externalization for both evaluated conditions. All ligands with high internalization rates also showed higher retention in the cells under re-internalization enabling conditions.

**Table 10.** Summary of the results of the externalization study. Cellular activity after externalization without ligand recycling (10  $\mu\text{M}$  AMD3100 in incubation medium) or with ligand recycling (incubation in normal medium) in % of specific internalized activity at  $t = 0$  min. Chem\_1 cells, 37  $^{\circ}\text{C}$ , RPMI + 5% BSA, 100,000 cells/well,  $c = 1.0$  nM for  $^{177}\text{Lu}$ -labeled ligands. Data are corrected for non-specific binding (10  $\mu\text{M}$  AMD3100) at  $t = 0$  min and expressed as mean  $\pm$  SD ( $n = 3$ ).

CXCR4 ligand	Cpd	No ligand recycling [%internalized activity at $t_0$ ]	Ligand recycling [%internalized activity at $t_0$ ]
[ $^{177}\text{Lu}$ ]DOTA-4-AMBA- <i>iodo</i> CPCR4	[ $^{177}\text{Lu}$ ] <b>24</b>	$21.8 \pm 0.8\%$	$41.0 \pm 1.0\%$
[ $^{177}\text{Lu}$ ]DOTA-4-ABA- <i>iodo</i> CPCR4	[ $^{177}\text{Lu}$ ] <b>25</b>	$25.1 \pm 0.4\%$	$41.3 \pm 0.6\%$
[ $^{177}\text{Lu}$ ]DOTA-D-Lys-Gly-4-ABA-CPCR4	[ $^{177}\text{Lu}$ ] <b>31</b>	$18.8 \pm 1.5\%$	$71.8 \pm 1.7\%$
[ $^{177}\text{Lu}$ ]DOTA-D-Arg-Gly-4-ABA-CPCR4	[ $^{177}\text{Lu}$ ] <b>33</b>	$21.8 \pm 0.4\%$	$82.3 \pm 0.8\%$
[ $^{177}\text{Lu}$ ]DOTA-D-Arg-Gly-4-ABA- <i>iodo</i> CPCR4	[ $^{177}\text{Lu}$ ] <b>34</b>	$21.8 \pm 0.8\%$	$80.5 \pm 2.2\%$
[ $^{177}\text{Lu}$ ]DOTA-D-Arg-D-Arg-4-ABA-CPCR4	[ $^{177}\text{Lu}$ ] <b>35</b>	$14.9 \pm 1.1\%$	$93.1 \pm 6.3\%$
[ $^{177}\text{Lu}$ ]DOTA-D-Arg-D-Arg-4-ABA- <i>iodo</i> CPCR4	[ $^{177}\text{Lu}$ ] <b>36</b>	$27.6 \pm 1.0\%$	$85.8 \pm 1.0\%$

**Mode of binding and signal transduction:** In consequence of the significantly enhanced binding affinity and internalization efficiency of the novel peptide **35** (DOTA-D-Arg-D-Arg-4-ABA-CPCR4) and due to its more favourable lipophilicity compared to **36** (DOTA-D-Arg-D-Arg-4-ABA-*iodo*CPCR4, see III.4.), the potential theranostic compound was examined in regards to the ligand binding profile during a three month research stay at the Emory University Hospital in Atlanta under the supervision of Prof. Hyunsuk Shim. The group of Prof. Shim

## RESULTS AND DISCUSSION

kindly provided different functional assays to investigate the nature of signal transduction through CXCR4 ligand binding. The gold standard for CXCR4 PET imaging, Pentixafor (**23**) and the first endoradiotherapeutic compound Pentixather (**24**) were also examined. For binding affinity screening, a competitive binding assay was performed on MDA-MB-213 cells employing the biotin-labeled CXCR4 antagonist TN14003 <sup>88</sup>.

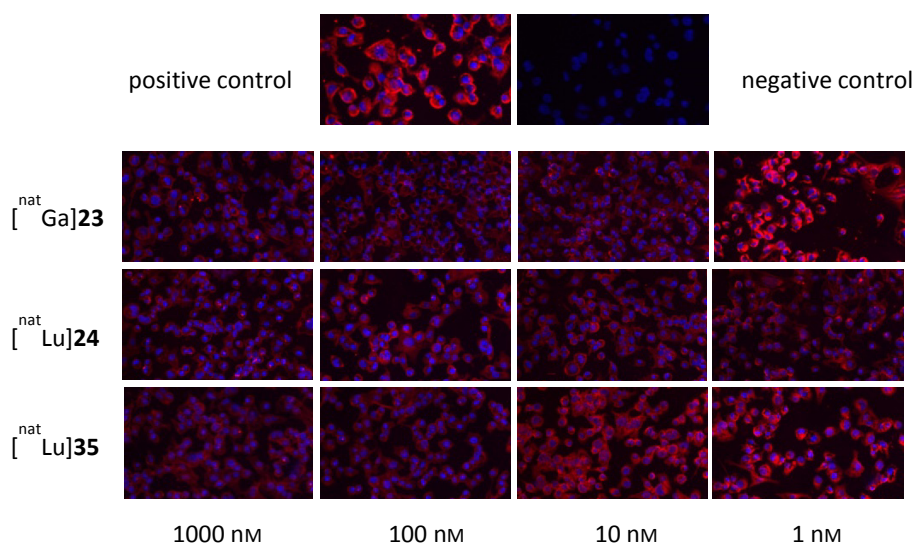


**Figure 22.** Representative immunofluorescence images for primary drug screening. MDA-MB-231 cells were treated with TN14003 (positive control),  $[\text{natGa}]\mathbf{23}$  ( $[\text{natGa}]$ Pentixafor),  $[\text{natLu}]\mathbf{24}$  ( $[\text{natLu}]$ Pentixather) or  $[\text{natLu}]\mathbf{35}$  ( $[\text{natLu}]$ DOTA-D-Arg-D-Ala-4-ABA-CPCR4) at various concentrations (15 min, 37 °C). The cells were subsequently fixed and incubated with biotin-labeled TN14003 (0.05 mg/ml). After washing, cells were incubated with streptavidin-rhodamine. Red color represents binding of TN14003 to CXCR4. Nuclei were counterstained with cytox blue.

The CXCR4 inhibition potency of  $[\text{natGa}]\mathbf{23}$ ,  $[\text{natLu}]\mathbf{24}$  and  $[\text{natLu}]\mathbf{35}$  was determined employing increasing concentrations (1 nM, 10 nM, 100 nM and 1000 nM, see Figure 22). Compared to the positive control, where no inhibitor was added (intense staining of the cells with rhodamine-labeled CXCR4 ligand), potent blocking of CXCR4 was observed for all tested compounds at a concentration as low as 10 nM. In contrast to the earlier determined  $IC_{50}$  values,  $[\text{natLu}]\mathbf{35}$  showed the lowest blocking potency with 10 to 100 nM. Nonetheless, the results depicted in Figure 22 confirm the high affinities towards  $h$ CXCR4 of the selected compounds as determined

## RESULTS AND DISCUSSION

before. A drawback of this assay is the incubation temperature of 37 °C, at which internalization of the receptor is freely possible and for this reason, this assay is not specific for binding to the target receptor, but rather reflects a combination of binding and internalization. This might also be the reason for the deviant results for  $[^{nat}\text{Lu}]\mathbf{35}$ , because of its considerably higher internalization rate in comparison to  $[^{nat}\text{Ga}]\mathbf{23}$  and  $[^{nat}\text{Lu}]\mathbf{24}$ .

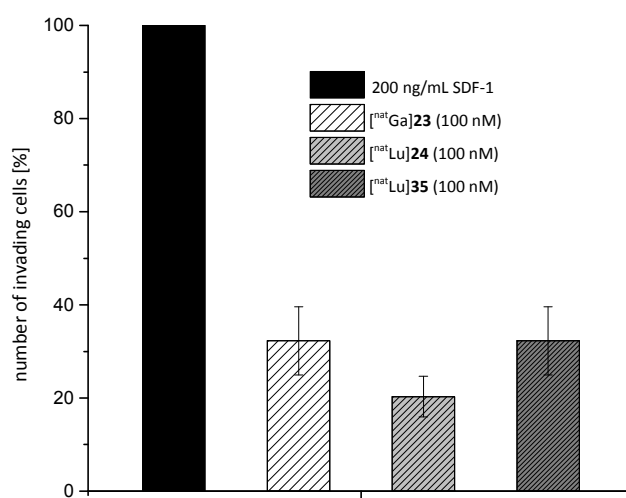


**Figure 23.** Matrigel Invasion assay. Inhibition of CXCR4/CXCL12-mediated matrigel invasion of CXCR4<sup>+</sup> cells (MDA-MB-231) *in vitro* by 100 nM of  $[^{nat}\text{Ga}]\mathbf{23}$  ( $[^{nat}\text{Ga}]\text{Pentixafor}$ ),  $[^{nat}\text{Lu}]\mathbf{24}$  ( $[^{nat}\text{Lu}]\text{Pentixather}$ ) or  $[^{nat}\text{Lu}]\mathbf{35}$  ( $[^{nat}\text{Lu}]\text{DOTA-D-Arg-D-Arg-4-ABA-CPCR4}$ ), respectively. Cells were seeded on top of the matrigel and CXCL12 (200 ng/mL) was added in the bottom side of the matrigel chamber. After H&E staining, invaded cells were counted and the average of the invading cell numbers of MDA-MB-231 with CXCL12 added to the lower chamber was set to 100%. Data are corrected for non-specific invading (no addition of CXCL12 in bottom chamber) and are expressed as mean  $\pm$  SD (n = 3).

In a second functional assay, the compounds were investigated in terms of inhibition potency for CXCL12 induced matrigel invasion of CXCR4<sup>+</sup> cells. As shown in Figure 23, 100 nM of each CXCR4 ligand effectively blocked the invasion of CXCR4<sup>+</sup> cells up to  $67.2 \pm 1.5\%$ ,  $79.7 \pm 4.4\%$  and  $67.7 \pm 7.3\%$  for  $[^{nat}\text{Ga}]\mathbf{23}$ ,  $[^{nat}\text{Lu}]\mathbf{24}$  and  $[^{nat}\text{Lu}]\mathbf{35}$ , respectively. These results contribute to the notion that all three ligands are able to block the association of CXCL12 to the receptor and therefore inhibit or at least weaken the signaling of ligand binding. However, a difference



## RESULTS AND DISCUSSION

between the weakly internalizing ligands [ $^{nat}\text{Ga}$ ]**23** and [ $^{nat}\text{Lu}$ ]**24** and the very effectively internalizing ligand [ $^{nat}\text{Lu}$ ]**35** could not be detected so far.

Therefore, a cyclic adenosine monophosphate (cAMP) assay was established. The utilized assay kit is optimized to quantify intracellular cAMP levels. The specific signal is inversely proportional to the concentration of cAMP in the samples. Binding of CXCL12 to CXCR4 activates G-protein mediated signaling through the  $G_i$  pathway, which inhibits adenylyl cyclase and consequently, reduces cAMP levels within the cell <sup>235</sup>. In order to receive a high signal-to-background ratio, forskolin and the resulting activation of adenylyl cyclase (high levels of cAMP) was utilized as a negative control <sup>236</sup> (activation of adenylyl cyclase results in high levels of cAMP and consequently a low signal in the assay, as the signal is inversely proportional).

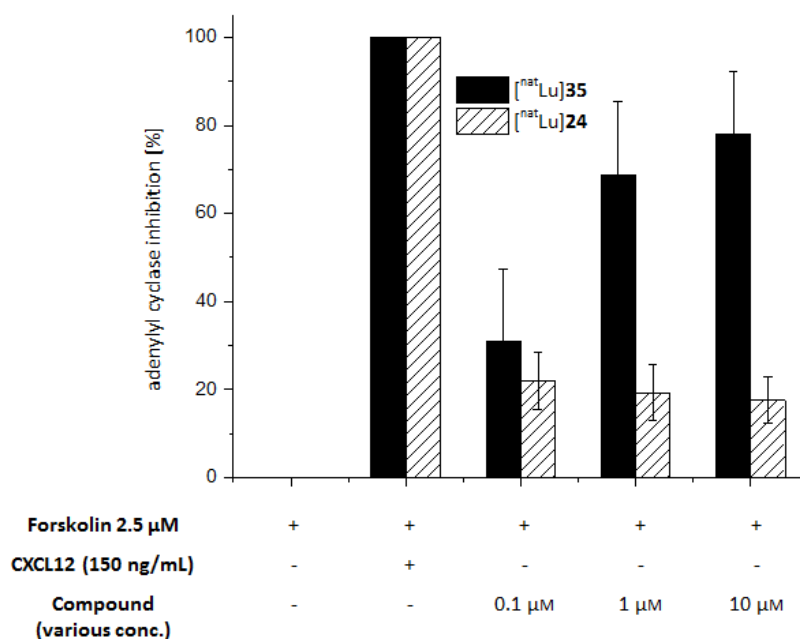


**Figure 24.** Agonist effects on CXCR4 using the TR-FRET based LANCE assay kit on U87 glioma cells. Inhibition of adenylyl cyclase induced by CXCL12, [ $^{nat}\text{Lu}$ ]**24** ([ $^{nat}\text{Lu}$ ]Pentixather) or [ $^{nat}\text{Lu}$ ]**35** ([ $^{nat}\text{Lu}$ ]DOTA-D-Arg-D-Ala-4-ABA-CPCR4). While [ $^{nat}\text{Lu}$ ]**35** counteracts forskolin at a concentration of 10  $\mu\text{M}$  to 80%, [ $^{nat}\text{Lu}$ ]**24** shows no agonist effect on CXCR4.

## RESULTS AND DISCUSSION

The range between low signal (induced by forskolin) and high signal (induced by CXCL12) was set to 0 and 100% of [cAMP], respectively. With this assay, it is possible to measure agonist and antagonist effects on CXCR4, depending on the experimental setup.

**Agonist effects:** [<sup>nat</sup>Lu]**35** and [<sup>nat</sup>Lu]**24** were added to human glioma U87 cells overexpressing CD4 and CXCR4. The experiment was performed according to the manufacturer's instructions using 5  $\mu$ M forskolin to activate adenylyl cyclase, which results in enhanced cAMP production. The presence of CXCL12 inhibits adenylyl cyclase as described earlier. These two conditions were set to 0 % of adenylyl cyclase inhibition (only forskolin) and 100% inhibition (forskolin and CXCL12, see Figure 24). Elevating concentrations of [<sup>nat</sup>Lu]**35** and [<sup>nat</sup>Lu]**24** were added to the forskolin pre-treated cells instead of CXCL12, to observe possible agonistic effects of the ligands. Figure 24 depicts a weak, but dose-dependent agonistic effect of [<sup>nat</sup>Lu]**35** on the production of cAMP in the cells. With a concentration of 10  $\mu$ M, [<sup>nat</sup>Lu]**35** reaches 80% of the effect induced by the endogenous ligand CXCL12. By contrast, [<sup>nat</sup>Lu]**24** was not able to affect the cAMP production induced by forskolin.

**Antagonist effects:** In the antagonistic setup, the cells were incubated with increasing concentrations of the test compounds for 30 min at 37 °C. After addition of forskolin and CXCL12, the concentration of cAMP ([cAMP]) in the cells was measured. For the positive control (100%), only forskolin was added to the cells, whereas for the negative control (0%) forskolin and CXCL12 was added. As a consequence, CXCL12 binds to CXCR4 on the cells, which induces the G<sub>i</sub>-signaling pathway and subsequently inhibits adenylyl cyclase, which results in reduced concentrations of cAMP. The test compounds, as antagonists, however should counteract the CXCL12 induced inhibition. As depicted in Figure 25, [<sup>nat</sup>Ga]**23** and [<sup>nat</sup>Lu]**24** showed increasing inhibition of CXCL12 in a dose-dependent way. Consequently, Pentixafor (**23**) and Pentixather (**24**) can be considered as antagonists or neutral ligands, since they also do not show high internalization efficiencies. [<sup>nat</sup>Lu]**35** on the contrary, was not able to block the G<sub>i</sub>-signaling pathway, but rather enhanced the CXCL12 induced signal with increasing

## RESULTS AND DISCUSSION

concentrations. Therefore, [<sup>nat</sup>Lu]**35** can be considered as weak partial agonist of CXCR4, which was expected due to the enhanced internalization efficiency of [<sup>177</sup>Lu]**35**.

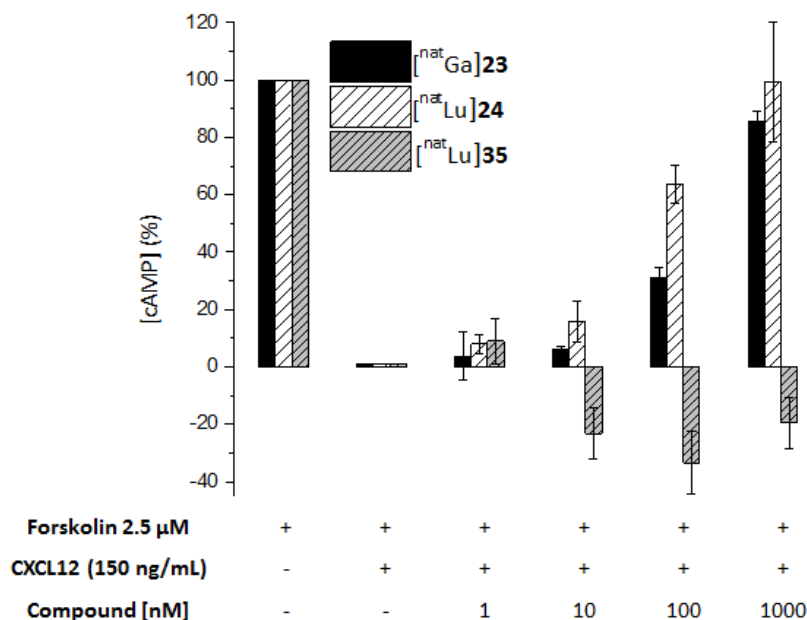


**Figure 25.** Antagonist setup of cAMP assay. Dose-dependent inhibition of cAMP production. With pretreatment (30 min at rt) of [<sup>nat</sup>Ga]**23** ([<sup>nat</sup>Lu]Pentixafor), [<sup>nat</sup>Lu]**24** ([<sup>nat</sup>Lu]Pentixather) or [<sup>nat</sup>Lu]**35** ([<sup>nat</sup>Lu]DOTA-D-Arg-D-Ala-4-ABA-CPCR4) at increasing concentrations, the effect of 150 ng/mL CXCL12 on cAMP reduction was measured by using the TR-FRET based LANCE assay kit. Note that [<sup>nat</sup>Lu]**35** enhances the reduction of [cAMP](%) together with CXCL12.

### 3.2.3. <sup>18</sup>F-labeled CXCR4 peptides

The introduction of the radio synthon AmBF<sub>3</sub> afforded an optimization of the current available highly affine CXCR4 ligands, in order to weaken the effect of the substitution of DOTA. As expected, a direct conjugation of AmBF<sub>3</sub> to 4-ABA (AmBF<sub>3</sub>-4-ABA-CPCR4 (**39**)) resulted in a massive decreased binding affinity with 134.3 ± 47 nM (Tab. 11). Given the fact that the diazotransfer on the *N*-terminus was more efficient on amino acids with high steric hindrance, D-valine was chosen as a spacer, which resulted in a 2-fold higher binding affinity of

## RESULTS AND DISCUSSION

65.2  $\pm$  10 nM for **40**. As shown in III.3.2.2., the optimized linking unit D-Lys-Gly-4-ABA as well as D-Arg-Gly-4-ABA introduced higher flexibility towards modifications and showed beneficial influences on the binding affinity of the CXCR4 ligands. Therefore, this linker concept was utilized and the resulting  $^{18}\text{F}$ -labeling precursor **42** (AmBF<sub>3</sub>-D-Arg-Gly-4-ABA-*iodo*CPCR4) and **43** (AmBF<sub>3</sub>-D-Lys-Gly-4-ABA-*iodo*CPCR4) showed, as anticipated, high binding affinities with 2.9  $\pm$  0.9 nM (**42**) and 3.8  $\pm$  0.9 nM (**43**), respectively. Surprisingly, the high binding affinity was also retained with the D-Tyr<sup>3</sup> uniodinated binding scaffold in peptide **41** (AmBF<sub>3</sub>-D-Arg-Gly-4-ABA-CPCR4,  $IC_{50}$  = 2.4  $\pm$  0.8 nM).

**Table 11.**  $IC_{50}$  values of selected  $^{19}\text{F}$ -peptides for *h*CXCR4 determined with Jurkat cells (2 h, rt, HBSS + 1% BSA) using [<sup>125</sup>I]FC131 ([<sup>125</sup>I]**R2**) (c = 0.1 nM) as radioligand. Data are expressed as mean  $\pm$  SD of three independent determinations. [<sup>nat</sup>Ga]Pentixafor ([<sup>nat</sup>Ga]**23**)<sup>91</sup> and [<sup>nat</sup>Ga]Pentixather ([<sup>nat</sup>Ga]**24**) were included in the study.

<i><sup>18</sup>F-labeling peptides</i>		
Peptide	Cpd	$IC_{50}$ [nM]
[ <sup>nat</sup> Ga]Pentixafor	[ <sup>nat</sup> Ga] <b>23</b>	24.8 $\pm$ 2.5
[ <sup>nat</sup> Ga]Pentixather	[ <sup>nat</sup> Ga] <b>24</b>	6.1 $\pm$ 1.5
AmBF <sub>3</sub> -4-ABA- <i>iodo</i> CPCR4	<b>39</b>	134.3 $\pm$ 47
AmBF <sub>3</sub> -D-Val-4-ABA- <i>iodo</i> CPCR4	<b>40</b>	65.2 $\pm$ 10
AmBF <sub>3</sub> -D-Arg-Gly-4-ABA-CPCR4	<b>41</b>	2.4 $\pm$ 0.8
AmBF <sub>3</sub> -D-Arg-Gly-4-ABA- <i>iodo</i> CPCR4	<b>42</b>	2.9 $\pm$ 0.9
AmBF <sub>3</sub> -D-Lys-Gly-4-ABA- <i>iodo</i> CPCR4	<b>43</b>	3.8 $\pm$ 0.9

Despite the highly promising binding affinities of the novel AmBF<sub>3</sub>-conjugated ligands, no internalization studies were performed, due to very low specific activities obtained after manual synthesis (as described in III.2.4.). The count rates would not be reasonable, if the internalization study was performed with 1.0 nM as standardized for all other ligands. Consequently, the synthesis has to be optimized prior to further preclinical studies on  $^{18}\text{F}$ -labeled CXCR4 ligands.

## RESULTS AND DISCUSSION

### 3.3. Ligands based on cyclo[D-Tyr-Pro-2-Nal-N(Me)-Arg-Arg] (**R3**) for addressing the CXCR chemokine receptor type 7

Since a variety of different assays were employed for the determination of binding affinity towards CXCR7 in the literature and to establish a reproducible system, simulating the *in vivo* binding situation as realistic as possible, living cells with endogenous CXCR7 expression (U343 human glioblastoma cells) were preferred over membrane aliquots<sup>158, 203</sup>. In addition, [<sup>125</sup>I]SDF-1 was not utilized as the radioligand, due to the very low stability of <sup>125</sup>I-labeled SDF-1 in solution ( $t_{1/2} < 7$  days, data not shown). Thus, the recently published CXCR7-specific ligand FC313 (**R3**)<sup>158</sup> was chosen as the radioligand. Prior to the establishment of a competitive binding assay, the specificity of **R3** had to be confirmed. Therefore, CHO cells were transfected with human and murine CXCR4 and CXCR7. The total cellular uptake of [<sup>125</sup>I]FC131 ([<sup>125</sup>I]**R2**) and [<sup>125</sup>I]FC313 ([<sup>125</sup>I]**R3**) are depicted in Figure 26 and all values are corrected for unspecific binding using 10  $\mu$ M of AMD3100.

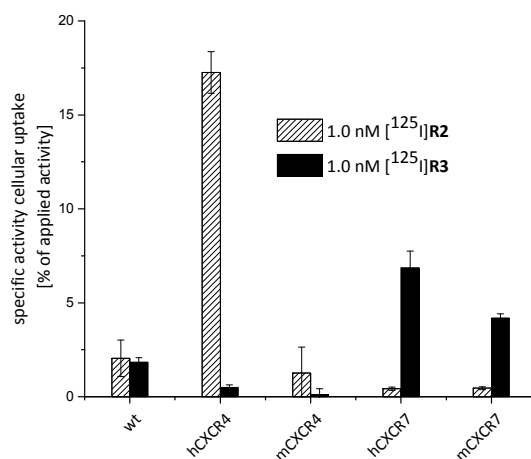


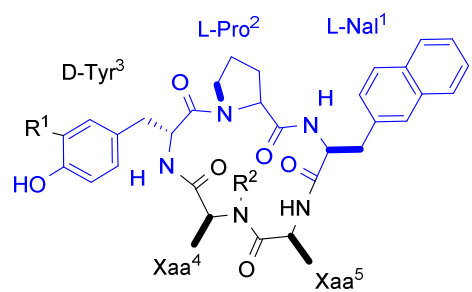
**Figure 26.** Specific cellular uptake of [<sup>125</sup>I]**R2** ([<sup>125</sup>I]FC131) and [<sup>125</sup>I]**R3** ([<sup>125</sup>I]FC313) on transfected CHO cells (wild type (no transfection), *hCXCR4*, *mCXCR4*, *hCXCR7* and *mCXCR7*). 150,000 cells/well were incubated in DMEM-F12 medium (5% BSA) for 2 h at 4 °C together with the respective radioligands ( $c = 1.0$  nM). The total cellular activity was corrected for non-specific binding (10  $\mu$ M AMD3100 for both CXCR4 and CXCR7). All data are expressed as mean  $\pm$  SD ( $n = 3$ ).

As already reported by *Oishi et al*, FC313 (cyclo(Nal-Pro-D-Tyr-Arg-N(Me)Arg), **R3**) showed specific binding to *h/mCXCR7*<sup>+</sup> cells, but almost no binding to *h/mCXCR4*<sup>+</sup> cells. This

## RESULTS AND DISCUSSION

prompted us to develop a competitive binding assay utilizing U343 cells, which are known to express *hCXCR7* in elevated levels and [ $^{125}\text{I}$ ]**R3** as the CXCR7 specific radioligand <sup>237</sup>.

To utilize the CXCR7 specific ligand **R3** as a potential PET probe, the structure has to be optimized in terms of hydrophilicity (calculated lipophilicity of **R3** using *ChemDraw Professional*,  $\log P_{\text{cal}} = 1.58$ ) to prevent elevated uptake *in vivo* due to hepatobiliary excretion <sup>169</sup>. As reported by *Oishi et al*, peptide modifications at position 2 (L-Pro) would lead to losses of CXCR7 specificity and therefore are not applicable. Additionally, subsequent SAR studies suggested that two aromatic groups (the phenol of D-Tyr<sup>3</sup> and the naphthalene of L-Nal<sup>1</sup>) are indispensable for the bioactivity *via* possible hydrophobic interactions <sup>158</sup>. Consequently, the two guanidino groups of L-Arg<sup>4</sup> and *N*-methylated L-Arg<sup>5</sup> were utilized for the design of novel derivatives (Fig. 27).



D-Tyr (R <sub>1</sub> )	Xaa <sup>4</sup>	Xaa <sup>5</sup>	R <sub>2</sub>	Cpd
H	L-Arg	L-Arg	Me	<b>R3</b>
I	L-Arg	L-Arg	Me	<b>44</b>
H	L-Orn	L-Arg	Me	<b>45</b>
H	D-Orn	L-Arg	Me	<b>46</b>
I	L-Orn	L-Arg	Me	<b>47</b>
H	L-Lys	L-Arg	Me	<b>48</b>
I	L-Lys	L-Arg	Me	<b>49</b>
H	L-Arg	L-Lys	Me	<b>50</b>
I	L-Arg	L-Lys	Me	<b>51</b>
H	L-Arg	L-Ala	aminohexyl	<b>52</b>
H	L-Arg	L-Ala	guanidinohexyl	<b>53</b>

**Figure 27.** Summary of structural modifications within the development of CXCR7 targeting peptides. Blue colored amino acids were not modified.

In order to provide a functional group for the introduction of linking units and chelators as anticipated for the development of novel PET probes and because cationic amino acids at these positions already inherited high binding affinities, ornithine and lysine were chosen for substitution.

## RESULTS AND DISCUSSION

Initially, to evaluate the influence of the conformation on the binding affinity of CXCR7 ligands, L-Orn (**45**) and D-Orn (**46**) were introduced at position 4, see Figure 27. Both peptides showed decreased binding affinities ( $675 \pm 171$  nM (**45**) and  $633 \pm 45$  nM (**46**) compared to  $180 \pm 16$  nM (**R3**), respectively), with no significant difference between **45** and **46** (Tab. 12). This finding led to the conclusion, that the conformation does not have a great influence on the  $IC_{50}$  values at this position, but since the lead structure FC131 (**R3**) contains L-Arg, only L-amino acids were employed in the following. The peptides containing L-Lys at position 4 (**48**) or 5 (**50**) exhibited a 1.5-fold higher binding affinity towards CXCR7 compared with the Orn-derivatives, but still showed 2.2-fold less potency than **R3**.

**Table 12.** Binding affinities towards *h*CXCR7 ( $IC_{50}$  values) of selected ligands determined using U343 glioblastoma multiforme (GBM) cells (150.000 cells/well). The cells were incubated with the respective ligands at 4 °C for 1 h together with [ $^{125}$ I]**R3** ( $c = 0.1$  nM) as radioligand. Each experiment was performed in triplicate, and results are means  $\pm$  SD from a minimum of three separate experiments.

<i>CXCR7 targeting peptides</i>			
peptide	$IC_{50}$ [nM]	peptide	$IC_{50}$ [nM]
<b>R3</b> (FC313)	$180 \pm 16$	<b>50</b>	$401 \pm 35$
<b>44</b>	$96 \pm 37$	<b>51</b>	$113 \pm 36$
<b>45</b>	$675 \pm 171$	<b>52</b>	$> 1000$
<b>46</b>	$633 \pm 45$	<b>53</b>	$342 \pm 2$
<b>47</b>	$179 \pm 56$	[ $^{nat}$ Ga] <b>54</b>	$834 \pm 38$
<b>48</b>	$484 \pm 226$	[ $^{nat}$ Cu] <b>54</b>	$> 1000$
<b>49</b>	$101 \pm 22$		

In computational docking studies with a homology model of CXCR7 a similar binding mode between CXCR4 and CXCR7 ligands could be observed<sup>158, 203, 238</sup>. Hence, the influence of side chain iodination of D-Tyr on the binding affinity of the CXCR7 ligands was investigated (as it had a beneficial effect on the CXCR4 ligands, see III.3.2.2.). Interestingly, all ligands (**44**, **47**, **49** and **51**, Fig. 27) exhibited a higher binding affinity than their parent, uniodinated peptides.

## RESULTS AND DISCUSSION

With  $IC_{50}$  values of  $96 \pm 37$  nM and  $101 \pm 22$  nM for **44** and **49**, these peptides showed an almost two-fold increased CXCR7 binding inhibition compared to **R3**. The resulting peptides feature enhanced lipophilicity due to the iodinated residue of D-Tyr (calculated lipophilicity of **49** using *ChemDraw Professional*,  $\log P_{\text{cal}} = 4.0$ ), which has to be balanced *via* condensation with hydrophilic chelators like NOTA, DOTA or DOTAGA for a suitable hydrophilicity. Thus, the chelator NOTA was conjugated to **49**, resulting in **54**. Unfortunately, the  $^{68}\text{Ga}$ -complex exhibited an 8-fold decreased binding affinity with  $834 \pm 38$  nM.

In conclusion, a more elaborate SAR studies has to be performed to assemble, on the one hand, the beneficial effects of iodination of the scaffold on the binding affinity and, on the other hand, the very high lipophilicity, which has to be decreased for suitable pharmacokinetics *in vivo*.

### 4. Determination of lipophilicity and specific cell binding

**Determination of lipophilicity:** Lipophilicity was measured as the partition coefficient of the  $^{68}\text{Ga}$ - or  $^{177}\text{Lu}$ -labeled peptides between n-octanol and PBS (pH 7.4) using the shake-flask method, see Table 13. Compared with reference ligand  $^{125}\text{I}$ **R2** ( $^{125}\text{I}$ FC131, all chelator coupled peptides showed increased hydrophilicity. From the experience with  $^{68}\text{Ga}$ Pentixafor ( $^{68}\text{Ga}$ **23**,  $\log P = -2.9 \pm 0.08$ ) and other radio-pharmaceuticals<sup>239</sup>, low lipophilicity in general results in rapid clearance from the circulation *via* the kidneys without increased renal uptake. Additionally, low hepatic uptake and biliary excretion improves tumor-to-background ratios and minimizes the effective whole body dose<sup>90, 91, 128, 169</sup>.

All peptides with D-Tyr iodinated scaffold showed enhanced lipophilicities ( $\log P = -1.8 \pm 0.2$  for  $^{177}\text{Lu}$ Pentixather ( $^{177}\text{Lu}$ **24**) vs.  $\log P = -2.9 \pm 0.08$  for  $^{68}\text{Ga}$ Pentixafor), whereas the  $^{68}\text{Ga}^{\text{III}}$ -chelates show an supplementary increase in hydrophilicity, as expected from the additional free carboxylate in the chelator compared to the  $^{177}\text{Lu}^{\text{III}}$ -chelate. The introduction of



## RESULTS AND DISCUSSION

the novel cationic “linking units” D-Arg-D-Ala-4-ABA ( $\log P = -2.75 \pm 0.24$  for  $[^{177}\text{Lu}]\mathbf{36}$ ) and D-Arg-Gly-4-ABA ( $\log P = -2.65 \pm 0.05$  for  $[^{177}\text{Lu}]\mathbf{34}$ ) resulted in hydrophilic peptides despite the D-Tyr iodinated scaffold. The CPCR4-based CXCR4 ligands **31**, **33** and **35** (cationic linking units, but without 3-*iodo*-D-Tyr) showed further increased hydrophilicity with  $\log P = -3.31 \pm 0.01$  for  $[^{177}\text{Lu}]\mathbf{31}$ ,  $\log P = -3.07 \pm 0.03$  for  $[^{177}\text{Lu}]\mathbf{33}$  and  $\log P = -2.95 \pm 0.13$  for  $[^{177}\text{Lu}]\mathbf{35}$ , respectively.

**Table 13.** Lipophilicity expressed as  $\log P$  (distribution coefficient in n-octanol/PBS) of radiolabeled CXCR4 ligands. Data are expressed as mean  $\pm$  SD (n = 6).

CXCR4 ligand	$\log P$
Reference ligands	
$[^{125}\text{I}]\mathbf{R2}^{90}$	$-0.35 \pm 0.02$
$[^{68}\text{Ga}]\mathbf{23}$	$-2.9 \pm 0.08$
$[^{177}\text{Lu}]\mathbf{24}$	$-1.8 \pm 0.2$
<b>R1</b> -based ligands	
$[^{68}\text{Ga}]\mathbf{9}$	$-2.8 \pm 0.1$
(iodo)CPCR4-based ligands	
$[^{177}\text{Lu}]\mathbf{31}$	$-3.31 \pm 0.01$
$[^{177}\text{Lu}]\mathbf{33}$	$-3.07 \pm 0.03$
$[^{68}\text{Ga}]\mathbf{34}$	$-3.03 \pm 0.02$
$[^{177}\text{Lu}]\mathbf{34}$	$-2.65 \pm 0.05$
$[^{68}\text{Ga}]\mathbf{35}$	$-3.58 \pm 0.06$
$[^{177}\text{Lu}]\mathbf{35}$	$-2.95 \pm 0.13$
$[^{68}\text{Ga}]\mathbf{36}$	$-3.29 \pm 0.02$
$[^{177}\text{Lu}]\mathbf{36}$	$-2.75 \pm 0.04$
$^{18}\text{F}$ -labeled peptides	
$[^{18}\text{F}]\mathbf{41}$	$-2.49 \pm 0.02$
$[^{18}\text{F}]\mathbf{42}$	$-1.47 \pm 0.01$

## RESULTS AND DISCUSSION

The novel  $^{18}\text{F}$ -labeled derivatives  $^{18}\text{F}$ **41** and  $^{18}\text{F}$ **42** inherited enhanced lipophilicity compared to  $^{68}\text{Ga}$ **23**, mostly due to the lack of the hydrophilic chelator. Nonetheless, the hydrophilicity of  $^{18}\text{F}$ **41** with a  $\log P = -2.49 \pm 0.02$  was considered to be sufficient for a fast renal clearance *in vivo*. Therefore,  $^{18}\text{F}$ AmBF<sub>3</sub>-D-Arg-Gly-4-ABA-CPCR4 ( $^{18}\text{F}$ **41**) was chosen for further evaluation using PET and Biodistribution studies (III.5.2.3.).

### Determination of plasma protein binding and binding to human blood cells:

Nonspecific interactions influence the fate of a radiopharmaceutical *in vivo*, which depends on the physicochemical properties, e.g. molecular weight, charge, lipophilicity, metabolic stability or elevated binding to red blood cells<sup>96, 223</sup>.

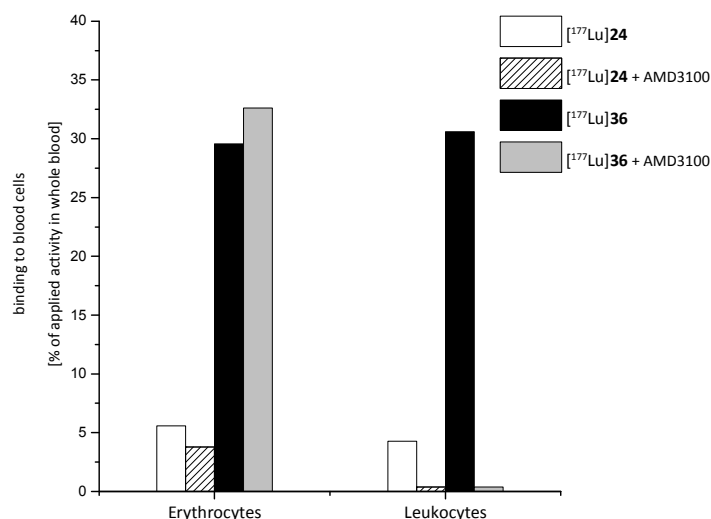


**Figure 28.** Binding of  $^{177}\text{Lu}$ **24** ( $^{177}\text{Lu}$ DOTA-4-AMBA-*iodo*CPCR4,  $^{177}\text{Lu}$ Pentixather) and  $^{177}\text{Lu}$ **36** ( $^{177}\text{Lu}$ DOTA-D-Arg-D-Ala-4-ABA-*iodo*CPCR4) to human blood cells (erythrocytes and leukocytes). Human blood was incubated with the respective radioligands ( $c = 1.0$  nM) for 30 min at 37 °C. CXCR4-mediated binding was determined using co-incubation of AMD3100 (100  $\mu\text{M}$ ).

On the contrary, high *in vivo* plasma protein binding increases the plasma half-life of the radiopharmaceutical and therefore might offer positive effects on the tracer distribution (higher uptake into target tissue over a longer period). Though, high unspecific binding to blood cells decreases the tumor to background ratio, especially at early time points, which might not be beneficial for diagnostic probes<sup>240</sup>. Several overlapping mechanisms have been identified for the

## RESULTS AND DISCUSSION

biologic profile of radiolabeled peptides and have to be evaluated for each compound independently. To estimate the bioavailability of the CXCR4 ligands *in vivo*, the plasma protein binding of [ $^{177}\text{Lu}$ ]**34**, (DOTA-D-Arg-Gly-4-ABA-*iodo*CPCR4) [ $^{177}\text{Lu}$ ]**35** (DOTA-D-Arg-D-Ala-4-ABA-CPCR4) and [ $^{177}\text{Lu}$ ]**36** (DOTA-D-Arg-D-Ala-4-ABA-*iodo*CPCR4) were determined and compared with [ $^{177}\text{Lu}$ ]Pentixather ([ $^{177}\text{Lu}$ ]**24**), applying ultracentrifugation. The 3-*iodo*-tyrosine group of [ $^{177}\text{Lu}$ ]**24** led to an increased  $\log P$  of  $-1.8 \pm 0.2$  and resulted in almost quantitative plasma protein binding (97%) as determined in our group<sup>182</sup>. The binding to human serum albumin was also quantitative for [ $^{177}\text{Lu}$ ]**35** and [ $^{177}\text{Lu}$ ]**36** (98% and >99%, respectively) despite the decreased lipophilicity and the absence of a halogenated tyrosine residue in [ $^{177}\text{Lu}$ ]**35**. [ $^{177}\text{Lu}$ ]**34** exhibited a plasma protein binding of 87%. Interestingly, [ $^{177}\text{Lu}$ ]**36** showed enhanced binding to human erythrocytes and CXCR4-mediated binding to human leukocytes see Figure 28. In comparison to [ $^{177}\text{Lu}$ ]**24**, six-fold more activity of [ $^{177}\text{Lu}$ ]**36** was bound to the leukocytes fraction after 30 min of incubation, while incubation together with an excess of AMD3100 prevented the CXCR4-mediated binding of [ $^{177}\text{Lu}$ ]**36** to leukocytes.

CXCR4 is known to be expressed on various types of leukocytes (monocytes, neutrophils and T-lymphocytes)<sup>6, 241</sup>. The specificity of binding could be demonstrated *via* co-incubation of the CXCR4 antagonist AMD3100 and the resulting significant reduction of tracer binding. Noteworthy, [ $^{68}\text{Ga}$ ]**23** ([ $^{68}\text{Ga}$ ]Pentixafor) was reported to bind to plasma proteins only to 64%. That fact should contribute to the low background uptake and the rapid whole-body clearance of [ $^{68}\text{Ga}$ ]**23**<sup>90</sup> rendering it superior for imaging studies. The combined effects of increased binding affinity and internalization rates, decreased lipophilicity, and higher binding to leukocytes (most probably due to enhanced binding affinity) on the pharmacokinetic behavior of the novel CXCR4 tracer were further investigated *in vivo* (III.5.).

## RESULTS AND DISCUSSION

### 5. *In vivo* evaluation

#### 5.1. Metabolite analysis

As confirmed by the clinical experience with [ $^{68}\text{Ga}$ ]Pentixafor and [ $^{177}\text{Lu}$ ]Pentixather, cyclic pentapeptides display excellent stability *in vivo* <sup>127, 128, 130, 153, 154</sup>. However, the metabolic *in vivo* stability of radioligands is a crucial prerequisite for clinical transfer of novel radioligands and *in vivo* metabolite analyses are thus a major component in their preclinical evaluation. For this reason, animals were sacrificed 30 min p.i. of the  $^{68}\text{Ga}$ - or  $^{177}\text{Lu}$ -labeled ligands ([ $^{68}\text{Ga}$ ]9, [ $^{68}\text{Ga}$ ]35 ([ $^{68}\text{Ga}$ ]DOTA-D-Arg-D-Ala-4-ABA-CPCR4) and [ $^{177}\text{Lu}$ ]36 ([ $^{177}\text{Lu}$ ]DOTA-D-Arg-D-Ala-4-ABA-*iodo*CPCR4). Liver and/or kidney homogenates, blood extract and the urine of healthy SCID mice were subsequently extracted and analyzed. All tested ligands showed high stability with >99% of intact injected tracer detected using radio-HPLC. Representative HPLC profiles of [ $^{177}\text{Lu}$ ]36 30 min p.i. of extracts and body fluids are shown in Figure 29.

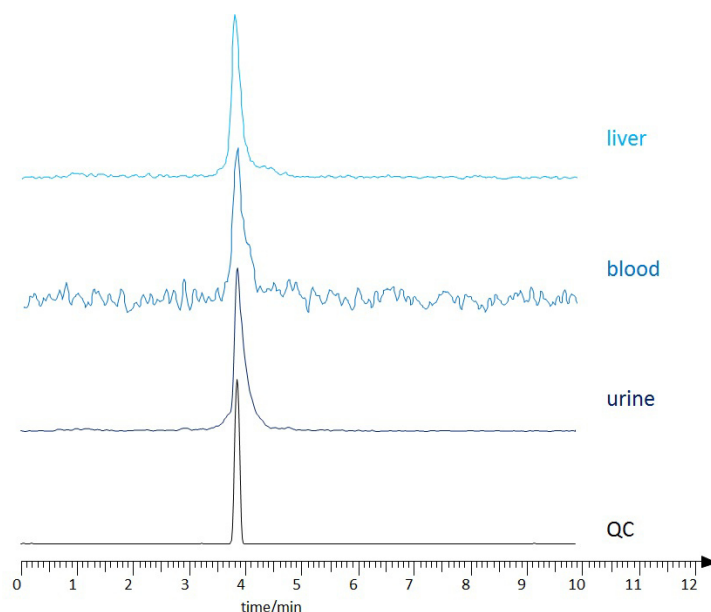


**Figure 29.** Exemplary radio-HPLC analyses of extracts from homogenized organs and body fluids (blood and urine) from CB17-SCID mice (30 min p.i. of 15 MBq of [ $^{177}\text{Lu}$ ]36, Chromolith column, flow rate 3 mL/min, 3 to 95% in 6 min, 95% for 3 min) injected with [ $^{177}\text{Lu}$ ]36.

## RESULTS AND DISCUSSION

### 5.2. Biodistribution

The physiological distribution of the CXCR4 targeting peptides at different time points was investigated in Daudi xenograft-bearing SCID mice. To provide comparability, the applied molar amount of peptide and the experimental setup were kept constant during the *in vivo* evaluation of the novel CXCR4 ligands (with the exception of [ $^{18}\text{F}$ ]**41**, due to low RCY), see Table 14.

**Table 14.** Biodistribution (in % ID/g) at 1 h p.i. in Daudi tumor-bearing SCID mice (or healthy mice): the **R1** derived ligand [ $^{68}\text{Ga}$ ]**9**, the ligands with iodinated binding scaffold [ $^{68}\text{Ga}$ ]**34** (D-Arg-Gly linker) and [ $^{68}\text{Ga}$ ]**36** (D-Arg-D-Ala linker) and their uniodinated analogue [ $^{68}\text{Ga}$ ]**35** (D-Arg-D-Ala linker), and the radiofluorinated CXCR4 ligand [ $^{18}\text{F}$ ]**41** (uniodinated scaffold).

<i>CPCR4.3 (R1) derived CXCR4 ligands</i>				
	<sup>[68Ga]</sup> <b>9</b> (n = 4)	<sup>[68Ga]</sup> <b>9</b> +50μg AMD3100 (n = 3)		
<hr/>				
blood	1.98 ± 0.09	4.33 ± 2.37		
heart	1.34 ± 0.76	2.31 ± 0.71		
lung	3.50 ± 0.65	4.79 ± 1.86		
liver	41.67 ± 4.84	8.55 ± 1.62		
pancreas	1.22 ± 1.32	0.96 ± 0.41		
spleen	10.87 ± 1.60	2.77 ± 0.63		
stomach	0.98 ± 0.19	1.92 ± 0.70		
small intestine	1.26 ± 0.27	2.63 ± 0.77		
colon	0.64 ± 0.16	1.08 ± 0.52		
adrenal gland	3.05 ± 1.06	2.71 ± 1.03		
kidney	6.83 ± 1.36	10.5 ± 2.22		
muscle	0.31 ± 0.11	0.68 ± 0.40		
bone	2.44 ± 0.60	1.42 ± 0.85		
brain	0.08 ± 0.02	0.45 ± 0.54		
<hr/>				
<i>Peptide 11/12 ((iodo)CPCR4) based ligands</i>				
	<sup>[68Ga]</sup> <b>34</b> (n = 4)	<sup>[68Ga]</sup> <b>35</b> (n = 4)	<sup>[68Ga]</sup> <b>35</b> + 50 μg AMD3100 (n = 3)	<sup>[68Ga]</sup> <b>36</b> (n = 4)
<hr/>				
blood	2.71 ± 0.52	4.01 ± 1.08	2.98 ± 0.57	8.85 ± 1.08
heart	1.77 ± 0.35	1.51 ± 0.30	1.37 ± 0.33	3.63 ± 0.71
lung	5.34 ± 1.09	3.07 ± 0.59	3.12 ± 0.57	6.82 ± 1.10

## RESULTS AND DISCUSSION

<b>liver</b>	$11.75 \pm 1.87$	$5.52 \pm 0.55$	$4.62 \pm 0.56$	$13.15 \pm 2.20$
<b>pancreas</b>	$0.83 \pm 0.12$	$0.68 \pm 0.01$	$0.69 \pm 0.07$	$2.01 \pm 0.39$
<b>spleen</b>	$4.46 \pm 0.69$	$1.94 \pm 0.17$	$2.38 \pm 0.23$	$6.95 \pm 1.51$
<b>stomach</b>	$1.85 \pm 0.34$	$1.20 \pm 0.13$	$0.97 \pm 0.32$	$2.13 \pm 0.49$
<b>small intestine</b>	$1.71 \pm 0.48$	$0.94 \pm 0.16$	$0.94 \pm 0.31$	$2.89 \pm 0.12$
<b>colon</b>	$1.50 \pm 0.29$	$0.71 \pm 0.13$	$0.47 \pm 0.09$	$1.48 \pm 0.67$
<b>adrenal gland</b>	$1.80 \pm 0.61$	$2.07 \pm 1.33$	$1.02 \pm 0.27$	$3.66 \pm 0.45$
<b>kidney</b>	$7.20 \pm 1.45$	$13.0 \pm 2.28$	$7.16 \pm 1.62$	$14.52 \pm 2.51$
<b>muscle</b>	$0.56 \pm 0.13$	$0.46 \pm 0.06$	$0.40 \pm 0.11$	$1.12 \pm 0.28$
<b>bone</b>	$1.45 \pm 0.61$	$1.42 \pm 0.13$	$0.74 \pm 0.11$	$3.33 \pm 0.51$
<b>brain</b>	$0.09 \pm 0.02$	-	-	-
<b>tumor</b>	$17.30 \pm 2.49$	$11.68 \pm 1.31$	$1.52 \pm 0.36$	$18.55 \pm 3.18$

### *Radiofluorinated PET probes*

	$[^{18}\text{F}]\mathbf{41}$ (n = 2)	$[^{18}\text{F}]\mathbf{41} + 50\mu\text{g}$ AMD3100 (n = 1)
<b>blood</b>	$1.40 \pm 0.07$	2.79
<b>heart</b>	$0.99 \pm 0.07$	1.98
<b>lung</b>	$3.31 \pm 0.16$	6.06
<b>liver</b>	$8.98 \pm 0.37$	9.76
<b>pancreas</b>	$0.44 \pm 0.05$	0.75
<b>spleen</b>	$2.06 \pm 0.19$	2.67
<b>stomach</b>	$1.18 \pm 0.22$	2.21
<b>small intestine</b>	$1.64 \pm 0.61$	3.02
<b>colon</b>	$0.71 \pm 0.26$	1.41
<b>adrenal gland</b>	$0.99 \pm 0.21$	1.45
<b>kidney</b>	$19.58 \pm 1.97$	30.47
<b>muscle</b>	$0.34 \pm 0.03$	0.76
<b>bone</b>	$1.37 \pm 0.22$	2.35
<b>tumor</b>	$4.40 \pm 0.65$	1.64

### *5.2.1. CXCR4 specific PET probes*

**CPCR4.3 (R1) derived CXCR4 ligands:**  $[^{68}\text{Ga}]\mathbf{9}$  ( $[^{68}\text{Ga}]\text{DOTA}-(1,4\text{-phenylenedimethanamine})\text{-cyclo}[\text{D-Tyr-N}(\text{hexylguanidino})\text{-D-Ala-Arg-2-Nal-D-Cys}]$ ) exhibited uptake predominantly in the liver (47% ID/g), but also in lung (4% ID/g) and kidneys (3% ID/g), Fig. 30. Activity uptake in blood (1.9% ID/g) and muscle (0.3% ID/g) was low, demonstrating high stability of the tracer 1 h p.i.. Interestingly, increased activity in the spleen (10.8% ID/g), in the

## RESULTS AND DISCUSSION

lung (3.5% ID/g) and in the bone (2.5% ID/g) displays the binding affinity towards murine CXCR4 ( $mIC_{50} = 63 \pm 19$  nM). Coinjection of AMD3100 resulted in a significant reduction of activity uptake (>80%) in the liver. Spleen, adrenal glands and bone also experienced a clear reduction of activity uptake, which supports the *in vitro* determined affinity towards murine CXCR4 of [ $^{68}\text{Ga}$ ]**9**.

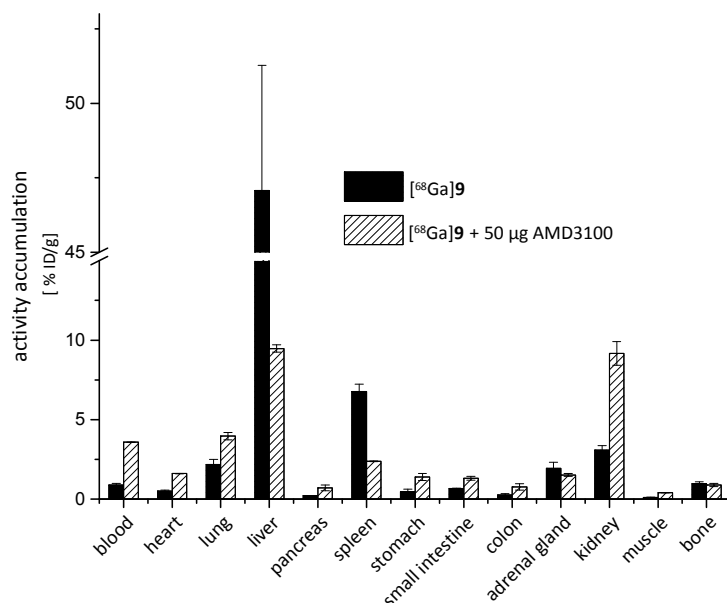


**Figure 30.** Biodistribution (in % ID/g) of CPCR4.3 derived ligand [ $^{68}\text{Ga}$ ]**9** and [ $^{68}\text{Ga}$ ]**9** together with 50 µg AMD3100 ( $n = 4$ , respectively) at 1 h p.i. in healthy SCID mice.

**Peptide 11/12 ((*iodo*)CPCR4) based ligands:** The improved binding affinity ( $IC_{50} = 0.4 \pm 0.1$  nM) and high internalization efficiency is clearly reflected in high activity accumulation of [ $^{68}\text{Ga}$ ]DOTA-D-Arg-D-Ala-4-ABA-CPCR4 ([ $^{68}\text{Ga}$ ]**35**) in the tumor ( $11.68 \pm 1.31\%$  ID/g, Fig. 31). The clearance from the background was slightly decelerated, most likely due to an enhanced association to blood plasma proteins and therefore, an elevated activity level in the blood ( $4.01 \pm 1.08\%$  ID/g). Compared to [ $^{68}\text{Ga}$ ]Pentixafor ([ $^{68}\text{Ga}$ ]**23**), which shows very little retention in the liver ( $<2\%$  ID/g), [ $^{68}\text{Ga}$ ]**35** accumulated in the liver with  $5.52 \pm 0.55\%$  ID/g at 1 h p.i., despite the significantly enhanced hydrophilicity ( $\log P = -2.9 \pm 0.08$  and  $\log P = -3.6 \pm 0.06$  for [ $^{68}\text{Ga}$ ]**23** and [ $^{68}\text{Ga}$ ]**35**, respectively). The introduction of a positively charged linking unit

## RESULTS AND DISCUSSION

seems to result in increased activity retention in the kidneys for both investigated peptides **35** and **36** ( $13.03 \pm 2.28\%$  ID/g and  $14.52 \pm 2.51\%$  ID/g, respectively).

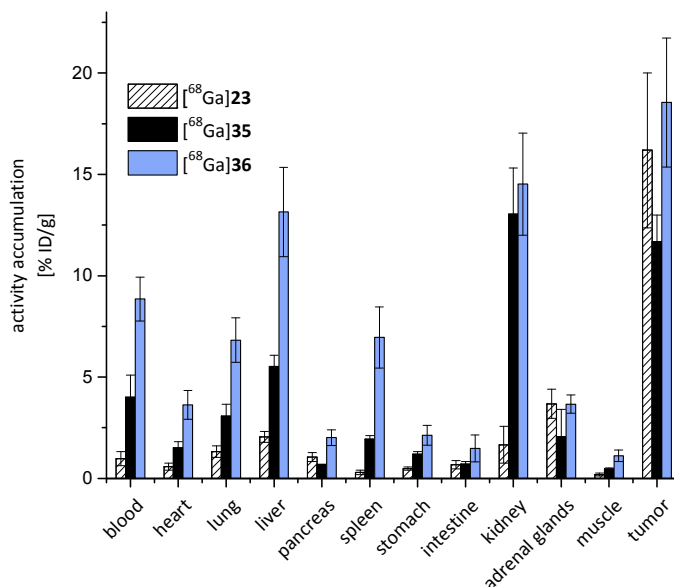


**Figure 31.** Biodistribution (in % ID/g) of the peptide **11** based ligand [<sup>68</sup>Ga]**35** and its iodinated analogue [<sup>68</sup>Ga]**36** in comparison to [<sup>68</sup>Ga]**23** at 1 h p.i. in Daudi tumor-bearing SCID mice.

The competition experiment with AMD3100 (see Tab. 14) clearly demonstrated the CXCR4 specificity of the activity accumulation in the Daudi xenograft. In contrast to the hepatic uptake of [<sup>68</sup>Ga]**9**, the liver uptake of [<sup>68</sup>Ga]**35** was not reduced by the competitor, which indicates, that only a part of the observed liver uptake was *m*CXCR4 mediated. However, due to low overall background activity, increased binding affinity and the optimized hydrophilicity, [<sup>68</sup>Ga]**35** can be considered suitable for PET imaging.

The combination of the high affinity linking unit and the iodinated scaffold in [<sup>68</sup>Ga]DOTA-D-Arg-D-Ala-4-ABA-*iodo*CPCR4 ([<sup>68</sup>Ga]**36**) led to a CXCR4 targeting peptide, which inherits high affinity towards human and murine CXCR4 ( $hIC_{50} = 2.6 \pm 1.0$  nM,  $mIC_{50} = 48.5 \pm 0.5$  nM, respectively). This is clearly reflected in high initial tumor uptake ( $18.6 \pm 3.18\%$  ID/g at 1 h p.i.), but also increased activity accumulation in the blood pool, lungs, spleen and adrenal glands. The effect of increasing murine binding affinity of [<sup>68</sup>Ga]**23** (no affinity >1000 nM), [<sup>68</sup>Ga]**35** (medium affinity  $182 \pm 26$  nM) and [<sup>68</sup>Ga]**36** (high affinity  $48.5 \pm 0.5$  nM) was clearly



## RESULTS AND DISCUSSION

reflected in the activity uptake of organs with elevated expression of *mCXCR4*<sup>242, 243, 244</sup> (e.g. lungs, liver and spleen, Fig. 31).

The efficient tumor targeting of [<sup>68</sup>Ga]**35** and [<sup>68</sup>Ga]**36** at 1 h p.i. in combination with the enhanced internalization and retention rates measured *in vitro*, were further investigated. In addition, the effect of the elevated plasma protein binding on the tumor uptake at late time points has been studied with the longer-lived isotope <sup>177</sup>Lu (III.5.2.2).

**<sup>18</sup>F-labeled CXCR4-targeting PET probes:** As already mentioned in III.2.4., the low specific activity (and therefore the high amount of injected, unlabeled peptide) of [<sup>18</sup>F]**41** ([<sup>18</sup>F]AmBF<sub>3</sub>-D-Arg-Gly-4-ABA-CPCR4) resulted in low activity accumulation in the tumor (4.40 ± 0.65% ID/g, Fig. 32).

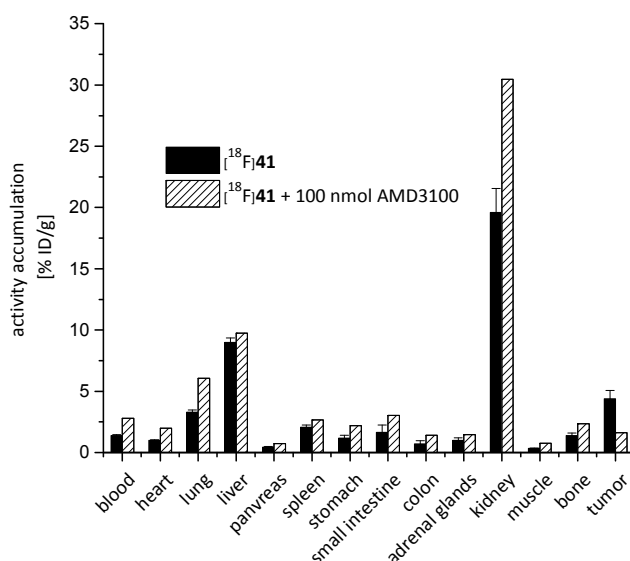


**Figure 32.** Biodistribution (in % ID/g) of [<sup>18</sup>F]**41** ([<sup>18</sup>F]AmBF<sub>3</sub>-D-Arg-Gly-4-ABA-CPCR4) and [<sup>18</sup>F]**41** together with 50 µg AMD3100 to visualize CXCR4 directed uptake at 90 min p.i. in Daudi xenograft-bearing SCID mice.

However, efficient clearance from the background was observed. The competition experiment with a blocking dose of AMD3100 led to a reduction of the tumor uptake from 4.4% ID/g to 1.6% ID/g indicating, that the tracer retains high affinity towards CXCR4 and good stability *in*

## RESULTS AND DISCUSSION

*vivo* (low bone uptake). Unfortunately, within the scope of this work, the automated synthesis could not be established and therefore has to be optimized in order to be able to utilize the advantages of the labeling strategies and the targeting traits of this class of compounds.

### 5.2.2. CXCR4-specific peptides for endoradiotherapeutic application

To determine the biodistribution of the novel  $^{177}\text{Lu}$ -labeled CXCR4 ligands at different time points and thus to gain insight into the kinetics of tracer elimination, biodistribution studies in Daudi tumor-bearing SCID mice were performed at 1, 6 and 48 h p.i. of [ $^{177}\text{Lu}$ ]**36** ([ $^{177}\text{Lu}$ ]DOTA-D-Arg-D-Ala-4-ABA-*iodo*CPCR4) and its uniodinated analogue [ $^{177}\text{Lu}$ ]**35**, respectively and are summarized in Table 15. All data were compared with the biodistribution of [ $^{177}\text{Lu}$ ]**24** ([ $^{177}\text{Lu}$ ]Pentixather), since it is the first CXCR4-directed cyclo pentapeptide applied for endoradiotherapy <sup>153, 182</sup>.

**Table 15.** Biodistribution (in %ID/g) at different time points p.i. in Daudi tumor-bearing SCID mice: iodinated peptide [ $^{177}\text{Lu}$ ]**36** (1 h, 6 h and 48 h p.i., respectively) and its more hydrophilic analogue [ $^{177}\text{Lu}$ ]**35** (1 h, 1 h with inhibition dose of AMD3100 (n =1), 6 h p.i. and 48 h p.i., respectively). The amount of co-administered unlabeled peptide was kept at 0.1 to 0.2 nmol for all peptides.

	[ $^{177}\text{Lu}$ ] <b>36</b> (n=3)	[ $^{177}\text{Lu}$ ] <b>36</b> (n=5)	[ $^{177}\text{Lu}$ ] <b>36</b> (n=4)
	1 h p.i.	6 h p.i.	48 h p.i.
<b>blood</b>	2.90 ± 0.32	0.17 ± 0.09	0.03 ± 0.01
<b>heart</b>	1.87 ± 0.32	0.28 ± 0.05	0.19 ± 0.02
<b>lung</b>	7.06 ± 0.67	1.07 ± 0.26	0.57 ± 0.04
<b>liver</b>	27.1 ± 1.87	17.1 ± 3.09	14.6 ± 2.00
<b>pancreas</b>	0.69 ± 0.14	0.11 ± 0.02	0.09 ± 0.01
<b>spleen</b>	6.72 ± 0.70	2.95 ± 0.75	2.72 ± 0.50
<b>stomach</b>	1.95 ± 0.17	0.25 ± 0.09	0.14 ± 0.02
<b>small intestine</b>	1.44 ± 0.22	0.24 ± 0.06	0.16 ± 0.06
<b>colon</b>	1.19 ± 0.35	0.49 ± 0.20	0.43 ± 0.30

## RESULTS AND DISCUSSION

<b>adrenal gland</b>	$4.54 \pm 1.06$	$0.68 \pm 0.21$	$0.60 \pm 0.12$
<b>kidney</b>	$10.3 \pm 0.26$	$3.20 \pm 0.45$	$2.58 \pm 0.69$
<b>muscle</b>	$0.58 \pm 0.07$	$0.06 \pm 0.01$	$0.04 \pm 0.00$
<b>bone</b>	$1.92 \pm 0.20$	$0.56 \pm 0.23$	$0.34 \pm 0.08$
<b>brain</b>	$0.08 \pm 0.01$	-	-
<b>tumor</b>	$17.2 \pm 2.01$	$12.5 \pm 2.56$	$8.11 \pm 0.96$

---

	$[^{177}\text{Lu}]\mathbf{35}$ (n=3)	$[^{177}\text{Lu}]\mathbf{35}$ (n=1)	$[^{177}\text{Lu}]\mathbf{35}$ (n=4)	$[^{177}\text{Lu}]\mathbf{35}$ (n=4)
	<b>1 h p.i.</b>	<b>1 h p.i. + 50<math>\mu</math>g AMD3100</b>	<b>6 h p.i.</b>	<b>48 h p.i.</b>

---

<b>blood</b>	$1.50 \pm 0.10$	1.9	$0.05 \pm 0.01$	$0.01 \pm 0.00$
<b>heart</b>	$0.90 \pm 0.07$	1.07	$0.13 \pm 0.02$	$0.08 \pm 0.01$
<b>lung</b>	$3.53 \pm 1.20$	3.34	$0.27 \pm 0.06$	$0.19 \pm 0.08$
<b>liver</b>	$11.9 \pm 1.57$	5.46	$11.3 \pm 2.83$	$8.99 \pm 1.62$
<b>pancreas</b>	$0.44 \pm 0.05$	0.61	$0.08 \pm 0.02$	$0.07 \pm 0.01$
<b>spleen</b>	$2.41 \pm 0.34$	1.11	$1.41 \pm 0.24$	$1.06 \pm 0.33$
<b>stomach</b>	$1.72 \pm 0.16$	2.46	$0.25 \pm 0.07$	$0.19 \pm 0.13$
<b>small intestine</b>	$1.23 \pm 0.18$	1.36	$0.30 \pm 0.06$	$0.16 \pm 0.11$
<b>colon</b>	$0.78 \pm 0.28$	0.74	$0.65 \pm 0.30$	$0.44 \pm 0.22$
<b>adrenal gland</b>	$1.16 \pm 0.18$	1.22	$0.51 \pm 0.12$	$0.33 \pm 0.08$
<b>kidney</b>	$9.74 \pm 0.91$	10.3	$7.10 \pm 2.06$	$3.05 \pm 0.15$
<b>muscle</b>	$0.28 \pm 0.02$	0.38	$0.04 \pm 0.01$	$0.02 \pm 0.00$
<b>bone</b>	$0.86 \pm 0.04$	0.74	$0.30 \pm 0.05$	$0.29 \pm 0.05$
<b>tumor</b>	$18.3 \pm 3.66$	3.04	$13.6 \pm 3.33$	$8.81 \pm 0.99$

One hour after injection, both tracers showed efficient tumor targeting with  $17.2 \pm 2.01\%$  ID/g  $[^{177}\text{Lu}]\mathbf{36}$  and  $18.3 \pm 3.66\%$  ID/g for  $[^{177}\text{Lu}]\mathbf{35}$ , respectively. High accumulation of radioactivity in the liver, spleen and lung, organs with elevated expression of *mCXCR4*<sup>242</sup>, was observed for  $[^{177}\text{Lu}]\mathbf{36}$  with  $27.08 \pm 1.87\%$  ID/g,  $6.72 \pm 0.70\%$  ID/g and  $7.06 \pm 0.67\%$  ID/g, as already seen for  $[^{68}\text{Ga}]\mathbf{36}$ . It is important to note, that the activity accumulation in the liver is not part of hepatobiliary clearance in the overall tracer elimination, which is evidenced by the absence of activity in the intestine at late time points (6 and 48 h p.i.). Additionally,  $[^{177}\text{Lu}]\mathbf{24}$  with a higher lipophilicity (log*P* value of  $-1.8 \pm 0.2$  vs.  $-2.8 \pm 0.04$  for  $[^{177}\text{Lu}]\mathbf{36}$ ) showed clearly decreased liver uptake compared to  $[^{177}\text{Lu}]\mathbf{36}$ .

## RESULTS AND DISCUSSION

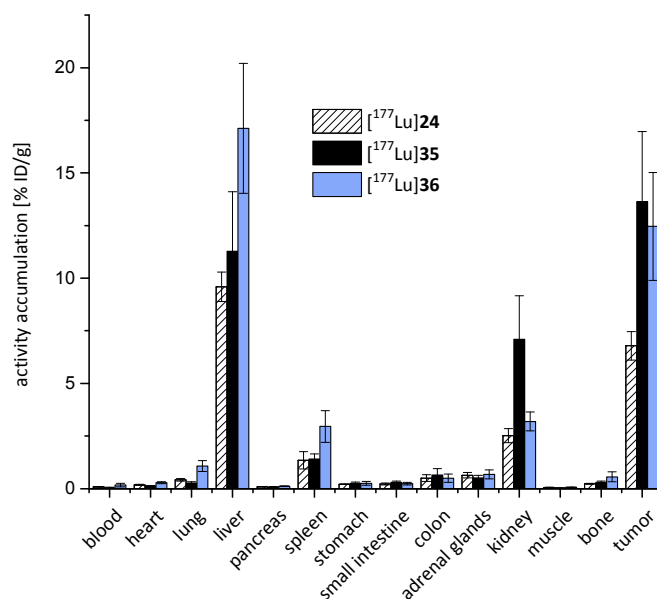


**Figure 33.** Comparison of the biodistribution of [<sup>177</sup>Lu]**24** ([<sup>177</sup>Lu]DOTA-4-AMBA-*iodo*CPCR4), [<sup>177</sup>Lu]**35** ([<sup>177</sup>Lu]DOTA-D-Arg-D-Ala-4-ABA-CPCR4) and [<sup>177</sup>Lu]**36** ([<sup>177</sup>Lu]DOTA-D-Arg-D-Ala-4-ABA-*iodo*CPCR4) (in % ID/g) in Daudi xenograft-bearing SCID mice at 6 h p.i..

Therefore, part of the observed liver uptake seems to be *mCXCR4* mediated, as demonstrated by the reduction of the hepatic activity by coinjection of a competitor (2 mg/kg AMD3100; Table 15). In accordance with the decreased murine binding affinity of [<sup>177</sup>Lu]**35**, the activity in the liver, spleen, adrenal glands and in the bone, was notably reduced. Possible binding to *mCXCR7* of both novel tracer, which is reported to be expressed in embryonic liver cells <sup>25</sup>, has to be further evaluated.

At 6 h p.i., tumor uptake, tumor/muscle ratios and tumor/liver ratios were highest for [<sup>177</sup>Lu]**35** and reached values of 13.6% ID/g, 378 and 1.2 for the Daudi xenograft (Fig. 33). [<sup>177</sup>Lu]**24** exhibited a tumor uptake of 6.7% ID/g and tumor/muscle and tumor/liver ratios of 122 and 0.7, respectively. Despite the elevated background accumulation of [<sup>177</sup>Lu]**36**, the tumor uptake, the tumor/muscle and tumor/liver ratios were 13.8% ID/g, 208 and 0.73, respectively.

To investigate the long-term biodistribution with focus on the retention of the <sup>177</sup>Lu-labeled peptides in the tumor tissue, mice were sacrificed at 48 h p.i. (see Figure 34). High retention of

## RESULTS AND DISCUSSION

activity in the tumor ( $8.8 \pm 1\%$  ID/g) was detected for [ $^{177}\text{Lu}$ ]**35** ([ $^{177}\text{Lu}$ ]DOTA-D-Arg-D-Ala-4-ABA-CPCR4), in contrast to [ $^{177}\text{Lu}$ ]**24** ([ $^{177}\text{Lu}$ ]Pentixather) with  $3.2 \pm 0.4\%$  ID/g).

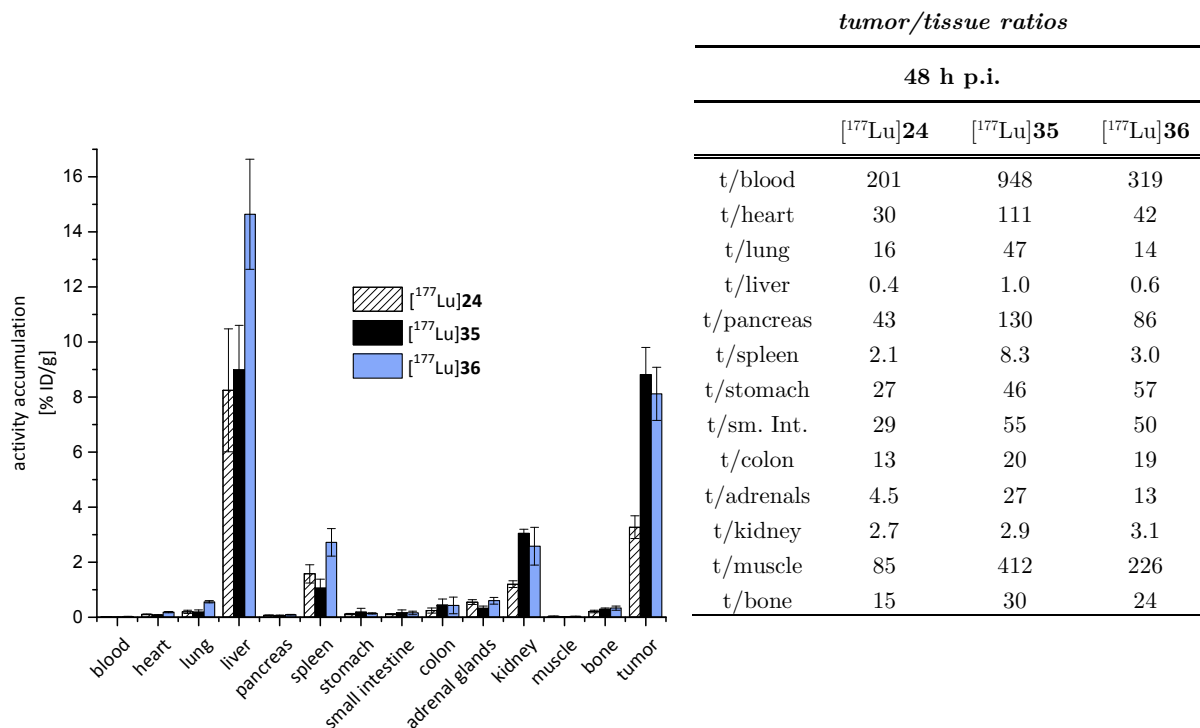


**Figure 34.** Comparison of the biodistribution of [ $^{177}\text{Lu}$ ]**24**, [ $^{177}\text{Lu}$ ]**35** and [ $^{177}\text{Lu}$ ]**36** (in % ID/g) in Daudi tumor-bearing SCID mice at 48 h p.i. and respective tumor/tissue ratios for [ $^{177}\text{Lu}$ ]**24**, [ $^{177}\text{Lu}$ ]**35** and [ $^{177}\text{Lu}$ ]**36**.

Probably due to the positive charged linker, the accumulation in the kidney was slightly enhanced for [ $^{177}\text{Lu}$ ]**35** with  $3.0 \pm 0.1\%$  ID/g compared to  $1.2 \pm 0.1\%$  ID/g for [ $^{177}\text{Lu}$ ]Pentixather ([ $^{177}\text{Lu}$ ]**24**). The tumor/tissue ratios depicted in the right panel of Figure 34 show an overall optimized biodistribution of [ $^{177}\text{Lu}$ ]**35** at 48 h p.i.. This finding is in accordance with the *in vitro* results, since radiolabeled **35** exhibited a high binding affinity, enhanced hydrophilicity, an enhanced internalization rate, but more importantly, the highest retention in tumor cells measured within this study (93% of added activity was still cell associated after 60 min).

## RESULTS AND DISCUSSION

The D-Tyr iodinated analogue [ $^{177}\text{Lu}$ ]**36** showed the highest internalization rate and total cellular uptake of all tested compounds, but also high binding affinity towards murine CXCR4. Further, the plasma protein binding of [ $^{177}\text{Lu}$ ]**36** was >99%, which in turn entailed a delayed clearance of the activity from the circulation at earlier time points. This property (in combination with the enhanced, specific binding towards CXCR4 expressing blood cells, see III.4.) was expected to have a beneficiary influence on tracer uptake in the target tissue, since it should lead to a prolonged tracer delivery to the tumor. The expected additional reservoir function was not clearly confirmed by the tracer distribution at 48 h p.i.. Compared to [ $^{177}\text{Lu}$ ]**35** no enhanced tumor activity of [ $^{177}\text{Lu}$ ]**36** was observed ( $8.1 \pm 0.96\%$  ID/g). Consequently, the tumor-to-organ ratios of [ $^{177}\text{Lu}$ ]**36** in the utilized xenograft model are thus, significantly improved compared to [ $^{177}\text{Lu}$ ]Pentixather ([ $^{177}\text{Lu}$ ]**24**), but are not superior to [ $^{177}\text{Lu}$ ]**35** (with exception of tumor/kidney).

First in-man results of [ $^{177}\text{Lu}$ ]**24** demonstrated, that the organ distribution and dosimetry in patients fundamentally differs from the mouse data. For example, the slightly enhanced hepatic retention of [ $^{177}\text{Lu}$ ]Pentixather in the mouse model was also observed in the first patients, but mean liver to kidney activity concentration ratios were significantly lower as opposed from the xenograft model <sup>154</sup>. Consequently, first patient dosimetry studies are necessary to be able to assess the potential of **35** and **36** as an endoradiotherapeutic tracer.

Interestingly, the introduction of a cationic amino acid in the “linking unit” of **35** and **36** seems to lead to elevated uptake and retention of activity in the kidneys ([ $^{177}\text{Lu}$ ]**35** tumor/kidney ratio = 1.9). A correlation between cationic amino acids in radiopharmaceuticals and enhanced renal uptake has already been reported for somatostatin analogs before. Albeit this fact is somewhat concerning, it was shown, that the risk of nephrotoxicity induced by endoradiotherapy could be reduced by coinjection of cationic amino acids or gelofusin <sup>233, 245</sup>.

## RESULTS AND DISCUSSION

### 5.3. Small-animal PET

#### 5.3.1. *CPCR4.3 (R1)* derived *CXCR4* ligands

The pharmacokinetic behavior of [ $^{68}\text{Ga}$ ]DOTA-(1,4-phenylen-dimethanamine)-cyclo[D-Tyr-N(hexylguanidino)-D-Ala-Arg-2-Nal-D-Cys] ([ $^{68}\text{Ga}$ ]**9**) was investigated using static small animal PET scans of normal SCID-mice. As expected from the biodistribution data, the maximum intensity projections (MIP), shown in Figure 35, demonstrated rapid clearance from circulation and renal excretion, resulting in accumulation of activity in the bladder. Metabolic stability was also evidenced by low unspecific whole body uptake of the tracer (metabolic stability was also confirmed under III.5.1.).

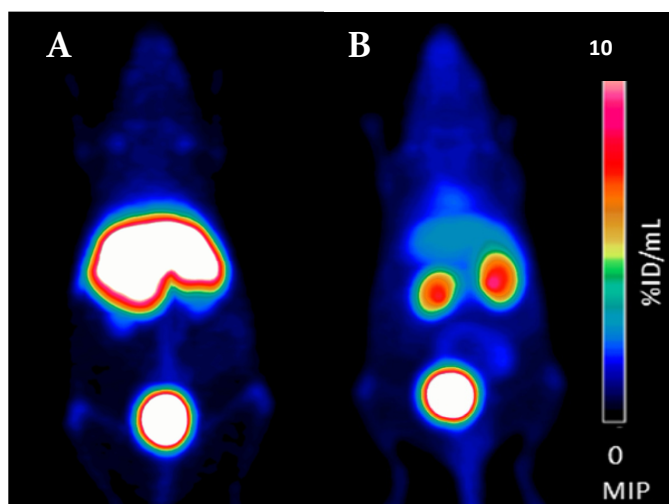


**Figure 35.** Maximum intensity projections (MIP) of  $\mu$ PET scans. MIP (1 h p.i. for 15 min, 0% to 10% ID/mL of two healthy SCID mice after injection of approximately 13 MBq (A) [ $^{68}\text{Ga}$ ]**9** or (B) [ $^{68}\text{Ga}$ ]**9** and 50  $\mu\text{g}$  AMD3100.

High tracer accumulation was detected in the liver, which could be reduced over 80% by coinjection of 50  $\mu\text{g}$  (2 mg/kg) AMD3100 (Figure 35, B). Given the high affinity of [ $^{nat}\text{Ga}$ ]**9** to both human and mouse CXCR4 ( $IC_{50} = 31 \pm 3$  nM and  $63 \pm 19$  nM for *h*CXCR4 and *m*CXCR4, respectively), the blockable liver accumulation strongly hints towards a species-specific CXCR4-mediated hepatic activity accumulation in mice. However, the high liver retention of [ $^{68}\text{Ga}$ ]**9** currently complicates the application of this tracer for the *in vivo* visualization of CXCR4-

## RESULTS AND DISCUSSION

expressing tissue in a mouse model, independently from the pronounced hydrophilicity ( $\log P = -2.8 \pm 0.1$ ). Several overlapping mechanisms have been identified for hepatic uptake of radiolabeled proteins and peptides (substrates for hepatic transporters, enhanced lipophilicity or positively charged conjugates)<sup>169, 223</sup>. Thus, further studies investigating the hepatic trafficking of *mCXCR4*-targeted peptidic probes are needed to fully elucidate their hepatic accumulation mechanism and to consequently develop strategies to reduce liver uptake, while maintaining efficient targeting of *mCXCR4* and *hCXCR4*.

### 5.3.2. Peptide 11/12 ((*iodo*)CPCR4) based ligands

In contrast to the suboptimal imaging properties of [<sup>68</sup>Ga]**9**, [<sup>68</sup>Ga]**23** ([<sup>68</sup>Ga]Pentixafor) has already been successfully used for PET imaging of CXCR4 expression in patients<sup>125-127, 129, 130</sup> and is currently entering clinical trials<sup>128, 131</sup>. As expected from the *in vitro* and biodistribution data, [<sup>68</sup>Ga]**33** ([<sup>68</sup>Ga]DOTA-D-Arg-Gly-4-ABA-CPCR4) and [<sup>68</sup>Ga]**35** ([<sup>68</sup>Ga]DOTA-D-Arg-D-Ala-4-ABA-CPCR4) revealed excellent CXCR4 receptor targeting and thus, high uptake in the Daudi xenograft with fast excretion (Figure 36). Besides the high tracer uptake in the tumor, slightly elevated accumulation in the liver and kidney was observed for [<sup>68</sup>Ga]**35** in comparison to [<sup>68</sup>Ga]**23**, despite the enhanced hydrophilicity of the CPCR4-based ligands ( $\log P$  of [<sup>68</sup>Ga]**35** is  $-3.58 \pm 0.06$  vs.  $-2.9 \pm 0.08$  for [<sup>68</sup>Ga]**23**). The higher internalization rates and increased binding affinities (as high as 60-fold in the case of [<sup>68</sup>Ga]**35**) did not result in higher tumor to background ratios, e.g. tumor/muscle is 26 for [<sup>68</sup>Ga]**35** and 85 for [<sup>68</sup>Ga]**23**. This might be due to the very pronounced specificity of [<sup>68</sup>Ga]**23** for human CXCR4, which shows literally no binding affinity for murine CXCR4 ( $IC_{50} > 1000$  nM in comparison to [<sup>nat</sup>Lu]**35** with  $IC_{50} = 182 \pm 26$  nM, see Table 8) and consequently no uptake in reported, *mCXCR4* expressing tissues like liver, lung, spleen or bone marrow<sup>172, 242</sup>. Given the significantly enhanced binding affinity of [<sup>68</sup>Ga]**35**, but also the slightly enhanced accumulation in the kidneys, a careful dosimetric investigation in patients is required to fully assess the potential of [<sup>68</sup>Ga]**35** as a clinical PET probe.



## RESULTS AND DISCUSSION

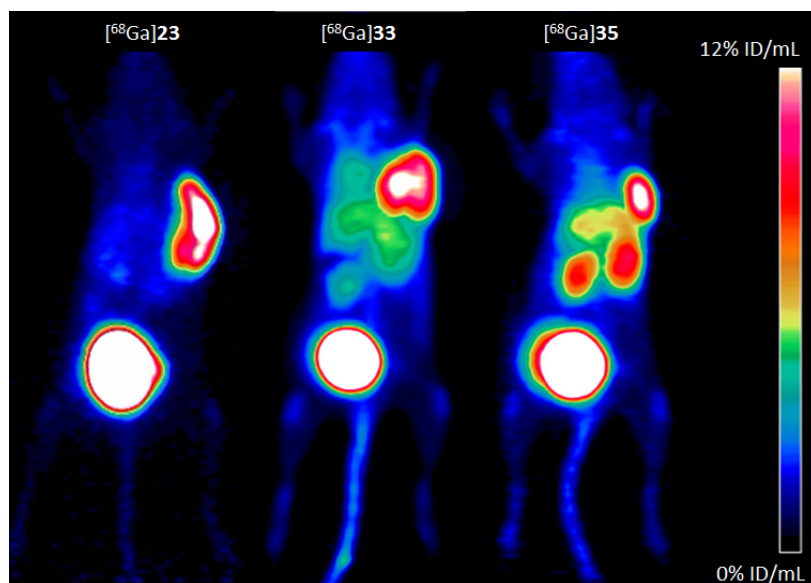


**Figure 36.** MIP (1 h p.i. for 15 min, 0% to 6/12% ID/mL) of Daudi tumor-bearing SCID mice after injection of approximately 12 MBq (0.2 nmol)  $[^{68}\text{Ga}]\mathbf{23}$  ( $[^{68}\text{Ga}]\text{Pentixafor}$ ) and cationic linker derivatives with non-iodinated scaffold  $[^{68}\text{Ga}]\mathbf{33}$  (D-Arg-Gly-4-ABA) and  $[^{68}\text{Ga}]\mathbf{35}$  (D-Arg-D-Ala-4-ABA).

In an additional experiment, the targeting efficiencies of the novel CXCR4 agents were determined in LNCaP xenograft-bearing SCID mice. As reported previously, the CXCL12/CXCR4 axis could be involved in prostate cancer cell migration and invasion. Functional CXCR4 was reported to be expressed by prostate cancer cell lines LNCaP and PC3, when compared with normal prostatic epithelial cells <sup>246</sup>. A noninvasive quantification of CXCR4 expression in prostate cancer could assist in the early assessment of enhanced metastatic potential of prostate cancer. Surprisingly, neither  $[^{68}\text{Ga}]\mathbf{23}$  nor  $[^{68}\text{Ga}]\mathbf{35}$  accumulated in the tumor to a greater extent than in background tissue (Figure 37). Both tracers were primarily taken up into the liver and kidneys, with excretion into the bladder. The utilized xenograft model, as well as the receptor density of CXCR4 on the surface of LNCaP cells may vary due to several parameters and has to be confirmed using histochemical methods <sup>247</sup>. Consequently, the suitability of CXCR4 targeting peptides for the quantification of the metastatic potential of prostate cancer has to be further evaluated in a more detailed fashion.

## RESULTS AND DISCUSSION

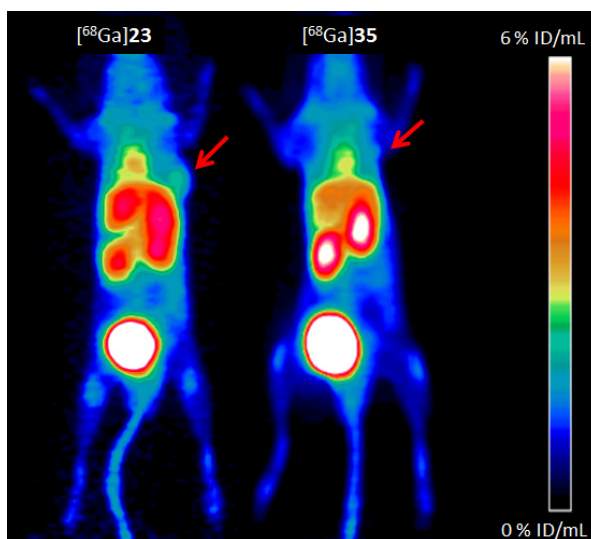


**Figure 37.** PET images (MIP at 1 h p.i. for 15 min, 0% to 6% ID/mL) of LNCaP (red arrow) xenograft-bearing SCID mice after injection of approximately 10 MBq (0.15 nmol)  $[^{68}\text{Ga}]\mathbf{23}$  ( $[^{68}\text{Ga}]\text{Pentixafor}$ ) and  $[^{68}\text{Ga}]\mathbf{35}$ .

Figure 38 shows exemplary PET images of the *iodoCPCR4*-based ligands  $[^{68}\text{Ga}]\mathbf{34}$  ( $[^{68}\text{Ga}]\text{DOTA-D-Arg-Gly-4-ABA-iodoCPCR4}$ ) and  $[^{68}\text{Ga}]\mathbf{36}$  ( $[^{68}\text{Ga}]\text{DOTA-D-Arg-D-Ala-4-ABA-iodoCPCR4}$ ) in comparison to  $[^{68}\text{Ga}]\mathbf{23}$ . As expected from the *in vitro* data, both tracers were primarily taken up into the tumor, but also into liver and kidneys. Interestingly, the significantly elevated binding to blood cells and plasma proteins of  $[^{68}\text{Ga}]\mathbf{36}$  (plasma protein binding >99% (III.4.), activity in blood  $8.85 \pm 1.08\%$  ID/g 1 h p.i., see Table 14) did not comprise the contrast of tumor to background in the MIP image. The pronounced activity accumulation of  $[^{68}\text{Ga}]\mathbf{34}$  in the kidneys could also not be confirmed in the biodistribution study (III.5.2.1.). As shown by the coinjection of 50  $\mu\text{g}$  AMD3100, tumor accumulation was almost exclusively CXCR4 mediated.

## RESULTS AND DISCUSSION

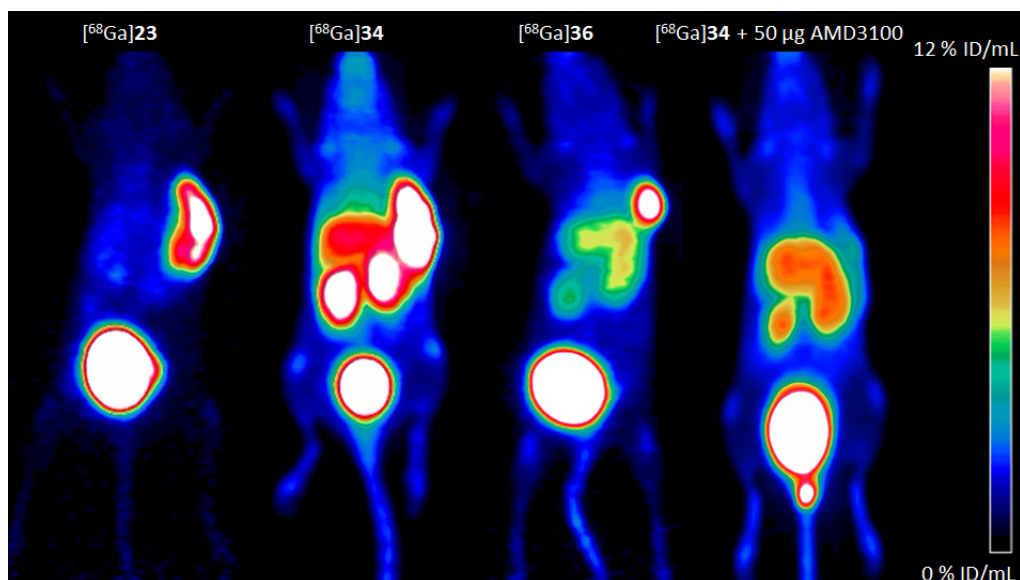


**Figure 38.** MIP (1 h p.i. for 15 min, 0% to 12% ID/mL) of Daudi tumor-bearing SCID mice after injection of approximately 12 MBq (0.2 nmol)  $[^{68}\text{Ga}]\mathbf{23}$  ( $[^{68}\text{Ga}]\text{Pentixafor}$ ) and cationic linker derivatives with iodinated scaffold  $[^{68}\text{Ga}]\mathbf{34}$ ,  $[^{68}\text{Ga}]\mathbf{36}$  as well as  $[^{68}\text{Ga}]\mathbf{34}$  coinjected with 50  $\mu\text{g}$  AMD3100.

**Tracer kinetic analysis:** Dynamic PET imaging offers the possibility of determination of the optimal imaging/biodistribution time point, as well as investigation of organ uptake and excretion kinetics. For the tracer kinetics, assuming a two-compartment model *in vivo*, the signal of non-specifically accumulated activity is characterized by a linear decrease of the graph in the logarithmic plot of time-activity curves<sup>111</sup>. In OSEM 3D reconstructed images, three dimensional regions of interest (ROI) were drawn, quantified and the resulting time-activity curves (TACs) for the CXCR4 ligands are shown in a logarithmic plot (Figure 39).

## RESULTS AND DISCUSSION

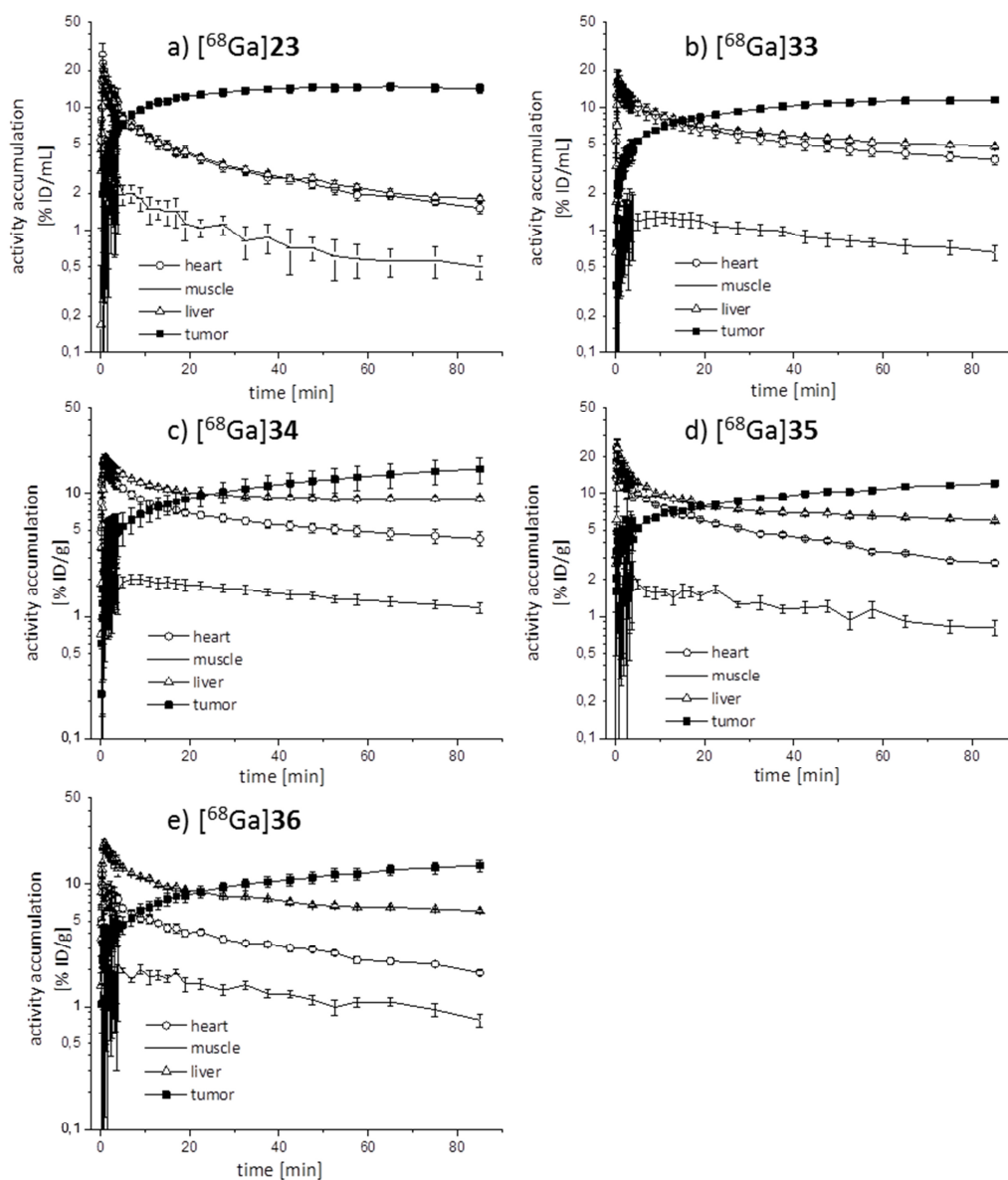


**Figure 39.** TACs (logarithmic plot) in %ID/mL derived from dynamic PET data (90 min acquisition time, OSEM 3D reconstruction) in Daudi xenografts, blood pool (heart), muscle and liver. Tumor-bearing SCID mice were injected with app. 10 MBq (0.05 - 0.15 nmol) of a)  $[^{68}\text{Ga}]\mathbf{23}$  as reference, b)  $[^{68}\text{Ga}]\mathbf{33}$ , c)  $[^{68}\text{Ga}]\mathbf{34}$ , d)  $[^{68}\text{Ga}]\mathbf{35}$ , and e)  $[^{68}\text{Ga}]\mathbf{36}$ .

$[^{68}\text{Ga}]\text{Pentixafor}$  ( $[^{68}\text{Ga}]\mathbf{23}$ ) demonstrated rapid accumulation in the tumor and an ideal clearance of activity from the background tissue. Despite the enhanced hydrophilicity of  $[^{68}\text{Ga}]\mathbf{35}$  ( $[^{68}\text{Ga}]\text{DOTA-D-Arg-D-Ala-4-ABA-CPCR4}$ ) and  $[^{68}\text{Ga}]\mathbf{36}$  ( $[^{68}\text{Ga}]\text{DOTA-D-Arg-D-Ala-4-ABA-}$

## RESULTS AND DISCUSSION

*iodoCPCR4*) with  $\log P = -3.58 \pm 0.06$  and  $-3.29 \pm 0.02$  compared to  $-2.90 \pm 0.08$  for [ $^{68}\text{Ga}$ ]Pentixafor (III.4., Table 13), high accumulation and only slow washout from the liver was observed in the  $\mu\text{PET}$  scans. Again, the reason for this could be the significantly increased murine binding affinity of [ $^{68}\text{Ga}$ ]**36**. The TACs of the liver were similar for all investigated tracers and seemed to be independent of the lipophilicity (which was lower for all ligands in comparison to [ $^{68}\text{Ga}$ ]Pentixafor). Nevertheless, efficient tumor targeting was observed for all ligands. The high retention of [ $^{68}\text{Ga}$ ]**36** in the blood pool, mostly due to elevated binding to plasma proteins, leads to a constant delivery of activity to CXCR4 positive tissue and therefore to an increased tumor activity over time (also visible for [ $^{68}\text{Ga}$ ]**34** ([ $^{68}\text{Ga}$ ]DOTA-D-Arg-Gly-4-ABA-*iodoCPCR4*)). To receive optimized tumor to background ratios, the slightly decelerated clearance of [ $^{68}\text{Ga}$ ]**36** and [ $^{68}\text{Ga}$ ]**35** from the liver and the constantly increasing tumor accumulation might result in somewhat delayed imaging time points.

### 5.3.3. Radiofluorinated CXCR4 PET probes

Due to the promising  $IC_{50}$  values for the CXCR4 ligands **41** and **42** ( $IC_{50} = 2.4 \pm 0.8$  nM and  $2.9 \pm 0.9$  nM, respectively) and to investigate the applicability of a novel labeling strategy utilizing a trifluoroborate precursor, Daudi tumor-bearing SCID mice were injected with [ $^{18}\text{F}$ ]**41** ([ $^{18}\text{F}$ ]AmBF<sub>3</sub>-D-Arg-Gly-4-ABA-CPCR4) and imaged at 1 h p.i..

[ $^{18}\text{F}$ ]**41** was chosen for the PET evaluation after determination of the lipophilicity. With a  $\log P$  of  $-1.47 \pm 0.01$ , [ $^{18}\text{F}$ ]**42** was considered too lipophilic for *in vivo* application with regard to hepatobiliary excretion and elevated liver uptake, in contrast to [ $^{18}\text{F}$ ]**41**, which revealed a significantly improved  $\log P$  of  $-2.49 \pm 0.02$ . One hour after injection, the tracer primarily accumulated in the kidneys and the bladder, but also in the tumor xenograft and to a lower extent in the liver (Fig. 40). Low activity uptake in the bones indicated metabolic inertness of [ $^{18}\text{F}$ ]**41** against *in vivo* defluorination. The activity accumulation into the Daudi xenograft was shown to be CXCR4 mediated by coinjection of 2 mg/kg AMD3100 in the competition study.

## RESULTS AND DISCUSSION



**Figure 40.** PET images (MIPs, 1 h p.i. for 15 min, 0% to 10% ID/mL) of two Daudi tumor-bearing SCID mice after injection of approximately 1 MBq. of  $[^{18}\text{F}]\mathbf{41}$  or for the competition study 1 MBq of  $[^{18}\text{F}]\mathbf{41}$  together with 50  $\mu\text{g}$  AMD3100.

As depicted in Figure 40, an almost quantitative reduction of activity accumulation in the tumor was achieved and interestingly, a clear reduction of liver uptake was detectable as well. Inconsistent with the very high binding affinity of  $\mathbf{41}$ , the tumor uptake in PET and in the biodistribution (Figure 32) is only 5% ID/g. This fact might be related to the very low specific activity of the  $^{18}\text{F}$ -labeled tracer. Compared to  $[^{68}\text{Ga}]\mathbf{34}$  PET imaging, an approximately 30-fold higher amount of unlabeled peptide was injected concomitant with  $[^{18}\text{F}]\mathbf{41}$ , since the specific activity of  $[^{18}\text{F}]\mathbf{41}$  was only 0.3 MBq/nmol, compared to 110 MBq/nmol for  $[^{68}\text{Ga}]\mathbf{34}$ . As already mentioned in III.2.4., the radiosynthesis has to be converted into a fully automated synthesis to be able to reach sufficient specific activities and consequently lower the amount of coinjected, unlabeled peptide in order to optimize the CXCR4 specific tumor accumulation.

## IV SUMMARY AND CONCLUSION

CXCR4 represents a highly relevant molecular target for imaging and ERT due to its expression pattern, which correlates with metastatic spread and disease progression. On account of this, two different binding scaffolds were utilized in this work (CPCR4.3 (cyclo[D-Tyr-N(hexylguanidino)-D-Ala-Arg-Nal-Gly], **R1**) and CPCR4 (cyclo[D-Tyr-N(Me)-D-Orn-Arg-2-Nal-Gly], **11**)) for the development of novel CXCR4 targeting ligands for imaging (PET or fluorescence imaging) and ERT. In addition, due to the pronounced involvement of CXCR7 in the CXCR4/CXCL12 axis and the upregulation of CXCR7 expression in several malignancies, novel CXCR7 targeting ligands were designed based on a third binding scaffold (FC313, cyclo[D-Tyr-Pro-2-Nal-N(Me)-Arg-Arg], **R3**).

The first approach focused on the highly affine cyclic pentapeptide CPCR4.3 (**R1**) and on the identification of modification points in combination with a linker that tolerates functionalization with structural diverse groups, without losing the encouraging *h/m*CXCR4 binding affinity of the parent peptide. A D-cysteine for glycine substitution in the binding scaffold of CPCR4.3 and additional optimization of the linking unit, resulted in cyclo[D-Tyr-N(hexylguanidino)-D-Ala-Arg-2-Nal-D-Cys(1,4-phenylen-bismethanamine)-acetamine] (**6**), a highly affine *m/h*CXCR4 targeting vector, which allows for conjugation with a chelator ( $[^{68}\text{Ga}]\mathbf{9}$ ) and decoration of QDs. Both conjugated derivatives demonstrated the potential of this CXCR4 targeting vector (fluorescence microscopy with ligand **6** modified QDs, III.3.1., Fig. 15 and  $\mu$ PET imaging with  $[^{68}\text{Ga}]\mathbf{9}$ , III.5.3.1., Fig. 35). Besides an encouraging pharmacokinetic profile, elevated accumulation in the liver was observed for  $[^{68}\text{Ga}]\mathbf{9}$  in healthy mice. Thus, further studies investigating the hepatic trafficking of *m*CXCR4-targeted peptidic probes are needed to fully elucidate the reasons of their hepatic accumulation mechanism and to consequently develop strategies to reduce liver uptake, while maintaining efficient targeting of *m*CXCR4. So far, targeted probes for murine CXCR4 receptors are barely known, which limits PET studies investigating CXCR4-associated pathologies currently to xenograft animal models<sup>131</sup>. Especially for applications in the mouse

## SUMMARY AND CONCLUSION

model, the novel CXCR4 ligand could help to gain closer insights into CXCR4 mediated pathological processes. With the ongoing improvement of binding affinity and pharmacokinetics, compound **6** could be a valuable lead structure for the development of CXCR4 ligands with optimized, species independent targeting characteristics.

The second approach included an  $IC_{50}$ -based SAR study to investigate the influence of additional (charged) amino acids in the linker between the binding scaffold and the chelator (III.3.2.1 and III.3.2.2.), since Pentixafor (**23**) provides only a limited choice of (radio)metal chelates with high binding affinity towards *h*CXCR4<sup>156, 248</sup>.

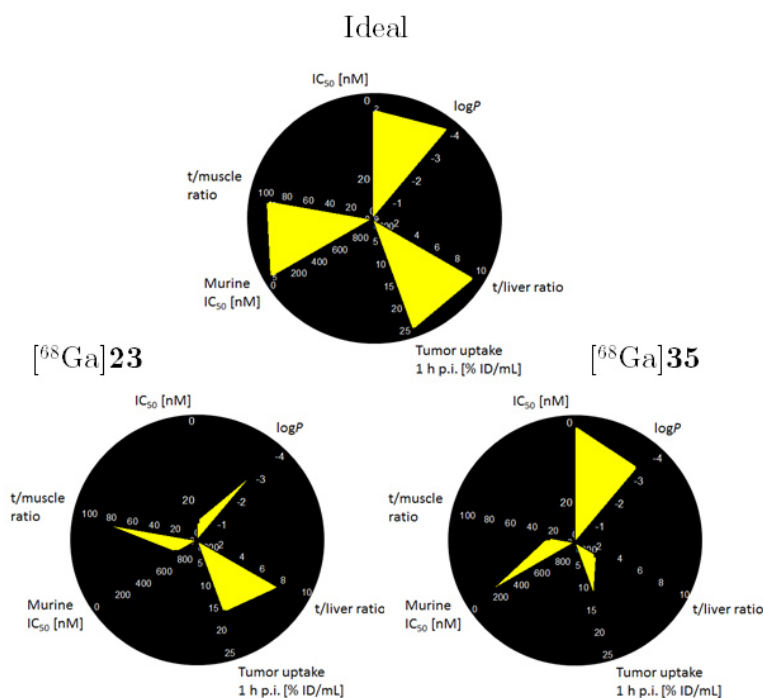


**Figure 41.** Web chart of characteristics for a PET tracer. **Top)** ideal PET tracer in theory, **left)**  $[^{68}\text{Ga}]\text{Pentixafor}$  ( $[^{68}\text{Ga}]\mathbf{23}$ ), **right)**  $[^{68}\text{Ga}]\mathbf{35}$ .

Therefore, the peptide spacer between the binding motif (*iodo*)CPCR4 (**11/12**) and the chelator (DOTA or DOTAGA) was modified step by step. The optimized CXCR4 ligands **35** (DOTA-D-Arg-D-Ala-4-ABA-CPCR4) and **36** (DOTA-D-Arg-D-Ala-4-ABA-*iodo*CPCR4) showed an up to



## SUMMARY AND CONCLUSION

60-fold enhanced binding affinity, which is almost independent of the incorporated metal (tested metals:  $^{\text{nat}}\text{Ga}^{3+}$ ,  $^{\text{nat}}\text{Lu}^{3+}$ ,  $^{\text{nat}}\text{Y}^{3+}$  and  $^{\text{nat}}\text{Bi}^{3+}$ ). The results of a comparative preclinical evaluation of **35** and the gold standard for PET,  $^{68}\text{Ga}$ ]Pentixafor, are summarized in Figure 41. In this visual chart an ideal PET tracer features a low  $IC_{50}$  (in the single digit nanomolar range), a  $\log P$  ideally between -3 to -4, high tumor to liver ratio *in vivo*, high tumor uptake (20% ID/g was selected to be ideal), pronounced murine binding affinity and a high tumor to muscle (background) ratio.  $^{68}\text{Ga}$ ]Pentixafor ( $^{68}\text{Ga}$ ]23) exhibited almost ideal tumor targeting characteristics with high tumor uptake, high tumor to liver and tumor to muscle ratios (III.5.3.2.). The novel compound  $^{68}\text{Ga}$ ]35 (DOTA-D-Arg-D-Ala-4-ABA-CPCR4) revealed improved binding affinity for human and murine CXCR4, a higher hydrophilicity and good tumor accumulation. Mostly due to the enhanced murine binding affinity, slightly elevated liver uptake and retention in the blood pool decreased the tumor to organ ratios compared to  $^{68}\text{Ga}$ ]Pentixafor. Given that  $^{177}\text{Lu}$ ]35 also exhibited excellent *in vitro* and *in vivo* characteristics (see III.5.2.2.), **35** is a promising CXCR4-targeting peptide, which can be used as a theranostic (therapeutic and diagnostic) tracer.

Its iodinated analogue **36** (DOTA-D-Arg-D-Ala-4-ABA-*iodo*CPCR4) revealed the highest internalization measured in this study, low  $IC_{50}$  values for  $^{\text{nat}}\text{Lu}$ - and  $^{\text{nat}}\text{Y}$ -complexes and elevated retention in tumor cells over 60 min, which in summary resulted in high tumor uptake and good tumor to organ ratios *in vivo*, see Figure 42. Ongoing clinical evaluation of  $^{177}\text{Lu}$ ]Pentixather ( $^{177}\text{Lu}$ ]24) in patients with hematological cancers will help to further assess the potential of endoradiotherapeutic treatment of CXCR4-overexpressing malignancies. In the comparative evaluation (Figure 42), however,  $^{177}\text{Lu}$ ]36 clearly demonstrated the beneficial effects of improved binding affinity, lipophilicity, and internalization/retention in tumor cells on the tumor targeting efficiency. High binding to human serum albumin (HSA) and increased, specific binding to human leukocytes with documented high CXCR4-expression<sup>249</sup>, might additionally lead to elongated half-life and therefore to a constant accumulation within the target over an extended period.

## SUMMARY AND CONCLUSION

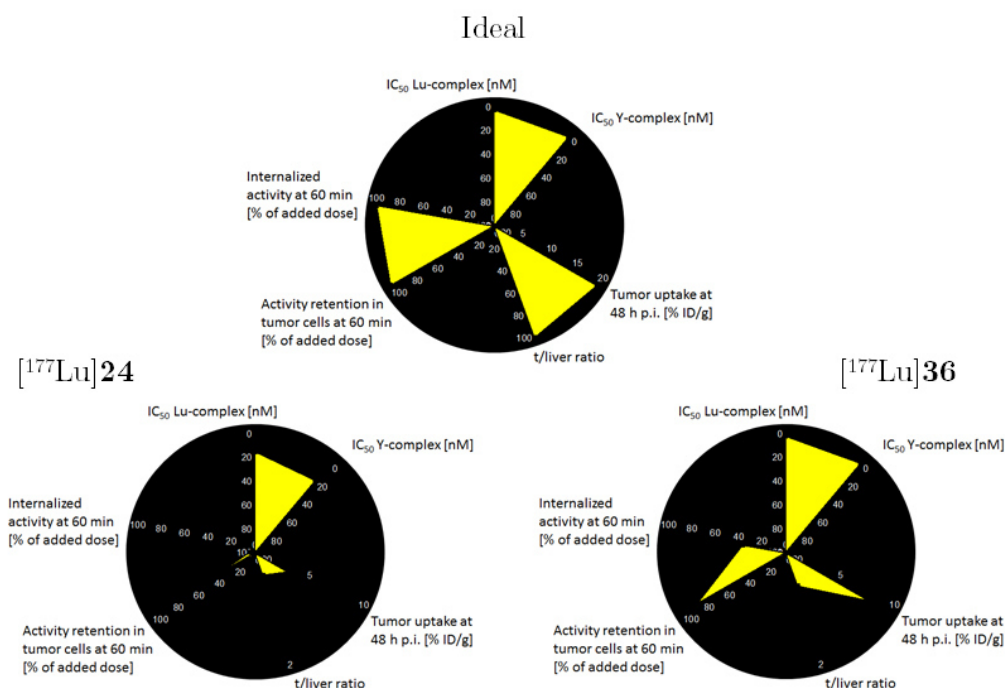


**Figure 42.** Web chart of characteristics for an endoradiotherapeutic tracer. **Top)** optimal tracer in theory with low  $\text{IC}_{50}$  values for  $^{\text{nat}}\text{Lu}$  and  $^{\text{nat}}\text{Y}$ -complex *in vitro*, high tumor uptake at late time points (48 h p.i.), high tumor to liver ratios, elevated retention of the activity in the externalization assay and efficient internalization of the radiolabeled tracer into tumor cells, **left)**  $[^{177}\text{Lu}]\mathbf{24}$ , **right)**  $[^{177}\text{Lu}]\mathbf{36}$ .

Importantly, the optimized linking unit led to a novel group of peptides (**33** - **36**), that are highly flexible with regards to structural modifications. This allows a straightforward implementation of various radiolabeling strategies including  $^{18}\text{F}$ -fluorination,  $^{99\text{m}}\text{Tc}$ -labeling, as well as the introduction of even bulky pharmacokinetic modifiers. When using this optimized linker concept, the affinities of the corresponding CPCR4- and *iodo*CPCR4-based derivatives are almost identical, which makes Tyr<sup>3</sup>-iodination dispensable as a tool to improve *hCXCR4* targeting. Surprisingly, however, using the *iodo*CPCR4 scaffold reduces species selectivity of the respective *iodo*CPCR4-based derivatives, which show almost 10-fold higher affinity towards *mCXCR4* compared to their CPCR4-based counterparts.

## SUMMARY AND CONCLUSION

The optimized linker concept was applied to develop  $^{18}\text{F}$ -labeled pentapeptides. Although the signaling unit was completely altered, high binding affinities were retained. Unfortunately, due to very low specific activities after manual synthesis, the initial  $\mu\text{PET}$  scans revealed only moderate activity accumulation in the tumor. For future applications of the promising  $^{18}\text{F}$ -labeled pentapeptides, further improvement of hydrophilicity ( $\log P = -2.49 \pm 0.02$ ) and most importantly, the establishment of an automated synthesis is necessary to lower the amount of concomitant injected, unlabeled peptide, since this has already been shown to decrease specific uptake *in vivo* for other ligand/receptor pairs<sup>250</sup>.

For the development of ACKR3 (CXCR7) targeting probes, a reliable *in vitro* assay was established to provide comparability with the reference ligands. An initial screening of structural modifications identified novel anchor points based on FC313 (**R3**) (e.g. substitution of L-Arg with L-Orn and subsequent iodination of D-Tyr). In future, a more elaborate SAR study has to decrease the lipophilicity and retain high binding affinity towards CXCR7 after conjugation with signaling units for PET imaging.

## V SUPPLEMENTARY MATERIAL

## 1. Figure and Table index

- Figure 1.** Involvement of the CXCR4 and CXCL12, in the tumor microenvironment and in the development of organ targeted metastasis. **A)** Within hypoxic areas of tumors, both CXCL12 and CXCR4 expression on tumor cells increases. Expression of CXCL12 promotes tumor cell growth and recruits circulating endothelial progenitors, which allow for tumor angiogenesis<sup>5</sup>. **B)** CXCL12 is released only by certain organs (bone marrow, liver and lung) or under certain physiological conditions (tissue damage, hypoxia etc.). CXCR4 expressing cells, such as stem cells or cancer cells are recruited by these sites and leave the circulation for differentiation or for the formation of metastasis (misuse of the physiological CXCR4/CXCL12 based stem cell axis) <sup>59</sup>.....**5**
- Figure 2.** Structure of CXCR4 and electrostatic surface area representation of CXCR4 and CXCL12. Left) Crystal structure of CXCR4 co-crystallized with small molecule inhibitor IT1t (magenta, PBD: 3ODU). Right) Surface representation of CXCR4 and CXCL12, colored according to the electrostatic potential from red (negative) to blue (positive). The CVX15 peptide (green ribbon) illustrates the binding site for peptide ligands <sup>83</sup>. ....**9**
- Figure 3.** Peptide and peptido-mimetic ligands for CXCR4. The amino acid sequence of CXCL12 (68 AS) is included with the two binding sites for CXCR4 labeled with purple (site 1) and blue (site 2) circles. Cysteines involved in disulfide bridges are labeled green and red, respectively. Structural modifications in the course of ligand development are indicated with blue color <sup>84-92</sup>.....**10**
- Figure 4.** Charge interactions in the crystal structure of CXCR4 in complex with the peptide CVX15 (A) (PDB code: 3OE0). Calculated binding mode of FC131 (**R2**), depicted in (B) and of the peptidomimetic ligand CPC4.3 (**R1**) (depicted in (C)) in CXCR4 using PDB code: 3OE0 and the software glide. Residues of the CXCR4 binding cavity, which are involved in ligand binding are highlighted in gray and green, respectively <sup>85, 89</sup>.....**13**
- Figure 5.** A) Helical wheel diagram of CXCR4 as seen from the extracellular side showing the upper halves of the TMs and parts of ECL-2. Residues on gray background were mutated during a site-directed mutagenesis study to determine crucial residues for FC131 interaction with CXCR4. B) Two-dimensional representation of FC131-binding to CXCR4. Residue colors: red, negative; purple, positive; cyan, polar; green, hydrophobic. Interactions: pink full and stippled arrows, H-bond with main and side chain respectively; green line,  $\pi$ - $\pi$  stacking; red line, cation- $\pi$  interaction; gray cloud, solvent-exposed atom <sup>104</sup>. ....**15**
- Figure 6.** Schematic representation of a PET scanner. The radioisotope decays by  $\beta^+$ -emission. Subsequent annihilation of the formed positronium results in two 511 keV  $\gamma$ -photons, which are counted by two opposite detector units electronically connected *via* a coincidence circuit. ....**18**
- Figure 7.** Structures of selected PET imaging agents for CXCR4 targeting.....**20**
- Figure 8.** Structures of CXCR4 targeting lead scaffolds **R1** <sup>89</sup> and **R2** <sup>88</sup> with thereof derived cyclic pentapeptides **2** and **11** <sup>91</sup> and the chemical structure of CXCR7 targeting lead scaffold FC313 (**R3**) <sup>158</sup>.....**87**

## SUPPLEMENTARY MATERIAL

- Figure 9.** Overview of the synthetic routes and the separation into chapters according to the utilized lead structure.....**88**
- Figure 10.** Synthetic route for the CXCR4 binding peptide (**2**). CXCR4 affine ligands in combination with different linkers (**3-8**). .....**90**
- Figure 11.** Schematic synthesis route for peptides employed in the “shifting the charge” study. For *in vitro* evaluation, the respective linear peptides were acetylated at the *N*-terminus to mimic an amide bond of further conjugation. ....**91**
- Figure 12.** Proposed reaction scheme of TFA catalyzed, direct iodination of peptide **11**. ....**93**
- Figure 13.** Reaction route for  $^{18}\text{F}$ -labeling precursor: I) construction of the peptidic linker on solid support ( $\text{R}^1$  represents different amino acids), II) diazo-transfer on solid support (a, b), III) preparation of  $\text{AmBF}_3$  synthon and *in situ* 1,3-dipolar cycloaddition (c, d), IV) preparation of the respective pentafluorophenolester (e), V) combination of iodinated scaffold **12** and the linker (f). ....**95**
- Figure 14.** Structural modifications used in the SAR study starting from FC313 (**R3**). Blue amino acids were kept constant during the structural modification process. ....**98**
- Figure 15.** Fluorescent microscopy of different CXCR4<sup>+</sup> cells. QDs-6 binding to (left) Daudi cells (100 nM, 1 h, rt), (middle) to Eμ-Myc1080 mouse B-cell lymphoma (25 nM, 1 h, rt), (right) to Chem\_1 cells (25 nM, 1 h, rt). ....**105**
- Figure 16.** Fluorescent microscopy of CXCR4 targeting specificity. (upper row) negative control with uncoated QDs on Chem\_1 cells (25 nM, 100.000 cells) and corresponding light microscopy image, (lower row) positive control with 25 nM **QDs-6** on Chem\_1 cells (25 nM, 100.000 cells) with corresponding light microscopy image. ....**105**
- Figure 17.** Structural Modifications (incl. Spacer, amino acids in the linking unit and the chelator) during the SAR study *Optimization of the linking unit* and the corresponding nomenclature of the peptides. ....**109**
- Figure 18.** Graphical summary of the SAR study *Optimization of the linking unit*.  $IC_{50}$  values were taken from Table 7 and represent  $IC_{50}$  values of at least three independent determinations. ....**112**
- Figure 19.** Internalization kinetics of [ $^{177}\text{Lu}$ ]**24** ([ $^{177}\text{Lu}$ ]Pentixather), [ $^{177}\text{Lu}$ ]**25** ([ $^{177}\text{Lu}$ ]DOTA-4-ABA-*iodo*CPCR4), [ $^{177}\text{Lu}$ ]**35** ([ $^{177}\text{Lu}$ ]DOTA-D-Arg-D-Ala-4-ABA-CPCR4) and [ $^{177}\text{Lu}$ ]**36** ([ $^{177}\text{Lu}$ ]DOTA-D-Arg-D-Ala-4-ABA-*iodo*CPCR4) into Chem\_1 cells. 100,000 cells/well were incubated with the respective radioligand ( $c = 1.0$  nM) at 37 °C in RPMI-medium (5% BSA). The total cellular activity was corrected for non-specific binding (10 μM AMD3100). All data are expressed as mean ± SD ( $n = 3$ ). ....**115**
- Figure 20.** Activity uptake kinetics (membrane bound and total cellular uptake) of [ $^{177}\text{Lu}$ ]**24** ([ $^{177}\text{Lu}$ ]Pentixather) and [ $^{177}\text{Lu}$ ]**36** ([ $^{177}\text{Lu}$ ]DOTA-D-Arg-D-Ala-4-ABA-*iodo*CPCR4) in Chem\_1 cells. 100,000 cells/well were incubated with the respective radioligand ( $c = 1.0$  nM) at 37 °C in RPMI-medium (5% BSA). The total cellular activity was corrected for non-specific binding (10 μM AMD3100). All data are expressed as mean ± SD ( $n = 3$ ). ....**116**
- Figure 21.** Externalization kinetics of selected CXCR4 ligands from Chem\_1 cells. 100,000 cells/well were incubated for 2 h with the respective radioligand ( $c = 1.0$  nM) at 37 °C in RPMI-medium (5% BSA). Then (left) RPMI-medium (5% BSA and 10 μM AMD3100) or (right) only RPMI-medium (5%

## SUPPLEMENTARY MATERIAL

BSA) was added for replacement. The total cellular internalized activity at  $t = 0$  min was corrected for non-specific binding (10  $\mu$ M AMD3100) and normalized to 100%. All data are expressed as mean  $\pm$  SD ( $n = 3$ ). ..... **118**

**Figure 22.** Representative immunofluorescence images for primary drug screening. MDA-MB-231 cells were treated with TN14003 (positive control), [ $^{nat}$ Ga]**23** ([ $^{nat}$ Ga]Pentixafor), [ $^{nat}$ Lu]**24** ([ $^{nat}$ Lu]Pentixather) or [ $^{nat}$ Lu]**35** ([ $^{nat}$ Lu]DOTA-D-Arg-D-Ala-4-ABA-CPCR4) at various concentrations (15 min, 37 °C). The cells were subsequently fixed and incubated with biotin-labeled TN14003 (0.05 mg/ml). After washing, cells were incubated with streptavidin-rhodamine. Red color represents binding of TN14003 to CXCR4. Nuclei were counterstained with cytox blue. .... **120**

**Figure 23.** Matrigel Invasion assay. Inhibition of CXCR4/CXCL12-mediated matrigel invasion of CXCR4<sup>+</sup> cells (MDA-MB-231) *in vitro* by 100 nM of [ $^{nat}$ Ga]**23** ([ $^{nat}$ Ga]Pentixafor), [ $^{nat}$ Lu]**24** ([ $^{nat}$ Lu]Pentixather) or [ $^{nat}$ Lu]**35** ([ $^{nat}$ Lu]DOTA-D-Arg-D-Arg-4-ABA-CPCR4), respectively. Cells were seeded on top of the matrigel and CXCL12 (200 ng/mL) was added in the bottom side of the matrigel chamber. After H&E staining, invaded cells were counted and the average of the invading cell numbers of MDA-MB-231 with CXCL12 added to the lower chamber was set to 100%. Data are corrected for non-specific invading (no addition of CXCL12 in bottom chamber) and are expressed as mean  $\pm$  SD ( $n = 3$ ). .... **121**

**Figure 24.** Agonist effects on CXCR4 using the TR-FRET based LANCE assay kit on U87 glioma cells. Inhibition of adenyl cyclase induced by CXCL12, [ $^{nat}$ Lu]**24** ([ $^{nat}$ Lu]Pentixather) or [ $^{nat}$ Lu]**35** ([ $^{nat}$ Lu]DOTA-D-Arg-D-Ala-4-ABA-CPCR4). While [ $^{nat}$ Lu]**35** counteracts forskolin at a concentration of 10  $\mu$ M to 80%, [ $^{nat}$ Lu]**24** shows no agonist effect on CXCR4. .... **122**

**Figure 25.** Antagonist setup of cAMP assay. Dose-dependent inhibition of cAMP production. With pretreatment (30 min at rt) of [ $^{nat}$ Ga]**23** ([ $^{nat}$ Lu]Pentixafor), [ $^{nat}$ Lu]**24** ([ $^{nat}$ Lu]Pentixather) or [ $^{nat}$ Lu]**35** ([ $^{nat}$ Lu]DOTA-D-Arg-D-Ala-4-ABA-CPCR4) at increasing concentrations, the effect of 150 ng/mL CXCL12 on cAMP reduction was measured by using the TR-FRET based LANCE assay kit. Note that [ $^{nat}$ Lu]**35** enhances the reduction of [cAMP](%) together with CXCL12. .... **124**

**Figure 26.** Specific cellular uptake of [ $^{125}$ I]**R2** ([ $^{125}$ I]FC131) and [ $^{125}$ I]**R3** ([ $^{125}$ I]FC313) on transfected CHO cells (wild type (no transfection), *h*CXCR4, *m*CXCR4, *h*CXCR7 and *m*CXCR7). 150,000 cells/well were incubated in DMEM-F12 medium (5% BSA) for 2 h at 4 °C together with the respective radioligands ( $c = 1.0$  nM). The total cellular activity was corrected for non-specific binding (10  $\mu$ M AMD3100 for both CXCR4 and CXCR7). All data are expressed as mean  $\pm$  SD ( $n = 3$ ). .... **126**

**Figure 27.** Summary of structural modifications within the development of CXCR7 targeting peptides. Blue colored amino acids were not modified. .... **127**

**Figure 28.** Binding of [ $^{177}$ Lu]**24** ([ $^{177}$ Lu]DOTA-4-AMBA-*iodo*CPCR4, [ $^{177}$ Lu]Pentixather) and [ $^{117}$ Lu]**36** ([ $^{177}$ Lu]DOTA-D-Arg-D-Ala-4-ABA-*iodo*CPCR4) to human blood cells (erythrocytes and leukocytes). Human blood was incubated with the respective radioligands ( $c = 1.0$  nM) for 30 min at 37 °C. CXCR4-mediated binding was determined using co-incubation of AMD3100 (100  $\mu$ M). .... **131**

**Figure 29.** Exemplary radio-HPLC analyses of extracts from homogenized organs and body fluids (blood and urine) from CB17-SCID mice (30 min p.i. of 15 MBq of [ $^{177}$ Lu]**36**, Chromolith column, flow rate 3 mL/min, 3 to 95% in 6 min, 95% for 3 min) injected with [ $^{177}$ Lu]**36**. .... **133**

## SUPPLEMENTARY MATERIAL

- Figure 30.** Biodistribution (in % ID/g) of CPCR4.3 derived ligand  $[^{68}\text{Ga}]\mathbf{9}$  and  $[^{68}\text{Ga}]\mathbf{9}$  together with 50  $\mu\text{g}$  AMD3100 ( $n = 4$ , respectively) at 1 h p.i. in healthy SCID mice. .... **136**
- Figure 31.** Biodistribution (in % ID/g) of the peptide 11 based ligand  $[^{68}\text{Ga}]\mathbf{35}$  and its iodinated analogue  $[^{68}\text{Ga}]\mathbf{36}$  in comparison to  $[^{68}\text{Ga}]\mathbf{23}$  at 1 h p.i. in Daudi tumor-bearing SCID mice..... **137**
- Figure 32.** Biodistribution (in % ID/g) of  $[^{18}\text{F}]\mathbf{41}$  ( $[^{18}\text{F}]\text{AmBF}_3\text{-D-Arg-Gly-4-ABA-CPCR4}$ ) and  $[^{18}\text{F}]\mathbf{41}$  together with 50  $\mu\text{g}$  AMD3100 to visualize CXCR4 directed uptake at 90 min p.i. in Daudi xenograft-bearing SCID mice. .... **138**
- Figure 33.** Comparison of the biodistribution of  $[^{177}\text{Lu}]\mathbf{24}$  ( $[^{177}\text{Lu}]\text{DOTA-4-AMBA-iodoCPCR4}$ ),  $[^{177}\text{Lu}]\mathbf{35}$  ( $[^{177}\text{Lu}]\text{DOTA-D-Arg-D-Ala-4-ABA-CPCR4}$ ) and  $[^{177}\text{Lu}]\mathbf{36}$  ( $[^{177}\text{Lu}]\text{DOTA-D-Arg-D-Ala-4-ABA-iodoCPCR4}$ ) (in % ID/g) in Daudi xenograft-bearing SCID mice at 6 h p.i.. .... **141**
- Figure 34.** Comparison of the biodistribution of  $[^{177}\text{Lu}]\mathbf{24}$ ,  $[^{177}\text{Lu}]\mathbf{35}$  and  $[^{177}\text{Lu}]\mathbf{36}$  (in % ID/g) in Daudi tumor-bearing SCID mice at 48 h p.i. and respective tumor/tissue ratios for  $[^{177}\text{Lu}]\mathbf{24}$ ,  $[^{177}\text{Lu}]\mathbf{35}$  and  $[^{177}\text{Lu}]\mathbf{36}$ . .... **142**
- Figure 35.** Maximum intensity projections (MIP) of  $\mu\text{PET}$  scans. MIP (1 h p.i. for 15 min, 0% to 10% ID/mL of two healthy SCID mice after injection of approximately 13 MBq (A)  $[^{68}\text{Ga}]\mathbf{9}$  or (B)  $[^{68}\text{Ga}]\mathbf{9}$  and 50  $\mu\text{g}$  AMD3100..... **144**
- Figure 36.** MIP (1 h p.i. for 15 min, 0% to 6/12% ID/mL) of Daudi tumor-bearing SCID mice after injection of approximately 12 MBq (0.2 nmol)  $[^{68}\text{Ga}]\mathbf{23}$  ( $[^{68}\text{Ga}]\text{Pentixafor}$ ) and cationic linker derivatives with non-iodinated scaffold  $[^{68}\text{Ga}]\mathbf{33}$  (D-Arg-Gly-4-ABA) and  $[^{68}\text{Ga}]\mathbf{35}$  (D-Arg-D-Ala-4-ABA). .... **146**
- Figure 37.** PET images (MIP at 1 h p.i. for 15 min, 0% to 6% ID/mL) of LNCaP (red arrow) xenograft-bearing SCID mice after injection of approximately 10 MBq (0.15 nmol)  $[^{68}\text{Ga}]\mathbf{23}$  ( $[^{68}\text{Ga}]\text{Pentixafor}$ ) and  $[^{68}\text{Ga}]\mathbf{35}$ . .... **147**
- Figure 38.** MIP (1 h p.i. for 15 min, 0% to 12% ID/mL) of Daudi tumor-bearing SCID mice after injection of approximately 12 MBq (0.2 nmol)  $[^{68}\text{Ga}]\mathbf{23}$  ( $[^{68}\text{Ga}]\text{Pentixafor}$ ) and cationic linker derivatives with iodinated scaffold  $[^{68}\text{Ga}]\mathbf{34}$ ,  $[^{68}\text{Ga}]\mathbf{36}$  as well as  $[^{68}\text{Ga}]\mathbf{34}$  coinjected with 50  $\mu\text{g}$  AMD3100..... **148**
- Figure 39.** TACs (logarithmic plot) in %ID/mL derived from dynamic PET data (90 min acquisition time, OSEM 3D reconstruction) in Daudi xenografts, blood pool (heart), muscle and liver. Tumor-bearing SCID mice were injected with app. 10 MBq (0.05 - 0.15 nmol) of a)  $[^{68}\text{Ga}]\mathbf{23}$  as reference, b)  $[^{68}\text{Ga}]\mathbf{33}$ , c)  $[^{68}\text{Ga}]\mathbf{34}$ , d)  $[^{68}\text{Ga}]\mathbf{35}$ , and e)  $[^{68}\text{Ga}]\mathbf{36}$ . .... **149**
- Figure 40.** PET images (MIPs, 1 h p.i. for 15 min, 0% to 10% ID/mL) of two Daudi tumor-bearing SCID mice after injection of approximately 1 MBq. of  $[^{18}\text{F}]\mathbf{41}$  or for the competition study 1 MBq of  $[^{18}\text{F}]\mathbf{41}$  together with 50  $\mu\text{g}$  AMD3100. .... **151**
- Figure 41.** Web chart of characteristics for a PET tracer. Top) ideal PET tracer in theory, left)  $[^{68}\text{Ga}]\text{Pentixafor}$  ( $[^{68}\text{Ga}]\mathbf{23}$ ), right)  $[^{68}\text{Ga}]\mathbf{35}$ . .... **153**
- Figure 42.** Web chart of characteristics for an endoradiotherapeutic tracer. Top) optimal tracer in theory with low  $IC_{50}$  values for  $^{nat}\text{Lu}$  and  $^{nat}\text{Y}$ -complex *in vitro*, high tumor uptake at late time points (48 h p.i.), high tumor to liver ratios, elevated retention of the activity in the externalization assay and

## SUPPLEMENTARY MATERIAL

efficient internalization of the radiolabeled tracer into tumor cells, left) [ $^{177}\text{Lu}$ ]Pentixather ([ $^{177}\text{Lu}$ ] <b>24</b> ), right) [ $^{177}\text{Lu}$ ] <b>36</b> .....	<b>155</b>
---	------------



## SUPPLEMENTARY MATERIAL

<b>Table 1.</b> Overexpression of CXCR4 in different types of malignancies based on literature from <sup>5, 8, 15, 33</sup> ....	<b>4</b>
<b>Table 2.</b> Physical properties of selected PET isotopes (positron emitters) <sup>106</sup> .....	<b>17</b>
<b>Table 3.</b> Physical properties of selected therapeutic radioisotopes ( <sup>106, 140-142</sup> ).....	<b>22</b>
<b>Table 4.</b> The half maximal inhibitory concentration ( <i>IC</i> <sub>50</sub> [nM]) of <i>h</i> CXCR4 targeting cyclic pentapeptides determined in a competitive binding assay using Jurkat cells (4.0 * 10 <sup>5</sup> cells/well, 2 h, rt, HBSS + 1% BSA) and ([ <sup>125</sup> I] <b>R2</b> (c = 0.1 nM) as the radioligand. Data are expressed as mean ± SD of at least three independent determinations.....	<b>103</b>
<b>Table 5.</b> <i>IC</i> <sub>50</sub> values of selected ligands for murine CXCR4 determined with Ep-Myc1080 mouse B-cell lymphoma cells (2 * 10 <sup>5</sup> cells/well, 2 h, rt, HBSS + 1% BSA) using [ <sup>125</sup> I]CPCR4.3 ([ <sup>125</sup> I] <b>R1</b> ) (c = 0.1 nM) as radioligand. ....	<b>104</b>
<b>Table 6.</b> The half maximal inhibitory concentration ( <i>IC</i> <sub>50</sub> [nM]) of <i>h</i> CXCR4 targeting cyclic pentapeptides determined in a competitive binding assay using Jurkat cells (4.0 * 10 <sup>5</sup> cells/well, 2 h, rt, HBSS + 1% BSA) and ([ <sup>125</sup> I] <b>R2</b> (c = 0.1 nM) as radioligand. Data are expressed as mean ± SD of three independent determinations. [ <sup>nat</sup> Ga]Pentixafor ([ <sup>nat</sup> Ga] <b>23</b> ) <sup>91</sup> was also included in the study. ....	<b>107</b>
<b>Table 7.</b> The half maximal inhibitory concentration ( <i>IC</i> <sub>50</sub> [nM]) of <i>h</i> CXCR4 targeting cyclic pentapeptides determined in a competitive binding assay with Jurkat cells (4.0 * 10 <sup>5</sup> cells/well, 2 h, rt, HBSS + 1% BSA) using ([ <sup>125</sup> I] <b>R2</b> (c = 0.1 nM) as the radioligand. Data are expressed as mean ± SD of three independent determinations. [ <sup>nat</sup> M]Pentixafor ([ <sup>nat</sup> M] <b>23</b> ) <sup>91, 156</sup> and [ <sup>nat</sup> M]Pentixather ([ <sup>nat</sup> M] <b>24</b> ) <sup>182</sup> were included in the study for comparison. ....	<b>110</b>
<b>Table 8.</b> <i>IC</i> <sub>50</sub> values of selected ligands for murine CXCR4 determined with Ep-Myc1080 mouse B-cell lymphoma cells (2 h, rt, HBSS + 1% BSA) using [ <sup>125</sup> I]CPCR4.3 ([ <sup>125</sup> I] <b>R1</b> ) (c = 0.1 nM) as reference and radioligand. ....	<b>113</b>
<b>Table 9.</b> Summary of the total cellular activity, the internalized activity and the ratio of internalized activity to total cellular uptake at 60 min as % of applied activity of radiolabeled CXCR4 ligands, determined on Chem_1 cells (37 °C, RPMI + 5% BSA, 100,000 cells/well, c = 1.0 nM for <sup>68</sup> Ga- and <sup>177</sup> Lu-labeled ligands). Data are corrected for non-specific binding (10 µM AMD3100) and expressed as mean ± SD (n = 3). ....	<b>117</b>
<b>Table 10.</b> Summary of the results of the externalization study. Cellular activity after externalization without ligand recycling (10 µM AMD3100 in incubation medium) or with ligand recycling (incubation in normal medium) in % of specific internalized activity at t = 0 min. Chem_1 cells, 37 °C, RPMI + 5% BSA, 100,000 cells/well, c = 1.0 nM for <sup>177</sup> Lu-labeled ligands. Data are corrected for non-specific binding (10 µM AMD3100) at t = 0 min and expressed as mean ± SD (n = 3). ....	<b>119</b>
<b>Table 11.</b> <i>IC</i> <sub>50</sub> values of selected <sup>19</sup> F-peptides for <i>h</i> CXCR4 determined with Jurkat cells (2 h, rt, HBSS + 1% BSA) using [ <sup>125</sup> I]FC131 ([ <sup>125</sup> I] <b>R2</b> ) (c = 0.1 nM) as radioligand. Data are expressed as mean ± SD of three independent determinations. [ <sup>nat</sup> Ga]Pentixafor ([ <sup>nat</sup> Ga] <b>23</b> ) <sup>91</sup> and [ <sup>nat</sup> Ga]Pentixather ([ <sup>nat</sup> Ga] <b>24</b> ) were included in the study. ....	<b>125</b>
<b>Table 12.</b> Binding affinities towards <i>h</i> CXCR7 ( <i>IC</i> <sub>50</sub> values) of selected ligands determined using U343 glioblastoma multiforme (GBM) cells (150.000 cells/well). The cells were incubated with the respective ligands at 4 °C for 1 h together with [ <sup>125</sup> I] <b>R3</b> (c = 0.1 nM) as radioligand. Each experiment	

## SUPPLEMENTARY MATERIAL

was performed in triplicate, and results are means  $\pm$  SD from a minimum of three separate experiments. .... **128**

**Table 13.** Lipophilicity expressed as  $\log P$  (distribution coefficient in n-octanol/PBS) of radiolabeled CXCR4 ligands. Data are expressed as mean  $\pm$  SD (n = 6). .... **130**

**Table 14.** Biodistribution (in % ID/g) at 1 h p.i. in Daudi tumor-bearing SCID mice (or healthy mice): the **R1** derived ligand [ $^{68}\text{Ga}$ ]**9**, the ligands with iodinated binding scaffold [ $^{68}\text{Ga}$ ]**34** (D-Arg-Gly linker) and [ $^{68}\text{Ga}$ ]**36** (D-Arg-D-Ala linker) and their unlabeled analogue [ $^{68}\text{Ga}$ ]**35** (D-Arg-D-Ala linker), and the radiofluorinated CXCR4 ligand [ $^{18}\text{F}$ ]**41** (uniodinated scaffold). .... **134**

**Table 15.** Biodistribution (in %ID/g) at different time points p.i. in Daudi tumor-bearing SCID mice: iodinated peptide [ $^{177}\text{Lu}$ ]**36** (1 h, 6 h and 48 h p.i., respectively) and its more hydrophilic analogue [ $^{177}\text{Lu}$ ]**35** (1 h, 1 h with inhibition dose of AMD3100 (n =1), 6 h p.i. and 48 h p.i., respectively). The amount of co-administered unlabeled peptide was kept at 0.1 to 0.2 nmol for all peptides. .... **139**

## SUPPLEMENTARY MATERIAL

### 2. Abbreviations

<b>A<sub>s</sub></b>	specific activity
<b>ABA</b>	aminobenzoic acid
<b>ACD</b>	annihilation coincidence correction
<b>ACKR3</b>	atypical chemokine receptor type 3
<b>AMBA</b>	aminomethylbenzoic acid
<b>AmBF<sub>3</sub></b>	ammoniomethyltrifluoroborate
<b>AS</b>	amino acid
<b>Boc</b>	<i>tert</i> -butyloxycarbonyl (protecting group)
<b>BSA</b>	bovine serum albumin
<b>cAMP</b>	cyclic adenosine monophosphate
<b>Cit</b>	citrulline
<b>CXCL12</b>	C-X-C motif chemokine 12
<b>CXCR4</b>	C-X-C chemokine receptor type 4
<b>CXCR7</b>	C-X-C chemokine receptor type 7
<b>DBU</b>	1,8-diazabicyclo[5.4.0]undec-7-ene
<b>DCM</b>	dichloromethane
<b>Dde</b>	<i>N</i> -(1-(4,4-dimethyl-2,6-dioxocyclohexylidene)ethyl) (protecting group)
<b>DEMEM</b>	Dulbecco's modified eagle medium
<b>DIAD</b>	diisopropyl azodicarboxylate
<b>DIC</b>	<i>N,N'</i> -Diisopropylcarbodiimide
<b>DIPEA</b>	<i>N,N</i> -Diisopropylethylamine
<b>DMAP</b>	4-(dimethylamino)pyridine
<b>DMF</b>	dimethylformamide
<b>DMSO</b>	dimethyl sulfoxide
<b>DOTA</b>	1,4,7,10-tetraazacyclododecane-1,4,7,10-tetraacetic acid
<b>DOTAGA</b>	1,4,7,10-tetraazacyclododecane,1-(glutaric acid)-4,7,10-triacetic acid
<b>DPPA</b>	diphenylphosphoryl azide
<b>EDC</b>	1-ethyl-3-(3-dimethylaminopropyl)carbodiimide
<b>EGF</b>	epidermal growth factor
<b>ECL</b>	extra cellular loop

## SUPPLEMENTARY MATERIAL

<b>ERT</b>	endoradiotherapy
<b>ESI-MS</b>	electrospray ionization mass spectrometry
<b>FBA</b>	filtered back protection
<b>FCS</b>	fetal calf serum
<b>FDA</b>	Food and Drug Administration
<b>Fmoc</b>	9-fluorenylmethyloxycarbonyl (protecting group)
<b>GPCR</b>	G protein-coupled receptor
<b>HIF-1</b>	hypoxia induced factor-1
<b>HATU</b>	O-(7-azabenzotriazol-1-yl)- <i>N,N,N',N'</i> -tetramethyluronium hexafluoro-phosphate
<b>HBSS</b>	Hank's buffered salt solution
<b>HEPES</b>	2-(4-(2-hydroxyethyl)-1-piperazinyl)-ethanesulfonic acid
<b>HOAt</b>	1-hydroxy-7-azabenzotriazole
<b>HOBt</b>	1-hydroxybenzotriazole
<b>HPCs</b>	hematopoietic progenitor cells
<b>HPLC</b>	high-performance liquid chromatography
<b>HSA</b>	human serum albumin
<b>HSC</b>	hematopoietic stem cells
<b>IC<sub>50</sub></b>	half maximal inhibitory concentration
<b>Iodogen</b>	1,3,4,6-tetrachloro-3R,6R-diphenylglycoluril
<b><math>k'</math></b>	capacity factor
<b>LET</b>	linear energy transfer
<b>mAb</b>	monoclonal antibodies
<b>MeCN</b>	acetonitrile
<b>MeOH</b>	methanol
<b>MM</b>	multiple myeloma
<b>NIS</b>	<i>N</i> -iodosuccinimide
<b>NMP</b>	<i>N</i> -methyl-2-pyrrolidone
<b>NOTA</b>	1,4,7-triazacyclononane-triacetic acid
<b>OSEM</b>	ordered subset expectation maximization
<b>Pbf</b>	2,2,4,6,7-Pentamethyldihydrobenzofuran-5-sulfonyl (protecting group)

## SUPPLEMENTARY MATERIAL

<b>PDB</b>	protein data bank
<b>PBS</b>	phosphate-buffered saline
<b>PET</b>	positron emission tomography
<b><i>p</i>-Ns</b>	4-nitrobenzenesulfonyl (protecting group)
<b>QD</b>	quantum dot
<b>rt</b>	room temperature
<b>SAR</b>	structure-activity relation
<b>ROI</b>	region of interest
<b>SDF-1</b>	stromal derived factor-1
<b>SPECT</b>	single-photon emission computed tomography
<b>SUV</b>	standardized uptake value
<b><math>t_R</math></b>	retention time
<b><math>t_{Bu}</math></b>	<i>tert</i> -butyl (protecting group)
<b>TBTU</b>	<i>O</i> -(1H-benzotriazol-1-yl)- <i>N,N,N',N'</i> -tetramethyluronium-tetrafluoro-borate
<b>TCP</b>	tritylchloride polystyrene
<b>TEA</b>	triethylamine
<b>TFA</b>	trifluoroacetic acid
<b>TFE</b>	trifluoroethanol
<b>THF</b>	tetrahydrofuran
<b>TIPS</b>	triisopropylsilane
<b>TLC</b>	thin-layer chromatography
<b>TM</b>	transmembrane
<b>VEGF</b>	vascular endothelial growth factor

### 3. References

1. Nelson, P. J., and Krensky, A. M. (2001) Chemokines, chemokine receptors, and allograft rejection, *Immunity* 14, 377-386.
2. Murphy, P. M., Baggiolini, M., Charo, I. F., Hébert, C. A., Horuk, R., Matsushima, K., Miller, L. H., Oppenheim, J. J., and Power, C. A. (2000) International union of pharmacology. XXII. Nomenclature for chemokine receptors, *Pharmacological reviews* 52, 145-176.
3. Rossi, D., and Zlotnik, A. (2000) The biology of chemokines and their receptors, *Annual review of immunology* 18, 217-242.
4. Segerer, S., Nelson, P. J., and SCHLÖNDORFF, D. (2000) Chemokines, chemokine receptors, and renal disease: from basic science to pathophysiologic and therapeutic studies, *Journal of the American Society of Nephrology* 11, 152-176.
5. Burger, J. A., and Kipps, T. J. (2006) CXCR4: a key receptor in the crosstalk between tumor cells and their microenvironment, *Blood* 107, 1761-1767.
6. Baggiolini, M. (1998) Chemokines and leukocyte traffic, *Nature* 392, 565-568.
7. McGrath, K. E., Koniski, A. D., Maltby, K. M., McGann, J. K., and Palis, J. (1999) Embryonic expression and function of the chemokine SDF-1 and its receptor, CXCR4, *Developmental biology* 213, 442-456.
8. Domanska, U. M., Kruizinga, R. C., Nagengast, W. B., Timmer-Bosscha, H., Huls, G., de Vries, E. G., and Walenkamp, A. M. (2013) A review on CXCR4/CXCL12 axis in oncology: no place to hide, *European journal of cancer* 49, 219-230.
9. Ceradini, D. J., Kulkarni, A. R., Callaghan, M. J., Tepper, O. M., Bastidas, N., Kleinman, M. E., Capla, J. M., Galiano, R. D., Levine, J. P., and Gurtner, G. C. (2004) Progenitor cell trafficking is regulated by hypoxic gradients through HIF-1 induction of SDF-1, *Nature medicine* 10, 858-864.
10. Balabanian, K., Lagane, B., Infantino, S., Chow, K. Y., Harriague, J., Moepps, B., Arenzana-Seisdedos, F., Thelen, M., and Bachelier, F. (2005) The chemokine SDF-1/CXCL12 binds to and signals through the orphan receptor RDC1 in T lymphocytes, *Journal of Biological Chemistry* 280, 35760-35766.
11. Moser, B., and Loetscher, P. (2001) Lymphocyte traffic control by chemokines, *Nature immunology* 2, 123-128.
12. Butcher, E. C., and Picker, L. J. (1996) Lymphocyte homing and homeostasis, *Science* 272, 60-67.
13. Springer, T. A. (1994) Traffic signals for lymphocyte recirculation and leukocyte emigration: the multistep paradigm, *Cell* 76, 301-314.
14. Campbell, J. J., Hedrick, J., Zlotnik, A., Siani, M. A., Thompson, D. A., and Butcher, E. C. (1998) Chemokines and the arrest of lymphocytes rolling under flow conditions, *Science* 279, 381-384.
15. Müller, A., Homey, B., Soto, H., Ge, N., Catron, D., Buchanan, M. E., McClanahan, T., Murphy, E., Yuan, W., and Wagner, S. N. (2001) Involvement of chemokine receptors in breast cancer metastasis, *nature* 410, 50-56.
16. Nagasawa, T., Kikutani, H., and Kishimoto, T. (1994) Molecular cloning and structure of a pre-B-cell growth-stimulating factor, *Proceedings of the National Academy of Sciences* 91, 2305-2309.
17. Feng, Y., Broder, C. C., Kennedy, P. E., and Berger, E. A. (1996) HIV-1 entry cofactor: functional cDNA cloning of a seven-transmembrane, G protein-coupled receptor, *Science* 272, 872-877.
18. Loetscher, M., Geiser, T., O'Reilly, T., Zwahlen, R., Baggiolini, M., and Moser, B. (1994) Cloning of a human seven-transmembrane domain receptor, LESTR, that is highly expressed in leukocytes, *Journal of Biological Chemistry* 269, 232-237.
19. Hattermann, K., and Mentlein, R. (2013) An infernal trio: the chemokine CXCL12 and its receptors CXCR4 and CXCR7 in tumor biology, *Annals of Anatomy-Anatomischer Anzeiger* 195, 103-110.

## SUPPLEMENTARY MATERIAL

20. Zlotnik, A., and Yoshie, O. (2000) Chemokines: a new classification system and their role in immunity, *Immunity* 12, 121-127.
21. Nagasawa, T., Hirota, S., Tachibana, K., Takakura, N., Nishikawa, S.-i., Kitamura, Y., Yoshida, N., Kikutani, H., and Kishimoto, T. (1996) Defects of B-cell lymphopoiesis and bone-marrow myelopoiesis in mice lacking the CXC chemokine PBSF/SDF-1, *Nature* 382, 635-638.
22. Loetscher, P., Moser, B., and Baggiolini, M. (2000) Chemokines and their receptors in lymphocyte traffic and HIV infection, *Advances in immunology* 74, 127-180.
23. Aiuti, A., Webb, I., Bleul, C., Springer, T., and Gutierrez-Ramos, J. (1997) The chemokine SDF-1 is a chemoattractant for human CD34+ hematopoietic progenitor cells and provides a new mechanism to explain the mobilization of CD34+ progenitors to peripheral blood, *The Journal of experimental medicine* 185, 111-120.
24. Ma, Q., Jones, D., Borghesani, P. R., Segal, R. A., Nagasawa, T., Kishimoto, T., Bronson, R. T., and Springer, T. A. (1998) Impaired B-lymphopoiesis, myelopoiesis, and derailed cerebellar neuron migration in CXCR4- and SDF-1-deficient mice, *Proceedings of the National Academy of Sciences* 95, 9448-9453.
25. Burns, J. M., Summers, B. C., Wang, Y., Melikian, A., Berahovich, R., Miao, Z., Penfold, M. E., Sunshine, M. J., Littman, D. R., and Kuo, C. J. (2006) A novel chemokine receptor for SDF-1 and I-TAC involved in cell survival, cell adhesion, and tumor development, *The Journal of experimental medicine* 203, 2201-2213.
26. Jones, S., Brockbank, S., Mobbs, M., Le Good, N., Soma-Haddrick, S., Heuze, A., Langham, C., Timms, D., Newham, P., and Needham, M. (2006) The orphan G-protein coupled receptor RDC1: evidence for a role in chondrocyte hypertrophy and articular cartilage matrix turnover, *Osteoarthritis and cartilage* 14, 597-608.
27. Raggo, C., Ruhl, R., McAllister, S., Koon, H., Dezube, B. J., Früh, K., and Moses, A. V. (2005) Novel Cellular Genes Essential for Transformation of Endothelial Cells by Kaposi's Sarcoma-Associated Herpesvirus, *Cancer research* 65, 5084-5095.
28. Sun, X., Cheng, G., Hao, M., Zheng, J., Zhou, X., Zhang, J., Taichman, R. S., Pienta, K. J., and Wang, J. (2010) CXCL12/CXCR4/CXCR7 chemokine axis and cancer progression, *Cancer and Metastasis Reviews* 29, 709-722.
29. Burger, J. A., Burger, M., and Kipps, T. J. (1999) Chronic lymphocytic leukemia B cells express functional CXCR4 chemokine receptors that mediate spontaneous migration beneath bone marrow stromal cells, *Blood* 94, 3658-3667.
30. Jin, D. K., Shido, K., Kopp, H.-G., Petit, I., Shmelkov, S. V., Young, L. M., Hooper, A. T., Amano, H., Avecilla, S. T., and Heissig, B. (2006) Cytokine-mediated deployment of SDF-1 induces revascularization through recruitment of CXCR4+ hemangiocytes, *Nature medicine* 12, 557-567.
31. Du, R., Lu, K. V., Petritsch, C., Liu, P., Ganss, R., Passequé, E., Song, H., VandenBerg, S., Johnson, R. S., and Werb, Z. (2008) HIF1  $\alpha$  induces the recruitment of bone marrow-derived vascular modulatory cells to regulate tumor angiogenesis and invasion, *Cancer cell* 13, 206-220.
32. Orimo, A., Gupta, P. B., Sgroi, D. C., Arenzana-Seisdedos, F., Delaunay, T., Naeem, R., Carey, V. J., Richardson, A. L., and Weinberg, R. A. (2005) Stromal fibroblasts present in invasive human breast carcinomas promote tumor growth and angiogenesis through elevated SDF-1/CXCL12 secretion, *Cell* 121, 335-348.
33. Chatterjee, S., Azad, B. B., and Nimmagadda, S. (2014) The intricate role of CXCR4 in cancer, *Advances in cancer research* 124, 31.
34. Hargreaves, D. C., Hyman, P. L., Lu, T. T., Ngo, V. N., Bidgol, A., Suzuki, G., Zou, Y.-R., Littman, D. R., and Cyster, J. G. (2001) A coordinated change in chemokine responsiveness guides plasma cell movements, *The Journal of experimental medicine* 194, 45-56.

## SUPPLEMENTARY MATERIAL

35. Trentin, L., Cabrelle, A., Facco, M., Carollo, D., Miorin, M., Tosoni, A., Pizzo, P., Binotto, G., Nicolardi, L., and Zambello, R. (2004) Homeostatic chemokines drive migration of malignant B cells in patients with non-Hodgkin lymphomas, *Blood* 104, 502-508.
36. Bradstock, K., Makrynika, V., Bianchi, A., Shen, W., Hewson, J., and Gottlieb, D. (2000) Effects of the chemokine stromal cell-derived factor-1 on the migration and localization of precursor-B acute lymphoblastic leukemia cells within bone marrow stromal layers, *Leukemia* (08876924) 14.
37. Tavor, S., Petit, I., Porozov, S., Avigdor, A., Dar, A., Leider-Trejo, L., Shemtov, N., Deutsch, V., Naparstek, E., and Nagler, A. (2004) CXCR4 regulates migration and development of human acute myelogenous leukemia stem cells in transplanted NOD/SCID mice, *Cancer research* 64, 2817-2824.
38. Zhou, Y., Larsen, P. H., Hao, C., and Yong, V. W. (2002) CXCR4 is a major chemokine receptor on glioma cells and mediates their survival, *Journal of Biological Chemistry* 277, 49481-49487.
39. Tang, W., Wang, X., Chen, Y., Zhang, J., and Lin, Z. (2015) CXCL12 and CXCR4 as predictive biomarkers of glioma recurrence pattern after total resection, *Pathologie Biologie* 63, 190-198.
40. Geminder, H., Sagi-Assif, O., Goldberg, L., Meshel, T., Rechavi, G., Witz, I. P., and Ben-Baruch, A. (2001) A possible role for CXCR4 and its ligand, the CXCL12 chemokine stromal cell-derived factor-1, in the development of bone marrow metastases in neuroblastoma, *The Journal of Immunology* 167, 4747-4757.
41. Hattermann, K., Sebens, S., Helm, O., Schmitt, A. D., Mentlein, R., Mehdorn, H. M., and Held-Feindt, J. (2014) Chemokine expression profile of freshly isolated human glioblastoma-associated macrophages/microglia, *Oncology reports* 32, 270-276.
42. Ozawa, P. M. M., Ariza, C. B., Ishibashi, C. M., Fujita, T. C., Banin-Hirata, B. K., Oda, J. M. M., and Watanabe, M. A. E. (2016) Role of CXCL12 and CXCR4 in normal cerebellar development and medulloblastoma, *International Journal of Cancer* 138, 10-13.
43. Zeelenberg, I. S., Ruuls-Van Stalle, L., and Roos, E. (2003) The chemokine receptor CXCR4 is required for outgrowth of colon carcinoma micrometastases, *Cancer research* 63, 3833-3839.
44. Shakir, M., Tang, D., Zeh, H. J., Tang, S. W., Anderson, C. J., Bahary, N., and Lotze, M. T. (2015) The Chemokine Receptors CXCR4/CXCR7 and Their Primary Heterodimeric Ligands CXCL12 and CXCL12/High Mobility Group Box 1 in Pancreatic Cancer Growth and Development: Finding Flow, *Pancreas* 44, 528-534.
45. Xiang, Z.-l., Zeng, Z.-c., Tang, Z.-y., Fan, J., Zhuang, P.-y., Liang, Y., Tan, Y.-s., and He, J. (2009) Chemokine receptor CXCR4 expression in hepatocellular carcinoma patients increases the risk of bone metastases and poor survival, *BMC cancer* 9, 1.
46. Han, M., Lv, S., Zhang, Y., Yi, R., Huang, B., Fu, H., Bian, R., and Li, X. (2014) The prognosis and clinicopathology of CXCR4 in gastric cancer patients: a meta-analysis, *Tumor Biology* 35, 4589-4597.
47. Kaifi, J. T., Yekebas, E. F., Schurr, P., Obonyo, D., Wachowiak, R., Busch, P., Heinecke, A., Pantel, K., and Izbicki, J. R. (2005) Tumor-cell homing to lymph nodes and bone marrow and CXCR4 expression in esophageal cancer, *Journal of the National Cancer Institute* 97, 1840-1847.
48. Scotton, C. J., Wilson, J. L., Scott, K., Stamp, G., Wilbanks, G. D., Fricker, S., Bridger, G., and Balkwill, F. R. (2002) Multiple actions of the chemokine CXCL12 on epithelial tumor cells in human ovarian cancer, *Cancer Research* 62, 5930-5938.
49. Wang, J., Wang, J., Sun, Y., Song, W., Nor, J. E., Wang, C. Y., and Taichman, R. S. (2005) Diverse signaling pathways through the SDF-1/CXCR4 chemokine axis in prostate cancer cell lines leads to altered patterns of cytokine secretion and angiogenesis, *Cellular signalling* 17, 1578-1592.
50. Zagzag, D., Krishnamachary, B., Yee, H., Okuyama, H., Chiriboga, L., Ali, M. A., Melamed, J., and Semenza, G. L. (2005) Stromal cell-derived factor-1  $\alpha$  and CXCR4 expression in hemangioblastoma and clear cell-renal cell carcinoma: von Hippel-Lindau loss-of-function induces expression of a ligand and its receptor, *Cancer research* 65, 6178-6188.



## SUPPLEMENTARY MATERIAL

51. He, X., Wei, Q., Zhang, X., Xiao, J., Jin, X., Zhu, Y., Cui, B., and Ning, G. (2010) Immunohistochemical expression of CXCR4 in thyroid carcinomas and thyroid benign lesions, *Pathology-Research and Practice* 206, 712-715.
52. Bai, S., Wang, D., Klein, M. J., and Siegal, G. P. (2011) Characterization of CXCR4 expression in chondrosarcoma of bone, *Archives of pathology & laboratory medicine* 135, 753-758.
53. Burger, M., Glodek, A., Hartmann, T., Schmitt-Gräff, A., Silberstein, L. E., Fujii, N., Kipps, T. J., and Burger, J. A. (2003) Functional expression of CXCR4 (CD184) on small-cell lung cancer cells mediates migration, integrin activation, and adhesion to stromal cells, *Oncogene* 22, 8093-8101.
54. Wang, N., Wu, Q.-L., Fang, Y., Mai, H.-Q., Zeng, M.-S., Shen, G.-P., Hou, J.-H., and Zeng, Y.-X. (2005) Expression of chemokine receptor CXCR4 in nasopharyngeal carcinoma: pattern of expression and correlation with clinical outcome, *Journal of translational medicine* 3, 26.
55. Scala, S., Ottaiano, A., Ascierto, P. A., Cavalli, M., Simeone, E., Giuliano, P., Napolitano, M., Franco, R., Botti, G., and Castello, G. (2005) Expression of CXCR4 predicts poor prognosis in patients with malignant melanoma, *Clinical Cancer Research* 11, 1835-1841.
56. Ho, T. K., Shiwen, X., Abraham, D., Tsui, J., and Baker, D. (2012) Stromal-cell-derived factor-1 (SDF-1)/CXCL12 as potential target of therapeutic angiogenesis in critical leg ischaemia, *Cardiology research and practice* 2012.
57. Janowski, M. (2009) Functional diversity of SDF-1 splicing variants, *Cell adhesion & migration* 3, 243-249.
58. Nervi, B., Ramirez, P., Rettig, M. P., Uy, G. L., Holt, M. S., Ritchey, J. K., Prior, J. L., Piwnica-Worms, D., Bridger, G., and Ley, T. J. (2009) Chemosensitization of acute myeloid leukemia (AML) following mobilization by the CXCR4 antagonist AMD3100, *Blood* 113, 6206-6214.
59. Liotta, L. A. (2001) Cancer: an attractive force in metastasis, *Nature* 410, 24-25.
60. Meads, M. B., Hazlehurst, L. A., and Dalton, W. S. (2008) The bone marrow microenvironment as a tumor sanctuary and contributor to drug resistance, *Clinical Cancer Research* 14, 2519-2526.
61. Hanahan, D., and Weinberg, R. A. (2011) Hallmarks of cancer: the next generation, *cell* 144, 646-674.
62. Ishikawa, T., Nakashiro, K.-I., Klosek, S. K., Goda, H., Hara, S., Uchida, D., and Hamakawa, H. (2009) Hypoxia enhances CXCR4 expression by activating HIF-1 in oral squamous cell carcinoma, *Oncology reports* 21, 707-712.
63. Salcedo, R., Wasserman, K., Young, H. A., Grimm, M. C., Howard, O. Z., Anver, M. R., Kleinman, H. K., Murphy, W. J., and Oppenheim, J. J. (1999) Vascular endothelial growth factor and basic fibroblast growth factor induce expression of CXCR4 on human endothelial cells: in vivo neovascularization induced by stromal-derived factor-1  $\alpha$ , *The American journal of pathology* 154, 1125-1135.
64. Phillips, R. J., Mestas, J., Gharaee-Kermani, M., Burdick, M. D., Sica, A., Belperio, J. A., Keane, M. P., and Strieter, R. M. (2005) Epidermal growth factor and hypoxia-induced expression of CXC chemokine receptor 4 on non-small cell lung cancer cells is regulated by the phosphatidylinositol 3-kinase/PTEN/AKT/mammalian target of rapamycin signaling pathway and activation of hypoxia inducible factor-1  $\alpha$ , *Journal of Biological Chemistry* 280, 22473-22481.
65. Staller, P., Sulitkova, J., Lisztwan, J., Moch, H., Oakeley, E. J., and Krek, W. (2003) Chemokine receptor CXCR4 downregulated by von Hippel-Lindau tumour suppressor pVHL, *Nature* 425, 307-311.
66. Burger, J., and Peled, A. (2009) CXCR4 antagonists: targeting the microenvironment in leukemia and other cancers, *Leukemia* 23, 43-52.
67. Konopleva, M. Y., and Jordan, C. T. (2011) Leukemia stem cells and microenvironment: biology and therapeutic targeting, *Journal of Clinical Oncology* 29, 591-599.
68. Frassanito, M. A., Cusmai, A., Iodice, G., and Dammacco, F. (2001) Autocrine interleukin-6 production and highly malignant multiple myeloma: relation with resistance to drug-induced apoptosis, *Blood* 97, 483-489.

## SUPPLEMENTARY MATERIAL

69. Gilbert, L. A., and Hemann, M. T. (2010) DNA damage-mediated induction of a chemoresistant niche, *Cell* 143, 355-366.
70. Mesguich, C., Zanotti-Fregonara, P., and Hindié, E. (2015) New Perspectives Offered by Nuclear Medicine for the Imaging and Therapy of Multiple Myeloma.
71. Zhao, H., Guo, L., Zhao, J., Weng, H., and Zhao, B. (2015) CXCR4 over-expression and survival in cancer: A system review and meta-analysis, *Oncotarget* 6, 5022-5040.
72. Woodard, L. E., and Nimmagadda, S. (2011) CXCR4-based imaging agents, *Journal of Nuclear Medicine* 52, 1665-1669.
73. Hattermann, K., Held-Feindt, J., Lucius, R., Mürköster, S. S., Penfold, M. E., Schall, T. J., and Mentlein, R. (2010) The chemokine receptor CXCR7 is highly expressed in human glioma cells and mediates antiapoptotic effects, *Cancer research* 70, 3299-3308.
74. Pawig, L., Klasen, C., Weber, C., Bernhagen, J., and Noels, H. (2015) Diversity and inter-connections in the CXCR4 chemokine receptor/ligand family: molecular perspectives, *Frontiers in immunology* 6.
75. Valentin, G., Haas, P., and Gilmour, D. (2007) The chemokine SDF1a coordinates tissue migration through the spatially restricted activation of Cxcr7 and Cxcr4b, *Current Biology* 17, 1026-1031.
76. Mazzinghi, B., Ronconi, E., Lazzeri, E., Sagrinati, C., Ballerini, L., Angelotti, M. L., Parente, E., Mancina, R., Netti, G. S., and Becherucci, F. (2008) Essential but differential role for CXCR4 and CXCR7 in the therapeutic homing of human renal progenitor cells, *The Journal of experimental medicine* 205, 479-490.
77. Zlotnik, A., Burkhardt, A. M., and Homey, B. (2011) Homeostatic chemokine receptors and organ-specific metastasis, *Nature Reviews Immunology* 11, 597-606.
78. Shim, H., Oishi, S., and Fujii, N. (2009) Chemokine receptor CXCR4 as a therapeutic target for neuroectodermal tumors, In *Seminars in cancer biology*, pp 123-134, Elsevier.
79. De Clercq, E. (2009) The AMD3100 story: the path to the discovery of a stem cell mobilizer (Mozobil), *Biochemical pharmacology* 77, 1655-1664.
80. Kashyap, M. K., Kumar, D., Jones, H., Amaya-Chanaga, C. I., Choi, M. Y., Melo-Cardenas, J., Ale-Ali, A., Kuhne, M. R., Sabbatini, P., and Cohen, L. J. (2015) Ulocuplumab (BMS-936564/MDX1338): a fully human anti-CXCR4 antibody induces cell death in chronic lymphocytic leukemia mediated through a reactive oxygen species-dependent pathway, *Oncotarget*.
81. Kuhne, M. R., Mulvey, T., Belanger, B., Chen, S., Pan, C., Chong, C., Cao, F., Niekro, W., Kempe, T., and Henning, K. A. (2013) BMS-936564/MDX-1338: a fully human anti-CXCR4 antibody induces apoptosis in vitro and shows antitumor activity in vivo in hematologic malignancies, *Clinical Cancer Research* 19, 357-366.
82. Misra, P., Lebeche, D., Ly, H., Schwarzkopf, M., Diaz, G., Hajjar, R. J., Schecter, A. D., and Frangioni, J. V. (2008) Quantitation of CXCR4 expression in myocardial infarction using 99mTc-labeled SDF-1  $\alpha$ , *Journal of Nuclear Medicine* 49, 963-969.
83. Wu, B., Chien, E. Y., Mol, C. D., Fenalti, G., Liu, W., Katritch, V., Abagyan, R., Brooun, A., Wells, P., and Bi, F. C. (2010) Structures of the CXCR4 chemokine GPCR with small-molecule and cyclic peptide antagonists, *Science* 330, 1066-1071.
84. Crump, M. P., Gong, J. H., Loetscher, P., Rajarathnam, K., Amara, A., Arenzana-Seisdedos, F., Virelizier, J. L., Baggolini, M., Sykes, B. D., and Clark-Lewis, I. (1997) Solution structure and basis for functional activity of stromal cell-derived factor-1; dissociation of CXCR4 activation from binding and inhibition of HIV-1, *The EMBO journal* 16, 6996-7007.
85. Oishi, S., and Fujii, N. (2012) Peptide and peptidomimetic ligands for CXC chemokine receptor 4 (CXCR4), *Organic & biomolecular chemistry* 10, 5720-5731.
86. Tamamura, H., Kuroda, M., Masuda, M., Otaka, A., Funakoshi, S., Nakashima, H., Yamamoto, N., Waki, M., Matsumoto, A., and Lancelin, J. M. (1993) A comparative study of the solution structures of tachyplesin I and a novel anti-HIV synthetic peptide, T22 ([Tyr 5, 12, Lys 7]-

## SUPPLEMENTARY MATERIAL

- polyphemusin II), determined by nuclear magnetic resonance, *Biochimica et Biophysica Acta (BBA)-Protein Structure and Molecular Enzymology* 1163, 209-216.
87. Tamamura, H., Waki, M., Imai, M., Otaka, A., Ibuka, T., Waki, K., Miyamoto, K., Matsumoto, A., Murakami, T., and Nakashima, H. (1998) Downsizing of an HIV–cell fusion inhibitor, T22 ([Tyr 5, 12, Lys 7]-Polyphemusin II), with the maintenance of anti-HIV activity and solution structure 1, *Bioorganic & medicinal chemistry* 6, 473-479.
  88. Fujii, N., Oishi, S., Hiramatsu, K., Araki, T., Ueda, S., Tamamura, H., Otaka, A., Kusano, S., Terakubo, S., and Nakashima, H. (2003) Molecular-Size Reduction of a Potent CXCR4-Chemokine Antagonist Using Orthogonal Combination of Conformation-and Sequence-Based Libraries, *Angewandte Chemie* 115, 3373-3375.
  89. Demmer, O., Frank, A. O., Hagn, F., Schottelius, M., Marinelli, L., Cosconati, S., Brack-Werner, R., Kremb, S., Wester, H. J., and Kessler, H. (2012) A Conformationally Frozen Peptoid Boosts CXCR4 Affinity and Anti-HIV Activity, *Angewandte Chemie International Edition* 51, 8110-8113.
  90. Gourni, E., Demmer, O., Schottelius, M., D'Alessandria, C., Schulz, S., Dijkgraaf, I., Schumacher, U., Schwaiger, M., Kessler, H., and Wester, H.-J. (2011) PET of CXCR4 expression by a 68Ga-labeled highly specific targeted contrast agent, *Journal of Nuclear Medicine* 52, 1803-1810.
  91. Demmer, O., Gourni, E., Schumacher, U., Kessler, H., and Wester, H. J. (2011) PET imaging of CXCR4 receptors in cancer by a new optimized ligand, *ChemMedChem* 6, 1789-1791.
  92. <http://www.foodreference.com/html/f-horseshoe-crab-trivia.html>. horseshoe crab.
  93. Tamamura, H., Hiramatsu, K., Mizumoto, M., Ueda, S., Kusano, S., Terakubo, S., Akamatsu, M., Yamamoto, N., Trent, J. O., and Wang, Z. (2003) Enhancement of the T140-based pharmacophores leads to the development of more potent and bio-stable CXCR4 antagonists, *Organic & biomolecular chemistry* 1, 3663-3669.
  94. George, G. P., Stevens, E., Åberg, O., Nguyen, Q.-D., Pisaneschi, F., Spivey, A. C., and Aboagye, E. O. (2014) Preclinical evaluation of a CXCR4-specific 68 Ga-labelled TN14003 derivative for cancer PET imaging, *Bioorganic & medicinal chemistry* 22, 796-803.
  95. Yan, X., Niu, G., Wang, Z., Yang, X., Kiesewetter, D. O., Jacobson, O., Shen, B., and Chen, X. (2015) Al [18F] NOTA-T140 Peptide for Noninvasive Visualization of CXCR4 Expression, *Molecular Imaging and Biology*, 1-8.
  96. Jacobson, O., Weiss, I. D., Kiesewetter, D. O., Farber, J. M., and Chen, X. (2010) PET of tumor CXCR4 expression with 4-18F-T140, *Journal of Nuclear Medicine* 51, 1796-1804.
  97. Tamamura, H., Esaka, A., Ogawa, T., Araki, T., Ueda, S., Wang, Z., Trent, J. O., Tsutsumi, H., Masuno, H., and Nakashima, H. (2005) Structure–activity relationship studies on CXCR4 antagonists having cyclic pentapeptide scaffolds, *Org. Biomol. Chem.* 3, 4392-4394.
  98. Tamamura, H., Araki, T., Ueda, S., Wang, Z., Oishi, S., Esaka, A., Trent, J. O., Nakashima, H., Yamamoto, N., and Peiper, S. C. (2005) Identification of novel low molecular weight CXCR4 antagonists by structural tuning of cyclic tetrapeptide scaffolds, *Journal of medicinal chemistry* 48, 3280-3289.
  99. Tanaka, T., Nomura, W., Narumi, T., Esaka, A., Oishi, S., Ohashi, N., Itotani, K., Evans, B. J., Wang, Z.-x., and Peiper, S. C. (2009) Structure-activity relationship study on artificial CXCR4 ligands possessing the cyclic pentapeptide scaffold: the exploration of amino acid residues of pentapeptides by substitutions of several aromatic amino acids, *Organic & biomolecular chemistry* 7, 3805-3809.
  100. Ueda, S., Oishi, S., Wang, Z.-x., Araki, T., Tamamura, H., Cluzeau, J., Ohno, H., Kusano, S., Nakashima, H., and Trent, J. O. (2007) Structure-activity relationships of cyclic peptide-based chemokine receptor CXCR4 antagonists: disclosing the importance of side-chain and backbone functionalities, *Journal of medicinal chemistry* 50, 192-198.
  101. Kobayashi, K., Oishi, S., Hayashi, R., Tomita, K., Kubo, T., Tanahara, N., Ohno, H., Yoshikawa, Y., Furuya, T., and Hoshino, M. (2012) Structure–activity relationship study of a CXC chemokine

## SUPPLEMENTARY MATERIAL

- receptor type 4 antagonist, FC131, using a series of alkene dipeptide isosteres, *Journal of medicinal chemistry* 55, 2746-2757.
102. Demmer, O., Dijkgraaf, I., Schumacher, U., Marinelli, L., Cosconati, S., Gourni, E., Wester, H.-J. r., and Kessler, H. (2011) Design, synthesis, and functionalization of dimeric peptides targeting chemokine receptor CXCR4, *Journal of medicinal chemistry* 54, 7648-7662.
  103. Demmer, O., Dijkgraaf, I., Schottelius, M., Wester, H.-J., and Kessler, H. (2008) Introduction of functional groups into peptides via N-alkylation, *Organic letters* 10, 2015-2018.
  104. Thiele, S., Mungalpara, J., Steen, A., Rosenkilde, M. M., and Våbenø, J. (2014) Determination of the binding mode for the cyclopentapeptide CXCR4 antagonist FC131 using a dual approach of ligand modifications and receptor mutagenesis, *British journal of pharmacology* 171, 5313-5329.
  105. Cherry, S. R., Sorenson, J. A., and Phelps, M. E. (2012) *Physics in nuclear medicine*, Elsevier Health Sciences.
  106. Magill, J., Pfennig, G., Dreher, R., and Söti, Z. (2012) *Karlsruher Nuclidkarte*, Nucleonica.
  107. Turkington, T. G. (2001) Introduction to PET instrumentation, *Journal of nuclear medicine technology* 29, 4-11.
  108. Turkington, T. G. (2011) PET Imaging Basics, In *Clinical PET-CT in Radiology*, pp 21-28, Springer.
  109. Thie, J. A. (2004) Understanding the standardized uptake value, its methods, and implications for usage, *Journal of Nuclear Medicine* 45, 1431-1434.
  110. Soret, M., Bacharach, S. L., and Buvat, I. (2007) Partial-volume effect in PET tumor imaging, *Journal of Nuclear Medicine* 48, 932-945.
  111. Watabe, H., Ikoma, Y., Kimura, Y., Naganawa, M., and Shidahara, M. (2006) PET kinetic analysis—compartmental model, *Annals of nuclear medicine* 20, 583-588.
  112. Nimmagadda, S., Pullambhatla, M., Stone, K., Green, G., Bhujwalla, Z. M., and Pomper, M. G. (2010) Molecular imaging of CXCR4 receptor expression in human cancer xenografts with [64Cu] AMD3100 positron emission tomography, *Cancer research* 70, 3935-3944.
  113. Jacobson, O., Weiss, I. D., Szajek, L., Farber, J. M., and Kiesewetter, D. O. (2009) 64 Cu-AMD3100—A novel imaging agent for targeting chemokine receptor CXCR4, *Bioorganic & medicinal chemistry* 17, 1486-1493.
  114. Hartimath, S., van Waarde, A., Dierckx, R. A., and de Vries, E. F. (2014) Evaluation of N-[11C] methyl-AMD3465 as a PET tracer for imaging of CXCR4 receptor expression in a C6 glioma tumor model.
  115. De Silva, R. A., Peyre, K., Pullambhatla, M., Fox, J. J., Pomper, M. G., and Nimmagadda, S. (2011) Imaging CXCR4 expression in human cancer xenografts: evaluation of monocyclam 64Cu-AMD3465, *Journal of Nuclear Medicine* 52, 986-993.
  116. Liang, Z., Zhan, W., Zhu, A., Yoon, Y., Lin, S., Sasaki, M., Klapproth, J.-M. A., Yang, H., Grossniklaus, H. E., and Xu, J. (2012) Development of a unique small molecule modulator of CXCR4, *PLoS One* 7, e34038.
  117. Shim, H., Liotta, D. C., Goodman, M. M., and Zhu, A. (2011) CXCR4 antagonists for imaging of cancer and inflammatory disorders, Google Patents.
  118. Misra, P., Humblet, V., Pannier, N., Maison, W., and Frangioni, J. V. (2007) Production of multimeric prostate-specific membrane antigen small-molecule radiotracers using a solid-phase 99mTc preloading strategy, *Journal of Nuclear Medicine* 48, 1379-1389.
  119. Banisadr, G., Dicou, E., Berbar, T., Rostène, W., Lombet, A., and Haour, F. (2000) Characterization and visualization of [125 I] stromal cell-derived factor-1  $\alpha$  binding to CXCR4 receptors in rat brain and human neuroblastoma cells, *Journal of neuroimmunology* 110, 151-160.
  120. Nimmagadda, S., Pullambhatla, M., and Pomper, M. G. (2009) Immunoimaging of CXCR4 expression in brain tumor xenografts using SPECT/CT, *Journal of Nuclear Medicine* 50, 1124-1130.
  121. Azad, B. B., Chatterjee, S., Lesniak, W. G., Lisok, A., Pullambhatla, M., Bhujwalla, Z. M., Pomper, M. G., and Nimmagadda, S. (2016) A fully human CXCR4 antibody demonstrates diagnostic utility and therapeutic efficacy in solid tumor xenografts, *Oncotarget*.

## SUPPLEMENTARY MATERIAL

122. Jacobson, O., Weiss, I. D., Szajek, L. P., Niu, G., Ma, Y., Kiesewetter, D. O., Peled, A., Eden, H. S., Farber, J. M., and Chen, X. (2012) Improvement of CXCR4 tracer specificity for PET imaging, *Journal of controlled release* 157, 216-223.
123. Wang, Z., Zhang, M., Wang, L., Wang, S., Kang, F., Li, G., Jacobson, O., Niu, G., Yang, W., and Wang, J. (2015) Prospective Study of (68) Ga-NOTA-NFB: Radiation dosimetry in healthy volunteers and first application in glioma patients, *Theranostics* 5, 882-889.
124. Wester, H. J., Koglin, N., Schwaiger, M., Kessler, H., Laufer, B., Demmer, O., and Anton, M. (2007) Cancer imaging and treatment, Google Patents.
125. Rischpler, C., Nekolla, S., Kossmann, H., Dirschinger, R., Schottelius, M., Hyafil, F., Wester, H., Laugwitz, K., and Schwaiger, M. (2016) Upregulated myocardial CXCR4-expression after myocardial infarction assessed by simultaneous GA-68 pentixafor PET/MRI, *Journal of Nuclear Cardiology* 23, 131-133.
126. Vag, T., Gerngross, C., Herhaus, P., Eiber, M., Philipp-Abbrederis, K., Graner, F.-P., Ettl, J., Keller, U., Wester, H.-J., and Schwaiger, M. (2016) First Experience on Chemokine Receptor CXCR4 Targeted Positron Emission Tomography (PET) Imaging in Patients with Solid Cancers, *Journal of Nuclear Medicine*, jnumed. 115.161034.
127. Wester, H. J., Keller, U., Schottelius, M., Beer, A., Philipp-Abbrederis, K., Hoffmann, F., Šimeček, J., Gerngross, C., Lassmann, M., and Herrmann, K. (2015) Disclosing the CXCR4 expression in lymphoproliferative diseases by targeted molecular imaging, *Theranostics* 5, 618.
128. Herrmann, K., Lapa, C., Wester, H.-J., Schottelius, M., Schiepers, C., Eberlein, U., Bluemel, C., Keller, U., Knop, S., and Kropf, S. (2015) Biodistribution and Radiation Dosimetry for the Chemokine Receptor CXCR4-Targeting Probe 68Ga-Pentixafor, *Journal of Nuclear Medicine* 56, 410-416.
129. Lapa, C., Reiter, T., Werner, R. A., Ertl, G., Wester, H.-J., Buck, A. K., Bauer, W. R., and Herrmann, K. (2015) [Ga] Pentixafor-PET/CT for Imaging of Chemokine Receptor 4 Expression After Myocardial Infarction, *JACC: Cardiovascular Imaging* 8, 1466-1468.
130. Wester, H., Beer, A., Keller, U., Schottelius, M., Hoffmann, F., Abbrederis, K., Kessler, H., and Schwaiger, M. (2014) Imaging of CXCR4 chemokine receptor expression with [68Ga] pentixafor: first experience in cancer patients, *Journal of Nuclear Medicine* 55, 118-118.
131. Philipp-Abbrederis, K., Herrmann, K., Knop, S., Schottelius, M., Eiber, M., Lückerrath, K., Pietschmann, E., Habringer, S., Gerngroß, C., and Franke, K. (2015) In vivo molecular imaging of chemokine receptor CXCR4 expression in patients with advanced multiple myeloma, *EMBO molecular medicine*, e201404698.
132. Lapa, C., Lückerrath, K., Rudelius, M., Schmid, J.-S., Schoene, A., Schirbel, A., Samnick, S., Pelzer, T., Buck, A. K., and Kropf, S. (2016) [68Ga] Pentixafor-PET/CT for imaging of chemokine receptor 4 expression in small cell lung cancer-initial experience, *Oncotarget*.
133. Lapa, C., Lückerrath, K., Kleinlein, I., Monoranu, C. M., Linsenmann, T., Kessler, A. F., Rudelius, M., Kropf, S., Buck, A. K., and Ernestus, R.-I. (2016) 68Ga-Pentixafor-PET/CT for Imaging of Chemokine Receptor 4 Expression in Glioblastoma, *Theranostics* 6, 428.
134. Kwong, J., Kulbe, H., Wong, D., Chakravarty, P., and Balkwill, F. (2009) An antagonist of the chemokine receptor CXCR4 induces mitotic catastrophe in ovarian cancer cells, *Molecular cancer therapeutics* 8, 1893-1905.
135. Peled, A., Abraham, M., Avivi, I., Rowe, J. M., Beider, K., Wald, H., Tiomkin, L., Ribakovsky, L., Riback, Y., and Ramati, Y. (2014) The high-affinity CXCR4 antagonist BKT140 is safe and induces a robust mobilization of human CD34+ cells in patients with multiple myeloma, *Clinical Cancer Research* 20, 469-479.
136. Peng, S.-B., Zhang, X., Paul, D., Kays, L. M., Ye, M., Vaillancourt, P., Dowless, M., Stancato, L. F., Stewart, J., and Uhlik, M. T. (2016) Inhibition of CXCR4 by LY2624587, a Fully Humanized Anti-CXCR4 Antibody Induces Apoptosis of Hematologic Malignancies, *PloS one* 11, e0150585.

## SUPPLEMENTARY MATERIAL

137. Peled, A., and Tavor, S. (2013) Role of CXCR4 in the pathogenesis of acute myeloid leukemia, *Theranostics* 3, 34-39.
138. Zoller, F., Eisenhut, M., Haberkorn, U., and Mier, W. (2009) Endoradiotherapy in cancer treatment—basic concepts and future trends, *European journal of pharmacology* 625, 55-62.
139. Wangler, C., Buchmann, I., Eisenhut, M., Haberkorn, U., and Mier, W. (2007) Radiolabeled peptides and proteins in cancer therapy, *Protein and peptide letters* 14, 273-279.
140. Hindie, E., Zanotti-Fregonara, P., Quinto, M., Morgat, C., and Champion, C. (2016) Dose Deposits from <sup>90</sup>Y, <sup>177</sup>Lu, <sup>111</sup>In, and <sup>161</sup>Tb in Micrometastases of Various Sizes: Implications for Radiopharmaceutical Therapy, *Journal of Nuclear Medicine*, jnumed. 115.170423.
141. Kocher, D. C. (1981) A Handbook of Decay Data for Application to Radiation Dosimetry and Radiological.
142. Kassis, A. I. (2008) Therapeutic radionuclides: biophysical and radiobiologic principles, In *Seminars in nuclear medicine*, pp 358-366, Elsevier.
143. Snyder, A. R. (2004) Review of radiation-induced bystander effects, *Human & experimental toxicology* 23, 87-89.
144. Ward, J. F. (1986) Mechanisms of DNA repair and their potential modification for radiotherapy, *International Journal of Radiation Oncology\* Biology\* Physics* 12, 1027-1032.
145. Kassis, A. I., and Adelstein, S. J. (2005) Radiobiologic principles in radionuclide therapy, *Journal of Nuclear Medicine* 46, 4S-12S.
146. Wessels, B. W., and Rogus, R. D. (1984) Radionuclide selection and model absorbed dose calculations for radiolabeled tumor associated antibodies, *Medical physics* 11, 638-645.
147. Zanzonico, P. B. (2000) Internal Radionuclide Radiation Dosimetry: A Review of Basic Concepts and Recent, *J Nucl Med* 41, 297-308.
148. Sautter-Bihl, M.-L., Herbold, G., and Bihl, H. (1996) Minimal residual disease: a target for radioimmunotherapy with <sup>131</sup>I-labeled monoclonal antibodies? Some dosimetric considerations, In *Systemic Radiotherapy with Monoclonal Antibodies*, pp 67-75, Springer.
149. Graham, K., Wang, Q., Boy, R. G., Eisenhut, M., Haberkorn, U., and Mier, W. (2007) Synthesis and evaluation of intercalating somatostatin receptor binding peptide conjugates for endoradiotherapy, *J Pharm Pharmaceut Sci* 10, 286-297.
150. van Essen, M., Krenning, E. P., Kam, B. L., de Jong, M., Valkema, R., and Kwekkeboom, D. J. (2009) Peptide-receptor radionuclide therapy for endocrine tumors, *Nature Reviews Endocrinology* 5, 382-393.
151. Witzig, T. E., Gordon, L. I., Cabanillas, F., Czuczman, M. S., Emmanouilides, C., Joyce, R., Pohlman, B. L., Bartlett, N. L., Wiseman, G. A., and Padre, N. (2002) Randomized controlled trial of yttrium-90-labeled ibritumomab tiuxetan radioimmunotherapy versus rituximab immunotherapy for patients with relapsed or refractory low-grade, follicular, or transformed B-cell non-Hodgkin's lymphoma, *Journal of clinical oncology* 20, 2453-2463.
152. Morschhauser, F., Radford, J., Van Hoof, A., Vitolo, U., Soubeyran, P., Tilly, H., Huijgens, P. C., Kolstad, A., d'Amore, F., and Diaz, M. G. (2008) Phase III trial of consolidation therapy with yttrium-90-ibritumomab tiuxetan compared with no additional therapy after first remission in advanced follicular lymphoma, *Journal of Clinical Oncology* 26, 5156-5164.
153. Herrmann, K., Schottelius, M., Lapa, C., Osl, T., Poschenrieder, A., Haenscheid, H., Lueckerath, K., Schreder, M., Bluemel, C., and Knott, M. (2015) First-in-man experience of CXCR4-directed endoradiotherapy with <sup>177</sup>Lu-and <sup>90</sup>Y-labelled pentixather in advanced stage multiple myeloma with extensive intra-and extramedullary disease, *Journal of Nuclear Medicine*, jnumed. 115.167361.
154. Herrmann, K., Schottelius, M., Lapa, C., Osl, T., Poschenrieder, A., Hanscheid, H., Lueckerath, K., Schreder, M., Bluemel, C., Knott, M., Keller, U., Schirbel, A., Samnick, S., Lassmann, M., Kropf, S., Buck, A. K., Einsele, H., Wester, H. J., and Knop, S. (2016) First-in-Human Experience of CXCR4-

## SUPPLEMENTARY MATERIAL

- Directed Endoradiotherapy with <sup>177</sup>Lu- and <sup>90</sup>Y-Labeled Pentixather in Advanced-Stage Multiple Myeloma with Extensive Intra- and Extramedullary Disease, *J Nucl Med* 57, 248-251.
155. Uy, G. L., Rettig, M. P., Motabi, I. H., McFarland, K., Trinkaus, K. M., Hladnik, L. M., Kulkarni, S., Abboud, C. N., Cashen, A. F., and Stockerl-Goldstein, K. E. (2012) A phase 1/2 study of chemosensitization with the CXCR4 antagonist plerixafor in relapsed or refractory acute myeloid leukemia, *Blood* 119, 3917-3924.
  156. Poschenrieder, A., Schottelius, M., Schwaiger, M., Kessler, H., and Wester, H.-J. (2016) The influence of different metal-chelate conjugates of pentixafor on the CXCR4 affinity, *EJNMMI research* 6, 1-8.
  157. Perrin, D. M. (2016) [18F]-Organotrifluoroborates as Radioprosthetic Groups for PET Imaging: From Design Principles to Preclinical Applications, *Accounts of chemical research*.
  158. Oishi, S., Kuroyanagi, T., Kubo, T., Montpas, N., Yoshikawa, Y., Misu, R., Kobayashi, Y., Ohno, H., Heveker, N., and Furuya, T. (2015) Development of Novel CXC Chemokine Receptor 7 (CXCR7) Ligands: Selectivity Switch from CXCR4 Antagonists with a Cyclic Pentapeptide Scaffold, *Journal of medicinal chemistry* 58, 5218-5225.
  159. Montalbetti, C. A., and Falque, V. (2005) Amide bond formation and peptide coupling, *Tetrahedron* 61, 10827-10852.
  160. Schottelius, M., Konrad, M., Osl, T., Poschenrieder, A., and Wester, H.-J. (2015) An optimized strategy for the mild and efficient solution phase iodination of tyrosine residues in bioactive peptides, *Tetrahedron Letters* 56, 6602-6605.
  161. Weineisen, M., Simecek, J., Schottelius, M., Schwaiger, M., and Wester, H.-J. (2014) Synthesis and preclinical evaluation of DOTAGA-conjugated PSMA ligands for functional imaging and endoradiotherapy of prostate cancer, *EJNMMI Research* 1, 1-15.
  162. Schottelius, M., Schwaiger, M., and Wester, H.-J. (2003) Rapid and high-yield solution-phase synthesis of DOTA-Tyr 3-octreotide and DOTA-Tyr 3-octreotate using unprotected DOTA, *Tetrahedron letters* 44, 2393-2396.
  163. Liu, S., and Edwards, D. S. (2001) Bifunctional chelators for therapeutic lanthanide radiopharmaceuticals, *Bioconjugate chemistry* 12, 7-34.
  164. Hansen, M. B., van Gorp, T. H., van Hest, J. C., and Löwik, D. W. (2012) Simple and efficient solid-phase preparation of azido-peptides, *Organic letters* 14, 2330-2333.
  165. Pourghiasian, M., Liu, Z., Pan, J., Zhang, Z., Colpo, N., Lin, K.-S., Perrin, D. M., and Bénard, F. (2015) 18 F-AmBF 3-MJ9: A novel radiofluorinated bombesin derivative for prostate cancer imaging, *Bioorganic & medicinal chemistry* 23, 1500-1506.
  166. Liu, Z., Pourghiasian, M., Radtke, M. A., Lau, J., Pan, J., Dias, G. M., Yapp, D., Lin, K. S., Bénard, F., and Perrin, D. M. (2014) An Organotrifluoroborate for Broadly Applicable One-Step 18F-Labeling, *Angewandte Chemie International Edition* 53, 11876-11880.
  167. Saha, G. B., Whitten, J., and Go, R. T. (1989) Conditions of radioiodination with iodogen as oxidizing agent, *International Journal of Radiation Applications and Instrumentation. Part B. Nuclear Medicine and Biology* 16, 431-433.
  168. Schottelius, M., Reubi, J. C., Eltschinger, V., Schwaiger, M., and Wester, H.-J. (2005) N-terminal sugar conjugation and C-terminal Thr-for-Thr (ol) exchange in radioiodinated Tyr3-octreotide: effect on cellular ligand trafficking in vitro and tumor accumulation in vivo, *Journal of medicinal chemistry* 48, 2778-2789.
  169. Schottelius, M., Wester, H.-J., Reubi, J. C., Senekowitsch-Schmidtke, R., and Schwaiger, M. (2002) Improvement of pharmacokinetics of radioiodinated Tyr3-octreotide by conjugation with carbohydrates, *Bioconjugate chemistry* 13, 1021-1030.
  170. Notni, J., Pohle, K., and Wester, H.-J. (2012) Comparative gallium-68 labeling of TRAP-, NOTA-, and DOTA-peptides: practical consequences for the future of gallium-68-PET, *EJNMMI research* 2, 1-5.

## SUPPLEMENTARY MATERIAL

171. Notni, J., Šimeček, J., Hermann, P., and Wester, H. J. (2011) TRAP, a Powerful and Versatile Framework for Gallium-68 Radiopharmaceuticals, *Chemistry—A European Journal* 17, 14718-14722.
172. Donnou, S., Galand, C., Touitou, V., Sautès-Fridman, C., Fabry, Z., and Fisson, S. (2012) Murine models of B-cell lymphomas: promising tools for designing cancer therapies, *Advances in hematology* 2012.
173. Tamamura, H., Hiramatsu, K., Ueda, S., Wang, Z., Kusano, S., Terakubo, S., Trent, J. O., Peiper, S. C., Yamamoto, N., and Nakashima, H. (2005) Stereoselective synthesis of [L-Arg-L/D-3-(2-naphthyl) alanine]-type (E)-alkene dipeptide isosteres and its application to the synthesis and biological evaluation of pseudopeptide analogues of the CXCR4 antagonist FC131, *Journal of medicinal chemistry* 48, 380-391.
174. Masuda, M., Nakashima, H., Ueda, T., Naba, H., Ikoma, R., Otaka, A., Terakawa, Y., Tamamura, H., Ibuka, T., and Murakami, T. (1992) A novel anti-HIV synthetic peptide, T-22 ([Tyr5, 12, Lys7]-polyphemusin II), *Biochemical and biophysical research communications* 189, 845-850.
175. Fields, G. B., and NOBLE, R. L. (1990) Solid phase peptide synthesis utilizing 9-fluorenylmethoxycarbonyl amino acids, *International journal of peptide and protein research* 35, 161-214.
176. Tanaka, T., Nomura, W., Narumi, T., Masuda, A., and Tamamura, H. (2010) Bivalent ligands of CXCR4 with rigid linkers for elucidation of the dimerization state in cells, *Journal of the American Chemical Society* 132, 15899-15901.
177. Narumi, T., Hayashi, R., Tomita, K., Kobayashi, K., Tanahara, N., Ohno, H., Naito, T., Kodama, E., Matsuoka, M., and Oishi, S. (2010) Synthesis and biological evaluation of selective CXCR4 antagonists containing alkene dipeptide isosteres, *Organic & biomolecular chemistry* 8, 616-621.
178. Deshmukh, M. V., Voll, G., Kühlewein, A., Mäcke, H., Schmitt, J., Kessler, H., and Gemmecker, G. (2005) NMR Studies Reveal Structural Differences between the Gallium and Yttrium Complexes of DOTA-d-Phe 1-Tyr3-octreotide, *Journal of medicinal chemistry* 48, 1506-1514.
179. Reubi, J. C., Schär, J.-C., Waser, B., Wenger, S., Heppeler, A., Schmitt, J. S., and Mäcke, H. R. (2000) Affinity profiles for human somatostatin receptor subtypes SST1–SST5 of somatostatin radiotracers selected for scintigraphic and radiotherapeutic use, *European journal of nuclear medicine* 27, 273-282.
180. Gourni, E., Canovas, C., Goncalves, V., Denat, F., Meyer, P. T., and Maecke, H. R. (2015) (R)-NODAGA-PSMA: A Versatile Precursor for Radiometal Labeling and Nuclear Imaging of PSMA-Positive Tumors, *PLoS one* 10, e0145755.
181. Willibald, M. (2014) Comparative evaluation of peptidic CXCR4-ligands, In *chair of pharmaceutical radiochemistry*, Technical University Munich, Munich.
182. Schottelius, M., Osl, T., Poschenrieder, A., Herrmann, K., Lapa, C., Hoffmann, F., Schwaiger, M., Lassmann, M., Buck, A., and Wester, H. (2015) [177] Lu-pentixather: preclinical and first patient results with a highly promising CXCR4-directed endoradiotherapeutic agent, *Journal of Nuclear Medicine* 56, 339-339.
183. Castanet, A.-S., Colobert, F., and Broutin, P.-E. (2002) Mild and regioselective iodination of electron-rich aromatics with N-iodosuccinimide and catalytic trifluoroacetic acid, *Tetrahedron Letters* 43, 5047-5048.
184. Poschenrieder, A., Osl, T., Schottelius, M., Hoffmann, F., Wirtz, M., Schwaiger, M., and Wester, H.-J. (2016) First 18F-Labeled Pentixafor-Based Imaging Agent for PET Imaging of CXCR4 Expression In Vivo.
185. Cai, W., Zhang, X., Wu, Y., and Chen, X. (2006) A thiol-reactive 18F-labeling agent, N-[2-(4-18F-fluorobenzamido) ethyl] maleimide, and synthesis of RGD peptide-based tracer for PET imaging of  $\alpha v \beta 3$  integrin expression, *Journal of Nuclear Medicine* 47, 1172-1180.



## SUPPLEMENTARY MATERIAL

186. Poethko, T., Schottelius, M., Thumshirn, G., Hersel, U., Herz, M., Henriksen, G., Kessler, H., Schwaiger, M., and Wester, H.-J. (2004) Two-step methodology for high-yield routine radiohalogenation of peptides: 18F-labeled RGD and octreotide analogs, *Journal of Nuclear Medicine* 45, 892-902.
187. Bernard-Gauthier, V., Bailey, J. J., Liu, Z., Wängler, B. r., Wängler, C., Jurkschat, K., Perrin, D. M., and Schirrmacher, R. (2015) From Unorthodox to Established: The Current Status of 18F-Trifluoroborate and 18F-SiFA-Based Radiopharmaceuticals in PET Nuclear Imaging, *Bioconjugate chemistry*.
188. Zeng, J.-L., Wang, J., and Ma, J.-A. (2015) New strategies for rapid 18F-radiolabeling of biomolecules for radionuclide-based in vivo imaging, *Bioconjugate chemistry* 26, 1000-1003.
189. Burke, B. P., Clemente, G. S., and Archibald, S. J. (2015) Boron-18F containing positron emission tomography radiotracers: advances and opportunities, *Contrast media & molecular imaging* 10, 96-110.
190. Mu, L., August Schubiger, P., and M Ametamey, S. (2010) [18F] fluorosilicon and [18F] fluoroboron-based biomolecules for PET imaging, *Current Radiopharmaceuticals* 3, 224-242.
191. Richter, S., and Wuest, F. (2014) 18F-Labeled Peptides: The Future Is Bright, *Molecules* 19, 20536-20556.
192. Ting, R., Harwig, C., auf dem Keller, U., McCormick, S., Austin, P., Overall, C. M., Adam, M. J., Ruth, T. J., and Perrin, D. M. (2008) Toward [18F]-labeled aryltrifluoroborate radiotracers: in vivo positron emission tomography imaging of stable aryltrifluoroborate clearance in mice, *Journal of the American Chemical Society* 130, 12045-12055.
193. Ting, R., Lo, J., Adam, M. J., Ruth, T. J., and Perrin, D. M. (2008) Capturing aqueous [18 F]-fluoride with an arylboronic ester for PET: Synthesis and aqueous stability of a fluorescent [18 F]-labeled aryltrifluoroborate, *Journal of Fluorine Chemistry* 129, 349-358.
194. Liu, Z., Li, Y., Lozada, J., Pan, J., Lin, K. S., Schaffer, P., and Perrin, D. M. (2012) Rapid, one-step, high yielding 18F-labeling of an aryltrifluoroborate bioconjugate by isotope exchange at very high specific activity, *Journal of Labelled Compounds and Radiopharmaceuticals* 55, 491-496.
195. Liu, Z., Li, Y., Lozada, J., Wong, M. Q., Greene, J., Lin, K.-S., Yapp, D., and Perrin, D. M. (2013) Kit-like 18 F-labeling of RGD-19 F-Arytrifluoroborate in high yield and at extraordinarily high specific activity with preliminary in vivo tumor imaging, *Nuclear medicine and biology* 40, 841-849.
196. Ting, R., Harwig, C. W., Lo, J., Li, Y., Adam, M. J., Ruth, T. J., and Perrin, D. M. (2008) Substituent effects on aryltrifluoroborate solvolysis in water: implications for Suzuki– Miyaura coupling and the design of stable 18F-labeled aryltrifluoroborates for use in PET imaging, *The Journal of organic chemistry* 73, 4662-4670.
197. Ting, R., Adam, M. J., Ruth, T. J., and Perrin, D. M. (2005) Arylfluoroborates and alkylfluorosilicates as potential PET imaging agents: high-yielding aqueous biomolecular 18F-labeling, *Journal of the American Chemical Society* 127, 13094-13095.
198. Liu, Z., Pourghasian, M., Bénard, F., Pan, J., Lin, K.-S., and Perrin, D. M. (2014) Preclinical evaluation of a high-affinity 18F-trifluoroborate octreotate derivative for somatostatin receptor imaging, *Journal of nuclear medicine* 55, 1499-1505.
199. Hansen, T. V., Wu, P., Sharpless, W. D., and Lindberg, J. G. (2005) Just click it: undergraduate procedures for the copper (I)-catalyzed formation of 1, 2, 3-triazoles from azides and terminal acetylenes, *Journal of chemical education* 82, 1833.
200. Hatse, S., Princen, K., Bridger, G., De Clercq, E., and Schols, D. (2002) Chemokine receptor inhibition by AMD3100 is strictly confined to CXCR4, *FEBS letters* 527, 255-262.
201. Kalatskaya, I., Berchiche, Y. A., Gravel, S., Limberg, B. J., Rosenbaum, J. S., and Heveker, N. (2009) AMD3100 is a CXCR7 ligand with allosteric agonist properties, *Molecular pharmacology* 75, 1240-1247.

## SUPPLEMENTARY MATERIAL

202. Ehrlich, A., Ray, P., Luker, K. E., Lolis, E. J., and Luker, G. D. (2013) Allosteric peptide regulators of chemokine receptors CXCR4 and CXCR7, *Biochemical pharmacology* 86, 1263-1271.
203. Montpas, N., Cabana, J., St-Onge, G., Gravel, S., Morin, G., Kuroyanagi, T., Lavigne, P., Fujii, N., Oishi, S., and Heveker, N. (2015) Mode of binding of the cyclic agonist peptide TC14012 to CXCR7: identification of receptor and compound determinants, *Biochemistry* 54, 1505-1515.
204. Fraker, P. J., and Speck, J. C. (1978) Protein and cell membrane iodinations with a sparingly soluble chloroamide, 1, 3, 4, 6-tetrachloro-3a, 6a-diphenylglycoluril, *Biochemical and biophysical research communications* 80, 849-857.
205. Notni, J., Pohle, K., and Wester, H.-J. (2013) Be spoilt for choice with radiolabelled RGD peptides: preclinical evaluation of 68 Ga-TRAP (RGD) 3, *Nuclear medicine and biology* 40, 33-41.
206. Mueller, D., Klette, I., Baum, R. P., Gottschaldt, M., Schultz, M. K., and Breeman, W. A. (2012) Simplified NaCl based 68Ga concentration and labeling procedure for rapid synthesis of 68Ga radiopharmaceuticals in high radiochemical purity, *Bioconjugate chemistry* 23, 1712-1717.
207. Breeman, W. A., de Jong, M., Visser, T. J., Erion, J. L., and Krenning, E. P. (2003) Optimising conditions for radiolabelling of DOTA-peptides with 90Y, 111In and 177Lu at high specific activities, *European journal of nuclear medicine and molecular imaging* 30, 917-920.
208. AP Breeman, W., MS de Zanger, R., Sze Chan, H., and de Blois, E. (2015) Alternative method to determine Specific Activity of 177Lu by HPLC, *Current radiopharmaceuticals* 8, 119-122.
209. Sosabowski, J. K., and Mather, S. J. (2006) Conjugation of DOTA-like chelating agents to peptides and radiolabeling with trivalent metallic isotopes, *Nature protocols* 1, 972-976.
210. Zhan, W., Liang, Z., Zhu, A., Kurtkaya, S., Shim, H., Snyder, J. P., and Liotta, D. C. (2007) Discovery of small molecule CXCR4 antagonists, *Journal of medicinal chemistry* 50, 5655-5664.
211. Mooring, S. R., Gaines, T., Liang, Z., and Shim, H. (2014) Synthesis of pyridine derivatives as potential antagonists of chemokine receptor type 4, *Heterocyclic communications* 20, 149-153.
212. Mashinchian, O., Johari-Ahar, M., Ghaemi, B., Rashidi, M., Barar, J., and Omid, Y. (2014) Impacts of quantum dots in molecular detection and bioimaging of cancer, *BioImpacts: BI* 4, 149.
213. Jin, T., Fujii, F., Yamada, E., Nodasaka, Y., and Kinjo, M. (2006) Control of the optical properties of quantum dots by surface coating with calix [n] arene carboxylic acids, *Journal of the American Chemical Society* 128, 9288-9289.
214. Cai, W., Chen, K., Li, Z.-B., Gambhir, S. S., and Chen, X. (2007) Dual-function probe for PET and near-infrared fluorescence imaging of tumor vasculature, *Journal of Nuclear Medicine* 48, 1862-1870.
215. Michalet, X., Pinaud, F., Bentolila, L., Tsay, J., Doose, S., Li, J., Sundaresan, G., Wu, A., Gambhir, S., and Weiss, S. (2005) Quantum dots for live cells, in vivo imaging, and diagnostics, *science* 307, 538-544.
216. Medintz, I. L., Uyeda, H. T., Goldman, E. R., and Mattoussi, H. (2005) Quantum dot bioconjugates for imaging, labelling and sensing, *Nature materials* 4, 435-446.
217. Choi, H. S., Liu, W., Misra, P., Tanaka, E., Zimmer, J. P., Ipe, B. I., Bawendi, M. G., and Frangioni, J. V. (2007) Renal clearance of quantum dots, *Nature biotechnology* 25, 1165-1170.
218. Hardman, R. (2006) A toxicologic review of quantum dots: toxicity depends on physicochemical and environmental factors, *Environmental health perspectives*, 165-172.
219. Mungalpara, J., Thiele, S., Eriksen, Ø., Eksteen, J., Rosenkilde, M. M., and Våbenø, J. (2012) Rational design of conformationally constrained cyclopentapeptide antagonists for CXCR4 chemokine receptor 4 (CXCR4), *Journal of medicinal chemistry* 55, 10287-10291.
220. Mungalpara, J., Zachariassen, Z. G., Thiele, S., Rosenkilde, M. M., and Våbenø, J. (2013) Structure-activity relationship studies of the aromatic positions in cyclopentapeptide CXCR4 antagonists, *Organic & biomolecular chemistry* 11, 8202-8208.
221. Shankaramma, S. C., Moehle, K., James, S., Vrijbloed, J. W., Obrecht, D., and Robinson, J. A. (2003) A family of macrocyclic antibiotics with a mixed peptide-peptoid  $\beta$ -hairpin backbone conformation, *Chemical Communications*, 1842-1843.

## SUPPLEMENTARY MATERIAL

222. Yoshikawa, Y., Kobayashi, K., Oishi, S., Fujii, N., and Furuya, T. (2012) Molecular modeling study of cyclic pentapeptide CXCR4 antagonists: New insight into CXCR4–FC131 interactions, *Bioorganic & medicinal chemistry letters* 22, 2146-2150.
223. Hosseinimehr, S. J., Tolmachev, V., and Orlova, A. (2012) Liver uptake of radiolabeled targeting proteins and peptides: considerations for targeting peptide conjugate design, *Drug discovery today* 17, 1224-1232.
224. Koenig, J. A., and Edwardson, J. M. (1997) Endocytosis and recycling of G protein-coupled receptors, *Trends in pharmacological sciences* 18, 276-287.
225. Cescato, R., Schulz, S., Waser, B., Eltschinger, V., Rivier, J. E., Wester, H.-J., Culler, M., Gjinj, M., Liu, Q., and Schonbrunn, A. (2006) Internalization of sst2, sst3, and sst5 receptors: effects of somatostatin agonists and antagonists, *Journal of Nuclear Medicine* 47, 502-511.
226. Reubi, J. C. (2003) Peptide receptors as molecular targets for cancer diagnosis and therapy, *Endocrine reviews* 24, 389-427.
227. Bodei, L., Paganelli, G., and Mariani, G. (2006) Receptor radionuclide therapy of tumors: a road from basic research to clinical applications, *Journal of Nuclear Medicine* 47, 375-377.
228. Storch, D., Béhé, M., Walter, M. A., Chen, J., Powell, P., Mikolajczak, R., and Mäcke, H. R. (2005) Evaluation of [99mTc/EDDA/HYNIC0] octreotide derivatives compared with [111In-DOTA0, Tyr3, Thr8] octreotide and [111In-DTPA0] octreotide: does tumor or pancreas uptake correlate with the rate of internalization?, *Journal of nuclear medicine* 46, 1561-1569.
229. Gjinj, M., Zhang, H., Waser, B., Cescato, R., Wild, D., Wang, X., Erchegyi, J., Rivier, J., Mäcke, H. R., and Reubi, J. C. (2006) Radiolabeled somatostatin receptor antagonists are preferable to agonists for in vivo peptide receptor targeting of tumors, *Proceedings of the National Academy of Sciences* 103, 16436-16441.
230. Cescato, R., Waser, B., Fani, M., and Reubi, J. C. (2011) Evaluation of 177Lu-DOTA-sst2 antagonist versus 177Lu-DOTA-sst2 agonist binding in human cancers in vitro, *Journal of Nuclear Medicine* 52, 1886-1890.
231. Wild, D., Fani, M., Behe, M., Brink, I., Rivier, J. E., Reubi, J. C., Maecke, H. R., and Weber, W. A. (2011) First clinical evidence that imaging with somatostatin receptor antagonists is feasible, *Journal of nuclear Medicine* 52, 1412-1417.
232. Wild, D., Fani, M., Fischer, R., Del Pozzo, L., Kaul, F., Krebs, S., Rivier, J. E., Reubi, J. C., Maecke, H. R., and Weber, W. A. (2014) Comparison of somatostatin receptor agonist and antagonist for peptide receptor radionuclide therapy: a pilot study, *Journal of Nuclear Medicine* 55, 1248-1252.
233. Dalm, S. U., Nonnekens, J., Doeswijk, G. N., de Blois, E., van Gent, D. C., Konijnenberg, M. W., and de Jong, M. (2015) Comparison of the therapeutic response to treatment with a 177-lutetium labeled somatostatin receptor agonist and antagonist in preclinical models, *Journal of Nuclear Medicine*, jnumed. 115.167007.
234. Cescato, R., Maina, T., Nock, B., Nikolopoulou, A., Charalambidis, D., Piccand, V., and Reubi, J. C. (2008) Bombesin receptor antagonists may be preferable to agonists for tumor targeting, *Journal of Nuclear Medicine* 49, 318-326.
235. Cooper, D., Mons, N., and Karpen, J. W. (1995) Adenylyl cyclases and the interaction between calcium and cAMP signalling, *Nature* 374, 421-424.
236. Awad, J., Johnson, R., Jakobs, K., and Schultz, G. (1983) Interactions of forskolin and adenylyl cyclase. Effects on substrate kinetics and protection against inactivation by heat and N-ethylmaleimide, *Journal of Biological Chemistry* 258, 2960-2965.
237. Hattermann, K., Holzenburg, E., Hans, F., Lucius, R., Held-Feindt, J., and Mentlein, R. (2014) Effects of the chemokine CXCL12 and combined internalization of its receptors CXCR4 and CXCR7 in human MCF-7 breast cancer cells, *Cell and tissue research* 357, 253-266.

## SUPPLEMENTARY MATERIAL

238. Yoshikawa, Y., Oishi, S., Kubo, T., Tanahara, N., Fujii, N., and Furuya, T. (2013) Optimized method of G-protein-coupled receptor homology modeling: its application to the discovery of novel CXCR7 ligands, *Journal of medicinal chemistry* 56, 4236-4251.
239. Eder, M., Schäfer, M., Bauder-Wüst, U., Hull, W.-E., Wängler, C., Mier, W., Haberkorn, U., and Eisenhut, M. (2012) 68Ga-complex lipophilicity and the targeting property of a urea-based PSMA inhibitor for PET imaging, *Bioconjugate chemistry* 23, 688-697.
240. Kratochwil, N. A., Huber, W., Müller, F., Kansy, M., and Gerber, P. R. (2002) Predicting plasma protein binding of drugs: a new approach, *Biochemical pharmacology* 64, 1355-1374.
241. Raman, D., Sobolik-Delmaire, T., and Richmond, A. (2011) Chemokines in health and disease, *Experimental cell research* 317, 575-589.
242. Bieniasz, P. D., Fridell, R. A., Anthony, K., and Cullen, B. R. (1997) Murine CXCR-4 is a functional coreceptor for T-cell-tropic and dual-tropic strains of human immunodeficiency virus type 1, *Journal of virology* 71, 7097-7100.
243. Klein, I., Cornejo, J. C., Polakos, N. K., John, B., Wuensch, S. A., Topham, D. J., Pierce, R. H., and Crispe, I. N. (2007) Kupffer cell heterogeneity: functional properties of bone marrow derived and sessile hepatic macrophages, *Blood* 110, 4077-4085.
244. Mendt, M., and Cardier, J. E. (2012) Stromal-derived factor-1 and its receptor, CXCR4, are constitutively expressed by mouse liver sinusoidal endothelial cells: implications for the regulation of hematopoietic cell migration to the liver during extramedullary hematopoiesis, *Stem Cells Dev* 21, 2142-2151.
245. Vegt, E., De Jong, M., Wetzels, J. F., Masereeuw, R., Melis, M., Oyen, W. J., Gotthardt, M., and Boerman, O. C. (2010) Renal toxicity of radiolabeled peptides and antibody fragments: mechanisms, impact on radionuclide therapy, and strategies for prevention, *Journal of nuclear medicine* 51, 1049-1058.
246. Singh, S., Singh, U. P., Grizzle, W. E., and Lillard, J. W. (2004) CXCL12–CXCR4 interactions modulate prostate cancer cell migration, metalloproteinase expression and invasion, *Laboratory investigation* 84, 1666-1676.
247. Shanmugam, M. K., Manu, K. A., Ong, T. H., Ramachandran, L., Surana, R., Bist, P., Lim, L. H., Prem Kumar, A., Hui, K. M., and Sethi, G. (2011) Inhibition of CXCR4/CXCL12 signaling axis by ursolic acid leads to suppression of metastasis in transgenic adenocarcinoma of mouse prostate model, *International Journal of Cancer* 129, 1552-1563.
248. Schottelius, M., Hoffmann, F., Willibald, M., Simecek, J., Schwaiger, M., and Wester, H. (2014) Pentixafor-based radiopharmaceuticals: A promising route towards CXCR4-targeted theranostics, *Journal of Nuclear Medicine* 55, 495-495.
249. Lee, B., Sharron, M., Montaner, L. J., Weissman, D., and Doms, R. W. (1999) Quantification of CD4, CCR5, and CXCR4 levels on lymphocyte subsets, dendritic cells, and differentially conditioned monocyte-derived macrophages, *Proc Natl Acad Sci U S A* 96, 5215-5220.
250. Kratochwil, C., Giesel, F. L., Leotta, K., Eder, M., Hoppe-Tich, T., Youssoufian, H., Kopka, K., Babich, J. W., and Haberkorn, U. (2015) PMPA for nephroprotection in PSMA-targeted radionuclide therapy of prostate cancer, *Journal of Nuclear Medicine* 56, 293-298.

## SUPPLEMENTARY MATERIAL

### 4. Publications

#### Peer-reviewed journal articles

- Poschenrieder A, Osl T, Schottelius M, Hoffmann F, Wirtz M, Schwaiger M, et al. First 18 F-Labeled Pentixafor-Based Imaging Agent for PET Imaging of CXCR4 Expression In Vivo. Tomography. 2016;2(2):85-93.
- Herrmann K, Schottelius M, Lapa C, Osl T, Poschenrieder A, Hanscheid H et al. First-in-Human Experience of CXCR4-Directed Endoradiotherapy with Lu-177- and Y-90-Labeled Pentixather in Advanced-Stage Multiple Myeloma with Extensive Intra- and Extramedullary Disease. J Nucl Med. 2016;57(2):248-51.
- Schottelius M, Konrad M, Osl T, Poschenrieder A, Wester H-J. An optimized strategy for the mild and efficient solution phase iodination of tyrosine residues in bioactive peptides. Tetrahedron Lett. 2015;56(47):6602-5.

#### Articles in preparation

- Theresa Osl, Margret Schottelius, Frauke Hoffmann, Horst Kessler, Markus Schwaiger, Hans-Jürgen Wester. Design and synthesis of novel chemokine receptor 4-targeted ligands for molecular imaging. Bioconjugate Chemistry,
- Theresa Osl, Alexander Schmidt, Margret Schottelius, Markus Schwaiger and Hans-Jürgen Wester. Synthesis and preclinical evaluation of a novel theranostic probe for CXCR4 positive malignancies. J Nucl Med,

#### Selected conference abstracts

- T.Osl, M. Schottelius, F. Hoffmann, A. Poschenrieder, M. Schwaiger, H.-J. Wester. Neue CXCR4-Liganden für die optische Bildgebung und die PET. Arbeitsgemeinschaft Radiochemie/Radiopharmazie. 2015; VII.2.
- Constantin Lapa, Stefan Knop, Andreas Schirbel, Theresa Osl, Andreas Poschenrieder, Heribert Haenscheid, Margret Schottelius, Andreas Buck, Hermann Einsele and Hans Wester. First in man experience of CXCR4-directed endoradiotherapy with <sup>177</sup>Lu- and <sup>90</sup>Y-labelled Pentixather in multiple myeloma patients, *J Nucl Med May 1, 2015 vol. 56 no. supplement 3 14*

#### Patents

- Wester HJ, Schottelius M, Osl T, Poschenrieder A, Willibald M. Modified cyclopentapeptides and uses thereof. WO 2015185162A1; 2015.

## SUPPLEMENTARY MATERIAL

### Patent applications

- Osl T, Wester HJ, Schottelius. Erfindungsmeldung – „High affinity linkers for the modification of cyclicpentapeptides and uses thereof“, 2016-09E02
- Osl T, Kapp T, Schottelius M, Kessler H, Wester HJ. Erfindungsmeldung „CPCR4.3-based CXCR4-targeted radio- and fluorescent ligands with reduced species selectivity“, 2016-11E01

## 5. Acknowledgements

First of all, I would like to thank Prof. Dr. Hans-Jürgen Wester for giving me the chance to perform a doctorate in his group, for the exquisite research project, the support in all scientific questions and the accreditation for summer schools or conferences. I am very grateful for supporting and finally realizing my research internship at the Emory University Hospital in Atlanta.

I would like to thank PD Dr. Margret Schottelius for the fruitful discussions on the CXCR4 project, synthetic impact, reading abstracts, presentations, posters, patents and papers and most of all for the funny moments in the lab.

Prof. Dr. Horst Kessler I would like to thank for providing several starting materials and scientific support with his knowledge about cyclic pentapeptides.

Thanks to Dr. Jakub Simecek for the support with the synthesis module and your advices in scientific aspects. Dr. Behrooz Yousefi and PD Dr. Johannes Notni, I would like to thank for your advice and discussions about all the important things of lab and life and for  $^{68}\text{Ga}$ -synthesis at any time! Most important, I very much appreciate all the support from Alex Schmidt, Steffi Robu, Tina Wirtz and Andi Poschenrieder and for the great times in the lab. Special thanks to Alex for helping out so many times with  $^{177}\text{Lu}$ -labeling, biodistribution, metabolism, internalization and especially for the numberless hours of discussion about work and life itself and for the constant support you provided to me. Steffi and Tina you were simply the best colleagues for work! Matthias Konrad, Daniel Di Carlo and Thomas Günther thanks for proof reading of my thesis (and making hard lab days more tolerable). I am very grateful Moni, that you always supported me with your excellent lab work and your talent for organization. Thanks Sven for helping out with binding assays and for several good parties. The lab work conducted by the students Lena Staiger, Mara Parzinger, Carla Courtis, Thomas Löhr, Chris Kiwus, Julia Evers, Chris Schiefer, Philipp Streich and the extraordinary Hifis Daniel Di Carlo (purification of tons of CPCR4) and Matthias Konrad is highly acknowledged.

## SUPPLEMENTARY MATERIAL

Prof Hyunsuk Shim, MD Zhongxing Liang, Dr. Younghyun Yoon, Yoon Hyeun Oum, Renren Bai, Saumya Gurbani and Scott Cordova I would like to thank for the support in all the experiments and for the great time in Atlanta. Special thanks to Saumya and Scot for showing me Atlanta's pub culture.

Prof. Dr. Markus Schwaiger I would like to thank for the lab space, and for the chance to use all the great facilities at Klinikum rechts der Isar. The contribution of the PET/SPECT-MTAs for taking blood samples and assistance with the activity deliveries and ordering is highly recognized. Thank goes to the GMP team and cyclotron operators Michael Herz and R. Klitsch for the support in  $^{18}\text{F}$  production and for the support with the synthesis module. Special thanks are due to the small animal PET Team, Sybille Reder and Markus Mittelhäuser, for always making additional scans possible, especially when the tumor growth was unpredictable and for your help with catheter injections of animals at any time.

Finally, I have to thank my family and friends for the support over all the years and for the encouragement during several ups and downs. Thanks dad for all your work with the horses, it wouldn't have been possible without you.